The University of Nottingham

Faculty of Engineering

Development of biomaterial applications for the investigation of the influence of dynamic mechanical cues and matrix apparent stiffness on the behaviour of contractile cells

Ana L Encerrado Flores, MSc

November 2021

Thesis submitted to the University of Nottingham for the degree of Doctor of Philosophy

ABSTRACT

Cells are continually exposed to forces from their microenvironment, i.e., the forces exerted by the extracellular matrix (ECM) and cell stiffness naturally varies within the body from hard bone to soft brain tissue. It has been observed that cell function is partly influenced by the variations in stiffness, which has been attributed to the phenomenon of cells sensing the mechanical properties of their microenvironment, and the pathways involved in this phenomenon are strongly linked to tissue healing and regeneration. Cellular functions such as proliferation, migration and differentiation have shown to be highly sensitive to changes in ECM stiffness. It is by applying force, when attached to the ECM, that most mammalian cells can sense these ECM variations in stiffness as a result of its resistance to deformation. Several mechanotransduction studies, aimed to elucidate the mechanisms behind this phenomenon, have focused on the fabrication of hydrogels with tuneable mechanical properties by the modification of the hydrogel intrinsic elastic modulus. This modification does not exclusively alter the hydrogel stiffness, however, but also other properties such as topography, architecture and chemistry of the hydrogel surfaces. This has the effect of obscuring the interpretation of results. The stiffness cells can sense can also be manipulated by altering the hydrogel thickness when constraint boundaries exist. Individual cells have been observed to sense stiff boundaries through soft synthetic hydrogels when the thickness is less than 10 μm. In contrast to these linear elastic synthetic polymers – which are the option of choice – biological tissue ECM is hard to replicate. Its mechanical complexity and fibrous inhomogeneous architecture are among factors that

make its study and artificial recreation challenging. The ECM is a fibrillar non-linear elastic protein-based complex, whose elastic modulus increases in magnitude as the applied strain increases. Not many mechanotransduction studies have used protein-based hydrogels but they have demonstrated that individual cells can sense stiff materials underneath these soft non-linearly elastic hydrogels at far deeper distances (50µ to 1440µm) compared to those reported by synthetic materials (10 µm). In this study, a chitosan-gelatin cross-linked hydrogel (ChG_PA) was developed and used to design, fabricate and test a range of applications to explore the effect of mechanical cues – matrix tension, apparent stiffness, stiffness gradients and flow-induced shear stress – on cell growth, migration, and differentiation, *in vitro*. Diverse cell lines were used to study the potentiality of these models, especially human mesenchymal stem cells (hMSC), which proved to proliferate and differentiate within hydrogels of varying uniform and graduated stiffness. All cell lines used where observed to sense the stiff materials underneath the ChG_PA hydrogels at distances ranging from 2500µm to 3000µm, depending on cell line and cell seeding density. Cell number, morphology and differentiation were seen to be strongly dependent on matrix apparent stiffness (287KPa to 3KPa), stiffness gradient (126Pa/µm to 2Pa/µm), and the combined effect of flow-induced shear (1.157 dyne/cm^2) and matrix apparent stiffness (213KPa to 5KPa). Therefore, the developed artificial ECM model presented in this research project is well suited to study the role of ECM mechanical cues on the behaviour of contractile cell lines.

Acknowledgments

Firstly, I would like to thank my grandma, whose encouragement and life example – to do what is right even when sometimes is the hardest thing to do – have always inspired me to do better, grow and seek personal understanding, and at the end her inspiration brought me to England and undertake my PhD studies.

To my beloved country of origin Mexico, which sourced the context for my continuous growth, and to my sponsor CONACYT, which provided the finances and the opportunity for me to complete my investigation project.

To my PhD supervisors Dr Colin Scotchford and Dr Alastair Campbell Ritchie, for their trust, enthusiasm, guidance and support during the length of this project. Special thanks to Dr Scotchford, whose trust, supervised freedom and support encouraged me to go deeper into my curiosity. Also, special thanks go to Prof George Roberts[1] for his generosity in sharing his vast knowledge, advice and expertise on chitosan chemistry and his chitosan.

Further acknowledgements are reserved for Julie Thomson and Kayla Kert (at Wolfson's cell lab) whose continuous support, chats and silent company made hard cell culture times not quite so hard – but enjoyable! Thank you, ladies.

Finally, thanks to my family, especially mama, who unfailingly daily would text "how are you doing my love? Thinking about you", and my husband who trust me even when it was hard to understand what I was doing and why I decided to tackle drawbacks the way I did, thank you both for all your unconditional love. This thesis is dedicated to you!

Psalm 139:13-14 (NLT)

13 You made all the delicate, inner parts of my body
and knit me together in my mother's womb.
14 Thank you for making me so wonderfully complex!
Your workmanship is marvellous—how well I know it.

Contributors

All experiments and data analysis were performed by the author at the Advance Materials and Bioengineering research group cell and materials laboratories, Faculty of Engineering, University of Nottingham, with the following exceptions:

Chapter 4-5: ChG_PA hydrogels of different PA% porosity

ChG_PA Hydrogel Cryo FIB-SEM (Figure 4.4, and 5.2) was performed, and images obtained by Dr Christopher Parmenter at the Nanoscale and Microscale Research Centre (nmRC), University of Nottingham.

Chapter 4-5 ChG_PA hydrogels X-ray photoelectron spectroscopy (XPS)

ChG_PA Hydrogels XPS (Figure 4.15 and 5.4) was performed and analysed by Dr Emily Smith at the Nanoscale and Microscale Research Centre (nmRC), University of Nottingham.

Chapter 5: Hydrogel apparent stiffness as a function of sample thickness

AFM measurements for hydrogel apparent stiffness (Figure 5.6) were performed and analysed by Xiaoli Zhang and Dr Nuria Gavara at Queen Mary University of London.

Chapter 6: Hydrogel apparent stiffness as a function of sample thickness

AFM measurements for gradient hydrogel apparent stiffness (Figure 6.3) were performed and analysed by Xiaoli Zhang at Queen Mary University of London.

Chapter 6: Cell orientation θ

Confocal imaging (Figure 6.9A) was performed by Christopher Gell at the Advanced Microscopy Unit part of School of Life Sciences Imaging (SLIM) facility, at the University of Nottingham.

Table of Contents

CHAPTER

1

Introduction

1.Introduction

Overview

Organisms of all kinds are constantly exposed to forces; these forces contribute to development, survival, and diseases. By sensing and responding to the external environment, organisms communicate and cooperate with each other, and human cells are no exception. It is well known most cell lineages possess a well-developed sense of 'taste' or 'smell', mediated by chemical factors, and research groups have recently turned their attention to another sense not yet fully explored or understood: a sense of 'touch' [1]. Cells react to specific mechanical forces and their immediate microenvironment stiffness, and transmit these cues through the extracellular matrix (ECM) and cell-to-cell interactions [2]. Such interchanges of chemical and mechanical signals constitute a wide range of means for cells to communicate with one another, and with their ECM; this complex, strongly regulated process plays a role in many essential homeostasis related processes, including cell migration, proliferation, differentiation, and apoptosis [3-5].

It is not surprising that mechanical interactions between cells and substrates are becoming an area of intense study in fields relevant to regenerative medicine, such as tissue healing and tissue regeneration. This is partly fuelled by the creative advances in the development of suitable elastic biomaterials [6-8] and cell culture models *in vitro* [9-11] for the study of cellular responses to their ECM stiffness. The majority of cell mechanotransduction studies evaluate discrete changes in stiffness, however cells *in vivo* are subjected to varying stiffness, as they migrate within tissues; therefore, gradients of

mechanical stiffness offer a more feasible way to study cell response to the mechanical cues in a more physiological manner.

A range of biomaterial systems have been developed toward this goal, including patterned glass substrates [12], elastomeric hydrogels [13], hydroxyapatite ceramics [14] and fibrillar foams [15]. However, hydrogels have arisen as the most promising option for these models and the resulting regenerative therapies; systems that better mimic the high complexity of *in vivo* biological environments, hydrogels have similar mechanical properties as those of many soft and connective tissues [16]. Most cell-culture hydrogels used in these studies are made of hydrogels, in which changes in mechanical properties are attained by altering the ratio of polymer or the degree of cross-linking, which alters the hydrogel elastic modulus. However, in practice the hydrogel's mesh size and cross-link-induced surface chemistry will also vary [10]. When fabricating stiffness gradients using this approach, the resulting gradient is often limited by the minimum possible shear modulus; the steepness of the gradient, which is usually rather shallow; or the simplicity of the stiffness gradients, which are often linear [29].

To overcome these limitations in this study, an approach was used based on the fact that cells can sense stiff substrates through soft ones [17]. In this approach, how much an underlying stiff surface can be felt through a second layer of a softer material is governed by the thickness of the superficial compliant layer and the magnitude of its deformation concept known as apparent stiffness [18].

Cells respond not only to static physiological cues, such as stiffness, but also to the environmental dynamic stimuli to which they are exposed once implanted *in vivo* [20]. It has been observed that extracellular dynamic environmental factors resulting from the exposure to mechanical stimuli, for example interstitial fluid shear, have several effects

on fibroblast proliferation, morphology, gene expression, and protein secretion [24]. However, it is impossible for researchers to assess the effects of mechanical forces on cultured cells, if systems for applying the suitable forces do not exist [26].

General Project Aim

The general aims of this research were to formulate a novel cross-linked chitosan-gelatin (ChG) hydrogel that support cell attachment and growth, to validate the design of cell-seeded applications for the investigation of the matrix stiffness influence on cell growth, migration and differentiation of mammalian cells; and to develop a bioreactor to investigate the static and dynamic mechanical stimuli in a 2D format.

Project Experimental Objectives

- Development of chitosan-gelatin hydrogels cross-linked with a polyphenol.
- Analysis of cell viability when cultured on the developed hydrogel.
- Characterise cell responses to variations in matrix stiffness.
- Introduce the use of stiffness gradients and compared cell response against matrices of uniform stiffness.
- Develop a bioreactor to enable assessment of cell responses to combine static and dynamic stimuli.

CHAPTER

2

Literature Review

2. Literature Review

Cell mechanotransduction and mechanosensing

The interaction of cells with surfaces is a complex phenomenon that has been widely studied from many different angles, including those relevant to the fields of Biology and Chemistry. The importance of the mechanical properties and the cell-surface interplay of biomaterials have been investigated due to their undeniable influence on cell behaviour [19]. This is in part due to the important role intracellular tensile forces – resulting from cytoskeletal reorganization of a cell's physical surroundings – play in regulating cell function [20]. Theoretically, an adherent cell is able to sense stiffness by anchoring onto the ECM and exerting traction forces using focal adhesions [21] and creating a deformation in the material that is proportional to the material's stiffness [22]. It is thought that cells are able to sense or to measure these deformations as a function of the force they exert, and translate them into phenotypic responses allowing them, for example, to migrate in response to stiffness gradients, resulting in durotaxis [23]. This biological response is now known to affect a variety of cellular processes, including proliferation and growth [11, 18, 24, 25], migration [11, 26-28], morphology [29-33], differentiation [10, 13, 34, 35], mature cell function [2, 36-38], and processes connected to cancer metastasis [19, 23]. The mechanism by which cells recognize mechanical properties and translate them into intracellular cues is governed by mechanosensitive receptors or structures, that sense and convert mechanical cues into cascades of biochemical signalling pathways; a process known as mechanotransduction (Figure 2.1) [39].

Mechanotransduction influences the development and maintenance of living tissues, but it is particularly important in mechanically-stressed tissues such as muscle, bone, cartilage and blood vessels, as these require adaptive flexible responses to rapidly adjust to

fluctuating loading conditions [40]. In order to translate mechanical cues into biochemical signals, cells recognize force differentials through molecular sensors, and then amplify and propagate these signals to induce changes in cellular fate and behaviour [5].

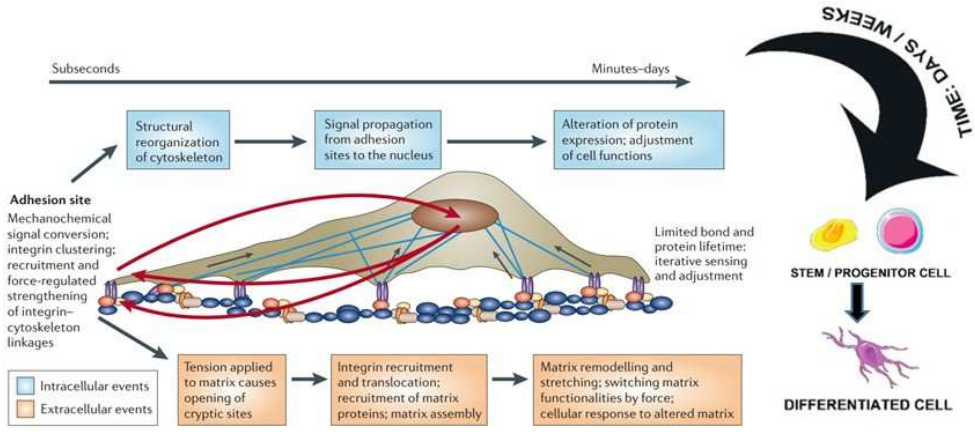

Figure 2. 1 The cellular process of mechanotransduction response from seconds to days. Mechanotransduction converts mechanical cues into biochemical signals to modulate cell behaviour and function. Generally, the processes involve receptors at the focal adhesions, mechanosensors, integrins, nuclear signalling factors, and nuclear deformation mediated by Laminin A, leading to the mediation of gene expression. The timescale for this 'pathway phases' ranges from seconds for the appearance of mechanosensors, hours for alteration in gene expression, days for modification in cell behaviour and function, while severe and permanent changes in phenotype, such as differentiation, require weeks. Adapted from Vogel et. al. [5].

The leading mechanical cues are controlled by flow shear stress, tensile forces, geometric and biomaterial derived cues, as well as the mechanical properties of the substrate, Figure 2.2. In this manner, mechanotransduction plays an important role in the regulation of cell behaviour, Figure 2.3.

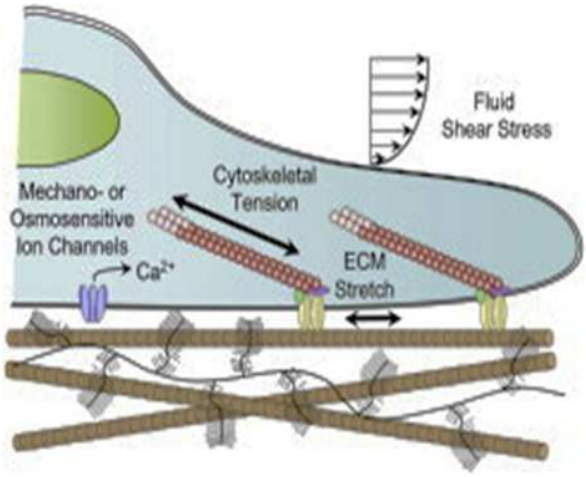

Figure 2. 2 The translation of Mechanical Cues and the Manipulation of Stem Cell Fate. During development and over lifetime, stem cells will be subjected to a plethora of physical cues, including compressive, elastic, tensile, and shear fluid stresses, often as a result to interactions with their ECM. Matrix stiffness, for example, can induce stretch of the cytoskeleton and nucleus through focal adhesions, whereas compression of the ECM can significantly modify local charge density and ion concentrations, hypothetically activating osmotically sensitive ion channels. Previous studies have shown that these mechanical stimuli alone can strongly influence stem cell growth, migration and differentiation *in vivo* and *in vitro*. Adapted from [41].

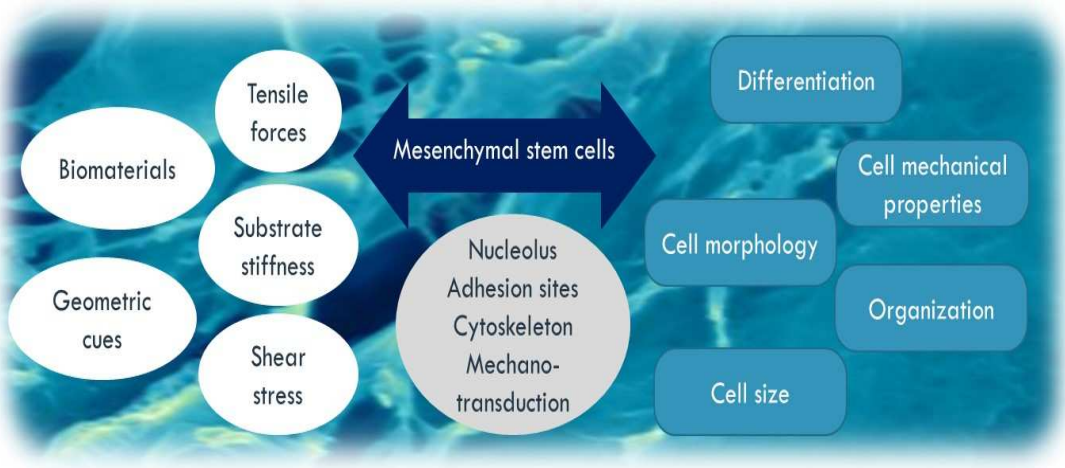

Figure 2. 3 The effect of mechanical signals on mesenchymal stem cell behaviour. Numerous mechanical properties, including matrix stiffness, tensile strength, shear stress, geometric cues, and matrix compositions are applied to mesenchymal stem cells. The cell responses to such influences include differentiation, organization, and changes in cell mechanical properties, morphology, and size. These pathways are mediated by several mechanisms, comprising nuclear deformations, mechanotransduction and changes in adhesion sites and the cytoskeleton. Adapted from [42].

Matrix elastic modulus, stiffness, stiffness gradients, thickness, and its role on cellular function.

Most healthy cells typically do not survive well when suspended in a fluid, as they need a surface to attach to; these cells are known to be anchorage dependent. Anchorage dependent cells need to adhere to other cells, ECM, or tissue culture substrates [43]. The substrate may vary in stiffness for example between cortical bone (~1-10GPa), brain (1-4KPa) or adipose tissue (~0.5-1KPa) [44]. Moreover studies have shown that some cells can modify the mechanical properties of their surroundings [45], furthermore the phenotype of cells, cultured *in vitro,* has been observed to be influenced by the stiffness of the substrates on which they rest [46, 47]; e.g. cells grown on soft agar hydrogels are used to identify risk of metastasis and the aggressiveness of cancer cells [48]. It is well known that cell-ECM interactions impact cell behaviour either directly or through cytokines [49, 50], e.g. stem cells and their niche, communicate not only by chemical but also through mechanical cues to regulate, cell behaviour and fate, and also to guide developmental processes [51, 52]. Other matrix physical cues, including surface characteristics such as, roughness, surface energy [53], and porosity [54, 55]; have also shown to influence cell behaviour.

Moreover, natural tissues come in a variety of stiffness, for example brain tissue is soft (1-4 KPa) whereas bone tissue is very hard (~1-10, GPa). Figure 2.4 shows the wide range of stiffness found in live tissues [38, 44, 56, 57]. 'Stiff' mineralized bone has a quite high Young's modulus, and needs very high stress to extend it, whereas brain tissue requires very little stress. Handorf and Cox et. al. [38, 44] individually reported that the ECM stiffness changes when involved in different pathologies, as in scar tissue and tumour samples, where it generally has higher stiffness compared to healthy tissue of the same kind, i.e. breast cancer tissue has shown to be 10-fold

stiffer than healthy breast tissue (1.5 KPa and 150 Pa, respectively) [38].

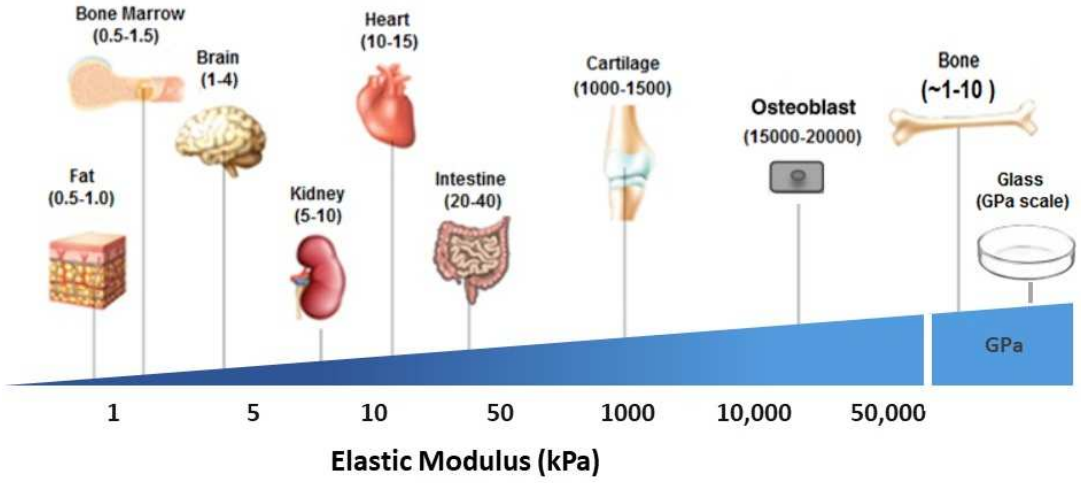

Figure 2. 4 Distinct modulus of human tissues suggesting tissue-specific stiffness. Different tissues with their explicit elastic modulus in the body. For reference, a tissue culture glass is shown, which is off the scale, in the gigapascal range (adapted from Cox et. al.)[44].

Cells possess a complex intracellular system that allows them to mechanosense their physical microenvironment. Theoretically, an anchorage dependant cell can sense rigidity by applying force on a surface and causing deformation in the material that is proportional to the material's intrinsic modulus [9]. It is thought that cells are able to sense or to measure these deformations as a function of the force they exert, and transduce them through the cytoskeleton to the nucleus to trigger a phenotypic response [29]. Mechanosensing by cells is now understood to be important or fundamental in a wide range of cellular processes, including division [25, 29, 58, 59], migration [11, 60-62], morphology [32, 60, 63, 64] differentiation [10, 65-68], and mature cell function [60, 69, 70], although the underlying molecular and mechanical control of mechanosensing is still poorly understood or controversial.

Matrix elastic modulus

The stiffness of a given material can be described as its ability to deform under applied forces, where less deformation results as matrix stiffness increases. Young's modulus (E) defines the stiffness of a substrate as the ratio of applied stress to resultant strain and has units of measurement in N/m^2 (Eq. 2.1).

$$E_{(Pascals)} = \frac{\sigma}{\varepsilon} = \frac{stress}{strain} \qquad \text{Eq. 2.1}$$

Stress is given by the applied force divided by the surface and strain; a dimensionless quantity defined by the stress-induced delta change in length of the material divided by its initial length [71].

Matrix stiffness

Matrix stiffness has been proven to affect cell function and behaviour at the signalling pathway level [27, 57, 72, 73]. This mechanotransductive process is mediated by integrin-focal adhesion (FA) signalling, which is manipulated by external forces and by the contractility of the cytoskeleton (CSK), both affecting cell-ECM adhesions [39]. Engler et al. [64] showed that controlling matrix stiffness can activate the differentiation pathways of hMSCs to the main cell lines of a tissue with comparable stiffness. Their studies show hMSCs differentiate into muscle, brain, and bone cells. Likewise Park et al. [74] proved hMSC differentiation into smooth muscle cells (SMCs) could be achieved by varying substrate stiffness, where stiff substrates (15 KPa) directed differentiation into SMCs, but softer ones (1 KPa) encouraged chondrogenic and adipogenic differentiation as a function of substrate stiffness (Figure 2.6).

Furthermore, their results show that over a period of several days to weeks, cells adhered to soft matrices (<1 KPa) began to show lean elongated morphologies and differentiate into neuronal lineages; those on intermediate stiffness (~10 KPa) started to show fibre-like morphologies, and express markers of muscle differentiation, and those on stiffer surfaces spread and flattened,

expressing markers of bone-cell differentiation (~30 KPa). Morphology changes are part of a cascade reflecting the cytoskeletal rearrangements taking place inside the cellular membrane

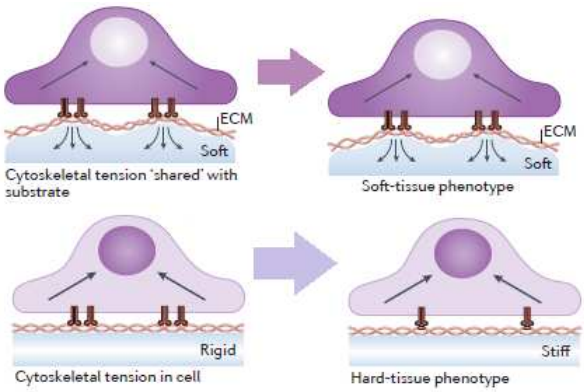

Figure 2. 5 hMSCs and Substrate Stiffness. Mesenchymal stem cells (MSCs) preferentially differentiate into soft tissue types on soft surfaces and into osteoblasts on stiff, rigid substrates. Cytoskeletal tension will change to match the tension of the substrates.

[75]. It has not been long since the effect of the ECM's stiffness started to be investigated, but the results demonstrate this characteristic is a strong regulator of stem cell behaviour and outcome [32, 67]. Discher et al. [1] have demonstrated that this passive mechanical cue seems to be, in some cases, more critical than soluble factors.

Stiffness gradients

Cells *in vivo* are subjected to varying stiffness as they migrate alongside tissues. Biological tissues are mechanically inhomogeneous, particularly during growth and migration, and cells are exposed to different mechanical stimuli and stiffness variations [46]. Variations can be found at the physiological scale (variations within tissues 1 Pa/μm) [76], at the soft-hard tissue interface (e.g. stiffness gradient at bone–cartilage interface and dentinal–enamel intersection 100 Pa/μm) [46], and also those stiffness variations can be produced during pathological processes (e.g. on cancer tumour progression and myocardial infarction 10 Pa/μm) [77, 78]. Therefore gradients of mechanical stiffness offer viable ways to study cell adhesion, distribution and alignment in a more physiological environment compared to hydrogels of uniform stiffness [79]. The development of

material gradients of varying stiffness represents an accessible way to investigate trends on cell behaviour which are closely related to continuous variations in the matrix stiffness, and can maximise the amount of the produced data, such as the critical stiffness threshold, points of stiffness regulating cell behaviours, the influence of stiffness itself, and also stiffness change ratios, stiffness gradients range, and changes in cell morphology and cell orientation during stiffness-induced migration (durotaxis) [80].

Furthermore, the ability of living cells to migrate guided by environmental gradients triggers a wide range of phenomena in development, homeostasis, and disease [81, 82]. The widely used approach of controlled cell migration is chemotaxis, the well-established ability of cells to follow gradients of soluble chemical cues [82]. However cells have the ability to sense mechanical cues, and they are able to be directed by rigidity gradients sensing the stiffness of their extracellular matrix (ECM), a process known as durotaxis [19, 23, 83-85]. Durotaxis has been linked to development [86], fibrosis [87], and cancer [88], although its underlying mechanisms remain unclear. Sharp transitions that are easy to replicate, such as bone and cartilage, have clearly illustrated this behaviour, however physiological conditions are more complex; most pathological conditions create gradients that are much less steep e.g. Berry et al. [78] demonstrated that myocardial infarction establishes gradients ~ 8 Pa/μm. It has also been reported that the favoured migration of vascular smooth muscle cells (VSMC) takes place on substrates ranging from ~2 to 40 KPa [89-91]. Both the range and the gradient or change in elastic modulus per unit length of the stiffness gradients described in these studies varies and are shown to have an impact on cell behaviour. However, these combined variations have caused confusion in the interpretation of results and make it difficult to segregate the effect of the elastic modulus range versus its rate of change (stiffness gradient) across the gradient. To better understand these

contributions separately in the durotactic phenomenon, it is desirable to fabricate a series of gradient surfaces that encompass the same stiffness range, whilst varying in the ratio of change of the stiffness gradient [92].

To fabricate stiffness gradients *in vitro*, a plethora of assorted methods have been explored, including manipulation of physical cross-linking (Figure 2.6) [93]. To understand some of the recent studies done in this mechanical landscape, refer to Table 2.1.

Table 2.1 Comparison of cell culture gradient hydrogel systems.

Ref	Year	Gradient surface area (cm2)	Cell seeding density	Stiffness gradient (Pa/μm)	Gradient range (MPa)	Linear
This study		2.54	250	2 to 104	0.002-0.503	
			1000	6 to 126	0.002-0.405	
Hadden et al.[94]	2017	4.80	2.40E+04	0.5	0.0001-0.0066	✓
				2.9	0.0024-0.0381	✓
				8.2	0.0032-0.1592	✓
Hartman et al.[95]	2016	0.1	500	2.9	0.00005-0.01	
Chao et al. [96]	2014	0.84	500	1.2	0.0004-0.0016	✓
Vincent et al.[76]	2013	2.5	12500	0.38	0.0015-0.0055	✓
				2.4	0.002-0.020	✓
				4.33	0.0025-0.0275	✓
Choi et al. [97]	2012	0.03	125	275	0.002-0.014	✓
Sunyer et al.[98]	2012	3.80	3000	~114	0.001-0.240	Semi
				~68	0.001-0.225	
				~7.4	0.003-.040	
Insenberg et al.[92]	2009	0.54	2700	10	0.029-0.0516	✓
				20	0.0093-0.041	✓
				40	0.0046-0.08	✓
Wong et al.[89]	2003	2.54	12700	~0.94	0.0025-0.011	✓

Adapted from Hadden et al. [94].

In addition, these methods are still limited in their fabrication; for example, for photopolymerization-based approaches, the toxicity of photo initiators, monomers and cross-linkers residues and UV radiation have limited their use. The surface chemistry of the substrate and its architecture often change along with the substrate stiffness gradient, which adversely combined the effect of surface chemistry and topography with substrate stiffness in cell studies [10, 97]. Therefore, having a uniform surface

architecture and chemistry along the stiffness gradient is desirable when studying the effect of stiffness on cell behaviour.

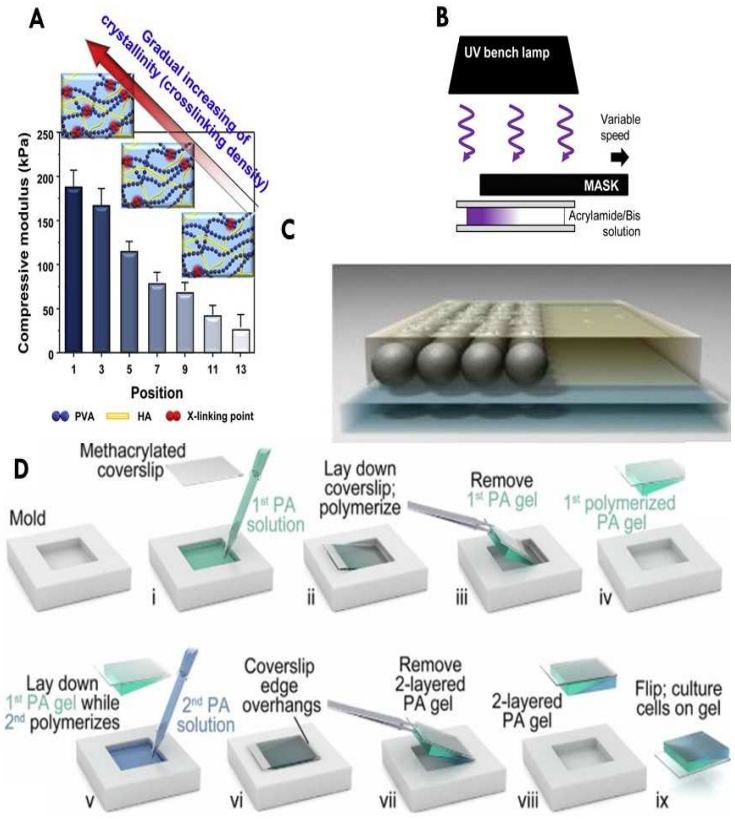

Figure 2. 6 Diverse techniques to fabricate stiffness gradients. A Gradual increasing of crystallinity (cross-linking density) **B** Gradual photo-polymerization **C** Inclusion of rigid particles fillers in soft hydrogel **D** Stiffness gradients using the principle that a cell can sense a hard material through a soft one (thickness gradients). Adapted from [84, 93, 94, 97, 98].

Matrix thickness

Most cell-culture materials used in mechanotransduction studies are hydrogels with tuneable mechanical properties. The manipulation of the hydrogel mechanical properties usually involves changes in the intrinsic elastic modulus of this gels by altering: the degree of cross-linking[73], the ratio of polymer[99], and the porosity and pore size [97] of these matrices. In practice, however, the hydrogel's mesh size and cross-link induced bulk and surface chemistry will vary, and these variations can alter the cell response to the matrix and complicate the interpretation of results [10]. Finding an

approach that overcomes these limitations and allows the study of variations in stiffness in isolation is desirable to understand the effect of matrix stiffness on cell response.

Adherent cells apply contractile forces to the material on which they adhere and sense the resistance of the material to deformation, i.e., its rigidity. Evans et al. [37] stated that this phenomenon is not entirely dependent on the matrix elastic modulus but also on the matrix dimensions (such as the thickness) and constraint boundaries. Tse et al. [100] reported that cells can sense underlying infinite stiff materials through soft hydrogels. This, according to Maloney et al. [18], is because the magnitude to which an underlying stiff substrate can be detected through a coating layer of a soft material will be a function not only of its intrinsic elastic modulus, but also of the thickness of the superficial elastic layer and the scale of its deformation (a concept known as apparent stiffness). Buxboim et al. [13, 101] developed a technique in which Polyacrylamide (PAAm) hydrogels were cast at different thicknesses (1-20μm) tightly attached to an underlying glass base. They observed that even at very low Young's modulus (1 and10 KPa which mimicked the elasticity of brain and muscle tissue respectively), at certain thickness (500nm-1μm) the cells behaved as if they were laying on much more rigid hydrogels comparable to hydrogels in the Young's module range of permineralized bone matrix (~100KPa). Lin et al. [102] provided the following theoretical explanation to the phenomenon. In summary, cells can sense substrate depth and translate to an apparent stiffness because of the way a cell probes the rigidity of its matrix. As a cell forms focal additions, it starts to contract, applying shear stress on the ECM and measuring the stiffness of the material by testing the resistance offered to this force. However, in this instance, the force needed to deform the surface of the ECM will rely not only on the Young's modulus of the hydrogel, but also on the thickness. One can make clearer sense

of this by using an analogy: it is much easier to pinch the surface of a deep bowl of jelly than that of a very shallow one, although the Young's modulus of both is the same. Evans et al. [37] explains that, since there is less jelly in the shallow bowl and because it is prevented from moving at its basal surface, a lateral shear deformation force of a specific scale will exert a much greater strain on the thin jelly than on the thick one. A complete explanation of this concept is illustrated and described in Figure 2.7.

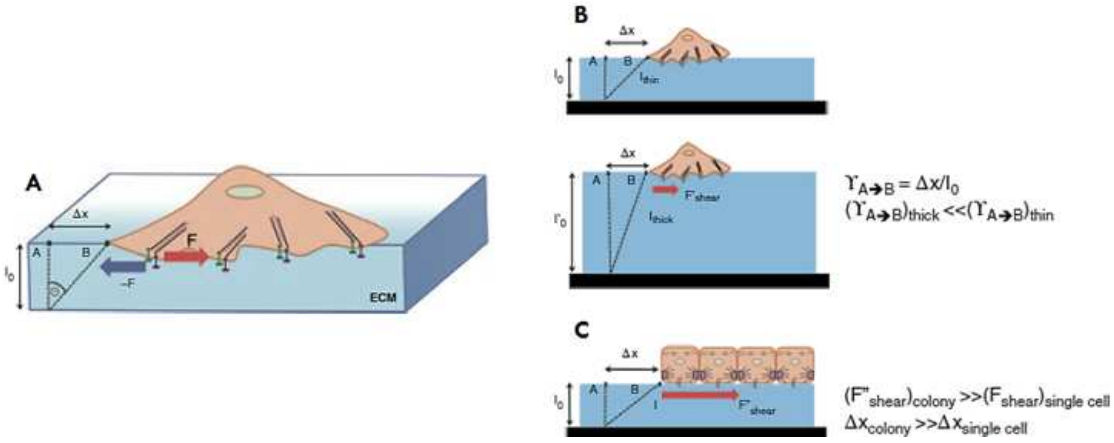

Figure 2. 7 Cellular mechanosensing of substrate thickness. Schematic explanation of Lin et al. [102] model **A** To contract a hydrogel from A to B for a given distance (Δx), a cell needs to make focal adhesions on a solid support, as shown in the image (the integrin connections are represented by the blue and green Ts), and then apply a force (blue arrow). Simultaneously and as a result of this process, a tensile strain is generated inside the cell at the cell cytoskeleton (tilted lines inside the cell represent the actin–myosin generated by the exerted contracting tension). The material must be able to withstand and accommodate to the force that the cell applies, in this scenario a shear force. **B** In a thin hydrogel the required force to deform the surface is higher. The shear stress is measured as the ratio among the transverse displacement of the hydrogel (Δx) and its initial length (l). A thick layer of the same modulus will require a smaller force to be contracted then a thin one. As a result, the tension produced in the cytoskeleton may reach a critical point on thin hydrogels, forcing the cell to spread more; on the other hand, on thick hydrogels, the cell may be unable to generate the same tension, and therefore stays rounded. **C** For colonies of cells, the transverse displacement is supposed to be greater than that for a single cell. This may be explained as a consequence of a collective behaviour mediated by tight intracellular interactions [103].

The influence of matrix stiffness on the behaviour of collective groups of cells.

Up to this point, a general overview on the influence of the ECM mechanical cues on cell behaviour has been described. In addition, the stiffness that the cells sense is determined not only by the hydrogel elastic modulus and but also by the thickness of this hydrogel

when it is firmly attached to a material of much higher stiffness. Most of the studies on mechanotransduction focus on the behaviour of single cells in response to their matrix rigidity. However, in most tissues, cells do not exist in their own but interact closely with neighbouring cells, both mechanically and chemically. In order to keep themselves attached to their ECM; they also must apply tensile force on the ECM to balance the forces they apply on each other. In some cases the forces that aggregates of cells convey to the ECM can become very large and then contraction of the matrix occurs [104]. This phenomenon has been explored by other groups, in which cell colonies stress hydrogels to a larger degree compared to single cells [105, 106]. It has been suggested that the larger lateral displacements that the groups of cells impart on ECMs compared to single cells may allow those forces to travel longer distances into matrices than single cells, sensing stiff materials beneath themselves through thicker softer substrates than single cells [22]. Moreover, most of the existing understanding of directed cell migration has been gathered from single-isolated cells studies. However, fundamental processes during development, tissue repairing, tissue regeneration, and some cancer cell invasion are governed by collective cell migration [82, 107, 108]. Cell-cell interactions within these groups provide cooperative mechanisms of cell guidance that are not appreciated on single cells studies [109].

Microenvironment dynamic mechanical cues, the influence of flow-induced shear stress

Shear forces are defined as unaligned forces applied parallel to the plane of activation, pushing one part of a body in one direction and another part of the body in the opposite direction. The stress is determined as the force per unit area (Eq. 2.2).

$$\sigma = \frac{F}{A}$$ Eq. 2.2

Where

σ Stress
F applied force [N]
A cross-sectional area [m^2]

Shear stress is particularly important for the functionality of blood vessels in which two types of shear stress are experienced. The first is the circumferential stress, consequential to the pulse pressure difference inside the vessel; the second is shear stress, generated from the blood flow [110]. As a result, many studies including shear stress focus on the effect of this mechanical cue on the differentiation, morphology and function of blood vessel cells, especially endothelia cells. However, in the past few years, the importance of those forces in altering cell function and inducing differentiation on other cell lineages is gaining higher popularity [111, 112]. Evidence of mechanically induced stem cell differentiation has been reported using several types of mechanical forces, including shear stress. Research supports that shear stress plays a role in osteogenic differentiation of hMSCs [112, 113]. The mechanosensitive nature of hMSCs allows them to respond to fluid shear stress [114, 115]. hMSCs cultured in 3D-engineered vascular scaffolds subjected to pulsatile flow have been observed to express endothelia markers [116]. Likewise, shear stress stimuli were observed to influence cell morphology and alignment of endothelial cells [117].

Fluid flow-induced shear bioreactors

Bioreactors are devices designed to culture cell-loaded constructs in a controlled and sterile environment [118]. They play a crucial role in the development of functional tissue, allowing the manipulation of the physiological environment of the culture.

Bioreactors provide the constructs or tissues with the suitable mechanical and chemical stimuli to achieve the desired phenotype expression [119, 120]. The mechanical stimuli selected for each application will vary according to those conditions found in the physiological environment of the native tissue [121]. Thus, the types of forces generated will be specific to the tissue to be built or reconstructed, and the bioreactor design.

Perfusion flow systems have demonstrated enhanced cell viability, proliferation, and extracellular matrix production within the whole construct, relative to static controls [122]. Recent research has shown that the limitations associated with traditional static cell culture can be reduced using dynamic cell-culture stimulation systems [123]. Fluid-flow stimulation of hMSCs, for example, has been widely used for fundamental research, and for the expansion and conditioning of cells for tissue engineering and regenerative medicine [77, 117, 118, 124]. Basically, cells subjected to fluid-flow shear stress interprets these mechanical cues as triggers for biochemical responses: the previously described mechanotransduction process [125]. Furthermore, in recent years the elucidation of mechanotransduction pathways is gaining interest in the field of Mechanobiology; for improving functional-tissue engineering, regenerative medicine treatment, and understanding diseases [38, 126-128]. For example, hMSCs will make use of the shear flow provided by the cardiovascular system, or the pressure gradients generated by natural body motion resulting in interstitial fluid-flow, to get to the place of injury. Cells subjected to fluid-flow shear stress interprets these mechanical cues as triggers for biochemical responses: the previously described mechanotransduction process [125]. Fluid-flow applications are good alternatives to take advantage of biomimetic flows to control cell responses *in vitro*. An explanatory sketch of a fluid flow perfusion column bioreactor can be seen in Figure 2.8.

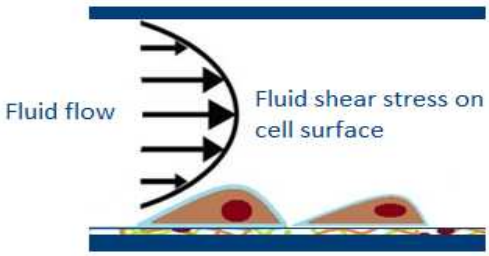

Figure 2. 8 Parallel plate flow cell culture bioreactor sketch. Perfusion column or parallel plate flow bioreactors use continuous fluid flow though sealed culture chambers that contain cell loaded scaffolds on the flow path. This causes the recirculated culture media flowing in the chamber to flow through the surface of the seeded cells [129, 130].

Cell source for mechanotransduction studies

The selection of the appropriate cell line for the study of the mechanisms behind how cells sense the mechanical make-up of their microenvironment will lie in the final biological application they are intended for. Stem cells are commonly used for bone tissue generation because of their higher proliferation rate over other osteo-like cell lines as osteoblasts and osteocytes. Adult stem cells are a favoured option; a class of stem cells that have shown therapeutic potential, despite their limited differentiation capacity compared to embryonic stem cells (ESCs). Various types of adult stem cells exist, including multipotent marrow stromal cells (hMSC). These cells hold a differentiation potential that varies widely, which makes them ideal as cell source for tissue injury/repair studies. In many cases, however, the mechanisms by which these cells regenerate tissues are poorly defined and require further understanding [131].

Mesenchymal Stem Cells

Stem cells from bone marrow are one of the most studied of all adult stem cells. Stromal mesenchymal stem cells such as hMSCs are 'multipotent' stem cells. These cells retain the ability to self-renew and differentiate into diverse lineages (Figure 2.9) [132-134]. hMSCs represent only 0.01% of the total nucleated cell population in the marrow, however they can be expanded *in vitro* to nearly one million times while maintaining their multi-lineage potential [132, 135]. Unlike other stem cell types, hMSCs do not express major histocompatibility antigens, which are responsible for immune reactions

[136]; they do not hold the possibility of malignant transformation [137] and also lack ethical issues which can restrict use [138] making them a suitable cell source candidate for a wide range of biomedical applications in tissue engineering.

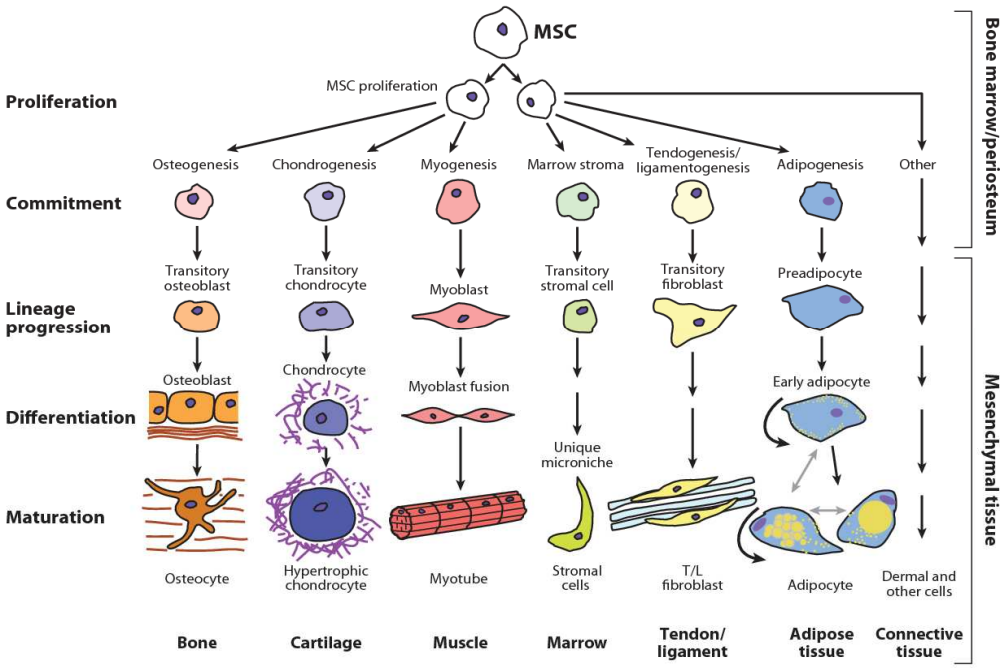

Figure 2. 9 The mesengenic process. Human mesenchymal stem cells (hMSCs) from bone marrow can progress to different linages, among which are bone, muscle, or adipose tissue, depending on their context and the stimuli to which they are subjected. Reproduced from Reference [139]

Since their initial description, mesenchymal stem cells (MSCs) have been shown to hold the ability to differentiate into several mesenchyme-derived tissues [140], including cellular phenotypes representative of the musculoskeletal tissues such as cartilage, bone, muscle, ligament and tendon, as well as adipose tissue and hematopoietic-supporting marrow stroma [134, 135, 141]. Additionally to these mesenchymal lineages, hMSCs can also differentiate into other tissue types, including hepatocytes, fibroblast and neural tissues [142-144].

It has been reported that hMSCs are highly responsive to the mechanical profile of their microenvironment. For example, Engler et al. [64] cultured MSCs on matrices of different stiffness. They reported that, on soft matrices matching the stiffness of the brain range (1-4 KPa), MSCs became neuronal-like, whereas raising the stiffness of those matrices to a harder muscle-like range caused the cells to switch to a myogenic cell fate. The group also reported that even harder substrates matching the collagenous bone led to osteoblast formation. Lin et al. [27] reported that, on hydrogels with stiffness gradients in the range of 1–20 KPa, MSCs showed higher migration speed on hard sections compared to those in the softer sections of the matrix. In addition, MSCs on the harder end decreased their nuclear stiffness and reduced the expression of Lamin A/C, which plays a main role in the regulation of nuclear stiffness. Biosynthetically active precursors and multi-potent cells are continued even in older individuals, another reason why MSCs are being used for tissue engineering of autologous implants without specific ethical issues [145]. Figure 2.10 shows a graphical representation of the human stem cell's microenvironment and the factors that regulate its behaviour.

Due to their ability to exit from the stem cell niche, travel among tissues, and re-home themselves to an injury site, Mesenchymal stem cells (MSCs) are highly migratory and differentiate in response to mechanical stimuli [146]. However, this characteristic makes their behaviour more complex and difficult to predict. While biochemical signals are commonly implicated and studied as migration cues, it has been hypothesised that mechanical cues of the ECM, such as stiffness gradients, may serve as an additional guide to MSC migration, ensuring the right cells arrive in the right location then immediately start to differentiate as part of the healing process [65, 92, 147, 148].

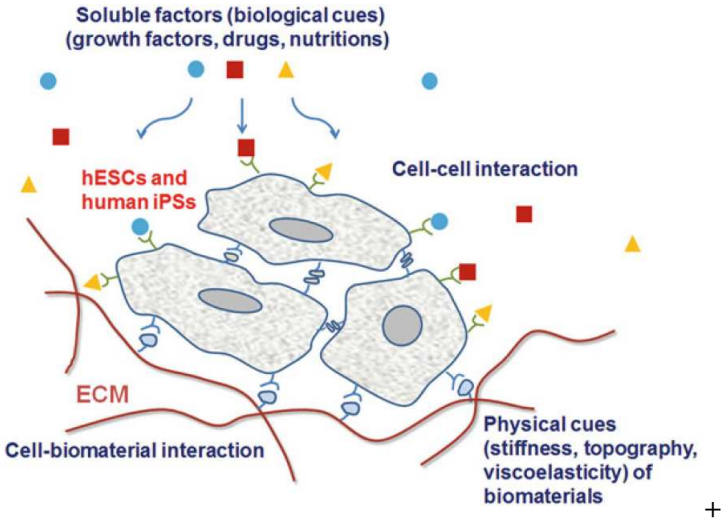

Figure 2. 10 Graphical representation of the human stem cells microenvironment and the factors that regulate it. A. Physical factors, such as matrix stiffness, topography and viscoelasticity B. Interactions among cells and biologically active molecules e.g. interactions cell-biomaterial C. Cell-cell interactions D. Soluble factors such as growth factors, adapted from [149].

MSCs are known to undergo durotactic rehoming; it has been reported that MSCs undergoing directed migration even in response to shallow, physiological (>~10 Pa/μm) stiffness gradients [34]. The process of durotaxis has shown to encourage MSC differentiation [45, 93, 150], making the understanding of this phenomenon relevant to therapeutic application of MSC. Given the existence of stiffness variation between and within tissues, it remains to be seen whether MSC homing is driven by the stiffness range or gradient (Pa/μm) [76].

Materials used in mechanotransduction studies

One of the most important aspects in evaluating cell response to the mechanical properties of its matrix is perhaps deciding the material the matrix should be made of. It is important to keep in mind the matrix will be an *in vitro* model of the ECM. Would a natural biopolymer that better resembles the complex composition and structure of the ECM be better? Or perhaps a well-controlled easy-to-replicate synthetic hydrogel?

Before describing the characteristics of both natural and synthetic biomaterials, physical aspects relevant to such work need to be delineated. A material is elastic if it deforms on application of a force and then, once the force is removed, the material returns to its initial shape. In contrast, an inelastic material is characterised by nonlinear deformations on application of a force, with slow recovery and permanent changes once the force is removed [43]. An elastic body or material is linear elastic if the force needed to extend or compress it by some distance is proportional to that distance [151]. The mechanical response of these homogeneous isotropic linearly elastic materials is easy to characterise by simple experiments. In contrast, biological materials that better mimic the complex fibrillar structure of the native ECM show large strain-hardening deformations, therefore the elasticity is inherently nonlinear. These tissue samples are anisotropic, meaning they have different properties in different directions [152, 153]. For instance, muscle fibres, bone and ligament are stiffer in the longitudinal direction as compared to the cross-sectional direction [151]. They also show viscoelastic behaviour; this means that they are elastic as, after a strain due to the application of a stress, they are capable of recovery, but they are also viscous because of their capability to creep after the strain [154].

Hydrogels

The study of cell-material interactions in hydrogels can provide information on cell behaviour that mimics cellular interactions with the ECM. They are perhaps the best-established elastic substrates for the development of soft tissue and cell-matrix interactions, making them suitable candidates for cell mechanobiology studies [155]. These elastic materials have structural similarity to the macromolecular-based highly-hydrated components in the body [156]. They support the application of contractile

forces, which allows anchorage-dependent cells to probe the physical properties of their microenvironment; they show mechanical strength, flexibility and structural integrity sufficient to withstand cell applied shear forces without permanent deformation or failure for a period of time [157]. Compliant substrates such as these highly-hydrated matrices deform as a result of contractile forces generated by adherent cells and, in turn, the mechanical response of this substrates profoundly influences numerous cellular functions [158]. Hydrogels, when used in mechanobiology studies, are prepared by a variety of methods; they are mechanically tuneable and use a diverse range of polymeric materials, mostly divided into two categories according to their origin: synthetic or natural.

Mechanical properties of hydrogel

In addition, the success of cell-compatible hydrogels is usually fixed to a set of appropriate mechanical properties. For example, tissue formation can rely on the mechanical properties of the hydrogel construct (e.g. matrix stiffness matching that of the desired tissue) [32, 159]. By now, it is well accepted that cell function is partly affected by the mechanical properties of the hydrogel substrate manipulating cell responses, such as cell migration, proliferation, and differentiation; for example, Discher et al. [1-3, 147] demonstrated in repeated occasions that stem cell fate can be manipulated by altering hydrogel matrix stiffness to match that of the desire tissue. Hydrogel degradation rate is critical in mechanotransduction studies; a well-designed degradable hydrogel will provide the mechanical integrity for proliferating and maturing cells and allow infiltration of blood vessels [160, 161]. A proper balance between degradability and mechanical properties, such as compliancy and matrix integrity, is critical to guarantee a suitable functionality of the hydrogel and cultured cells within the desired timespan [162]. The permeability of the hydrogel is also

associated with the mechanical properties of the hydrogel and its swelling behaviour, while variation in the permeability is a widely employed strategy for controlling nutrient diffusion, matrix integrity and load release [163-165].

Tuneable mechanical properties of the hydrogel are critical in mechanobiology studies and they are the result of the composition and structure of the hydrogel [166, 167]. Hydrogels are custom-made materials which can be mechanically optimised by tuning parameters such as cross-linking degree. For example, Sood et al. [167] demonstrated that a higher degree of cross-linking results in a strong, but brittle hydrogel with a reduction of the percentage of its elongation. The swelling degree, co-monomer composition, polymerization conditions, and cross-linking density have been shown to be the most important parameters influencing the mechanical properties of hydrogels [168-173]. Mechanical properties of hydrogels are also influenced by structural design or architectural parameters, such as porosity, pore size and pore shape [174, 175]. The effect of pore size was studied by Yamane et al. [175] and they observed a higher compression modulus for hydrogels with the smallest pore sizes (100 ml) than for the hydrogels with pore sizes in the range of 200 to 400 ml. Engler, Discher et al. [64] demonstrated the prominent role of matrix mechanical properties in guiding hMSC fate by studying cells attached to PAAm hydrogels of different stiffness. hMSCs were observed to commit to lineages based on the matrix stiffness; soft PAAm hydrogels (<1 KPa) promote neurogenesis, while intermediate stiffness hydrogels (~10 KPa) promote myogenesis and stiff hydrogels (>30 KPa) osteogenesis [29]. Therefore, a hydrogel designed for biomedical applications will permit control of biochemical as well as biophysical signals in the cell microenvironment.

Synthetic-based hydrogels

Synthetic-based hydrogels are a reliable option for mechanobiology studies, mostly due to their reproducibility and easy to control mechanical properties. Polyacrylamide (PAAm) hydrogels are maybe the most widely used synthetic substrates in the study of cell response to the mechanical properties of its matrix, and have also been used extensively for other cell-matrix interactions studies [29, 33, 176-178]. When used in mechanobiology studies, often substrate stiffness is controlled by adjusting the polymer concentration and cross-link density to match the stiffness of a diverse range of animal tissues, which have a broad range of elastic moduli (from just a few KPas in brain [1-4KPa] to the GPa scale for bone [1-10GPa]) [179, 180]. These hydrogels have been seen to have linear elasticity, therefore they are able to recover their original shape when an applied force is removed [178]. This is an important property, which allows accurate quantification of applied forces by simply measuring the deformations created in the hydrogel [181]. However, this characteristic differs from the non-linear elastic behaviour of the ECM in biological tissue, making the comparison with what cells experience *in vivo* difficult to determine [150, 153, 182]. It also has been suggested that contractile cells on this synthetic linearly elastic hydrogel may exert less force at early stages of focal adhesion formation, compared to the non-linear elastic ECM, and they respond likewise on other linear elastic substrates with the same elastic modulus [43]. Despite the fact that PAAm hydrogels are widely used in cell-material interaction, including mechanobiology studies, hydrogels with fine control of stiffness undergo significant swelling when exposed to aqueous solutions [183]. Swelling in hydrogels also may cause inconsistencies of hydrogel density throughout the hydrogel [13] and these variations in density across the thickness and width of the hydrogel may give rise to a

stiffness gradient through the hydrogel which, in turn, could significantly influence cellular responses [94, 129]. Furthermore, cells can't easily adhere to these polymers, therefore their surface needs to be functionalized with extracellular proteins before being used for cell culture [22, 29, 97].

Natural fibrillar biopolymers

While synthetic polymers display linear elastic behaviours in response to the forces applied by contractile cells, naturally-occurring biopolymers exhibit non-linear, viscoelastic behaviour [153]. This non-linear elastic behaviour refers to the increase of elastic response under stress or strain, which is characterised by a strain-stiffening response [37]. Natural biopolymers are even harder to characterize, with unusual mechanical properties (especially extracellular matrix proteins like collagen hydrogels), and they have provided novel insights into cell contractility and the mechanosensation field [152]. These naturally occurring biopolymers form entangled fibrillar, porous networks with heterogeneous structures (Figure 2.11 B C D), along with their derivative gelatin; while synthetic hydrogels such as PAAm exhibit much more homogeneous highly-ordered structures (see Figure 2.11A for full comparison) [152, 184-186].

Gelatin (Figure 2.11 D), as well as its precursor, exhibits non-linear elastic behaviour after application of forces, and may undergo strain-stiffening and irreversible fibre compaction. Its simpler structures, however, make it easier to characterise and therefore makes it a good alternative for mechanobiology studies [150, 153, 182].

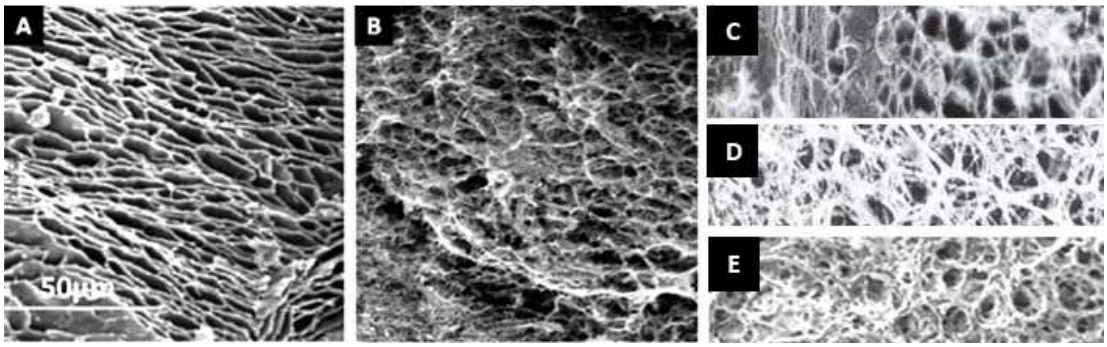

Figure 2.11. SEM of synthetic and natural fibrillar hydrogels. A Pure PAAm in an isotropic state reproduced from [187]. Fibrillar biopolymers B The fibrous entangled chitosan-gelatin hydrogel cross-linked with Proanthocyanidin used in this study. **C** Fibrillar collagen I [184]. **D** Pure gelatin 2% set hydrogel prepare under the same technique used in this study, where the fine and dense entangled network of thin filaments can be appreciated[184]. **E** Pure chitosan which in the gel state form the disorganized nano-fibril structures shown in the image[188].

Collagen networks (Figure 2.11C) have been widely used in mechanobiology studies. They exhibit anisotropic non-linear strain-dependent elastic behaviour that is a reversible property, and which is not associated with irreversible network deformation [189]. It has been observed that the mechanical properties of these collagen-based hydrogels are determined by physical entanglement of the fibres. Some of these mechanical properties manifest as complex behaviours such as strain-stiffening and negative normal stress [186, 190, 191].

Cells have shown to be able to sense stiff materials through the soft fibrillar hydrogels at longer-distances than on synthetic hydrogels. This was observed by Leong et al. [192], who reported that hMSCs were able to sense stiff glass through thick soft collagen hydrogels and change their morphology accordingly in the range of 130-µm to 1440-µm-thick, compared to the few microns previously reported on PAAm hydrogels (up to10-µm thick).

Chitosan-gelatin hydrogel (ChG) for mechanobiology studies

Strain-stiffening has lately emerged as a broad response of biological tissues to mechanical stimulation as well as a prevailing regulator of cell behaviour and fate [193]. While deforming, protein-based hydrogels composed of collagen, fibrin, actin and neurofilaments, as well as their derivatives, exhibit the nonlinear elasticity of the ECM [153]. Polysaccharide hydrogels can exhibit strain-stiffening behaviours in the same way [193]. Therefore, a composite formed from diverse natural biopolymers can be an option to explore since it will offer wider opportunity for customization while still closely mimic the mechanical properties of the ECM. Gelatin – a derivative of the fibrillar collagen I – can be degraded naturally via the use of the enzyme collagenase, allowing for local degradation controlled by the cells present in the engineered tissue themselves [194]. Gelatin protein shows a fibrillar composition, with a simpler single coil structure in the gel form than collagen I (Figure 2.11 D) [184]. It is able to form thermally-reversible hydrogels, formed by breaking the natural triple-helix structure of collagen (typically collagen I) into single-strand coil, like individual fibres, by thermal degradation [195]. In the solution state, the gelatin molecules will adopt a disordered conformation, but on cooling to approximately 25°C, they undergo a thermally reversible coil-helix transition, and the molecules partially reorganise into the collagen triple helical structure [184, 196]. The stiff helical coils will then self-associate to form a three-dimensional hydrogel structure. With a much simpler structure than the one of its precursor [197], gelatin retains informational signals such as the Arg–Gly–Asp (RGD) sequence, which promotes cell adhesion, migration, differentiation and proliferation [198]. The basic chemical structure of gelatin can be observed in Figure 2.12.

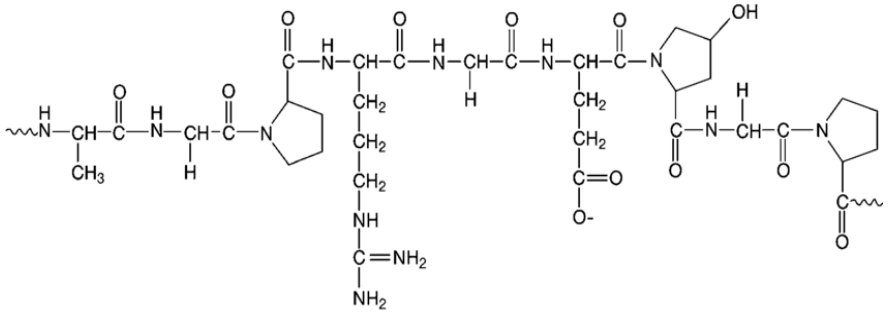

Figure 2.12. Basic chemical structure of gelatin. Structurally, gelatin contains repeating sequences of glycine, proline, and hydroxyproline, reproduced from [199].

the use of gelatin-based hydrogels is often restricted, however, because of concerns regarding potential immunogenic reactions and limited tunability of degradation kinetics, relatively poor mechanical properties, and batch-to-batch consistency, similar to its precursor, collagen [200]. A number of chemical modification methods have been investigated to improve the mechanical properties of these hydrogels [201, 202]. For instance, it has successfully been coupled to glycosaminoglycans such as hyaluronic acid and Chitosan in hydrogel scaffolds *in vitro*, where the protein is used to support cellular adhesion without losing the benefits of the GAG'S mechanical strength [203-206].

Chitosan is a highly surface-charged rigid bio-nano fibril glycosaminoglycan, which also exhibits strain hardening mechanical properties at physiological pH (Figure 2.11E), and is the deacetylated derivative of chitin [188, 193]. It is a polycationic polysaccharide composed of randomly distributed β-(1-4)-linked D-glucosamine, and usually less than 40% of N-acetyl-D-glucosamine residues (Figure 2.13). Chitosan has found many biomedical applications, including tissue-engineering applications, due to its excellent biocompatibility, low toxicity, structural similarity to natural GAGs of the ECM [207], and degradation by various mechanisms, including surface erosion, enzymatic degradation through chitosanase and lysozyme, and dissolution [207]. The mechanical properties of chitosan can be easily modified by regulating the degree of deacetylation of the

polymer [208], and also using the primary amino groups on the molecule, which are reactive and provide a mechanism for side group attachment using a variety of mild reaction conditions, amongst others [209]. This modification will disrupt the characteristic crystal structure of the material, and increase the amorphous fraction to fabricate a material with lower stiffness and higher elongation ability [210]. The precise nature of changes in chemical and biological properties, however, will depend on the nature of the side group added to it.

The degradation kinetics can be tuned by the deacetylation degree of the chitosan and using the appropriate cross-linking chemistries and density. The inherent properties of chitosan, such as excellent cytocompatibility, biodegradation, minimal foreign body response, and antimicrobial properties make chitosan-based hydrogels attractive candidates for tissue engineering applications. Additionally, the large number of accessible hydroxyl and amine groups in chitosan provide numerous possibilities to create hydrogels via chemical cross-linking [211]. These functional groups can react with many bi-functional small molecule cross-linkers, such as glutaraldehyde, polyphenols, formaldehyde, genepin, diethyl squarate and diacrylate, to form chemically cross-linked hydrogels [212].

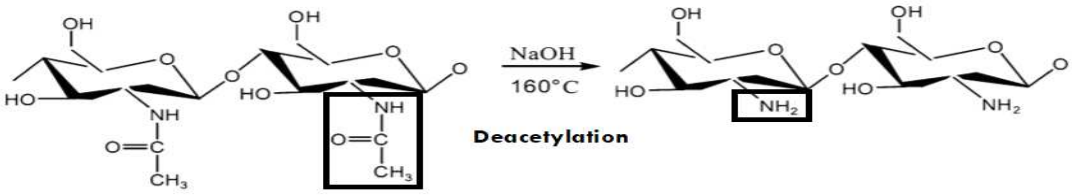

Figure 2. 13 Synthesis of hydrogels by chemical cross-linking. A Synthesis of hydrogels by polymerization of monomers and cross-linking agent; **B** Synthesis of hydrogels by cross-linking of pre-polymerized water-soluble polymers. Reproduced from [213].

Chitosan-gelatin (ChG) blends have been used in a wide range of biomedical applications [214-216]. When they are mixed together, gelatin and chitosan form

polyelectrolytic complexes in different gelated states based on the polymer concentrations and polymer ratios, as well as the ionic strength and the pH of the mixing solution [206, 217-219]. Chitosan-gelatin blends were a feasible option for this research. However, despite all of the above-mentioned advantages, chitosan-gelatin blends suffer from an important limitation relevant to the research carried out in this project: they exhibit weak mechanical stability, showing considerable room for improvement [197, 220-222].

Synthesis of the ChG hydrogels cross-linked with Proanthocyanidin

Hydrogels are 3D networks prepared by swelling hydrophilic polymer chains networks in an initiator aqueous solution such as water or alcohols, using various polymerization techniques such as bulk, solution and suspension, and by physical and chemical cross-linking routes [223, 224]. The cross-linked network contains either chemical or physical cross-links. As described by Hoffman et al. [217], when a polyelectrolyte is combined with a multivalent ion of the opposite charge, it may form a physical hydrogel known as an ionotropic hydrogel. When these polyelectrolytes of opposite charges are mixed, they may gel or precipitate depending on their concentrations, the ionic strength, and pH of the solution. The products of such ion-cross-linked systems are known as polyion complexes, or polyelectrolyte complexes [217]. All of these interactions are reversible, and can be disrupted by changes in physical conditions such as ionic strength, pH, temperature, application of stress, or addition of specific solutes that compete with the polymeric ligand for the affinity site – in this case, on the protein [225]. In this study, the interaction between the polymers (chitosan-gelatin) is an example of this kind of hydrogel; chitosan is cationic polymer and gelatin is amphipathic polymer showing anionic property in acidic solution. When mixed together, they gelled in accordance with their concentrations, the ionic strength and pH of the solution forming the chitosan-gelatin

(bio)polyelectrolyte complexes in an acidic medium, as previously reported by Voron'ko et al. [226]. Figure2.14 shows the formation of ionic hydrogels using as example the blend used in this study.

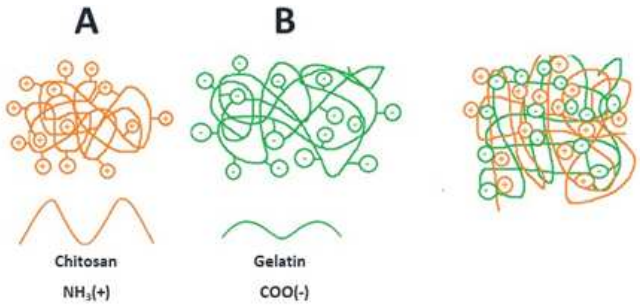

Figure 2. 14 The development of ionic physical hydrogels. The ChG blends form polyionic hydrogel complexes with **A** chitosan positive amide group (NH_3+) and **B** gelatin carboxylate ion functional group (COO-) mixed in acidic solution. **C** chitosan-gelatin ionic hydrogel adapted from [226].

Chemically cross-linked hydrogels

Chemically cross-linked hydrogels are popular options, mainly due to their good mechanical properties. These hydrogels contain covalent bonds which can be introduced by the following cross-linking techniques [227]: physical, chemical, photochemical grafting, high energy irradiation, and using enzymes. The chemical method is the most used. A schematic representation of hydrogel chemical cross-linking can be observed in Figure 2.15. To control mechanical properties, degradation and clearance rate, cross-linking of naturally derived materials has been explored using chemical reagents, including divinyl sulphone, epichlorhydrin and phosphoryl chloride [228]. However, all of these reactions produce hydrogels with low densities of cross-linking, while very high water content makes them very low in mechanical strength and readily biodegradable [228].

For example, in a previous study, researchers lowered the water content of hyaluronic acid hydrogels by cross-linking using water-soluble carbodiimides, and found this yielded

hyaluronic acid hydrogels with very low water content, but with high biodegradation rates [229].

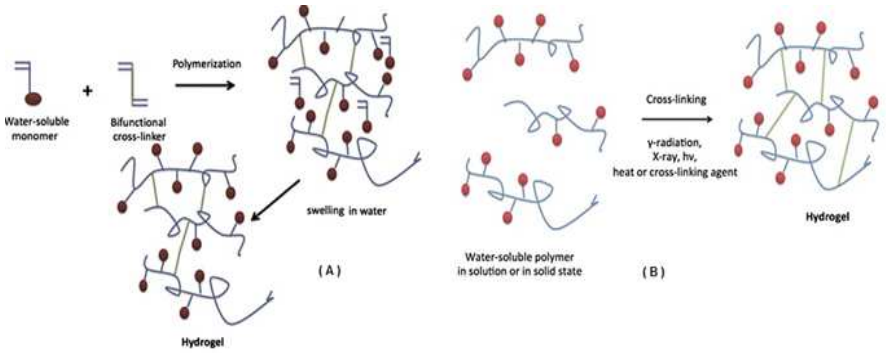

Figure 2. 15 Synthesis of hydrogels by chemical cross-linking. A Synthesis of hydrogels by polymerization of monomers and cross-linking agent; **B** Synthesis of hydrogels by cross-linking of pre-polymerized water-soluble polymers. Reproduced from [213].

Cross-linking agents such as glutaraldehyde, glyoxal, formaldehyde and other chemical cross-linking agents, are frequently added to hydrogel blends to improve mechanical properties and lower water content [230, 231]. However, these agents have shown to be cytotoxic and could cause undesirable side effects if implanted *in vivo* [230, 232]. Thus, research groups seek to replace these agents with safer or non-toxic cross-linking agents.

Plant based Proanthocyanidin (PA) compounds have shown to fulfil the requirements of a desirable cross-linker reagent [233]. They are naturally occurring plant metabolites widely available in fruit and vegetables, part of the category known as condensed tannins, which consist of highly hydroxylated structures capable of forming insoluble complexes with carbohydrates and proteins [234, 235]. PAs were found to increase collagen synthesis and accelerate the conversion of soluble collagen to insoluble collagen during development [236, 237]. Furthermore cytotoxicity, cross-linking rate and biocompatibility of PAs as collagen tissue fixative is much more favourable than

other reagents, as those blends use glutaraldehyde (GA) as a cross-linker [233]. The PA chemical structure can be observed in Figure 2.16.

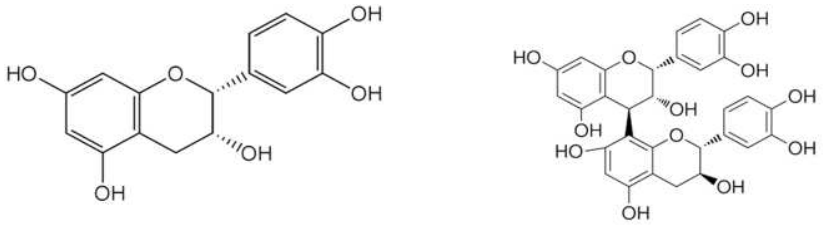

(A) (B)

Figure 2. 16 Chemical structure of Proanthocyanidins. A Individual monomer units of Proanthocyanidin; **B** Proanthocyanidin. Adapted from [238].

This study uses a chitosan-gelatin blend that has proved to be effective for tissue engineering [99, 219, 239, 240]. However, the instability of these formulations in the aqueous state, and particularly their mechanical weakness has limited their use and applications. This characteristic, however, can be improved by introducing chemical cross-linkers (glutaraldehyde, poly(ethylene glycol)s, carbodiimide and polyphenols) [194, 206, 241, 242]. Some studies have demonstrated that PA can cross-link chitosan-gelatin as a mixture, as well as individually, to produce more stable, less swellable and biocompatible hydrogels with tuneable mechanical properties, [206] forming chemical (also called permanent) hydrogels, which are covalently-crosslinked networks [243]. These hydrogels, according to Wichterle et.al. [243] can be fabricated by cross-linking of water-soluble polymers, or by the conversion of hydrophobic to hydrophilic polymers, plus cross-linking to form a network (Figure 2.17).

In this study, PA was used to crosslink the ChG physical hydrogel, resulting in a chemical hydrogel in low temperature (25˚C) (Figure 2.11B). According to Kim et al. [206] these hydrogels usually contain regions of low water swelling and high cross-link density. Based on their findings, keeping the deacetylation% of chitosan and polymer ratio

constant while varying the cross-linker (PA) concentration, provides a feasible method to modulate the hydrogel mechanical properties.

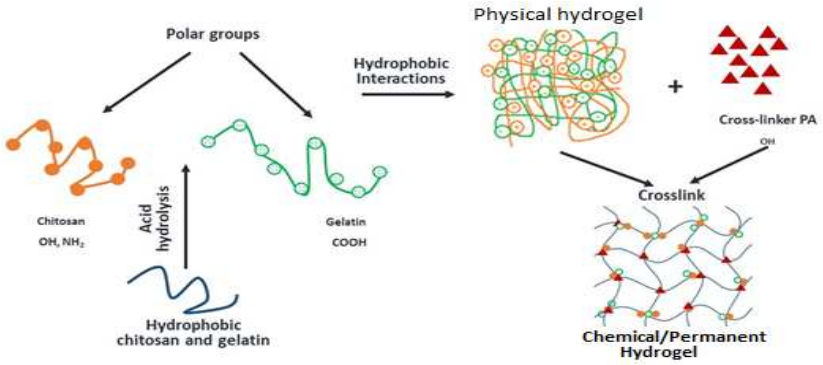

Figure 2. 17 Schematic representation of methods for the development of hydrogels by chemical modification of hydrophobic polymers. Examples of these types of hydrogels include (a) the partial hydrolysis of the acetate, ammonia and carboxyl groups to –OH $–NH_2$ and COOH groups in conversion of the insoluble chitosan and the thermal sensitive gelatin. Resulting hydrogel may be subsequently covalently cross-linked.

According to Kim et al. [206], the COOH groups of the gelatin – in these chitosan-gelatin hydrogels cross-linked with PA – react with the amino groups of chitosan resulting in amide linkages, while OH groups of both chitosan and PA react with COOH groups of the gelatin, resulting in ester linkages in a temperature-dependent reaction. If the temperature of gelatin and chitosan solution falls too low before adding the cross-linker PA, the gelatin precipitates out of solution with the chitosan, and the PA cannot react with the COOH groups of gelatin; the OH groups of chitosan have interacted with COOH groups of gelatin.

Regenerative medicine therapies and the role of cell mechanotransduction

Regenerative medicine is a growing biomedical research area which aims to repair injured body parts and restore their functions by using laboratory-grown tissues, materials and artificial implants [244]. Recent developments on this field focus on

strategies that better emulate the complexity of the native ECM that can respond in a more physiological manner to their local environment and cues [126, 245].

Stem cell stiffness-induced differentiation is one of a relevant biological response link to tissue regeneration and closely related to cell mechanosensing. Mechanical cues have proved to be dominant players in cell functionality; it has become clear that cell differentiation can be directed by mechanical cues, i.e. osteogenic differentiation of hMSCs in response to matrix stiffness has been well documented [97, 114, 246]. Rao et al. [247] demonstrated that vessel network formation could be enhanced by coculture of hMSCs and endothelial cells, while decreasing matrix stiffness to a range of 80-300 Pa. Furthermore Wingate et al. [248] showed that soft substrates (2KPa) with addition of vascular endothelial growth factor (VEGF) synergistically guided hMSC differentiation into endothelial cells.

Another aspect of relevance to these applications is the known link between changes in ECM stiffness and disease. Cells rely on cues from their physical surroundings-substrate elasticity or stiffness, physical shape and shear forces to direct their fate and function [10, 57, 105, 249]. Therefore, the elucidation of the pathways that allow cells to recognise the mechanical profile of their surroundings can lead to more effective therapies to address cell-biomechanical environment related diseases in a more systemic way. For example, drugs that alter the balance between physical parameters, such as rigid (e.g. bone) or elastic (e.g. arteriolar, dermal connective tissue), already exist and are in clinical use for conditions such as osteoporosis and metastatic bone disease [250]. Furthermore, some mechanisms behind cancer progression and spreading may be explained by cells mechanosensing ability. Recent findings have demonstrated that an increase of matrix stiffness (from <1 KPa to 2 and 4 KPa) is sufficient for activation of myofibroblast-like cells. Upon activation, cells were found to mechanically sense the

increased rigidity of the environment as they produce excess collagen [251]. Lachowski et al. [252, 253] has demonstrated that durotaxis is strongly involved on these myofibroblast-like cell tumour growth. They developed stiffness gradients and showed pancreatic stellate cells (PSCs) migrate from adjacent soft tissue (1KPa) towards the stiff tumour microenvironment (25KPa) and, as rigidity increases, distant PSCs become durotactic activated and recruited towards the stiff tissue, further enhancing the positive feedback loop.

Biomaterials play a pivotal role in the development of tissue engineering therapies, therefore a deeper more integrated understanding of the mechanisms regulating cell mechanosensory capabilities can aid, in the development of more sophisticated biomaterials, with the ability to spatially alter the environment of the cell *in vitro*. The development of dynamic surfaces is an exciting step towards creating multifactorial environments that better mimic the changing complexity of the *in vivo* extracellular environment. By combining techniques used in engineering and biology, this thesis presents a viable method to alter substrate stiffness through changes in gel thickness and constraint boundaries that can be used to match the mechanical profile of a variety of different living tissues. This can therefore provide useful information on creating and characterising biomaterials suitable for tissue repair, organ replacement and pathology treatment; materials that better mimic the mechanical and biophysical properties of those of the tissue they aim to replace or restore.

CHAPTER

3

Materials and Methods

3.Materials and Methods

Introduction

This section is dedicated to discussing the experimental techniques, materials and methods employed throughout the entire project. The chapter begins in section 3.2, outlining the protocols for the fabrication of the different constructs used through the research project. Section 3.3 details the characterization methods used to evaluate the properties of the diverse constructs. Section 3.4 introduces supportive culture conditions for the growth and maintenance of mammalian cells, and the subsequent analyses and quantifications. Section 3.5 describes the biological methods used to assess cell response as function of diverse mechanical cues for NIH 3T3 fibroblast, MG63 osteoblast-like cells, and Mesenchymal stem cells. Section 3.6 describes the use of assays ELISA to quantify cell differentiation. Section 3.7 centres on 2D culture in a perfusion bioreactor. The statistical analysis applied is summarized in section 3.8.

Hydrogel fabrication

PA 95% was purchased from UKmushroomsupplies; crab shell-derived chitosan was a gift from Dr George Roberts (Aerus Tech LTD, DSA 85%), cell culture media and reagents from Gibco Invitrogen (UK), all remaining materials and suspensions were purchased from Sigma Aldrich (UK).

Heavy metal ions purification from chitosan powder

The water insoluble chitosan precipitate and the water-soluble material are then separated, resulting in a purified chitosan material. A chitosan solution was produced by dissolving 250g of chitosan powder in1.5 litres of distilled H_2O. Glass wool was added to a filter column (to work as a filter), before the chitosan solution was poured into the column. Then, the column was topped-up with 1 M sulphuric acid and liquid was allowed

to flow through the column at 1 drop/ second. Next, the chitosan was treated with aqueous ammonia. After all liquid had passed through the column, the chitosan was collected and washed exhaustively with distilled H_2O, to remove any traces of sulphuric acid or ammonia (measuring pH repeatedly until reaching 7). Finally, the chitosan was dried and grounded to a powder.

Chitosan-gelatin hydrogel (ChG) cross-linked with Proanthocyanidin (PA) fabrication.

The cross-linked chitosan-gelatin (ChG_PA%) hydrogel was prepared as illustrated on Figure 3.1. 1:1 3% (wt/v) ChG solution cross-linked with PA were prepared as described, 1.5g of gelatin (from porcine skin) was magnetically stirred in 60ml of distilled water at 50°C until fully dissolved, temperature was then decreased to 37°C, once the solution cooled down 600µL of acetic acid was added (to reach a pH of ~4.7), followed by 1.5g of chitosan, to incite the polyelectrolyte complex formation with the negatively-charged gelatin and the positively-charged chitosan, and the solution was left to homogenize for 2 hours. 60ml of phosphate buffered saline (PBS) was slowly added alongside 5ml of HEPES buffer to rise the mixture just over pH 5. Solution was then divided into equal parts according and 0.5 to 5.0% (w/w) of PA powder dissolved in sterilised distilled water (SDW) then added to each of the previously divided parts. Hydrogels were then left stirring over night at 37°C for the PA chemical cross-linker to fully react, showing a change in colour from pink to purple. Sodium hydroxide (1M NaOH) was added drop-wise manner, to initiate the pH dependant cross-linking until a ~pH of 6.5 was reached the mixture was left to blend for another hour. Then the solutions were placed in the ultrasonic bath machine for 15 min to remove entrapped air bubbles see Figure 3.1 for further detail. ChG hydrogel at different PA concentrations were poured at different quantities into either glass petri dishes and air dried over

night to obtain membranes which were carefully peeled off from the bottom. The thickness of dry hydrogels ranged between 0.2 and 0.8mm or cast at controlled thickness of 200µm on well plates of different sizes. Well plates were then stored at 4°C until used.

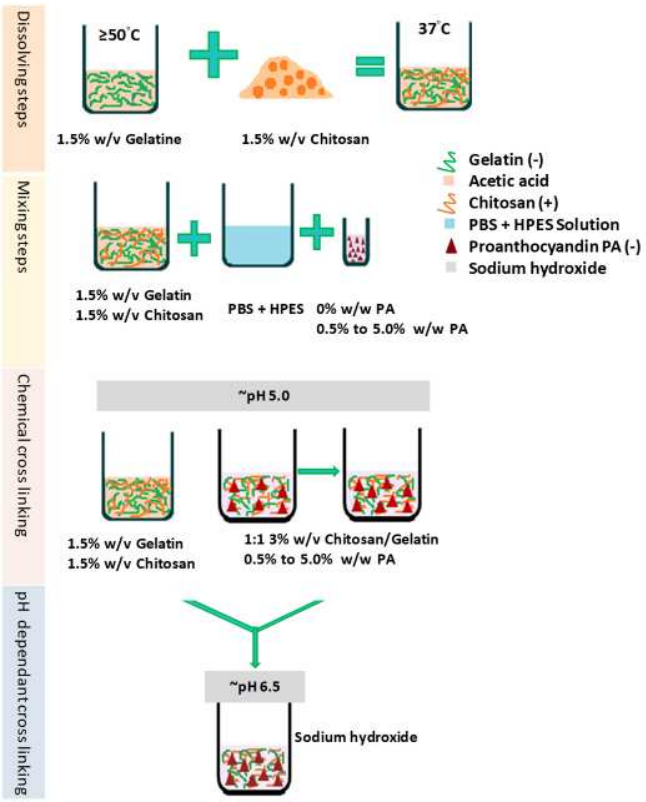

Figure 3. 1 Preparation and cross-linking of ChG hydrogel at different PA concentrations. Adapted from [222].

Variations in apparent stiffness experiment sample fabrication.

Substrates of varied apparent stiffness were built by varying the height of the superficial compliant ChG_PA hydrogel. A ChG hydrogel of 2.5% PA concentration and known young's modules (0.11MPa) was used for these studies. Two different sample geometries using this principle were built. Flat round samples of equal diameter and different uniform thickness (from 0.2mm to 6.0mm) and wedge-shaped samples with different steepness (θ8°, θ12°) and thickness.

For the flat geometry samples hydrogels (Figure 3.2) were cast, by varying the amount of hydrogel pipetted to each well according to the desired thickness (Eq3.1). Well plates were then stored at 4°C for the hydrogel to set, until needed (Figure 3.2).

$$V = \pi r^2 h \qquad \text{Eq3.1}$$

For gradient samples, a tilted food grade stainless steel stand with variable inclination was customized to facilitate the casting of a wedge shaped-like sample (Figure 3.3), with one right angle and two other unequal angles, one of each being controlled by the tiled stand itself. The amount of hydrogel needed to achieve a planar surface with a 180° leaning angle on sample top (to avoid the effect of gravity on cell response later the cell culture stage) was calculated using the equations 3.2 and 3.3 below.

$$V = \frac{\pi r^2 h}{2} \qquad \text{Eq3.2}$$

$$h = \frac{\tan\theta}{wp\emptyset} \qquad \text{Eq3.3}$$

Cast hydrogels were washed with distilled water, then neutralized as described in upcoming section and rinsed with PBS. Prepared Hydrogels were sterilized by UV radiation for 24hrs prior to use; hydrogels were protein conditioned in fresh media. ChG_PA hydrogel cast at different thicknesses is illustrated on Figure 3.2.

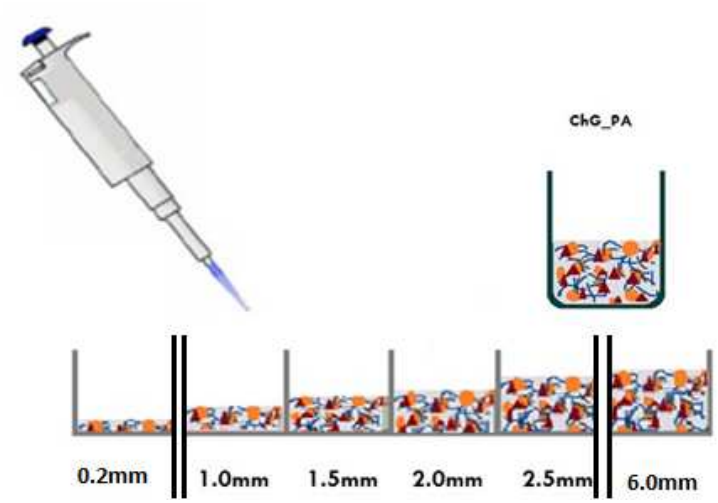

Figure 3. 2 **Casting of ChG_PA** 2.5% hydrogel at different thicknesses.

Hydrogel surface alkali treatment

For the alkaline treated sample, after overnight gelation, hydrogels cast in petri dishes were washed with distilled water then neutralized by pouring (10% v/v) diluted 1M NaOH on top of samples for 2h, to neutralize residual acetic acid, then the solution was removed and further washed with sterile distilled water to pH7.0 (SDW).

Hydrogel sterilisation.

Hydrogel samples were covered with 70% industrial methylated spirit (IMS) for 30 min then hydrogels were washed 2X5 with distilled water and placed under UV light for 24hrs and turned upside down for the last 2 hours of treatment, and then covered with PBS and either used directly or refrigerated until usage.

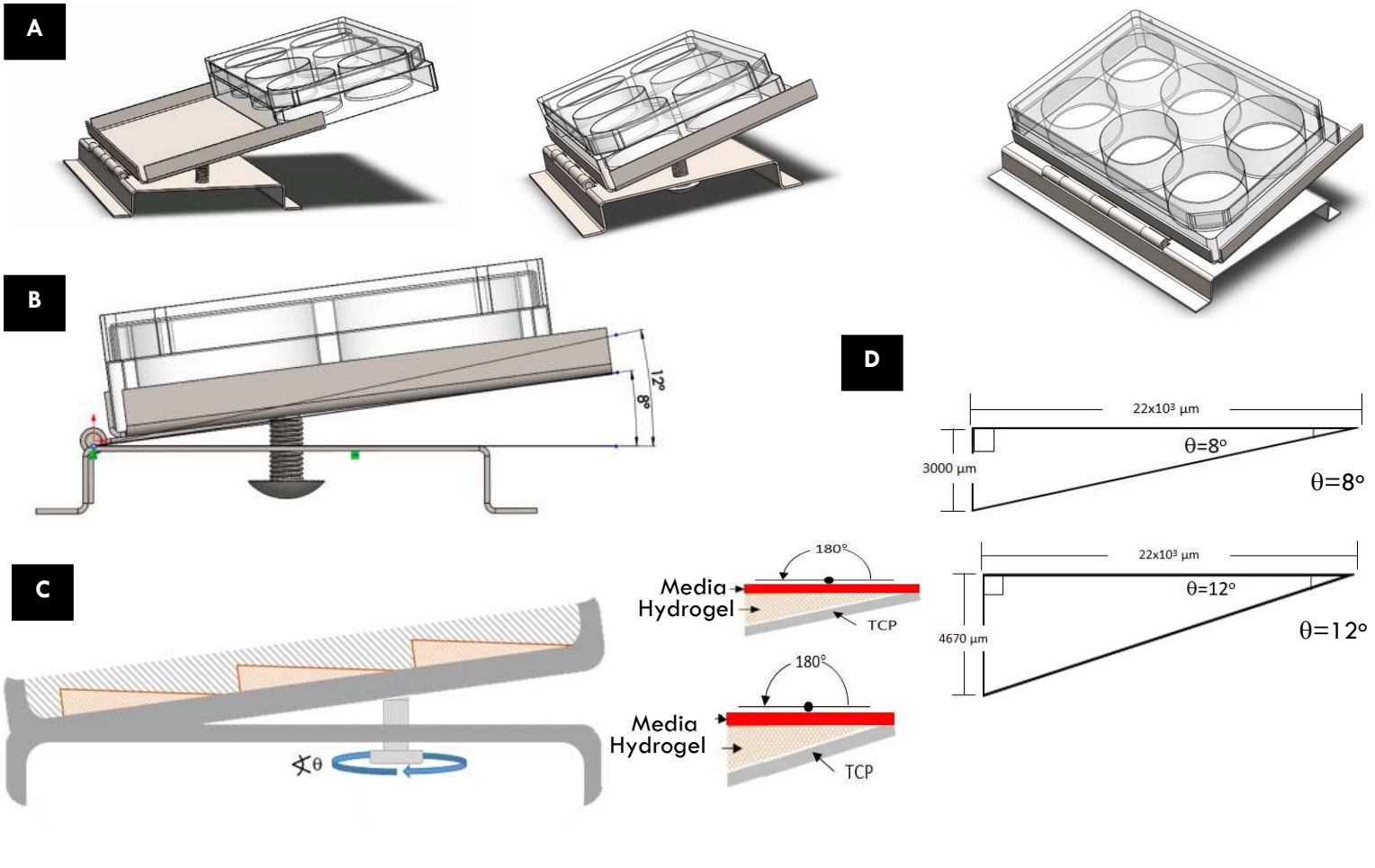

Figure 3. 3 Schematic representation of A. Tissue culture well-plate holder with a mechanism to give the tissue-culture well plate (TCWP) a gradient at different angles B θ8˚ and θ12˚ used in this study. C Image of a finished TCWP sample set. E, θ8˚ and θ12˚ gradient sample dimensions.

Hydrogel characterization

Sample physical properties

Sample thickness

Hydrogel thickness was determined by photographing cross-sectional sections of samples of different thicknesses and wedge dimensions and a calibrated graduated scale at the same magnification. The ImageJ software was used to assess sample height, using the straight tool [Image processing with ImageJ] measuring 3 representative samples from each variation [254].

Hydrogel capillary effect on gradient samples

Capillary effect: this phenomenon was observed on the gradient samples and characterised in order to avoid considering these regions as part of the experiment. It was found that the surface length affected by the phenomenon was greater for the steeper gradient (θ12) which had an average effect length of ~900µm. The affected surface on the sallower gradient (θ8) was ~663µm (Figure 3.4A). To facilitate analysis the immediate field of view after the sample edge (length 2000µm) was avoided for analysis purposes (Figure 3.4B).

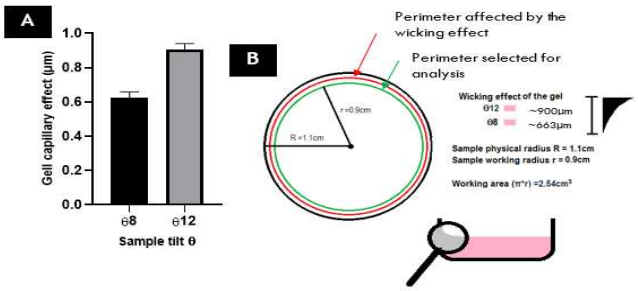

Figure 3. 4 Substrate thickness varies in proportion to the sample gradient. **A** Substrate wicking effects were measured using light microscope cross-section images of the gradient hydrogel and the imageJ software. The data is presented as group mean ± SE of the mean for the measurements (n=10) on each sample(n=12). **B.** wicking effect was found to be ~663µ for **θ8**˚ and ~900µm for **θ12**˚ first field of view from the external perimeter of the sample (2000µm length) was avoid for analysis. Final working area was given by $(R\text{-}2000\mu m)^2 * \pi$ equals 2.54cm^2.

Hydrogel porosity (cryo-FIB SEM)

Hydrogel samples of different cross-linker concentrations and different thicknesses were analysed using cryo-focused ion beam-scanning electron microscopy (cryo-FIBSEM) to investigate the porosity and structure of hydrogels in the presence of water. In this technique, the hydrogel samples were plunge-frozen in slush nitrogen or using a metal mirror freezer and transferred under liquid nitrogen to the sample shuttle of a Cryo-SEM system (Quorum PPT 2000, Quorum Technologies). In the prep-chamber, individual samples were coated for 60 seconds using a Pt sputter target. The sample was then loaded into the FIB-SEM (FEI Quanta 3D, FEI). Once in the SEM chamber, the hydrogels were prepared for FIB by deposition (3-4 seconds) of a platinum precursor from the gas injector (set to 27°C) of the microscope and milled using an initial current of 1-3 nA to make a rough cut, and then by further cuts at lower milling currents (0.3 nA-50 pA), to remove the common milling artefact, known as curtaining. SEM micrographs of the visible milled face showed dark patches with largely white areas in between. It was initially postulated that the darker areas were the pores of the hydrogel. In order to test this, the temperature in the SEM chamber was raised to -90°C, leading to slow sublimation of the water at the FIB milled face, (Figure 3.5 a-c) over approximately 20 minutes. The final sublimed hydrogel images are clearly interpretable as a porous hydrogel where now the lighter contrast features are identified as the hydrogel strands, and the pores are now darker and devoid of water. With a better understanding of the location of these components, the original non-sublimed images can be re-examined, and the black contrast correlated directly to the polymer and the white to the water. By inverting the contrast of the original milled face image, it is possible to give an image equivalent to the dehydrated image, but which has all the water bound, and is therefore a truer representation of the hydrogel's morphology. (Figure 3.5 e-f) This process has been

validated by [255]. The cross-sections of a variety of samples were statistically analysed with ImageJ software (National Institute of Health). The average pore size was calculated by measuring a total of 30 pores from 10 locations of 3 replicates for hydrogel combination. The total per cent porosity was determined to be the ratio of the total pore area to the total scaffold area in each image [256].

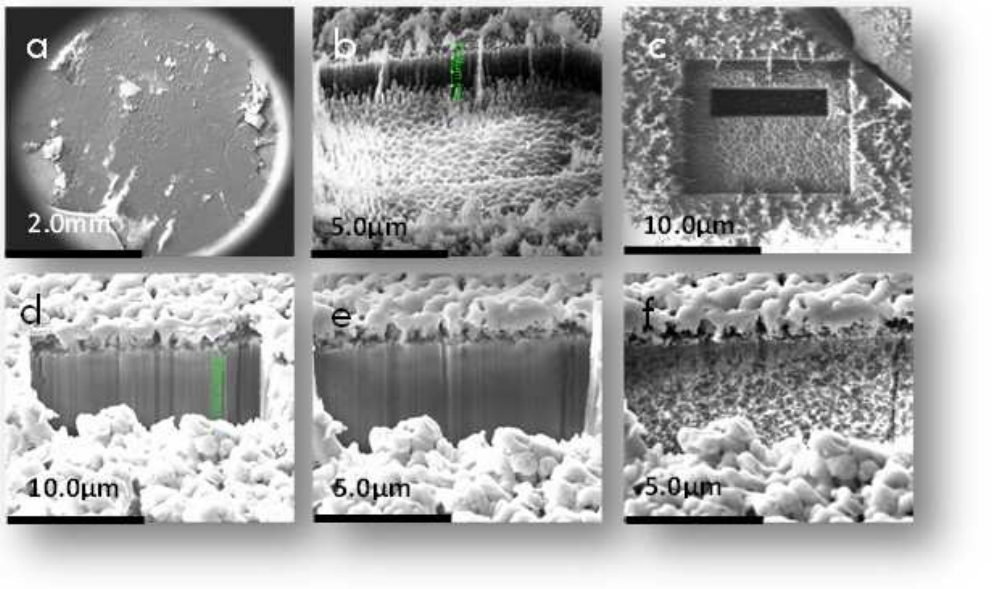

Figure 3. 5 Time lapse SEM images for the ChG_PA cryo-FIB SEM imaging technique for the characterization of pore size and porosity, from beginning (a) to end (f).

Mechanical properties

Compression Test

Mechanical properties of the cross-linked ChG_PA hydrogels were determined using a mechanical tester (Instron, Model 5567, Instron Corp). The cross-linked ChG_PA hydrogels were cut into disks (1.0 cm in radius) and kept covered by PBS at 25°C for 24 hours. Uniaxial compression tests were performed on the swollen ChG_PA hydrogels at 25°C, using a crosshead speed of 1.0cm/min and a load cell of 50 N. Each compressive test was performed for less than 1 minute to avoid loss of water during

measurement. The experiments were performed in quintuplicate. The compressive modulus (G) was obtained using compression-strain diagrams [40].

Macroscopic shear modulus measurements: atomic force microscopy

Apparent stiffness of the cross-linked G-CH hydrogels of different thickness was measured using a Catalyst AFM (Bruker Corp) instrument, mounted on the stage of an Axiovert 200 inverted microscope (Zeiss), employed on a vibration isolation table (Isostation). A V-shaped gold-coated silicon nitride cantilever with a four-sided pyramidal tip (MLCT, Bruker Corp) was used as probe. The spring constant of the cantilever was 0.047± 0.003 N m−1. Measurements on hydrogels were performed in liquid, using ultrapure water as bathing solution. Once the slide containing the hydrogel was placed on the stage of the microscope, the cantilever was positioned far above the glass surface, and allowed to thermally equilibrate. Then, the relationship between photodiode signal and cantilever deflection was calibrated, by taking a force-displacement curve at a bare region of the glass slide and measuring its slope. For the gradient hydrogel measurements, the point-and-shoot feature was used in contact mode to perform line scans along the direction of the thickest increase of the hydrogels. The trigger mode was set to 'relative'. In this option, the feedback system readjusts the initial piezo position for each force-displacement ramp, so that the maximal force applied to the sample remains constant. This option is particularly useful to perform line scans on sloped samples, because the piezo initial position is constantly readjusted, thus adapting to the varying height profile of a sample. Line scans were always started over a bare glass location close to the hydrogel edge. The recorded initial piezo position at that location was used later as a zero-height reference when computing the hydrogel height at each location. 10 force displacement curves were acquired at each hydrogel location, using 5-μm ramps with up to ~750nm indentations at 1 Hz, with a thickness of

at least 400nm. Spacing between locations on a line scan was held constant, and ranged between 100nm and 1µm, depending on the steepness of the hydrogel being measured. To perform measurements on thicker regions of the hydrogel (thickness >200µm), the same protocol was used but no initial measurements were performed on bare glass. Hydrogel thickness on those areas was estimated by focusing from the glass surface to the top of the hydrogel surface with the optical microscope, which was equipped with a motorized z-focus.

The force-distance curves were collected and analysed according to the Hertz model [257]. The hydrogel is treated as an incompressible material with Poisson ratio 0.5. Force curves obtained were analysed with force curve analysis module of the JPK software (Figure 3.6). 20 repeated force curves on 5 locations at the same thickness were obtained from 3 samples of each combination [258].

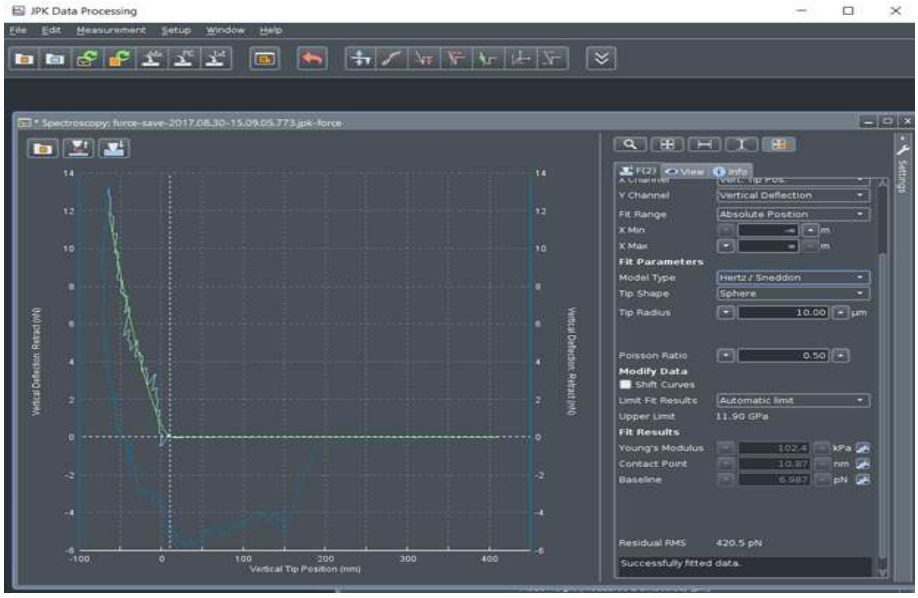

Figure 3. 6 Force curve analysis using JPK data processing software and the force curve analysis module.

Surface and bulk chemical properties

Contact angle goniometry

Hydrophilicity of hydrogels surface was determined by measuring the contact angle of a drop of sterilized de-ionised water. ChG_PA of different concentrations and thickness were assessed by measured 5 different locations on 3 samples 22mm diameter per each combination.

A First Ten Angstroms FTA200 dynamic contact angle system was used for measuring the water contact angle of the hydrogels. A droplet of water (5±0.1µl) was placed on to the surface using an air displacement pipette from fixed height of 5mm. An image of the droplet was captured using SLR camera with macro lens (Nikon D700 with Nikkor Micro 105mm; Nikon Coro Japan) within 10s of placing the droplet. The contact angle θ_c images were analysed by the FTÅ Video software as illustrated on Figure 3.7.

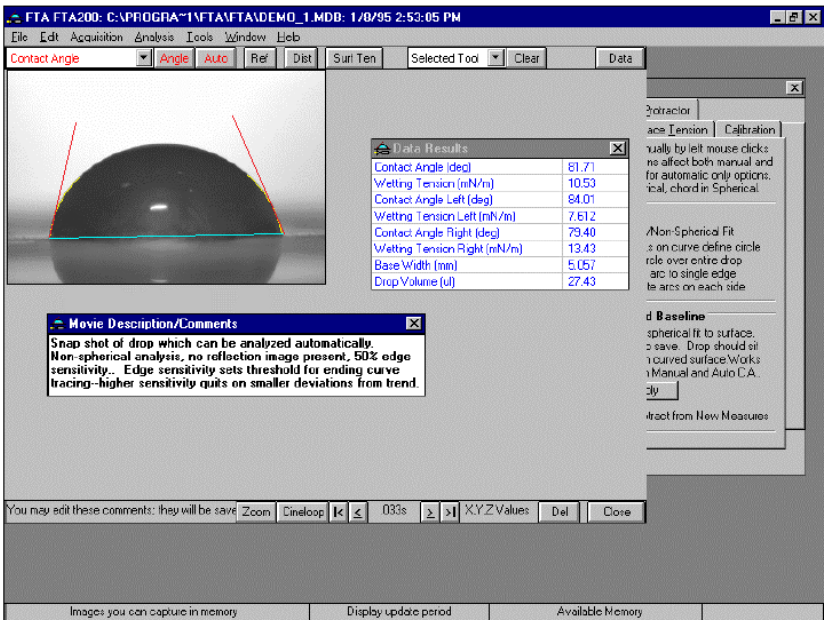

Figure 3. 7 Water contact angle. FTÅ Video Software image analysis.

Surface chemistry: XPS

XPS spectra of every combination were recorded using a Kratos Axis Ultra spectrometer employing a monochromated Al Kα X-ray source (hν = 1486.6 binding energy (eV)), hybrid (magnetic/electrostatic) optics, a hemispherical analyser, a multichannel plate, and a delay line detector (DLD) with a collection angle of 30° and a take-off angle of 90°. The X-ray gun power was set to either 100W or 150W, dependent on the quality of the vacuum obtained. All spectra were recorded using an aperture slot of 300 × 700μm^2 with a pass energy of 80 eV for survey scans and 20 eV for high-resolution core-level scans.

The cooling experiments were carried out using standard Kratos stage cooling methods, employing liquid nitrogen as the coolant. The temperature of the stage was monitored using a mounted thermocouple in contact with the sample stub; however, some thermal lag should be expected because the thermocouple is not directly in contact with the ChG_PA sample.

Two groups of samples were prepared for this analysis, ChG_PA samples of different PA (0.0 to 5.0%) concentrations were cast on glass cover slips with thickness of 1.0mm. The second group of samples were cast using ChG cross-linked with 2.5% PA and varying the sample thickness (0.5 – 6.0mm).

Prior to analysis, the ChG_PA samples were stored in an oven at 50° until each of them fully dried. ChG_PA hydrogels pumping times were recorded to assess the suitability of each sample; rough pumping was carried out in an external airlock before being introduced into the main analytical chamber. Pumping was performed until achieving the required airlock vacuum (~5 × 10-7 Torr) after 30−60 min. The base pressure of the analytical chamber was typically 3 × 10-9 Torr during the experiments. All XPS spectra

were recorded using the Kratos VISION II software; data files were translated to VAMAS. Data processing was conducted with CasaXPS software (version 2.3.19) [259].

Bulk chemistry: XDR

X-ray diffraction (XRD) area measurements were conducted with Siemens D-500 using Cu-Kα radiation at 40 mA emission current and 25 kV acceleration voltage, and 0.05° step size with 2s dwell time on each step. To investigate the phase make-up of these hydrogels, two groups of samples were prepared for this analysis. ChG_PA samples of different PA concentrations (0.0 to 5.0%) were cast on glass cover slips with thickness of 1.0mm. The second group of samples were cast using ChG cross-linked with 2.5% PA and varying the sample thickness (1.0 to 4.0mm) and point source XRD scans were conducted with a Bruker D8-Discover using Cr-Kα radiation at 35 mA emission current and 30 kV acceleration voltage, with 0.04° step size and 4s dwell time per step. The diameter of the nozzle used was 2mm, which resulted in a beam maximum length of up to ~ 5mm at the sample surface [260].

Characterization of kinetic properties

Swelling ratio

To determine the percentage of water adsorption and content, the swelling behaviour of the hydrogels was determined. Dry hydrogels were soaked in aqueous solutions. 10mm diameter hydrogels samples of different PA concentrations (0.0% to 5.0%) were prepared and dried at 50°C for 6 h in an oven, and then accurately weighed. Afterwards, the dried samples were immersed in solutions of different pH (4, 7, 10) for different times (1 minute to 7 days). Finally, the samples were removed from the solution, and weighed immediately after blotting with a filter paper to remove the

surface adsorbed liquid. The swelling ratio was calculated for each sample according to Eq.3.4

$$\mathrm{SW} = \frac{Ww - Wd}{Wd} \qquad \text{Eq. 3.4}$$

$$\mathrm{WC} = \frac{W2 - W1}{W2} X\ 100 \qquad \text{Eq. 3.5}$$

The water content was determined by applying the Eq. 3.5.

Where, *SW* is the swelling percentage of the hydrogels inside the solutions, *Ww* and *Wd* are the weights of the hydrogels in the swollen and dry states, respectively and *WC* water content. The dry weight of the hydrogel was recorded as *W1,* and the final wet weight (35 min) was denoted by *W2*. The reported results of the swelling and water content test are the average of three measurements for each sample [206, 239, 261].

Stability in water

The stability of ChG_PA% hydrogels alkaline and not treated (AT) in aqueous solutions were investigated. 10mm diameter hydrogels samples of different PA concentrations (0.0% to 5.0%) were prepared, dried at 50°C for 6 hours in an oven. A group was alkaline treated (AT) and then died again, and then both groups were accurately weighed at the beginning of the experiment. The dried hydrogels were immersed in two different aqueous solutions (pH 4 and pH 7) at 20°C. For intervals from 1 day up to 14 days hydrogels were removed and dried for 48h in a laminar-flow hood, and a second weighing was directed to determine the weight loss thereby stabilities of the hydrogels. Stability of the hydrogels in the aqueous solution is expressed with the use of Equation 3.6.

$$S = \frac{W2}{W1} \qquad \text{Eq. 3.6}$$

where S is the ratio of the weights of the hydrogels remaining after the test. *W1* and *W2* are, respectively, the weights of dried hydrogels before and after the test.

Gelation time

It is important for systems designed to gel in situ (ASTM, 2011), for example: wound healing treatment at wound site requires fast gelation time with a cross-linking mechanism suitable for gelation in situ [262]. To assess the gelation time of the ChG hydrogel as a function of PA% concentration, 1ml (x 5) of each different combination was mixed with a metallic spatula (Figure 3.8) until the hydrogel separated from the base of the vessel, where it was contained as shown in Figure 3.8 and the time required for the hydrogel to reach this state was recorded.

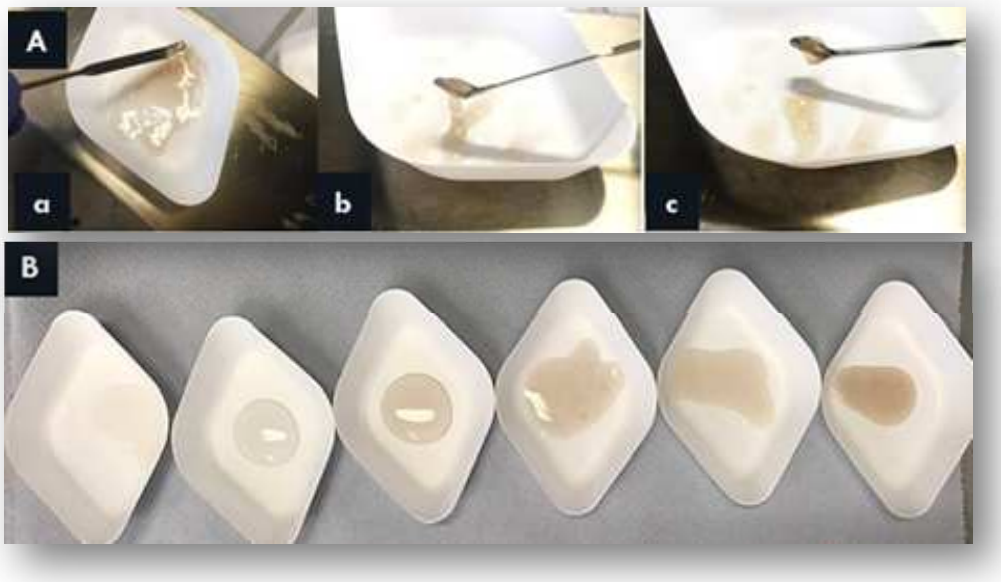

Figure 3. 8 Gelation time A Lapse time images of the gelation assessment technique used in this study, **a** from liquid state to **c** hydrogel. **B** ChG at different PA concentrations.

Characterization of biological properties

Cytotoxicity elution test

UV sterilised hydrogels were incubated in 37°C culture medium at a surface area/medium volume ratio of 3cm^2/ml (medium extraction method applied according to ISO 10993-12 of larger items with thickness > 1.0mm) for 24 h before removing for test. Fresh medium was used as control. Meanwhile, 3T3, MG63 and hMSCs cells were seeded at a density of 40 x 10^3 cells/cm^2 in each well of 48 well-plates and incubated for 24h until fully confluent. Then the culture medium was replaced with extracted test eluents and incubated for another 24h.

Cells cultured in complete DMEM were used as control. The extraction medium was removed, and cells were washed 3 times with PBS, and incubated in Alamar Blue solution (1:10 Alamar Blue: Hank's Balanced Salt Solution) for 80 min along with 3 blank wells. 100µl aliquots were transferred to a 96-well plate in triplicate, and the fluorescence was measured at the excitation wavelength at 530nm and emission at 590nm in FLx800 plate reader (BioTek Instruments Inc). In the current study, according to the ISO 10993-5, a sample would be considered to have cytotoxic potential if cellular metabolic activity reduced to less than 70% compared to the control group.

Cell Culture

Cell CultureSwiss-3T3 fibroblasts, MG63 Osteoblast-like were grown in culture of Dulbecco's modified minimum essential medium (DMEM CellGro) supplemented with 10% foetal bovine serum (FBS), 1% 200mm L-glutamine, 0.15 mgml^{-1} L-ascorbic acid (Vitamin C), 5% 100X AA/AM antibiotics-antimycotics, 5% 1M HEPES Buffer, and 1% 100X NEAA nonessential amino acids. Cells were cultured in a humidified 37°C, 5% CO2 NuAire HEPA-filtered CO^2 incubator.

Immortalised bone marrow-derived human mesenchymal stem cells (hMSCs) – a gift from Dr Virginie Sottile [14] – were maintained in a monolayer culture, stored in a humidified atmosphere at 37°C and 5% CO^2 NuAire HEPA-filtered CO^2 incubator. Cells were typically grown in standard medium consisting of low glucose Dulbecco's Modified Eagle Medium (DMEM), 1% (v/ v) L-Glutamine, 1% (v/v) non-essential amino acids (NEAA)and 2% (v/v) antibiotics/ antimycotics (Invitrogen, UK), supplemented 10% foetal bovine serum (FBS), [14].

Passaging cell culture

Once cells reached 80% confluence, cell culture media was discarded, and replaced with 5ml sterile PBS, flask was gently swirled to wash the cells and PBS was aspirated from the flask and then trypsinised with approx 1.5ml Trypsin/HEPES solution, the flask was again gently swirled to ensure the Trypsin/HEPES solution covered the entire monolayer and incubated for 5 min at 37°C. The flask was checked at regular intervals under light microscopy to see if the cells have detached from the tissue-culture plastic. Flask was gently tapped on the sides to loosen cells. 6ml of culture media was added to the flask and then transferred into a 20-ml universal container. This was repeated with 4ml media and added to the same universal. The cells were centrifuged at 250 x g and 4500rpm for 4 minutes, after which the supernatant was removed and then 6ml of fresh media was added. Then pallet was resuspended and 2ml of the suspension transferred into 3 new T25 flasks containing 8ml of media each, and then the flasks transferred to a 37°C, 5% CO^2 humidified incubator and culture media changed the following day.

Cryopreservation and Thawing

After trypsinisation and centrifugation, cell pellets were resuspended in 1:1 combination of culture media to freeze mix (80% (v/v) culture media with serum, and 20% (v/v) DMSO). Cell suspensions were transferred to sterile cryotubes and stored at -80 °C

overnight. Tubes were then moved to liquid nitrogen for long-term storage. Frozen cells were thawed in a 37°C water bath for less than 1 minute. DMSO was neutralised with culture media and the thawed cell suspension was centrifuged at 200g for 5 minutes. Cell pellets were resuspended in fresh culture media and stored in a humidified atmosphere at 37°C and 5% CO^2. Suspensions and materials were purchased from Sigma Aldrich (UK), and cell culture media, and supplements from Gibco Invitrogen (UK).

Cell seeding

Transferred hydrogels experiment

Hydrogels were cast in thin layers in glass petri dishes, then peeled out and transferred to tissue culture plastic well-plates. Each hydrogel was protein-conditioned by suspending in fresh media overnight, after which the culture media was tipped away. Passages 11–17 for NIH 3T3 and MG63 cells lines were used for this study. A cell seeding density rate of 25×10^4 cells/cm^2 was used, and media was changed every 48hrs.

Different cross-linker concentration experiment

24hrs prior to their use, hydrogels were cast in well plates, protein-conditioned, and covered by fresh media. Passages 11–17 for NIH 3T3 and MG63 cells lines were used for this study. All groups were cultured in flasks until reaching confluence at 80%, then washed with warm PBS, dissociated with 0.2% trypsin/EDTA, pelletized by centrifugation for 5 minutes and finally re-suspended in 1ml fresh media. A cell seeding rate of 25×10^4 cells/cm^2 and a working volume of 250µl were used to seed cells on each sample dropwise in a spiral manner. Then samples were placed inside the incubator for 2 hours waiting for cells to attach to the substrate; after that time 350µL

of fresh media was added to each sample. The samples were maintained at 37°C, 5% CO^2/95% air always; fresh medium was replaced every 48hrs.

Flat samples apparent stiffness experiment

24hrs prior to their use, hydrogels were cast in 48 well plates with samples of different thicknesses, ranging from 0.5mm – 4.0mm; they were protein conditioned, and covered by fresh media. MG63 and hMSC cells lines were used for this study. A cell seeding rate of 250 cells/cm^2 and 2500 cells/cm^2, and a working volume of 250µl were used to seed cells on each sample dropwise in a spiral manner. Then samples were placed inside the incubator for 2 hours, waiting for cells to attach to the substrate; after that time 350µL of fresh media was added to each sample. The samples were maintained at 37°C, 5% CO^2/95% air always, fresh medium was replaced every 48hrs.

Apparent stiffness gradients experiment

24hrs prior to their use, hydrogels were cast in 12 well plates of samples of local stiffness gradients were protein conditioned and covered by fresh media. MG63 and h MSC cells lines were used for this study. A seeding rate of 250 cells/cm^2 and 1000 cells/cm^2, and a working volume of 250µl were used to seed cells on each sample dropwise in a spiral manner. Then samples were placed inside the incubator for 2 hours waiting for cells to attach to the substrate; after that time 350µL of fresh media was added to each sample. The samples were maintained at 37°C, 5% CO^2/95% air always, fresh medium was replaced every 48h. For cell quantity and differentiation studies, after each incubation, timepoint samples were sectioned in 4 equal parts along the gradient (y axis) and each individual section placed with tweezers in individual wells at 12 well plates.

Observing effects of substrate stiffness on short term cell attachment.

hMSCs cells were seeded onto 1.0mm, 1.5mm and 2.0mm hydrogel samples. The hydrogels were divided in two groups, with one group being incubated for a 2-hour period and the other set incubated for a 6-hour period before fixation and imaging via ESEM. To generate quantitative results for these images, cell morphology was grouped into 3 different types, each describing different stages on the cell attachment process.

Cell viability studies

Cell metabolic activity Alamar Blue test

Alamar Blu e test was used to estimate viable relative cell number. Alamar Blue is non-toxic to cells and does not need killing the cells to achieve measurement. This allowed cells samples to be monitored in regular bases and be re-used for further investigations. Using microplates and analysing with microplate readers easily set up automatization. (AbD Serotec, Oxford, UK) diluted 1:10 in Hank's Balanced Salt Solution solutions was warmed for 10 minutes before use: cell cultures were washed with warm PBS (3 x 5min); for the gradient experiment samples were sectioned in 4 equal parts along the gradient direction (the y axis) and each section was placed using tweezers in a 12 well-plate well, then 0.4ml/cm2 Alamar blue solution was added to the samples and to additional 3 wells which worked as blanks. The culture plate was protected from light by being covered in aluminium foil, to be transported to the incubator where it remained for 80 minutes; then it was removed, wrapped in aluminium foil, and placed on the plate shaker at 150 rpm. The well plate was removed from the shaker, sprayed with IMS and placed into a Class II fume hood with the hood's light off. The silver foil was removed and 100µl of each sample was taken and dropped into a 96 well-plate solution from each sample, including blanks. The fluorescence (at 560nm, 590nm) of the samples was evaluated using a fluorescence reader (FLx800, Biotek Instruments, USA) and blanked

against non-reduced mixture.

Hoechst 33258 DNA Assay

Cell number was determined by assaying for total DNA contents after the 14, 21 and 28-day culture periods. In this assay, the Hoechst 33258 (Sigma-Aldrich, UK) stain binds cellular DNA resulting in enhanced fluorescence, which is directly proportional to the DNA content as described by Rage et al. [263]. To lyse the cells, the culture medium was replaced with 1ml sterile deionised water (SDW), and the well plate was stored at -20˚C. Once frozen, the well plate was placed into the incubator at 37˚C to thaw, and the cycle was repeated 3 times. Aliquots of 100µl from each sample were transferred to a 96-well plate, and 100µl Hoechst stain (10mg/ml SDW) added at a working dilution 1:50 in TNE buffer (10mm Tris (hydroxymethyl) methylamine, 1mm EDTA and 2mm NaCl in distilled water, pH 7.4). Then the well plate was wrapped in aluminium foil and placed on the plate shaker at 150rpm. The fluorescence (at 360nm, 460nm) of the samples was evaluated using a micro-plate fluorescence reader FLx800, Biotek. A standard curve of DNA was produced using known concentrations of DNA from calf thymus (Sigma-Aldrich, UK) reconstituted in 0.01M NaCl to a concentration of 20µg/ml.

PicoGreen DNA assay

The fluorochrome PicoGreen dsDNA reagent (Invitrogen) is an ultra-sensitive fluorescent nucleic acid stain for quantitating double-stranded DNA (dsDNA) in solution. It is a more sensitive DNA content test reagent, enabling one to quantitate as little as 25pg/ml of dsDNA (50pg dsDNA in a 2ml assay volume) with a standard spectro fluorometer and fluorescein excitation and emission wavelengths. PicoGreen binds cellular DNA resulting in enhanced fluorescence, which is directly proportional to the DNA content. To lyse the cells, the culture medium was replaced with 1ml SDW, and the well plate was stored at -20°C. Once frozen, the well plate was placed into the incubator at 37°C to thaw, and

the cycle was repeated 3 times. The stock PicoGreen reagent was diluted 200- fold in 1X dilution buffer. Aliquots of 100µl from each well were transferred to a 96-well plate, along with 100µl 1x PicoGreen reagent. The plate was gently agitated in the dark for 5 minutes. The fluorescence (at 490nm, 640nm) of the samples was evaluated using a micro-plate fluorescence reader FLx800, Biotek Instruments, USA. A standard curve of DNA was produced using known concentrations of lambda DNA (Invitrogen).

Cell osteogenic differentiation

Alkaline phosphatase

Alkaline phosphatase (ALP) enzyme activity was used as a marker for early osteogenic differentiation [264]. A Randox ALP kit was used for this experiment. The 10-mL vial labelled R1b containing p-nitrophenylphosphate was reconstituted, with 10ml of the buffer labelled R1a. Briefly, the cells were lysed as follows: the culture medium was first replaced with 1ml SDW and the well plate was stored at -20˚C. Once frozen, the well plate was placed into the incubator at 37˚C to thaw, and the cycle was repeated 3 times. Aliquots of 50µl from each sample were transferred to a 96-well and 50µl of p-Nitrophenyl phosphate substrate solution was added to each well. The plate cover from light for 30 minutes at room temperature, before 100µl duplicates of the p-Nitrophenyl phosphate substrate solution were transferred to a 96-well plate to be used as blanks. The absorbance for the reactions was read at 405nm, using ELx800, Biotek Instruments, USA microplate reader, and 1:5 dilutions were required for readings outside the range of the plate reader.

ELISA for Osteocalcin

An osteocalcin ELISA kit (Invitrogen, UK) was used to quantify osteocalcin concentrations after osteogenic differentiation of hMSCs, following the manufacturer's protocol. To lyse the

cells, the culture medium was replaced with 1ml SDW and the well plate was stored at -20°C. Once frozen, the well plate was placed into the incubator at 37°C to thaw, and the cycle was repeated 3 times. Aliquots of 200µl of the lysed cell solution in each sample, standards and controls were added to each well (well plate provided in kit). Next, 100µl of Anti-OST-HRP conjugate was added to each well and incubated in the dark at room temperature for 2 hours. After the incubation period, the solution was disposed of, and wells were washed 3 times with the provided wash solution. Then 100µl of stabilised chromogen solution was added to each well. The plate was covered and incubated in the dark for 30 minutes at room temperature. After the incubation period, 100µl of stop solution was added to each well. Then, the plate was agitated to encourage a colour change from blue to yellow. The absorbance was measured at 490nm within 1 hour of adding the Stop Solution using a ELx800, Biotek Instruments US. Untreated stabilised chromogen solution was added to 3 wells, and these absorbance readings were used as blanks. A standard curve was generated from the osteocalcin standards in the kit. This allowed the concentration of unknown samples to be calculated.

Morphology analysis

Phalloidin Stain for Actin Filaments

Phalloidin is a bicyclic peptide belonging to a family of toxins isolated from the deadly Amanita phalloides 'death cap' mushroom. The peptide is commonly used in imaging applications to selectively label filamentous actin. The phalloidin FITC (Invitrogen) was dissolved in 1.5ml methanol to yield a final stock concentration of 6.6µM. After the culture period, cells were washed twice in PBS and fixed in ice cold 4% paraformaldehyde for 15 minutes. Samples were washed twice with PBS before a 0.1% Triton X-100 solution was used for 5 minutes to perforate the cell membrane.

Samples were washed twice with PBS before 205µl of phalloidin stain was applied to each slide (5µl phallotoxin stock diluted with 200µl PBS). Slides were incubated with the stain in the dark for 20 minutes. Finally, samples were washed twice with PBS and mounted onto microscope slides, using Vectashield mounting medium containing DAPI (Vector Laboratories).

Phase Contrast Microscopy

Phase contrast microscopy (Nikon FS-100 WITH Nikon 10x, 20x, and 40x Objective lenses Japan) outfitted with a Nikon digital camera was used to obtained images of live cultures. Digital micrographs were captured from different locations and analysed for observations on cell spreading area, cell density, and shape factors such as cell circularity, aspect ratio, orientation degree and number of cell processes. For the PA cross-linker concentration and the uniform stiffness experiments., 18 images were analysed per timepoint, 3 images per sample (in the y axis top centre and bottom of each sample), 6 samples per condition. For the gradient hydrogel samples, starting from the thin end going down in the y axis to the thick end of the gradient sample, 3 images at different locations in the same x axis were taken 2.0mm apart in the y axis, avoiding the capillary effect affected region (2mm from each end of the sample) for a total of 9 locations, 27 images per sample.

To determine the cell superficial area in contact with the substrate, cell aspect ratio, circularity, orientation angle, and cell density per sample section, an image of a calibrated graduated scale was captured before capturing any group of micrographs at the same magnification.

The software ImageJ [254] was used to process images, selecting cells with tools like free-hand selection, straight line and multi point (Figure 3.9) to then calculate cell

density, cell spreading area, and shape descriptors such aspect ratio, circularity and other statistics such as orientation angle. Only cells with distinct outline were included in the results. A minimum of 60 cells were used to report the statistics over 3 different set locations per field of view, at 3 different fields of view per step samples on uniform stiffness samples, and 3 per location, on 9 locations per gradient samples.

Cell orientation in the gradient samples were morphologically analysed, phase-contrast images of 3 fix field of view and ~3 fixed regions of analysis (Figure 3.9A) were analysed using the software ImageJ and the free hand tool (Figure 3.9B) The presence of cell process lamellipodia was determined qualitatively by observation of a projection of cellular mass visually distinct from the main body of the cell. Rounded cells (lacking defined lamellipodia and filipodia) were defined as 'unpolarized', and data for orientation were not recorded. Long axes for cells were identified by morphological inspection. For gradient hydrogels, the angle between the gradient direction and the cell's long axis was measured using NIH ImageJ. For uniform hydrogels, this procedure was implemented by assigning a fixed arbitrary reference direction. Cell orientations of 90° indicate that the cell was oriented perfectly in the direction of the gradient; an average cell orientation of 180° or 0° corresponds to cells that were randomly oriented. For the flow-induced experiments, cell orientation angle of 0° indicated orientation in the direction of the flow.

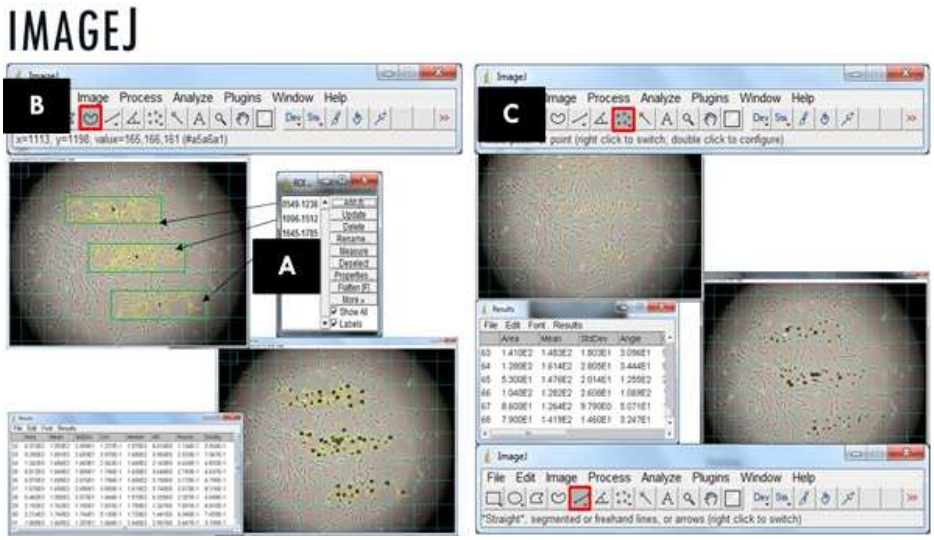

Figure 3. 9 The software ImageJ was used to process images; three regions of view were previously selected to analyse each image at three set locations Using the **A** ROI tool. Measurements were performed selecting cells with tools like **B** free-hand selection, and **C** and multi point.

Confocal microscopy

For screening, imaging was performed using an inverted Leica SP2 confocal laser scanning microscope with 40x oil immersion objective and Ar/HeNE (488nm) laser. Clones were imaged by generating z-stacks of 1µm planes from the cuticle to basal lamina at a resolution of 1024x1024. For other experiments requiring multi-channel acquisitions, a Zeiss LSM880 exciter confocal laser scanning microscope was used with 40x oil immersion objective, optimal resolution and lasers 405nm, 488nm, 543nm and 633nm. Collagen fibrils were imaged in reflectance mode, using a 488nm laser for excitation and imaging with a bandpass filter of 490–500nm [39]. Fiji (ImageJ) software was used to analyse images [254].

Scanning electron microscopy (SEM)

Cast hydrogels were washed with warm PBS (3x5min). Next, a 2.5% glutaraldehyde in distilled water was used for primary fixation followed by 1% osmium tetroxide in

distilled water for secondary fixation. After washed 3x5min in 0.1M sodium cacodylate buffer, the dehydration process of the specimens was conducted by washing with graded series of ethanol which is successively 20%, 40%, 60%, 70%, 80%, 90% and 100% ethanol, and finally dried via HMDS for 2×5min. HMDS was removed, and the samples were left to air-dry overnight in a fume cupboard. Hydrogels were coated with a thin layer of platinum (10nm).

Environmental scanning electron microscopy (eSEM)

Hydrogel samples were imaged with Environmental Scanning Electron Microscope (ESEM) using a FEI Quanta 650 ESEM with and without cells. The samples with cells were taken at day 7 after seeding. All samples were washed with PBS, fixed with 4% glutaraldehyde for 20 minutes, washed with PBS, and then washed with SDW in excess prior to imaging. The samples were imaged at a temperature range of 3-0°C, a humidity range of 100-85%, and pressure at 5.5-2.5 torr with a Peltier stage to control the temperature of the sample. At these parameters, the samples were able to be imaged for approximately 30 minutes.

Cell migration assay

Overall cell distributions on gradient hydrogel samples were determined for durotactic studies by assessing the spatial distribution of hMSCs at 3, 5, 7, 9, 14, 21 days incubation period. Briefly on samples seeded at low densities (250 cells/cm^2) starting from the thin end going down (on the y axis) to the thick end of the gradient sample. Three images at different locations in the same x axis were taken 2.0mm apart on the y axis, for a total of 9 locations, 27 images per sample. Individual cells were counted using the ImageJ software (Figure 3.10A, C) for the 27 fields of view, then the percentage of individual cells at each of the 9 locations was calculated.

Bioreactor

Parallel-plate flow chambers system

A perfusion system was used for the dynamic culturing experiment. In these systems, fluid is continuously introduced at one side of the chamber and flows out from the other side allowing continuous addition and removal of medium (Figure 3.11).

In the parallel-plate flow chamber systems used in these experiments, pressure gradients driving the flow were established by a peristaltic pump (Figure 3.11b); which allows rapid variations in flow and shear stress. These variations result from the incompressibility of the fluid, and any changes in flow rate through the pump must be matched by changes in flow rate through the flow chamber [26]. The whole closed loop comprises also a perfusion system included two media reservoirs, one for each bioreactor (Figure. 3.11a), a multi-channel peristaltic pump (Watson-Marlow 2500s, Figure. 3.11b), and interconnecting tubing (Figure. 3.11a) polymer ferrules, silicone tubes, tubing with lure endings, all biological inert materials which interconnect components exposed to the media in the system. For the study, culture media was pumped continuously through the chamber, at different flow rates depending on the experiment, for up to 14 days. The entire system was kept in a 100% humidity atmosphere in a NuAire HEPA-filtered CO^2 incubator (Figure 3.11). Gaseous exchange is achieved as media returns to the reservoir: droplets of media drop through an air gap between the return line and the media in the reservoir (Figure. 3.11a). For both systems, medium was recirculated and its quality validated after the experiment. The total media in the perfusion flow system was 250ml. In order to sustain media condition in both systems, media were replaced every 3 days. The samples were separately taken out of the bioreactors at different timepoints depending on the experiment

morphological change and increase in cell number.

Bioreactor validation

Cytotoxicity

Polycarbonate (the same as used to fabricate the bioreactor) was used as specimen to perform elution test. The specimen was place in a sterile container with at 1:5 weight (grammes) to volume (millilitres) ratio with 10%FBS/DMEM media for 24h at 37°C, then the specimen was extracted. At the same time NIH 3T3 cells were cultured in 6-well plate at a density of $30X10^4$ cells/cm^2 in 10% FBS/DMEM. Once 80% confluence was achieved, the medium was replaced with the one from the specimen medium. Cells were incubated for 72h before cell metabolic activity and morphological studies.

Device preparation

Before the start of experimentation, efficacy of sealing set up was validated soaking the assemble bioreactor and interconnecting tubing in SDW and pumping air into the system with a syringe; after this procedure, tubing and bioreactors were disassembled and submerged in high medical surface disinfectant (Distell diluted 1:10 deionized water) for 24 hours, then carefully rinsed with hot water and double-rinsed and wiped with 70% industrial methylated spirit (IMS) for 15min and washed again with SDW. Finally, the components were sterilized under UV light for two hrs as the components were exposed to a non-sterile environment while not in use.

Recirculating media quality

In the experiment recirculated media was replaced after 3 days by fresh media; in order to validate quality of the elution, the spent media was used as cell culture media in controlled 100ml flasks. Phase-contrast microscopy (Nikon FS-100 with Nikkon 103,

203, and 403 objective lenses, Nikon, Japan) was used to generate images of cultures and evaluate cell viability in response to elution (Figure 3.10f).

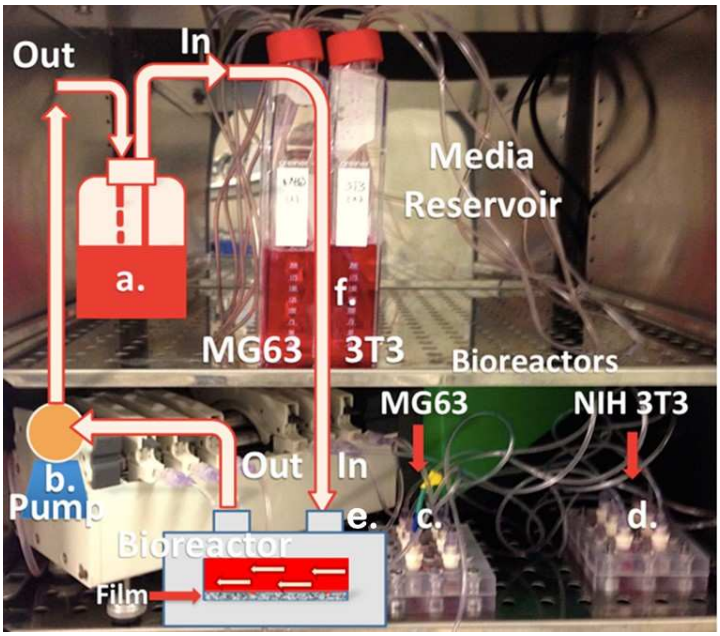

Figure 3. 10. Flow perfusion system consist of a) Two media reservoirs one for each cell line; b) a peristaltic pump (Watson-Marlow 2500s) two three flow culture wells bioreactors c) MG63 cell line bioreactor, d) NIH 3T3 Bioreactor; e) media flow runs parallel to the 2D Construct. The whole system is contained in a humidified CO2 incubator, allowing gas exchange to occur through the f) silicone rubber interconnecting tubing system.

Data analysis

For most of the experiments the samples were evaluated at different timepoints from 0 until 48 days for static and for perfusion culture, depending on the experiment. The samples taken at each timepoint were evaluated, and the results shown in different graphs for them to be assessed. Statistical analysis was performed to evaluate the spread and significant difference samples. The report uses bar plots, and error bars to do so, and a brief statistical analysis to assess significance. Data was represented as mean ± SEM when appropriate. GraphPad Prism version 8.0 for Windows was used to create graphs and help in comparison.

CHAPTER

4

Development of a chitosan-gelatin cross-linked hydrogel for the study of the influence of substrate mechanical cues on cell response.

4. Development of a Chitosan-Gelatin Cross-linked Hydrogel for the Study of the Influence of Substrate Mechanical Cues on Cell Response

Introduction

The aim of this chapter is to develop a naturally derived hydrogel with tuneable mechanical properties, then to characterise its physical, chemical and mechanical properties. Overall, the goal of this chapter is to develop and optimize a suitable material for studying the influence of the hydrogel mechanical properties on cell behaviour.

Hydrogels have gained attention over the years as cell transplantation vehicles for the regeneration of a variety of tissues [265, 266]. Their structural similarity to the macromolecular-based highly-hydrated components in the body makes them strong candidate materials for many applications in regenerative therapies [155, 156]. Well-designed gels must show mechanical strength, flexibility and structural integrity sufficient to withstand applied forces from cells and the adjacent tissues *in vivo* without deformation or failure for a certain period of time [157, 241]. Furthermore, the mechanical properties of materials to which cells adhere have been found to profoundly affect the function of the cells [158]. Hydrogels with controllable mechanical and biological properties have a promising future in the biomedical applications field.

Physical and mechanical properties of soft biological tissues are critical to their physiological function; however, it is hard to replicate them with synthetic materials. Unlike linear synthetic polymer hydrogels – which have been used to investigate how cells respond to the mechanical properties of their microenvironment – extracellular matrix proteins such as collagen or its derivative gelatin, are fibrillar materials with nonlinear

mechanical properties [153, 182]; their elastic modulus increases in magnitude as the applied strain increases, thus the resistance that a cell can sense would be a strong function of the contractile forces it exerts. Rudnicki et al. [185] reported that fibroblast cells on fibrin and collagen hydrogels sense mechanical signals over much larger distances (up to 150μm) than they do on linearly elastic synthetic PAAm (<5μm). Likewise Winer et al. [150] found that hMSCs and NIH 3T3 on fibrin hydrogels can significantly deform the hydrogel up to five cell lengths farther then on homogenous linearly elastic synthetic PAAm hydrogels of identical elastic intrinsic modulus. Although it is becoming clear that cells can sense substantially farther (both laterally and in depth) on protein-based hydrogels than on synthetic hydrogels, there has not been a considerable amount of work using the naturally derived options for mechanotransduction studies, thus the mechanism by which mechanical signals are propagated through protein hydrogels is not yet fully understood.

Gelatin, a soluble protein derivative of collagen, holds a variety of desirable features, such as good cytocompatibility, low immunogenicity, plasticity, promoting cell adhesion and proliferation, and it is available at very low cost. However, the natural weakness of the hydrogels is a problem. A number of chemical modification methods have been investigated to improve the mechanical properties of these hydrogels [201, 202]. For instance, gelatin has successfully been coupled to glycosaminoglycans in hydrogel scaffolds *in vitro*. Chitosan, the deacetylated derivative of chitin, provides a large number of accessible hydroxyl and amine groups, and therefore provides numerous possibilities to create hydrogels via chemical cross-linking [211]. However, when mixed, these blends are unstable matrices, and have rapid biodegradation rates; the instability of the structures of these polymers in the gelated state have limited their applications as biomaterials for regenerative therapies. A common approach to overcome those natural structural

limitations is the use of cross-linker reagents [225, 232]. Several synthetic and natural cross-linkers have been used, but some of which decrease the cytocompatibility. Proanthocyanidins (PA) are inexpensive compounds and oligomeric complexes, which can be used as cross-linker reagent for these polymers [242, 267]. The cytotoxicity, cross-linking rate, and biocompatibility of PAs as a collagen-tissue fixative is much more efficient than other reagents, such as glutaraldehyde (GA) [267]. PA has been used to cross-link ChG formulations producing a more stable, less swellable, and cyto-compatible hydrogels with tuneable mechanical properties [206, 238].

This section will describe the fabrication process, structure and properties of a biodegradable natural protein-based hydrogel substrate used as construct for cell culture. The aim was to develop a cyto-compatible, biomimetic material with tuneable mechanical properties, with the ability to match the inhomogeneous nonlinear mechanical profile of a plethora of living tissue, in order to enable the study of a variety of cell lineage behaviour as a response to the mechanical cues of the matrix.

Results

ChG Cross-linked Hydrogel Development

The use of hydrogels and similar biomaterials with controlled mechanical properties (with Young's moduli ranging from Pa to MPa) has allowed the systematic study of the effect of matrix stiffness on cell behaviour [7]. This section summarises the design, development, and optimization process to fabricate a chitosan-gelatin ChG hydrogel cross-linked with PA with tuneable mechanical properties, for the study of cell response to mechanical cues of its microenvironment. Several polymers to polymer, and polymer to cross-linker ratios, as well as solvent, temperatures and fabrication times were used in the early stages of the material design. Before starting any chitosan-gelatin blend

experimentation, the chitosan deacetylation% effect on chitosan mechanical properties was evaluated. Chitosan deacetylated at 85% and 50% at equal molecular weight were used for these trials. Hydrogels were prepared and compression tests for each combination were performed. It was observed that the higher the degree of deacetylation of chitosan, the higher was the compression modulus of the chitosan hydrogels (data not shown), the results of these trials support previous reports highlighting the importance of chitosan deacetylation% on mechanical properties of the fibrous hydrogel [210, 268]. Thereafter, chitosan at deacetylation percent of 85% was used for further experimentation. Once the appropriate Chitosan deacetylation% was obtained, an initial chitosan-gelatin blend study was performed to validate the efficacy of PA compared to that of glutaraldehyde (GA) solution for the cross-linking of these (chitosan-gelatin 1:1) blends. A concentration of 0.5% (GA v/w, PA w/w) was compared, using hydrogel setting times and cell response as means of evaluation. The evaluation showed that the setting time of those hydrogels treated with GA was shorter (20 min) compared to those treated with PA (4hrs at 4°C); however, the increase in cell number rate was 3 times more favourable for those hydrogels treated with PA (data not shown), making PA more suitable to fit the aims of this project. Next, polymer concentrations were tested. To maintain consistency with previous evaluation, a 1:1 ratio was maintained, 3%, 4% and 5% w/v concentration were evaluated comparing setting times of each blend. 3% 1:1 ChG was chosen, because 4% and 5% blends were shown to be very viscous, hard to pipette and trapping air bubbles leading to uncontrolled hydrogel porosity (data not shown). Hydrogels using purified chitosan and non-purified chitosan were manufactured, and mechanical properties and cell response were compared from both groups. No mechanical properties were observed to be affected, and a significant decline on cell number was detected for those hydrogels using the

purified chitosan – for this reason and to avoid adding additional variation to the study, it was decided to use chitosan, as it was without subjecting it to a purification process; a single batch was used in this project, so further validation was not needed.

The first chitosan-gelatin blend (FM1) was made from 3% chitosan dissolved in 2% acetic acid solution and stirred overnight at room temperature. Three percent gelatin was dissolved in sterile distilled water (DSW) at 50°C then incorporated to the chitosan solution. PA was used to cross-link ChG blends by the bulk cross-linking method. ChG solution was divided in 3 parts 5ml of PA solution at 0.5%, 2.5%, and 5% dissolved in PBS were added to each part of the chitosan-gelatin mixture described above. This solution was stirred for 1h and then cast on glass [206], dried hydrogel surfaces were neutralized with 1M NaOH [269]. The resulting hydrogel proved to support cell culture but performed poorly compared to tissue culture plastic (TCP) (Figure 4.1).

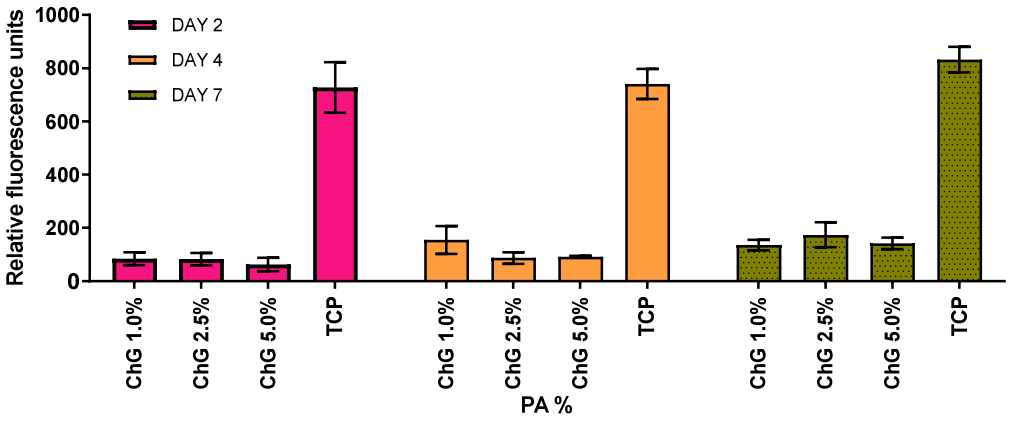

Figure 4. 1 NIH 3T3 Cell response to 400µm thick ChG-PA hydrogels cross-linked at different concentrations using fabrication method 1compared to TCP.

The amount of acetic acid proved to be too high, since conditioning media kept showing signs of acidity (changes in colour from red to yellow) even after the sample had been washed 3 times. 1MNaOH has also proved to be toxic at high concentrations [270]. To

reduce the amount of acetic acid to the minimum needed to dissolve chitosan and to find a suitable dilution factor and treatment time for the NaOH neutralization solution were the goals to be achieved by **the second fabrication method (FM2).** After several trials, it was found that a 0.6% acetic acid solution at 37°C was enough to fully dissolve chitosan over a period of 2hrs. 1MNaOH used to neutralize the samples surface was diluted at 30% and left to act on top of hydrogels for 1hr. Cell response improved, but the results were still significantly below TCP. After several attempts (data no shown) it was observed that bulk pH had a significant effect on cell response and integrity of the hydrogel (Figure 4.3). However, decreasing acetic acid concentration lower than 0.6% led to a very viscous chitosan solution: very hard to handle and not suitable for repeatable pipetting. For the third fabrication (FM3) method additional alternatives to increase the pH of the bulk were explored. Chitosan is soluble at low pH with its amine groups reminding protonated at pH lower than 6. As the pH increases above 6, the amine groups become deprotonated and chitosan becomes insoluble again [271]. So, ensuring full incorporation of chitosan, gelatin and PA before increasing pH over 6 was critical for the integrity of the hydrogel. This phenomenon also allowed an additional pH cross-linking reaction, as the pH of the incorporated blend was increased over 6 after the mix was fully blended. This became an important constraint addressed by the sequence of the final fabrication method (FM3). Gelatin was dissolved in SDW at 50°C for 25 min; temperature was then decreased to 37°C and 0.6% acetic acid and chitosan powder was added to the gelatin solution. pH at this stage varied from 4.5 to 4.7; once the chitosan fully dissolved (2hrs approx) PBS+HEPES (1:1to SDW) was added to the solution which rises pH to a range of 5.0 to 5.8, enough for the PA reagent to remain stable while reacting with the polymer, according to Slusarewicz et al. [230] PA displays stable activity between pH 5 and 9 inclusive, and for chitosan to stay soluble, the solution was

stirred magnetically until a change in colour (pink to dark purple as a result of pH change) was observed. A coagulation medium (1MNaOH) was then added to the mix until the bulk pH 6.5 was achieved, allowing an additional pH dependant cross-linking of the hydrogel. Also, the alkaline NaOH treatment concentration was decreased to 0.1M NaOH by extending treatment time to 120min. A cross-linker concentration of 2.5% PA was chosen to compare among the different fabrication methods, as was this concentration providing better results in early attempts. Results presented on Figure 4.2 A-D show the efficacy of **fabrication method 3 (FM3)** compared to the previous attempts. NIH 3T3 cells (Fig 4.2 A and C) and MG63 (Fig 4.2 A and C) were used to compare different cell type responses to the hydrogels. Both cell types responded favourable to FM2 and FM3. FM3 surpassed even the cell metabolic activity achieved on TCP for both cell types (Fig 4.2 A and B). The hydrogels were also compared to their non-cross-linked version and to the polymers on their own. The cell growth was higher for FM3 for both cell types. Table 4.1 shows a summary of the different formulations and their components. Figure 4.3 shows the preparation and post-cross-linking processing of each of the 3 fabrication methods (FM) and images of the end-product appearance.

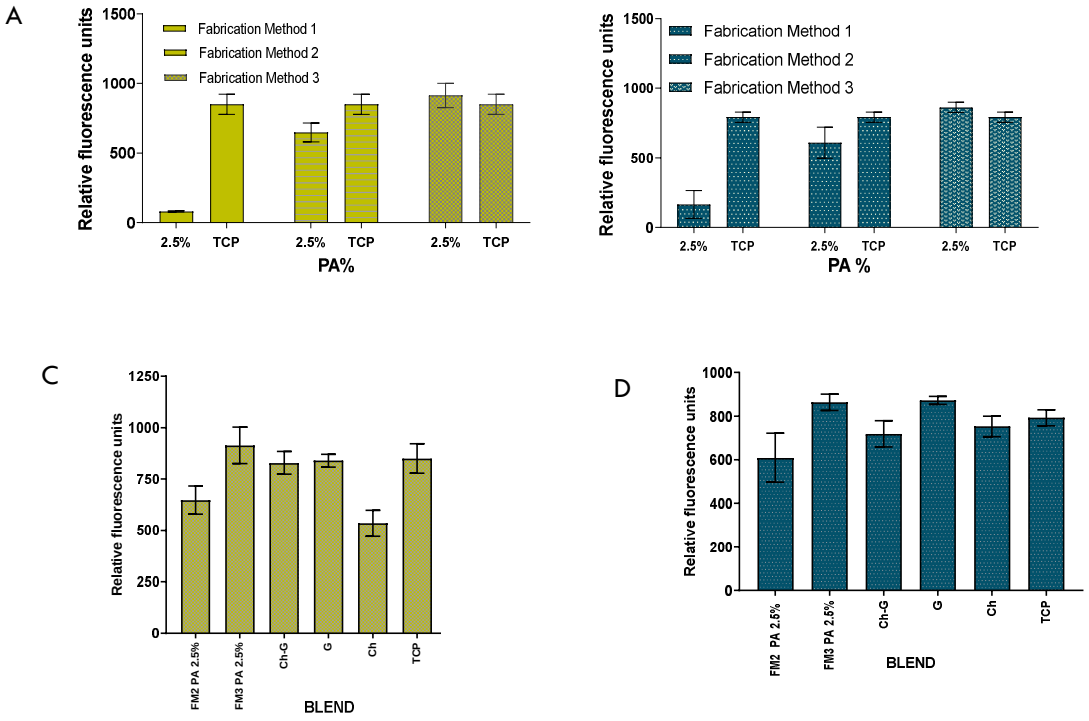

Figure 4. 2 Cell response to hydrogel fabrication methods A NIH 3T3 and **B** MG63 cell response to 400µm thick ChG-PA hydrogels cross-linked at 2.5% concentrations using fabrication method (FM) 1 to 3 compared to tissue-culture plastic (TCP). **C** NIH 3T3 and **D** MG63 cell response to 400µm thick ChG-PA, ChG, G, Ch hydrogels compared to tissue-culture plastic (TCP).

Table 4. 1 ChG_PA formulation development.

Formulation	Chitosan w/v%	Gelatin w/v%	PA w/w%	Solvent	Acetic acid	Coagula-tion media	Alkaline treatment (AT)	Cell growth vs TCP
FM 1	3	3	1.0,2.5,5.0	SDW	2%	NO	1M NaOH	Poor
FM 2	3	3	2.5	SDW+PBS +HEPES	0.60%	NO	0.1M NaOH	Similar
FM 3	3	3	2.5	SDW+PBS +HEPES	0.60%	1M NaOH	0.1M NaOH	Higher

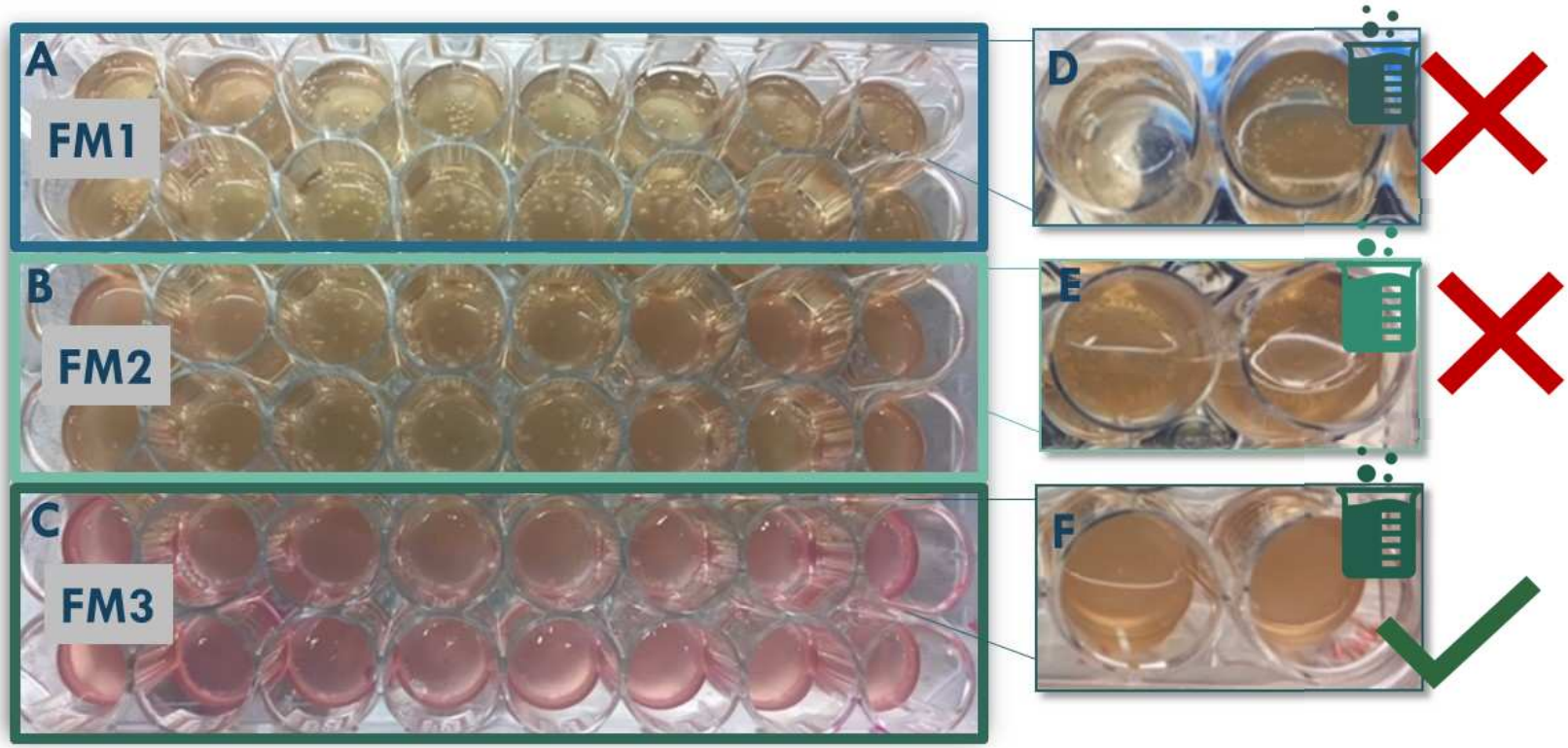

Figure 4. 3 ChG 2mm thick hydrogel samples preparation and post-cross-linking processing. **A** Fabrication Method 1(FM1) 3% ChG blend dissolved in 2% acetic acid solution and cross-linked with 2.5% PA. Samples leach acidic residues which turned pink media yellow. **B** Fabrication Method 2(FM2)3% Chitosan was dissolved in 0.6% acetic acid solution and incorporated to gelatin which was previously dissolved in PBS+HEPES and then cross-linked with 2.5% PA pH of the bulk reach 5 to 5.8 but once set samples still leached acidic residues which slightly turned pink media yellow. **C** Fabrication Method 3(FM3) 3% Chitosan was dissolved in 0.6% acetic acid solution and incorporated to gelatin which was previously dissolved in PBS+HEPES and then cross-linked with 2.5% PA the mix was left stirring overnight to fully blend and then 1M NaOH was drop ways added until the pH of the bulk reached 6.5 then samples were cast once set and washed acidic residues were not observed (pink media did not changed colour) **D** FM 1 thick samples showed a not cured highly absorbent liquid core, that burst as days passed. **E** FM 2 thick samples still showed to decrease the liquid core phenomena, however some of the samples still burst with time. **F** For FM 3 samples, the additional pH dependant cross-linking provided by the coagulation media (1M NaOH) decreased the leaching of acidic residues, and improved hydrogel integrity for over 60 days (data not shown). Liquid core was not a problem for this blend and none of the samples have been observed to disintegrate or burst with time.

Hydrogel Characterisation

Porosity

Figure 4.4 shows the observed differences on the porous morphology of the cross-linked hydrogel as cross-linker content was varied.

Chitosan-gelatin ChG hydrogel produced following formulation (Table 4.1 FM3): 3 were characterised in terms of pore morphology, size, interconnectivity and overall porosity.

Cryo FIB SEM micrographs of the visible milled face of the ChG hydrogel samples fabricated from different cross-linker contents were investigated, and shown in Figure 4.4 A-D, the obtained pore size as well as porosity are summarized in Table 4.2. Hydrogel exhibits numerous micro-pores uniformly distributed among the substrates. The interconnected and porous structures could be found in all fabricated samples. Observed marked differences in the pore shape, wall thickness and size across the range of micro to nanometre pore sizes. Evidently noted and statistically significant were the differences among pore size, which was inversely correlated with the hydrogel cross-linker content. For pure ChG hydrogels (0.0% w/w), the pores were bigger in size formed out of thin wall structures, while as the PA content increased, the thicker pore wall structures became more clearly observed (see in Figure 4.4 D). Table 4.2 shows that the pore sizes of the cross-linked ChG hydrogel were between 0.34 µm and 0.17 µm, and the porosity ranged from 60% to 40% as cross-linker content increased. Results shown significant differences on pore size figure 4.4.E and pore size variation Figure 4.4F among the cross-linked hydrogels.

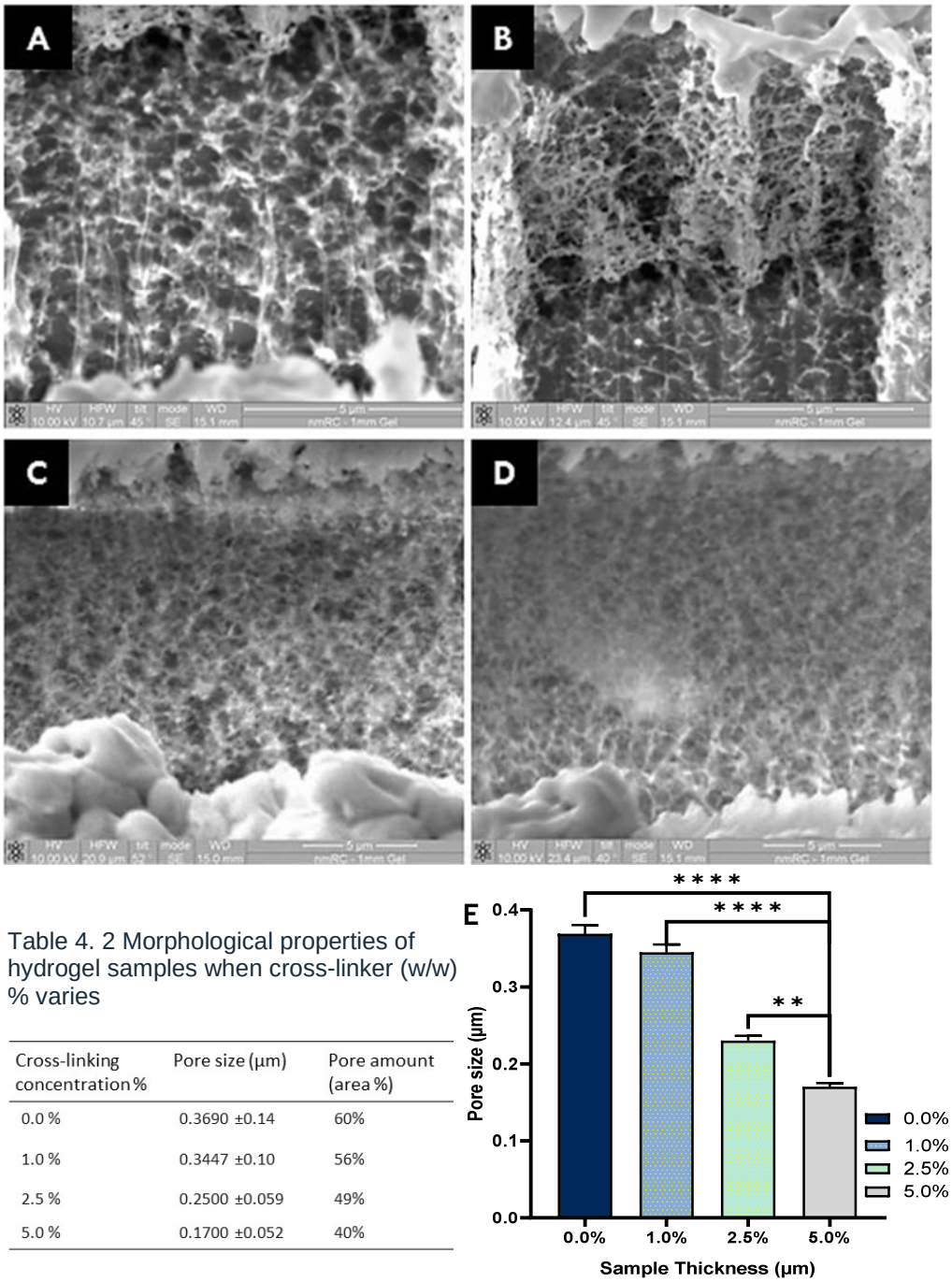

Table 4. 2 Morphological properties of hydrogel samples when cross-linker (w/w) % varies

Cross-linking concentration %	Pore size (µm)	Pore amount (area %)
0.0 %	0.3690 ±0.14	60%
1.0 %	0.3447 ±0.10	56%
2.5 %	0.2500 ±0.059	49%
5.0 %	0.1700 ±0.052	40%

Figure 4. 4 Effect of cross-linking concentration on matrix morphology. FIB-Scanning electron micrograph of ChG hydrogel discs crosslinked with PA A 0.0%, **B** 1.0% **C** 2.5% **D** and 5.0% **E** Porosity properties of ChG gels was quantified from FIB-Scanning electron micrograph analyses. Total pore number was determined for micro-, interconnecting- and micro-pores. (n=5 for each condition). Data shown as mean±SD.

Stability in water

While chitosan is insoluble in water (pH7), gelatin is soluble; however, both are soluble in solutions below pH4.7. Figure 4.5 shows the degree of stability obtained from non-cross-linked chitosan-gelatin (ChG) and alkaline treated chitosan-gelatin (AT-ChG), PA cross-linked chitosan-gelatin at different cross-linked concentrations (PA_%), and alkaline treated PA cross-linked chitosan-gelatin at different theoretical cross-linked concentrations (AT-PA_%) hydrogels in different pH contexts (Figure 4.5 A,C,E non-treated, B,D,E alkaline treated).

The assessment of the stability of the different hydrogels shows that non-cross-linked chitosan-gelatin (ChG) hydrogels, both non and alkaline treated with 0.1M NaOH are very unstable in acidic solutions (pH 4): 95% and 80%, mass loss by day 14 (Figure 4.5 A) was reported. This is because both chitosan and gelatin are soluble in low pH. However, the stability of these hydrogels increases as the acidity of the solution decreases (pH 7, pH 10) an explanation could be that because gelatin remains soluble at pH over 4. The hydrogels cross-linked with PA produced noticeable increases in stability for the three different pH solutions, even at the lowest cross-linker concentration (PA_0.5%). The effect of cross-linking on stability is more discrete at pH4. Alkaline treatment (AT) of the hydrogel surface showed a noteworthy effect on the construct's stability behaviour. Non-alkaline treated hydrogel showed a more significant pH sensitivity compared to the treated combinations. Alkaline treated (NaOH) hydrogels exhibited a significantly more stable behaviour compared to their counterparts, for most of the combinations, making the cross-linker % stability correlation increase. Mass integrity remained intact for 90% of the samples cross-linked with PA and alkaline treated (Figure 4.5 B, D and F). The alkaline treated samples cross-linked at 2.5 and 5 PA% showed to be the combinations that remained intact for the whole extent of the

experiment at all the pHs. Observation from experiments using the hydrogels (data not shown) exhibiting these combinations continued without apparent change for over 60 days.

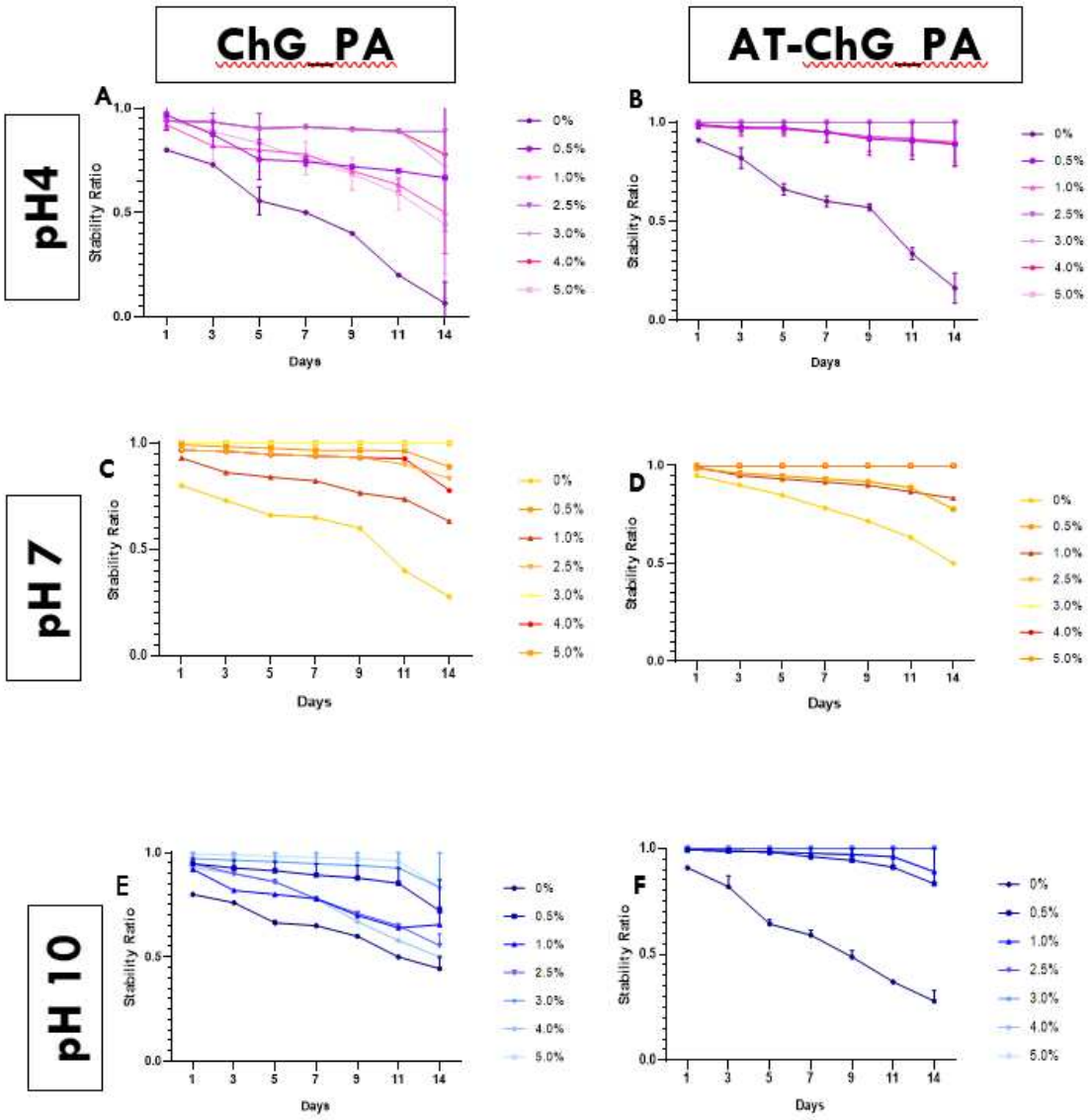

Figure 4. 5 The stability of the hydrogels in water the stability of the hydrogels was evaluated at different pHs at room temperature for 14 days. (A) ChG and PA_% at pH4 (B) AT-ChG and AT-PA_% at pH4(C) ChG and PA_% at pH7 (D) AT-ChG and AT-PA_% at Ph7(E) ChG and PA_% at pH10 (F) AT-ChG and AT-PA_% at Ph10. Stability of the hydrogel increased with the introduction of cross-linker and variability decreased for those samples alkaline treated with 0.1M Na OH.

The stability of the hydrogels evaluated at different pHs at the conclusion of the experiment Figure 4.6. shows that the stability of the hydrogel increased with the introduction of cross-linker, and variability among combinations decreased once the samples were alkaline treated with 0.1M Na OH (Figure 4.6 A-C, a-c). This effect was more evident for the acidic solutions.

Swelling

The swelling ratio of ChG hydrogels cross-linked with PA and alkaline treated with sodium hydroxide (0.1 NaOH) at different pH is shown in Figure 4.7. A to G. Non-cross-linked ChG hydrogels show the highest potential for swelling at the first 2hrs, however they started to present weight losses after 96hrs. PA cross-linked hydrogels showed lower potential for swelling, this being decreased as the theoretical cross-linking density increased from 2.5% to 4%. In general, the swelling ratio of materials decreases as the degree of cross-linking increases [272].

However, the reduction of swelling is not proportional to the extent of cross-linking, e. g. this tendency was interrupted as the theoretical concentration reached 4% which also reported weight losses after 96hrs. Increases in potential for swelling were significantly different in samples soaked in acidic solutions for this combination. The comparison between groups at pH7 can be evaluated on Figure 4.8.

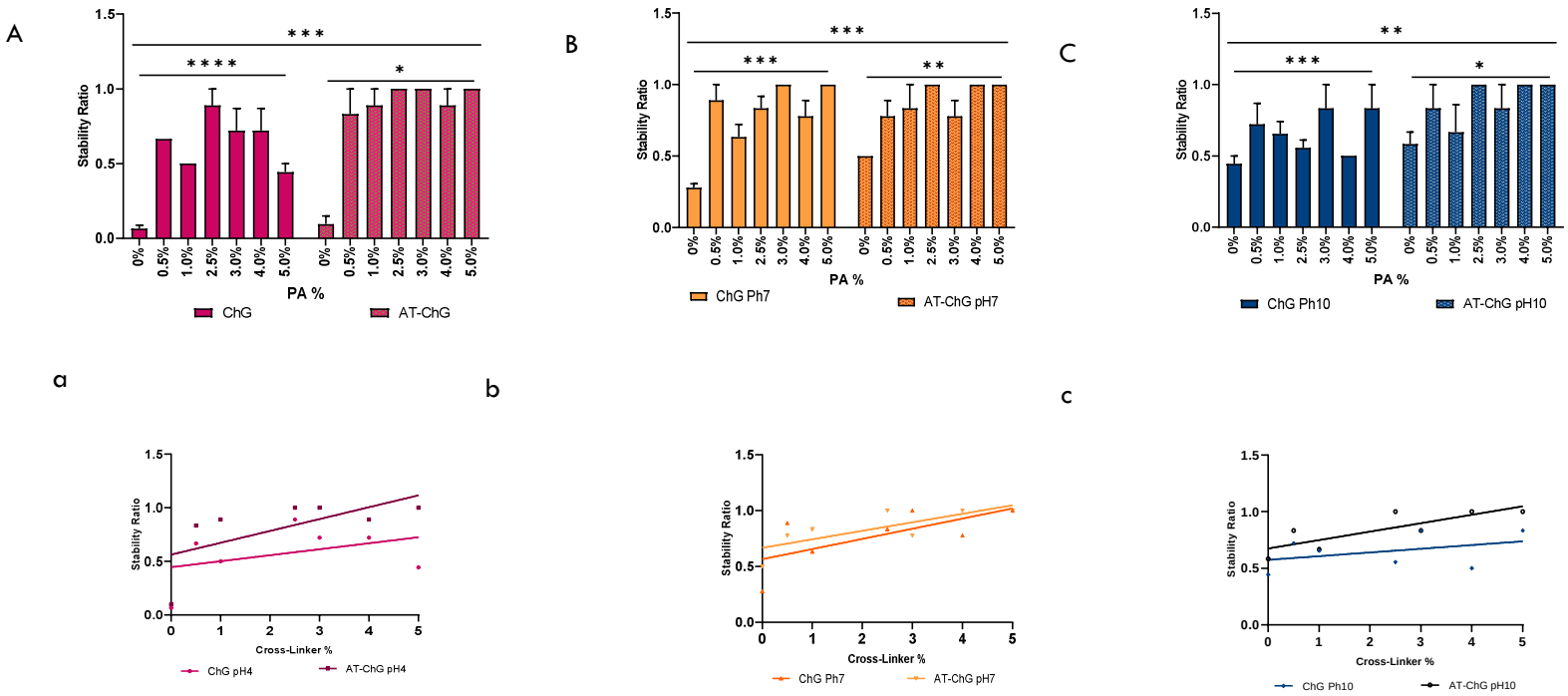

	pH 4		pH 7		pH 7	
	ChG	AT-ChG	ChG	AT-ChG	ChG	AT-ChG
Equation	Y = 0.05585*X + 0.4451	Y = 0.1107*X + 0.5623	Y = 0.09097*X + 0.5651	Y = 0.07622*X + 0.6670	Y = 0.03273*X + 0.5744	Y = 0.07452*X + 0.6749
R^2	0.1508	0.4063	0.45	0.6074	0.1534	0.6732

Figure 4. 6 The stability of the hydrogels in water the results of the stability of the hydrogels at different pHs and room temperature at day 14 for **A** ChG and AT-ChG and AT-ChG and AT-PA_% at pH4 **B** ChG and PA_% and AT-ChG and AT-PA_% at Ph7 **C** ChG and PA_% and AT-ChG and AT-PA_% at Ph10. And fitting lines for each combination **a** ChG and AT-ChG and AT-ChG and AT-PA_% at pH4 **b** ChG and PA_% and AT-ChG and AT-PA_% at Ph7 **c** ChG and PA_% and AT-ChG and AT-PA_% at Ph10.

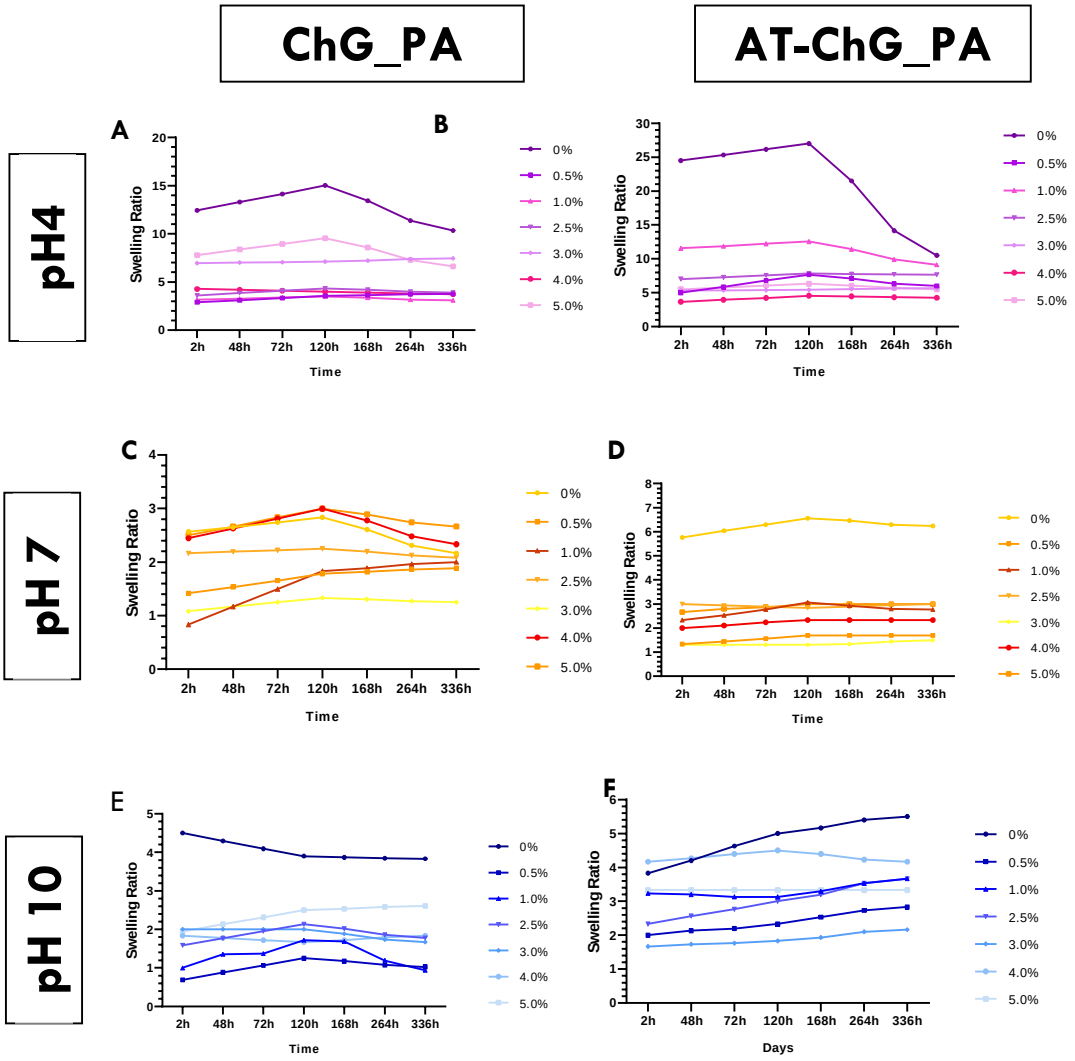

Figure 4. 7 The hydrogel swelling behaviour. The swelling behaviour of the hydrogels was evaluated at different pHs at room temperature for 14 days. (A) ChG and PA_% at pH4 (B) AT-ChG and AT-PA_% at pH4(C) ChG and PA_% at pH7 (D) AT-ChG and AT-PA_% at Ph7(E) ChG and PA_% at pH10 (F) AT-ChG and AT-PA_% at Ph10. Swelling of the hydrogel decreased with the introduction of cross-linker and further swelling reduction and variability decreased for those samples alkaline treated with 0.1M NaOH.

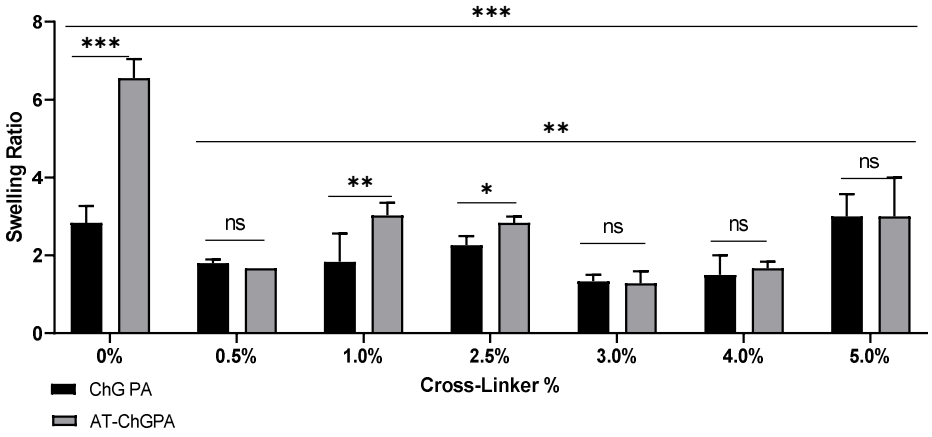

Figure 4. 8 The hydrogel swelling behaviour. The swelling behaviour of the hydrogels was evaluated at different pHs at room temperature at 96hrs. ChG significance comparison against PA_% at pH7. Swelling of the hydrogel decreased with the introduction of cross-linker and further swelling reduction and variability decreased for those samples alkaline treated with 0.1M NaOH.

Water Content

Water content of ChG hydrogels cross-linked with PA and alkaline treated with sodium hydroxide (0.1M NaOH) AT was evaluated, results are shown in Figure 4.9.

No significant variation in water absorption was observed for non-alkaline treated ChG_PA and alkaline treated AT-ChG_PA samples weight respectively, with a water content average of 130% and 265%, respectively. Interestingly, differences of 1- and 2-folds were observed among samples of the same cross-linker content, and alkaline and non-alkaline treated (Figure 4.9). Differences were more evident as the amount of cross-linker was increased, therefore the kinetics of water absorption showed to be significantly different. The water content was invariably higher for those samples alkaline treated with sodium hydroxide (0.1M NaOH). A similar pattern also existed for the stability in water and swelling ratio curves (Figure 4.5 and Figure 4.7) showing that this behaviour remains stable over time.

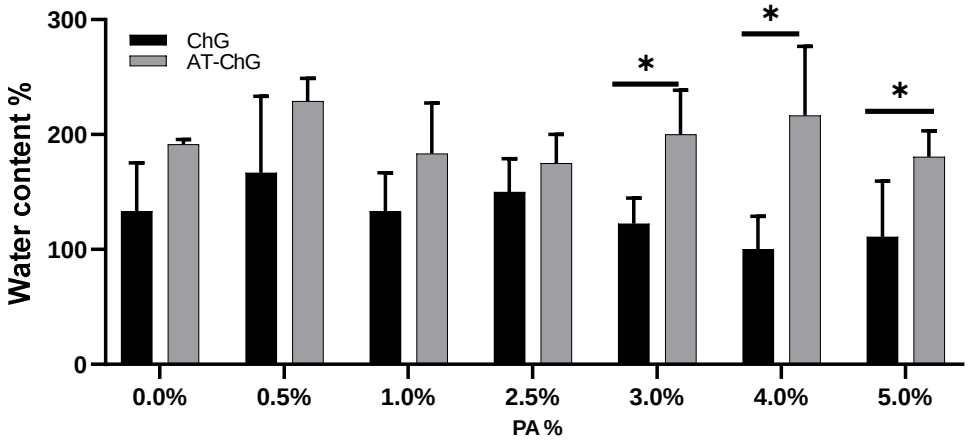

Figure 4. 9 The Water Content was evaluated at room temperature at 35min. ChG significance comparison against PA_% at pH7. Data shown as mean±SEM

Gelation Time

Hydrogels were prepared using formulation three (Table 4.1 FM3) to study the gelation behaviour of the hydrogel at room temperature at different PA concentrations ranging from 0% to 5% (w/w). Gelation times of the ChG hydrogels at different PA concentrations are given in Table 4.3. In general gelation time of the hydrogel decreased as concentration of PA increased. ChG samples without cross-linker took longer to set (15 – 44 min) and reported the highest variation among samples of the same kind. Gelation time exponentially decreased as the cross-linker was introduced to the blend. Except for 2.5 and 3.0_PA% which reported no significant differences, significant differences were found among each combination Figure 4.10. Another finding was that the variation among samples also decreased as cross-linker concentration increased; samples showing higher consistency on gelation times from 2.25% onwards as shown in Figure 4.10 D and Table 4.3.

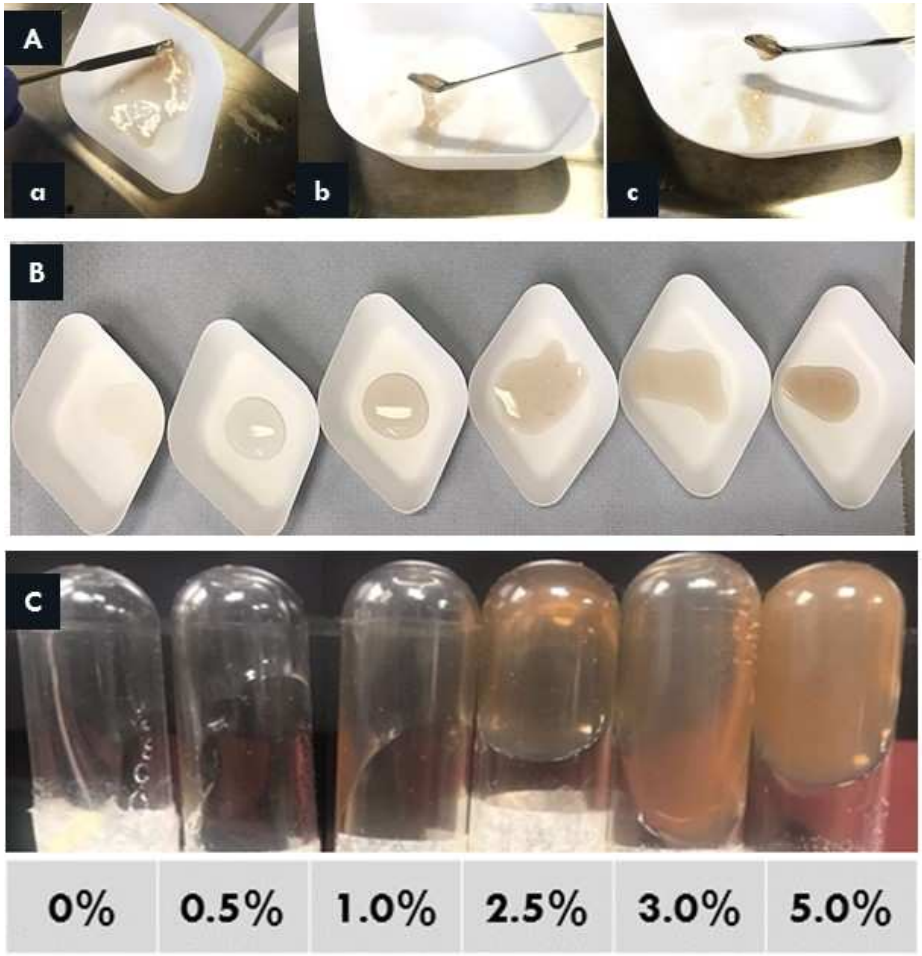

Table 4. 3 AT-ChG hydrogel gelation time summary varying cross-linker

PA% (w/w)	Time (min)			
	Min	Max	Mean	SD
0%	15	44	**23**	7.21
0.5%	14	47	**21**	6.66
1.0%	14	33	**15**	2.60
2.25%	8	13	**11**	0.57
2.5%	7	12	**8**	0.62
2.75%	7	8	**8**	0.34
3.0%	6	8	**6**	0.27
4.0%	3	7	**5**	0.98
5.0%	3	3	**3**	0.27

Figure 4. 10 Digital images of A a-c time lapse images of the blend from liquid to hydrogel **B** Samples: 1ml hydrogel solution at 0 to 5.0 PA concentration% at room temperature **C** Samples in testing tubes upside down at room temperature after 1hr of being cast.

Hydrophobic and hydrophilic properties of ChG hydrogels.

In order to explore the correlation between the microstructure of PA cross-linked ChG hydrogels and its surface property, the hydrophobic-hydrophilic properties of ChG hydrogels have been examined by water contact angle (WCA) tests as a function of PA%, and results can be observed in Figure 4.11. WCA is a good indicator of the degree of hydrophilicity of hydrogels. Generally, WCA decreases when surface hydrophilicity is higher. It can be seen that the addition of PA causes the initial WCA to decreased compared with no PA cross-linked hydrogels, which is likely due to the hydrophilic nature of Proanthocyanidin [273] property, that decreases as PA is increased, making the hydrogel more hydrophobic as cross-linker concentration increases. The hydrophobicity of the hydrogels remained constant with no significant difference until a concentration of up to 2.5 PA%, increasing exponentially for 3.0 PA% onwards, Figure 4.11A. Furthermore, analysis of the surface wettability of the alkaline-treated hydrogels were studied in detail (Figure 4.11B). It was found, compared with those not alkaline-treated, that the hydrophilicity of hydrogels Proanthocyanidins cross-linked and alkaline-treated improved, showing a decrease of ≈10° average for concentrations in the range of 0.5 to 2.5 PA%. Samples in the range of 1.0 to 2.5 PA% optimised WCA for alkaline-untreated and -treated samples, producing samples hydrophilic. Table 4.4 Table 4.4 ChG hydrogel WCA mean and standard deviation summary.

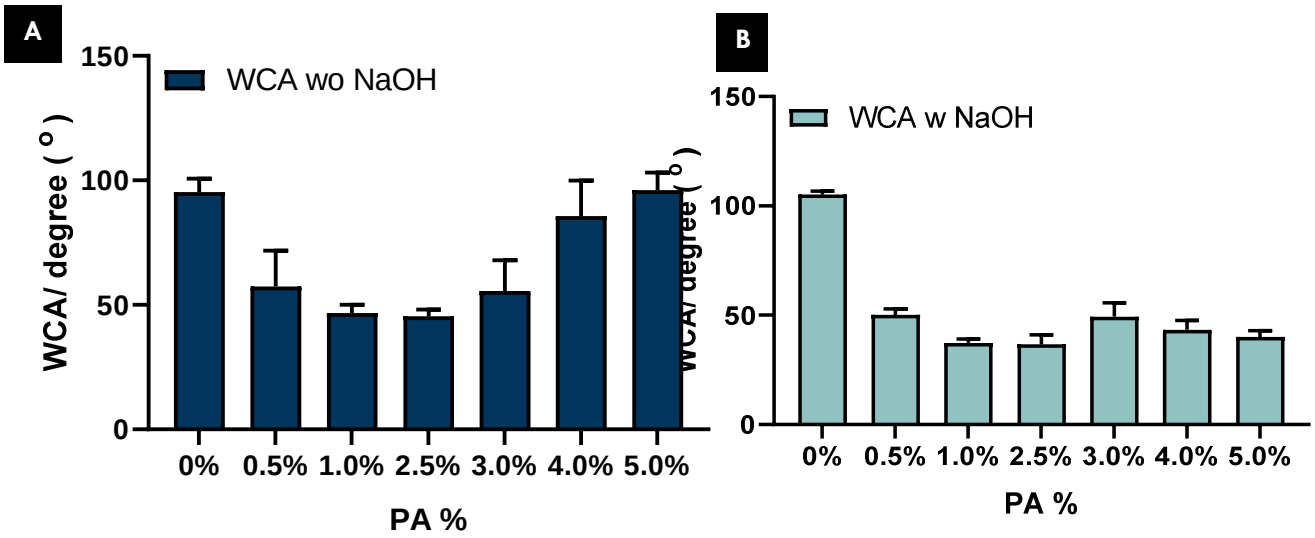

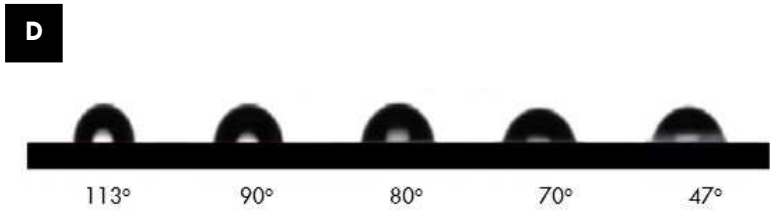

Table 4. 4 ChG gel WCA mean and standard deviation summary.

	WCA wo NaOH		WCA w NaOH	
	Mean	SD	Mean	SD
0%	95.33	9.29	97.00	8.54
0.5%	57.33	25.01	50.00	5.00
1.0%	46.67	5.77	37.33	3.06
2.5%	45.33	4.62	36.67	7.64
3.0%	55.53	21.44	49.33	11.02
4.0%	85.53	25.02	43.33	7.64
5.0%	96.00	12.17	40.00	5.00

Figure 4. 11 Water contact angle (WCA) of chitosan-gelatin (ChG) / Proanthocyanidin (PA) hydrogels as a function of PA%. The data were expressed as mean ± SEM.

It was also observed that alkaline NaOH concentration and treatment length affected the wettability of the samples (Figure 4.12). ChG_2.5 PA% hydrogels surface-neutralized with 4 different NaOH concentrations were studied at 2 different timepoints, see Table 4.5. Increasing the concentration of the 1M NaOH in the aqueous solution decreases contact angle, as does increasing the treatment duration. Also, variability among samples were observed to decrease as NaOH concentration and treatment length of the neutralize solution was increased. 1M NaOH produces samples with the highest hydrophilicity independent of treatment length. The 0.1M concentration at 120 min length produced high hydrophilicity.

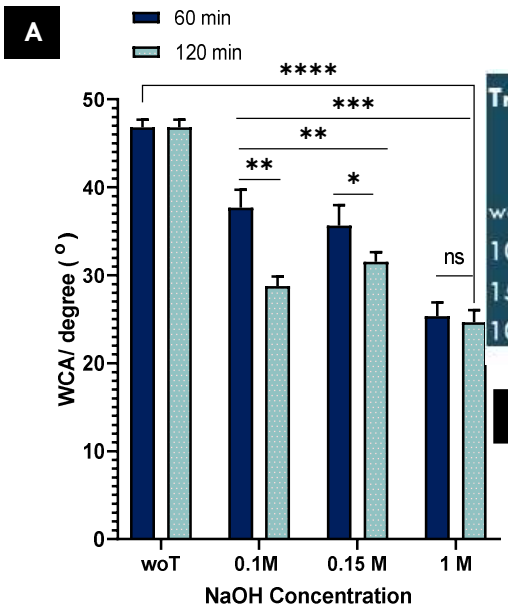

Table 4. 5 ChG hydrogel WCA of gels alkaline treated.

Treatment NaOH (v/v)	60 min		120 min	
	Mean	SD	Mean	SD
woT	46.80	0.90	46.82	0.89
10.0%	37.67	2.04	28.78	1.10
15.0%	35.65	2.31	31.51	1.13
100%	25.36	1.53	24.64	1.39

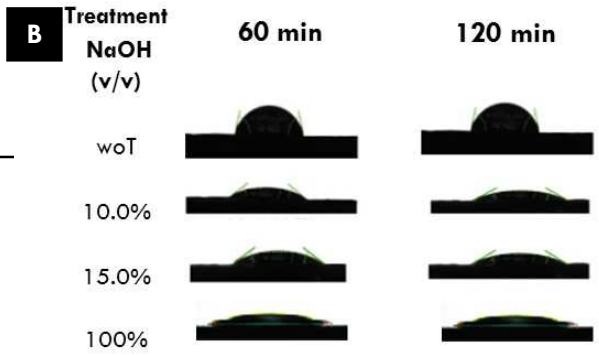

Figure 4. 12 Water contact angle (WCA) of chitosan-gelatin (ChG)/ Proanthocyanidin (PA) hydrogels as a function of PA%. The data were expressed as mean ± SD.

Mechanical properties of chitosan-gelatin based hydrogels.

To examine how cross-linker content affects the elasticity of the ChG hydrogels cross-linked with PA, 1:1 hydrogel ChG. The compositions range was chosen, as it has non cytotoxic effects, as previously reported by Kim et al. [206]. It can be observed that controlling the content of the cross-linker in the hydrogels has a significant effect on the hydrogel compressive modulus (Figure 4.13). The compressive modulus of the cross-linked ChG hydrogels was monitored performing compression test in an Instron machine. The stress-strain curves of hydrogels tested in unconfined compression showed resistance to failure to brake to increase as PA content increased, up to a concentration of 3%; after this the hydrogel becomes stronger, it breaks faster (Figure 4.13A). Compressive modulus response to cross-linker content is summarized in Table 4.6; hydrogel is shown in Figures 4.13 B which clearly illustrates that the compressive modulus of the ChG increased with increasing concentrations of PA%, thus indicating a higher resistance of the ChG matrices to deformation with an increasing content of cross-linking. Stronger structures of ChG hydrogels were obtained with increasing concentrations of PA for the same concentration of polymer. It was also observed that variation between samples were stronger on samples of high PA% content, Figure 4.13B suggesting unreactive PA particles in the hydrogel as content rises above 2.5 PA%. It was also observed that on alkaline-treated samples, the effect of PA% on sample compressive modulus was amplified, and standard variations diminished (Figure 4.13B).

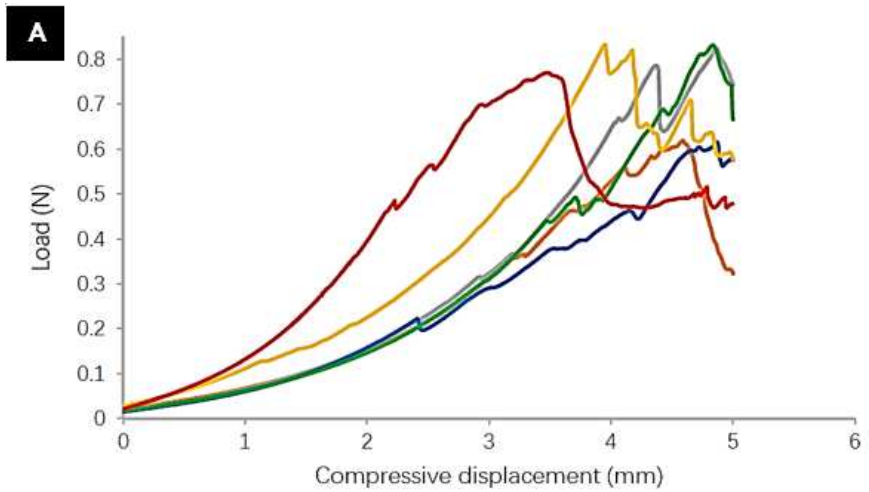

Table 4. 6 ChG hydrogel Compressive Modulus of gels modified by different PA%.

PA%	No-Alkaline Treated MPa	SEM	Alkaline Treated MPa	SEM
1.0%	0.03218	0.002	0.04908	0.007
2.5%	0.09883	0.008	0.1119	0.014
5.0%	0.26110	0.012	0.3187	0.019

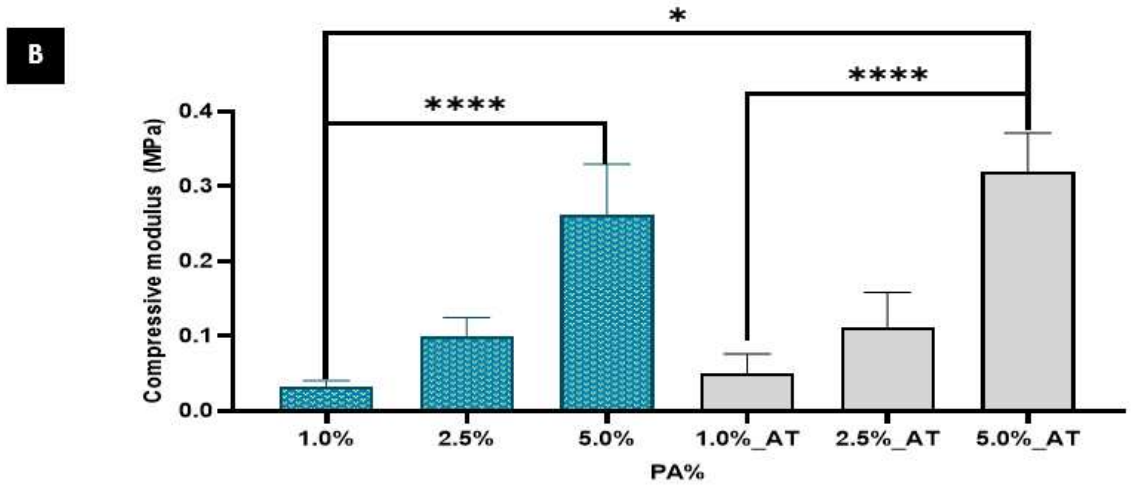

Figure 4. 13 Hydrogel stiffness A Failure to break**; l**oad (N) against Compressive displacement (mm) curves with different PA%). **Bb** Modulus (MPa) against PA% All the samples were stored in fridge (4°C). The data were expressed as mean ± SEM.

X-Ray diffraction (XRD)

The presence of intermolecular interactions among the chitosan-gelatin ChG_PA hydrogel components was confirmed by X-ray diffraction (XRD) analysis (Figure 4.14). The XRD pattern of pure chitosan-gelatin ChG hydrogels showed two broad peaks at 2θ = 8.0°and 20.0°, corresponding to the semi-crystalline nature of chitosan. The peaks are wider when compared to the XRD pattern of pure chitosan [274], which should be caused by the presence of non-crystalline gelatin that reduces the crystallinity of the blending. The diffraction peak at 2θ 8.0° corresponded to the triple-helix crystalline structure of gelatin, and the relatively regular crystal frame of chitosan [99, 275]. A broad peak centred at 2θ 21° matched to the amorphous structure of chitosan and gelatin [221].

All the hydrogels produced a diffraction pattern of a semi-crystalline to an amorphous phase. With the addition of PA into pure chitosan-gelatin hydrogels, peak at 2θ 8.0° moves to a hump at ~2θ =11°, still corresponding to the semi-crystalline structure of gelatin and chitosan; the intensity of XRD peaks decreased and gradually increased back again (Figure 14.14B), displaying a diffraction pattern of an amorphous phase with the background raised at around 2θ = 21°, demonstrating the behaviour of PA within the matrix of the hydrogels.

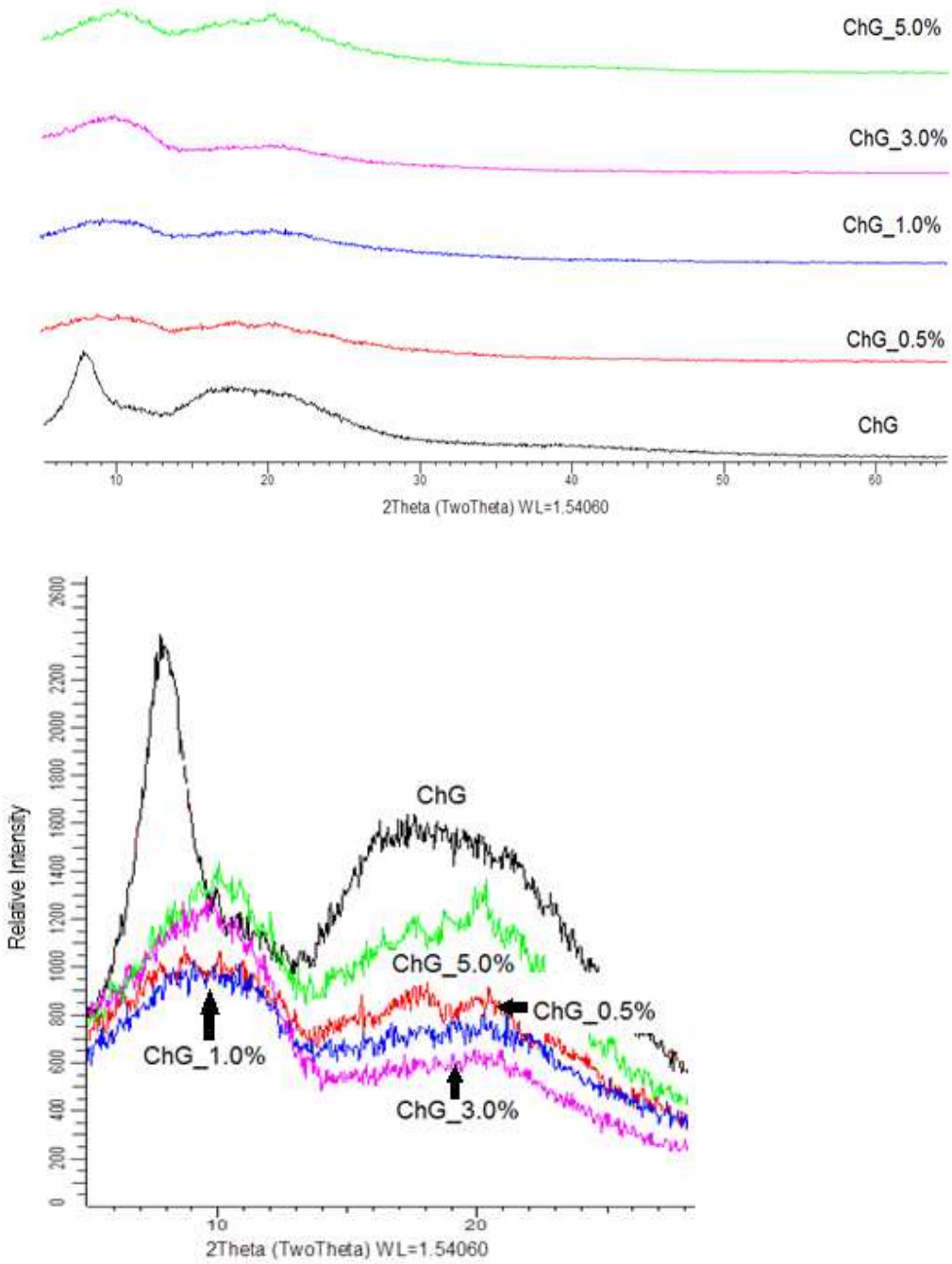

Figure 4. 14 XRD Hydrogel stiffness Load (N) against Compressive displacement (mm) curves with different PA%. All these samples were stored in fridge (4°C). Modulus (MPa) against PA% curves. All the samples were stored in fridge (4°C). The data were expressed as average ± standard deviation.

X-ray photoelectron spectroscopy (XPS)

Figure. 4.15A-F shows the qualitative XPS spectra of pure chitosan-gelatin ChG hydrogel (Figure4.15A) and those after modification with proanthocyanidins PA (Figure 14.15B-F). All samples were neutralised with 0.1M NaOH solution for 120min. ChG hydrogels presented 4 main elements as shown in Figure 4.15. The binding energies (eV) are 285.0 eV for C, 531.0 eV for O, 1072 eV for Na and 402 eV corresponding to nitrogen. Apart from the predominant C and O, which do not show significant atomic concentration % change (Table 4.6), among samples the additional two partly predominate elements, Na (1072 eV) and N (402 eV), are observed to significantly change in shape, intensity and % ($p>0.05$) as the amount of Proanthocyanidin (PA) was increased compared with the original pure ChG hydrogels. The changes on Na appearance on the surface could be attributed to the hydrophilicity of the hydrogels improving once cross-linked with PA, and gradually decreasing as PA was increased, facilitating the absorption of the Na added to alkaline-treat the hydrogel surface. Furthermore, the peak at 402 eV corresponded to nitrogen results from the abundant amino and amide groups that are widely present in both Chitosan and Gelatin.

Table 4. 6 ChG hydrogel main elements atomic concentration % summary.

	Atomic concentration %			
	C 1s %	O 1s %	N 1s %	Na 1s %
ChG	63.95	20.95	8.38	3.88
ChG_0.5%	62.13	22.66	5.43	0.67
ChG_1.0%	61.29	21.22	6.91	1.39
ChG_2.5%	60.90	22.92	7.37	1.50
ChG_3.0%	60.26	23.93	7.24	1.73
ChG_5.0%	60.01	24.29	7.62	1.89

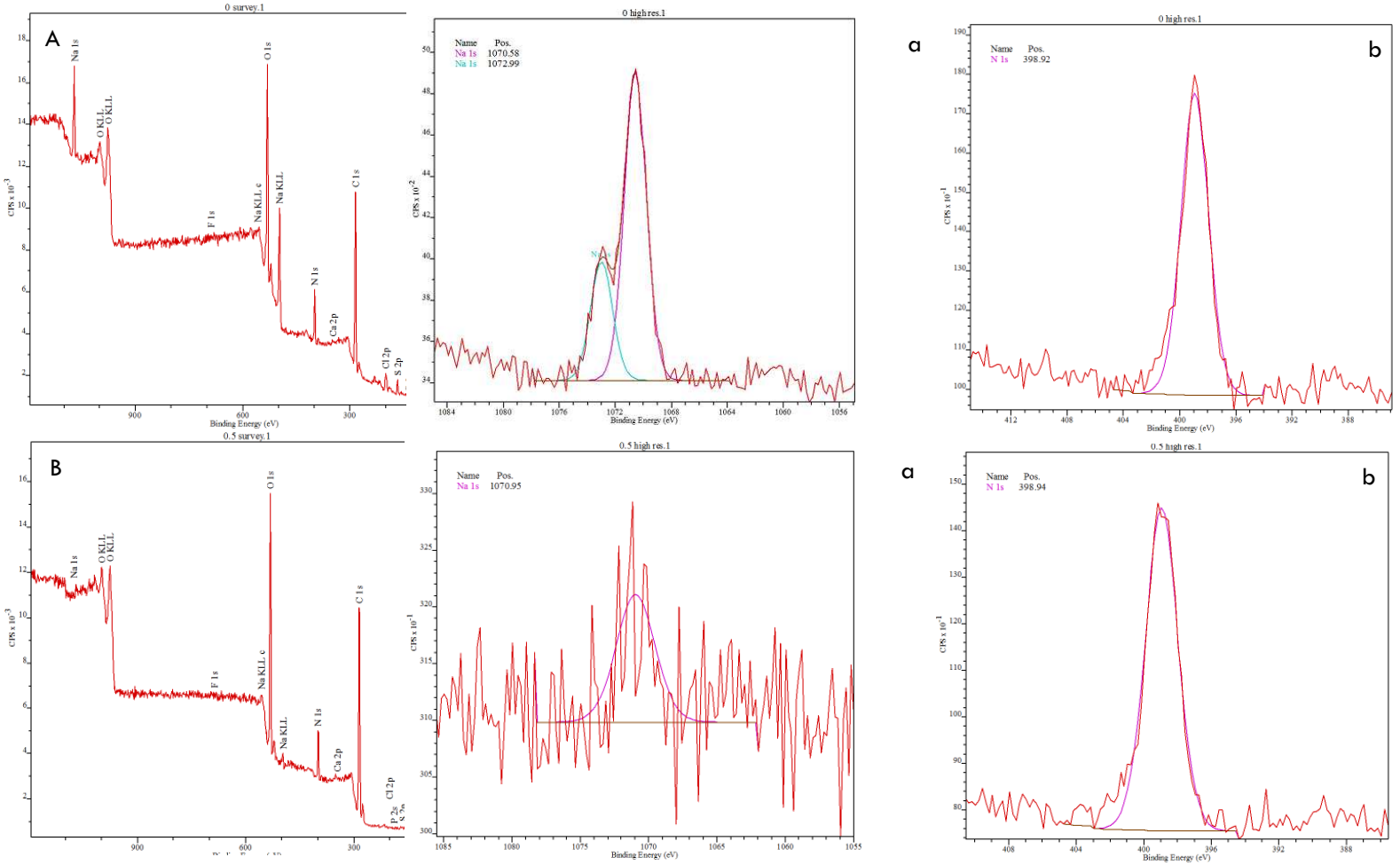

Figure 4. 15 A XPS spectra of **A** pure ChG hydrogel. a) ChG Na peak; A.b) ChG N peak **B XPS** spectra of ChG cross-linked with 0.5% PA hydrogel: B.a) ChG_0.5% PA Na peak ; B.b) N peak.

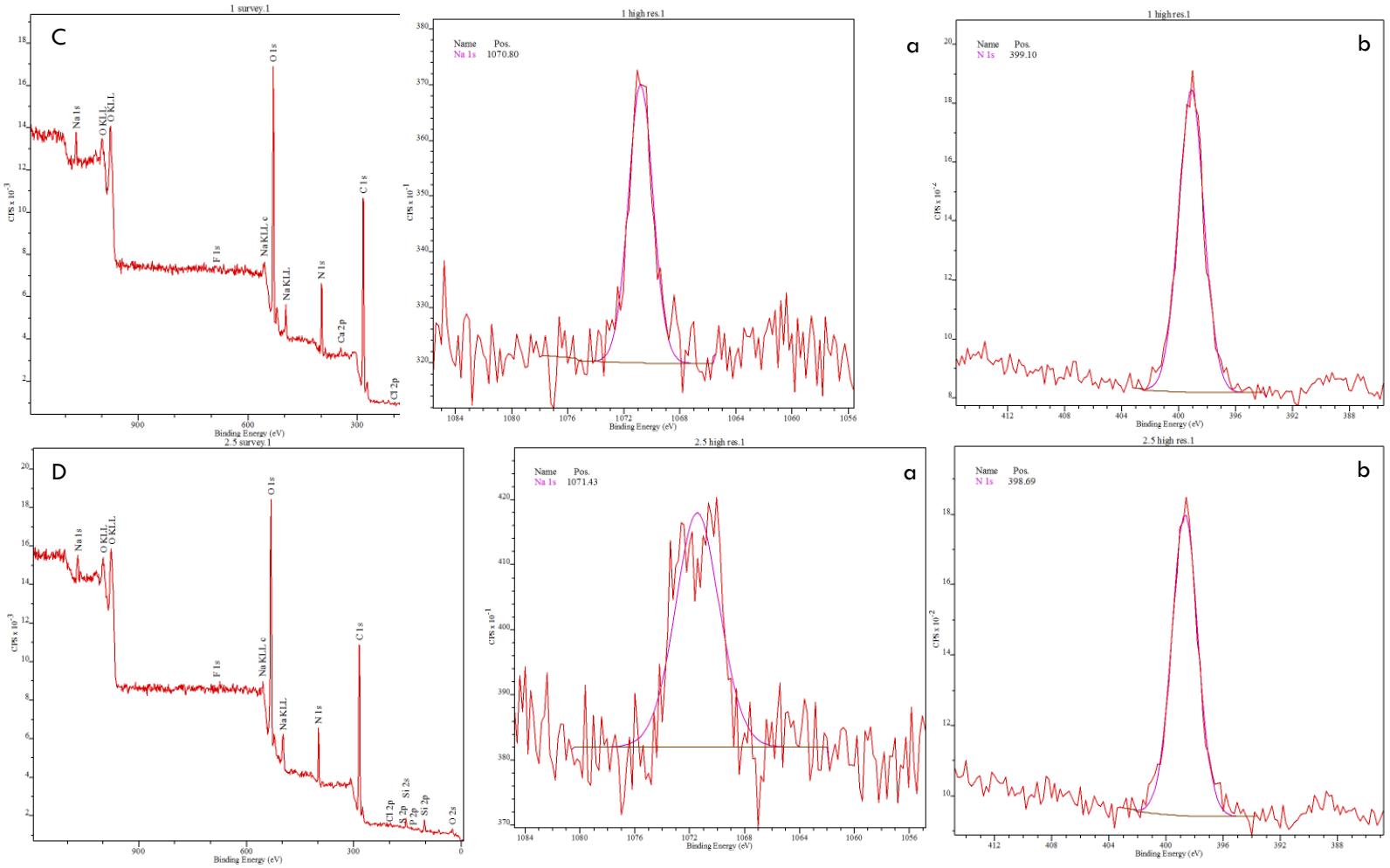

Figure 4. 15 C XPS spectra of ChG cross-linked with 1.0% PA hydrogel: C.a) ChG_1.0% PA Na peak; C.b) ChG N peak **D XPS** spectra of ChG cross-linked with 2.5% PA hydrogel: D.a) ChG_2.5% PA Na peak; D.b) N peak.

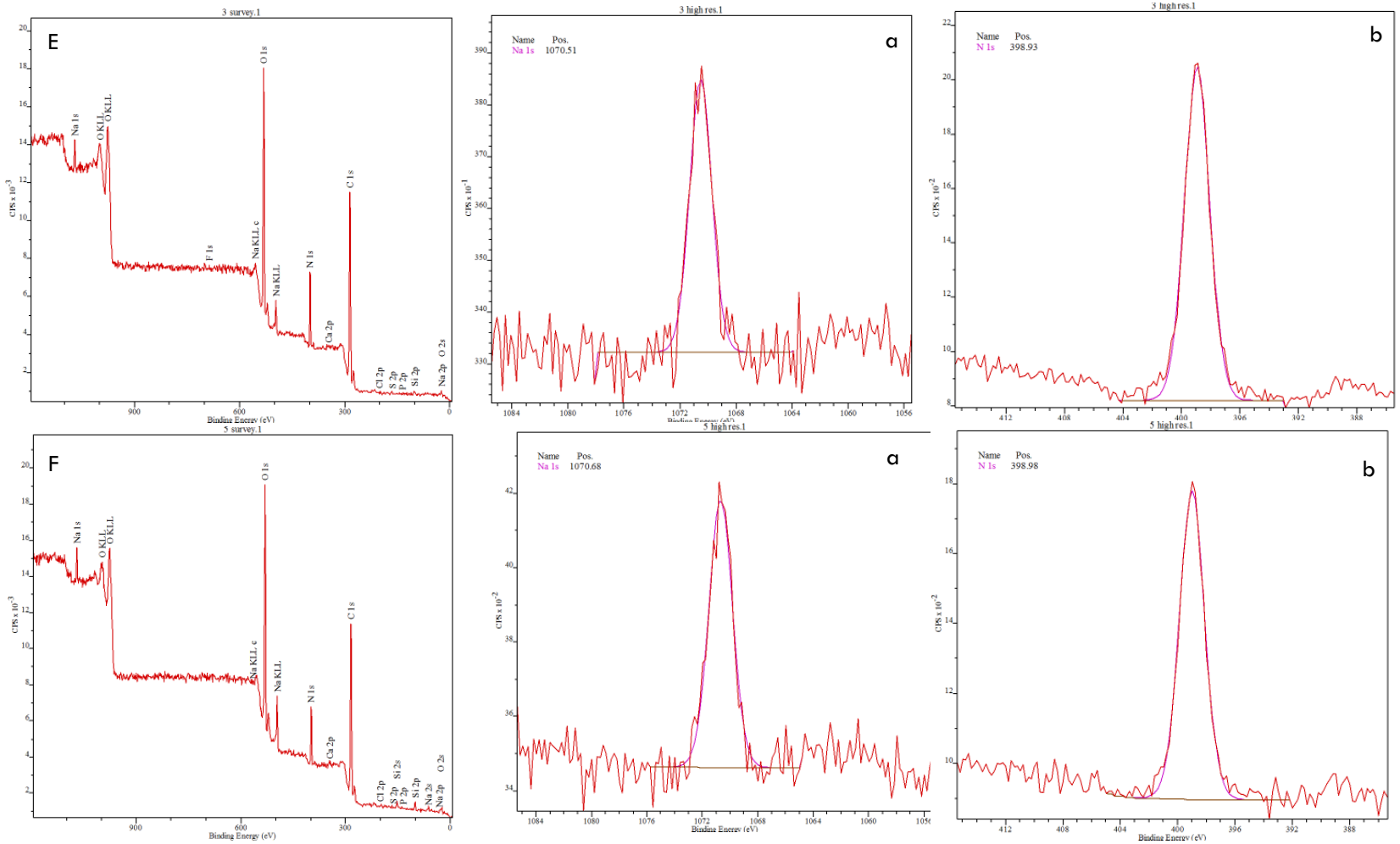

Figure 4. 15 C XPS spectra of ChG modified with 3.0% PA hydrogel: C.a) ChG_3.0% PA Na peak; C.b) ChG N peak D XPS spectra of ChG modified with 5.0% PA hydrogel: D.a) ChG_5.0% PA Na peak; D.b) N peak.

Cell-material interaction studies

Cytotoxicity

The metabolic activity results (Figure 4.16A) do not show statistically significant (Figure 4.16Aa-b) among the experimental groups in relation to positive control and test control groups. Metabolic activity of both groups shows cell viability after 48hrs.

Morphological evaluation of the cell cultures (Figure 4.16B-F) revealed no morphological difference between control and test groups for both cell lines, no cytotoxic hazard is apparent.

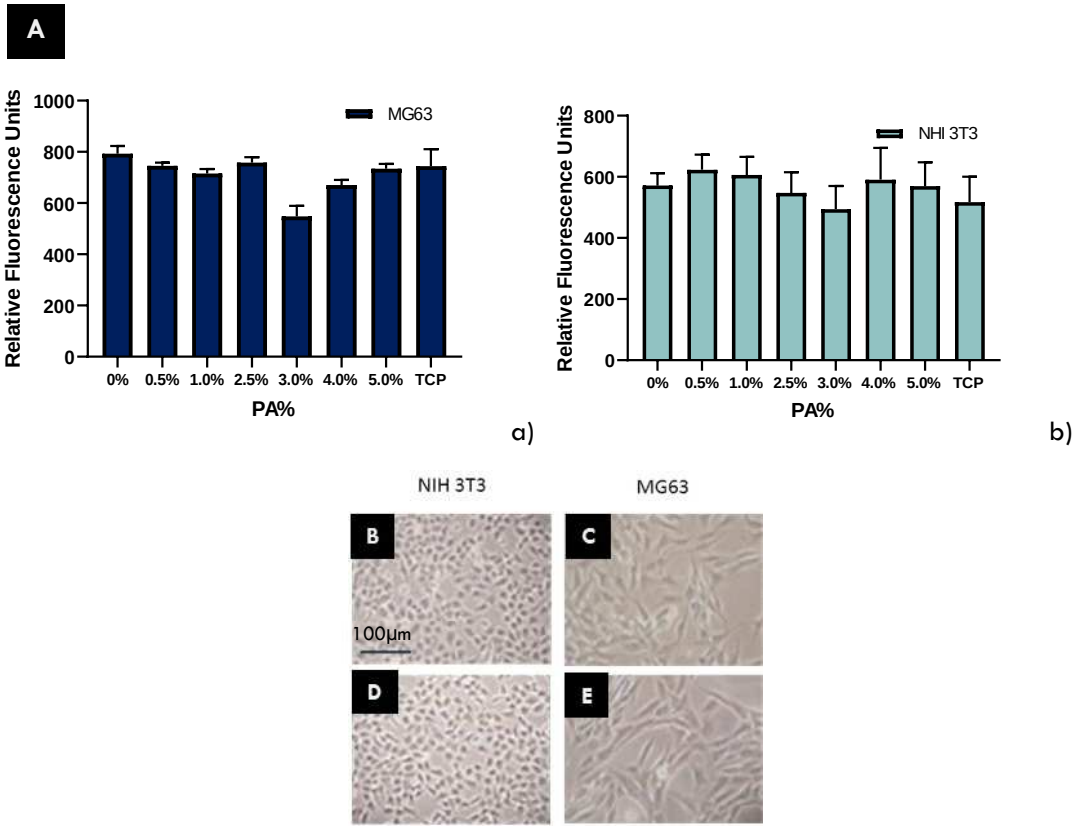

Figure 4. 16 Cytotoxicity of chitosan-gelatin ChG hydrogels cross-linked with Proanthocyanidin (PA). A Alamar Blue cell metabolic activity measurement for both, **a)** NIH 3T3 and **b)** MG63 cell lines; **B** NIH-3T3 control group (TCP) cells image; c) MG63 control group (TCP) cell image; **C** NIH-3T3 representative test group image (ChG_2.5 PA%); **D** MG63 representative test group image test group image (ChG_2.5 PA%). Data was expressed as mean ±SEM

Cell attachment to ChG hydrogels.

Figure 4.17 shows the cell attachment on neutralised chitosan-gelatin cross-linked with proanthocyanidins (AT-ChG_PA%) hydrogels. Osteoblast like (MG63) and fibroblast (NIH 3T3) cells were seeded on AT-ChG_PA% hydrogels. After 24 hrs, there was cell adhesion on all different variants of the ChG hydrogels for both cell lines NIH 3T3(Figure 4.18 Aa-c) and MG63 (Figure 4.18 Ba-c). For both cell lines no apparent variances were observed among AT-ChG_1.0% and AT-ChG_2.5% regarding attachment and spread of cells (Figure 4.18 Aa-b and 14.18 Ba-b). In the case of AT-ChG_5% double the amount of rounded not-well-spread and not-attached cells with less pseudopodia were observed for NIH 3T3 cell lines, the differences being three times greater for osteoblast like cells (Figure 4.18 B.c.).

After 96hrs of incubation, it was found that cells adhered and completely spread on the surface of all the 3 studied variants of the hydrogel (Figure 4.18C-D). For concentrations 1.0 and 2.5 PA% they all had many pseudopodia and formed a complete monolayer on the surface of the samples, for both NIH 3T3 (Figure 4.18 Ca-b) and MG63 (Figure 4.18 Da-b), so that the hydrogel surface was not at all visible. The trend previously observed at 24hrs of cultivation persisted in both cell lines NIH 3T3 (Figure 4.18 Cc) and MG63 (Figure 4.18 Dc) when cultured on AT-ChG_5% cells showed three times lower cell number and rounded cells compared to the other two PA (1.0% and 2.5%) concentrations after 96hrs of culture. This result suggests that chitosan-gelatin cross-linked with PA membranes support cell adherence and PA concentration influence the hydrogel performance for this property.

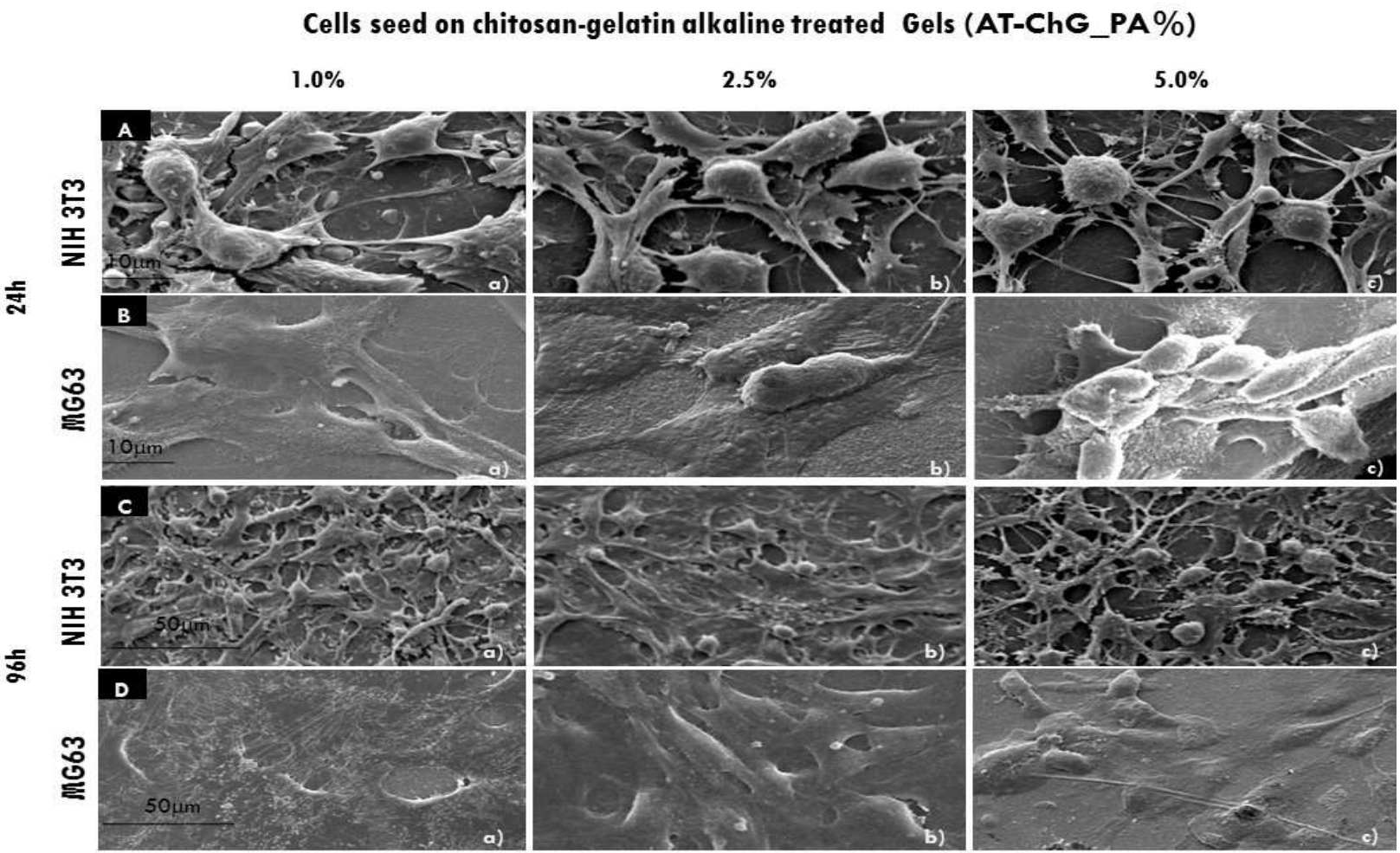

Figure 4. 17 Cell attachments to AT-ChG_PA% hydrogels SEM images A| NIH 3T3 cells on **a.** AT-ChG_1.0 PA%, **b.** AT-ChG_2.5 PA% **c.** AT-ChG_5.0 PA% **B| MG63 cells** on **a.** AT-ChG_1.0 PA%, **b.** AT-ChG_2.5 PA% **c.** AT-ChG_5.0 PA% **24 h** after been seeded, **C| NIH 3T3 cells** on **a.** AT-ChG_1.0 PA%, **b.** AT-ChG_2.5 PA% **c.** AT-ChG_5.0 PA% **D| MG63 cells** on **a.** AT-ChG_1.0 PA%, **b.** AT-ChG_2.5 PA% **c.** AT-ChG_5.0 PA% **24 h** after being seeded 96 h after seeding the cells.

Growth and morphological changes of mammalian cells on ChG hydrogels cross-linked with PA

The ability of the chitosan-gelatin ChG hydrogels cross-linked with PA to support mammalian cells growth was tested using mouse fibroblasts (NIH 3T3) and human osteoblast-like (MG63) as model cell lines. The results after cell culture on the hydrogels surface for 7 days are shown in Figures 14.18-20. Quantitative metabolic activity of both cell lines, mouse fibroblasts (NIH 3T3) and human osteoblast-like (MG63) cultured on ChG hydrogels for 1 week was established using Alamar blue-test (AB), and results can be seen on Figure 4.20. Results of AB-test expressed as mean ± standard deviation for 3 replicates. Cell metabolic activity of the cells cultivated on TCP was used as a control. It was found that the number of attached spread cells, 6 hours after being seeded, for both cell lines, was better for those grown on TCP. The number of attached and spread cells was also observed to be different among the hydrogels of different PA% concentrations (data no shown). ChG_2.5% hydrogels provided cell metabolic activity like that of TCP and ChG_5.0%; it was the combination that performed more poorly (Figure 4.18 A a) to d), and Figure 4.19 A a) to d)).

PA modification of the prepared hydrogels affected cell growth and cell morphology in different ways. The amount of PA used to cross-link the hydrogel has a significant effect on cell growth (Figure 14.18 b-d and 14.19 b-d). Notably, after 3 days of incubation, all cells on the 4 different sample combinations were spread (not visible round cells, on the hydrogel surface). However, differences on cell growth were still evident for both cell lines after a week of incubation (Figure 4.18 C a-d and 4.19 C a-d).

Figure 14.20 shows the AB test results of both cell lines fibroblasts NIH 3T3 (Figure 14.20A) and human osteoblast-like MG63 (Figure 14.20B) seeded on the different hydrogels and cultured for 7 days. The cell metabolic activity for hydrogels cross-linked

with 2.5 PA% had the highest value during this culture period, even above TCP. However, the number of cells seeded on all 3 ChG cross-linked with PA hydrogels increased gradually, indicating the hydrogels are cytocompatible and can support cell adhesion and an increase in cell number – although it can be seen that a concentration of 2.5 PA% can be used as an optimum concentration choice if what is needed is cell adherence and an increase in cell number (which for this concentration (2.5%) was significantly higher on both cell lines compared to that of 1.0 and 5.0 PA%).

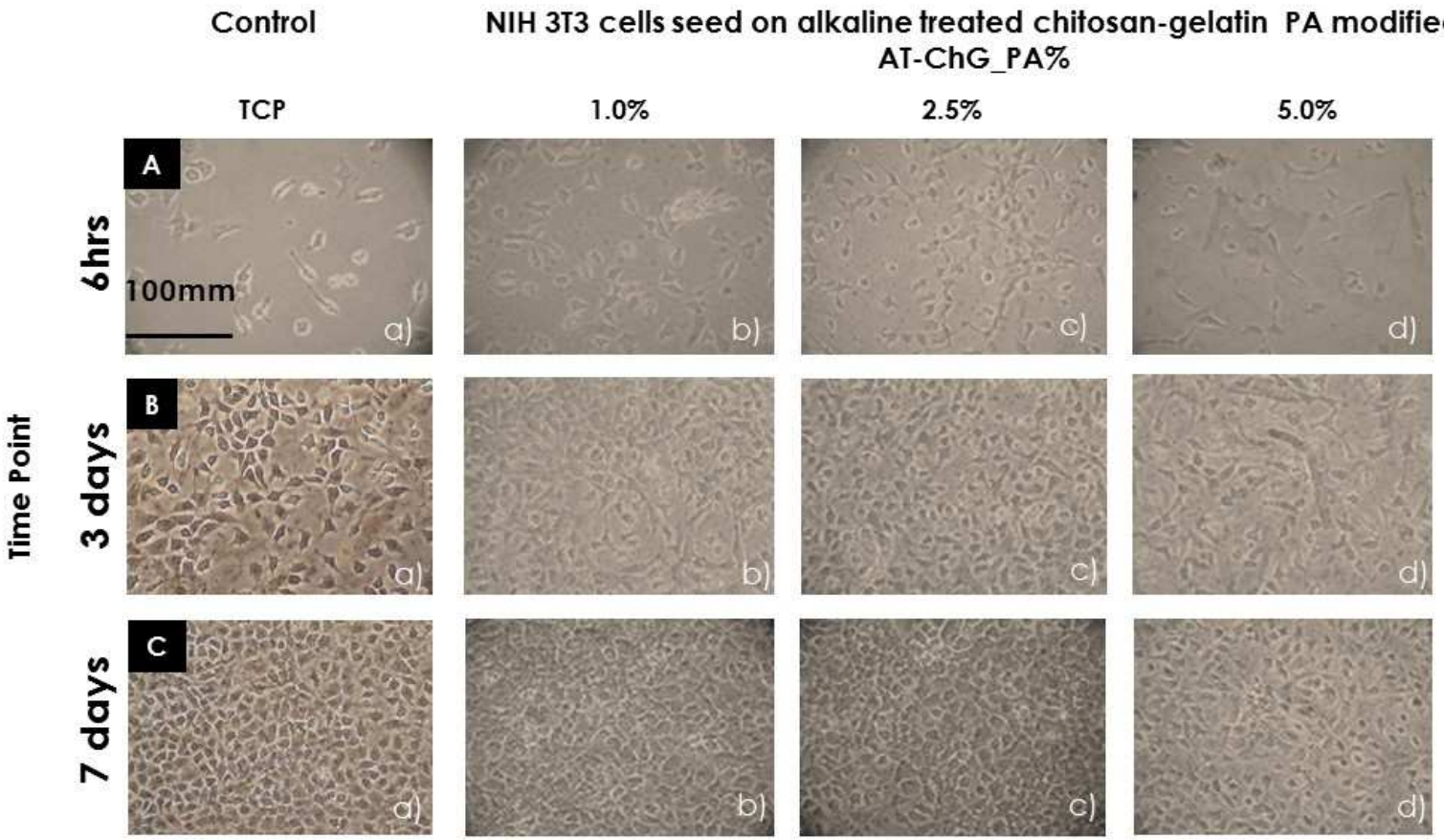

Figure 4. 18 Phase contrast micrographs of NIH 3T3 cells on **a)** TCP and **b)- d)** chitosan-gelatin ChG hydrogels at different PA% concentrations and **A-C** different timepoints.

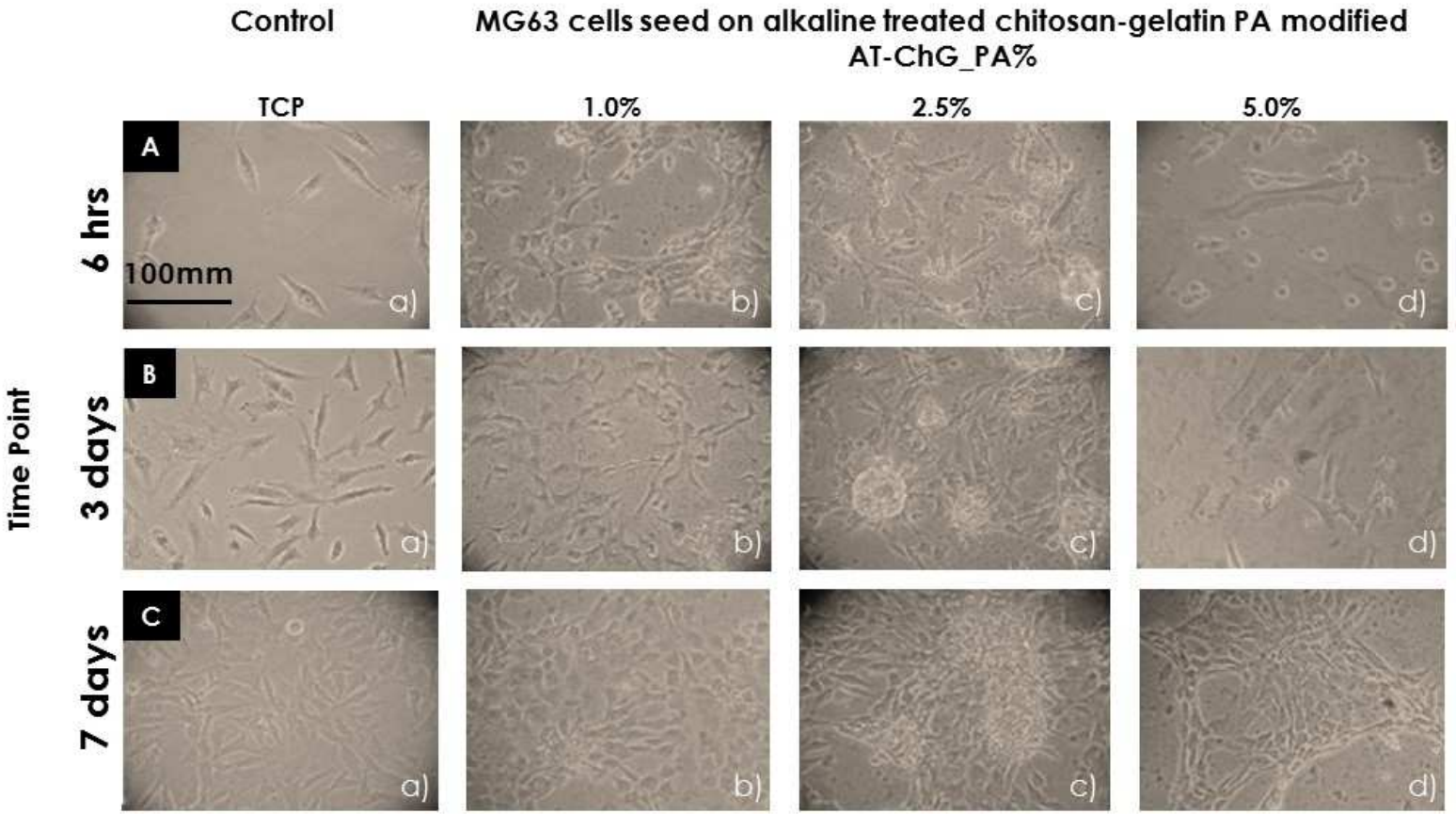

Figure 4. 19 Phase contrast micrographs of MG63 cells on **a)** TCP and **b)- d)** chitosan-gelatin ChG hydrogels at different PA% concentrations and **A-C** different timepoints.

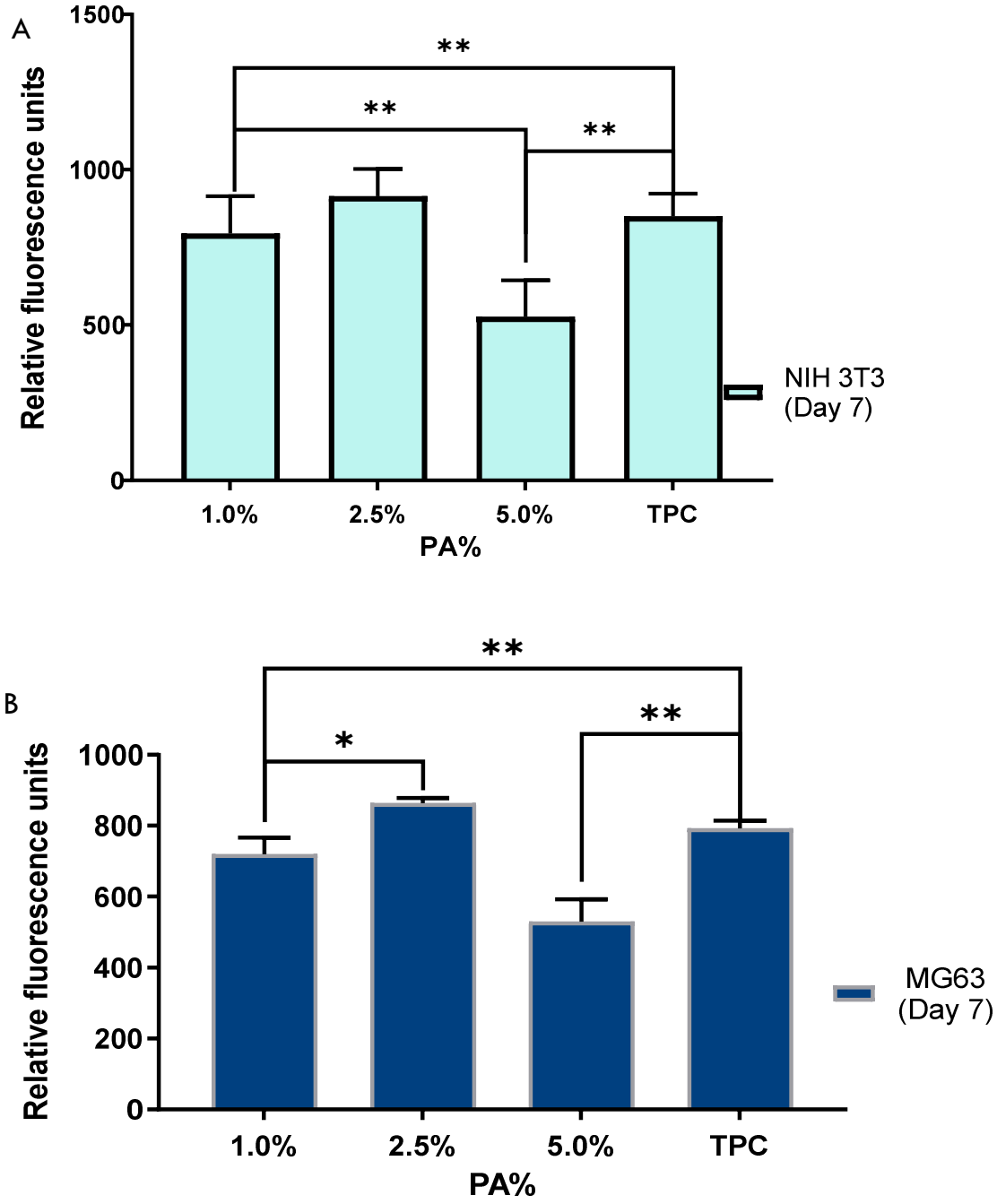

Figure 4. 20 Cell metabolic activity of A NIH mouse fibroblasts and **B** MG63 Human osteoblast like cells cultured on TCP and ChG_PA hydrogels for 1 week. Results of AB-test expressed as mean ± standard deviation for three replicates. Viability of the cells cultivated on TCP was used as a control.

Alamar blue assay and phase contrast micrographs were used to determine the cell morphology changes and increase in cell number rate on NaOH-treated substrates at different dilution concentrations. Figure. 4.21shows the cell morphology, growth and cell attachment of human osteoblast-like MG63 cells seeded on substrates of different PA content and alkaline-treated with different NaOH% after culturing for 48hrs. Significant reductions on cell number were found for specimens alkaline-treated with 1M NaOH treatment (Figure 14.21.1A and 14.21.3), an effect seen on all combinations independently of PA content, these results are in good agreement with the cell metabolic activity results, which showed cell response to be significant lower (Figure 14.21.2) for this treatment compared with diluted solution treatments and the control TCP, even when cells seeded on this specimens showed good attachment and spreading (Figure 14.21.3). Cell numbers in specimens treated with 0.1M and 0.15M NaOH are higher than those treated with 1M NaOH, and significant differences were observed on cell number, morphology (Figure 14.21.1) and metabolic activity (Figure 14.21.2, $P < 0.05$) among PA content and NaOH dilution%. 0.1M NaOH diluted was found to have overall the higher cell number and good cell attachment %. Being ChG_2.5% the combination with the highest cell number (Figure 14.21.1 Cb) and attached cell/mm^2 ratio. There was no significant difference between the control TCP and ChG_2.5% 0.1M NaOH treated samples (Figure 14.21 2). According to these results, it was observed the cell growth of specimens plated on ChG_2.5% alkaline treated with 0.1M NaOH was the highest, this was one of the reasons this combination was chosen to be used in subsequent experiments.

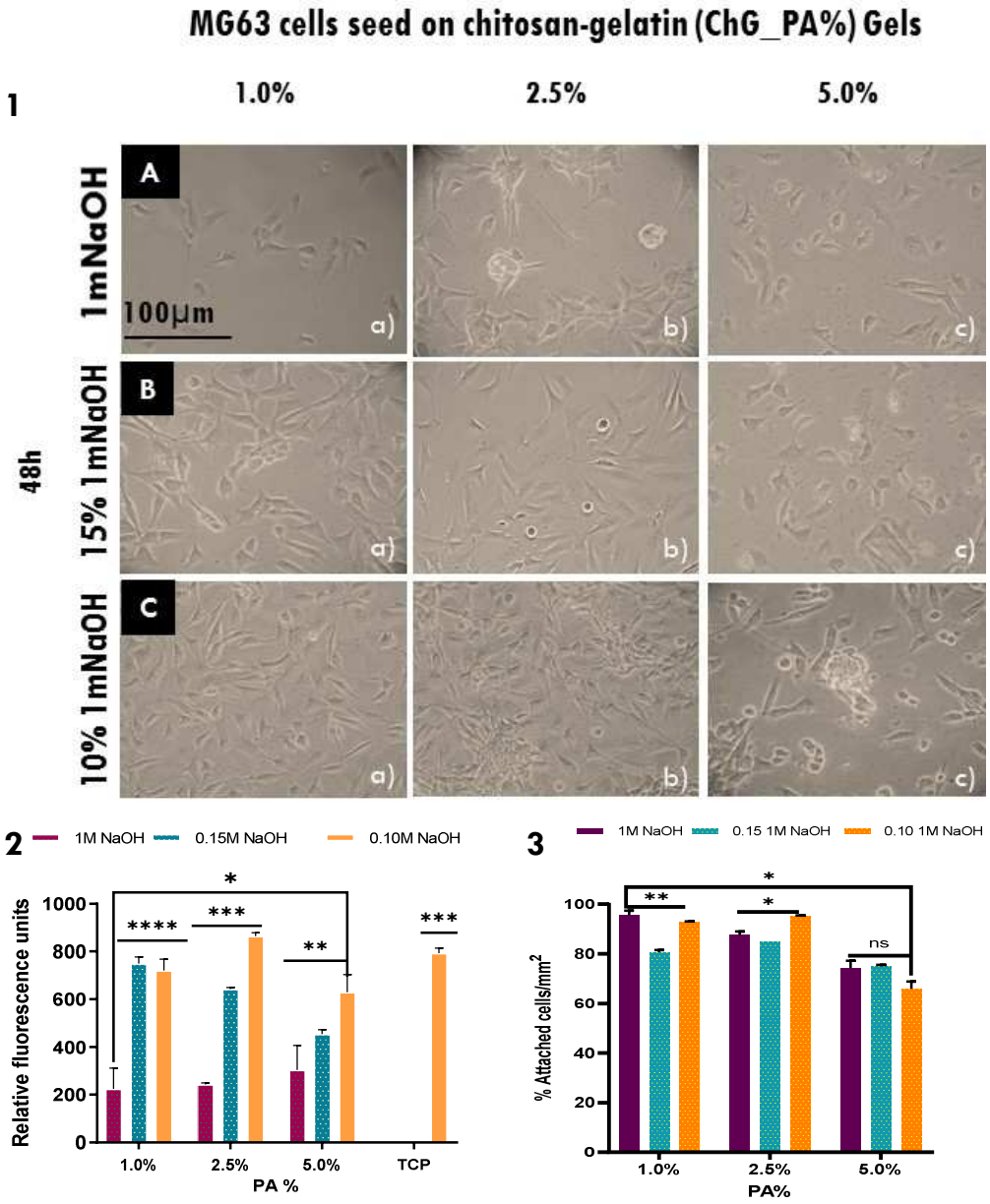

Figure 4. 21 Cell response to alkaline surface treatment with 1M NaOH 1) Phase contrast micrographs of MG63 cells culture for 48 hrs on A Treated with 1M NaOH solution leave it on top of the hydrogel **a-c)** chitosan-gelatin ChG hydrogels at different PA% concentrations for 10 min **B** Treated with 15% 1M NaOH dissolved in distilled water solution and leave it on top of the hydrogel **a-c** chitosan-gelatin ChG hydrogels at different PA% concentrations for 90 min and **B** Treated with 10% 1M NaOH dissolved in distilled water solution and leave it on top of the hydrogel **a-c** chitosan-gelatin ChG hydrogels at different PA% concentrations for 120 min. **2) MG63 cell viability response** measure as metabolic activity using Alamar Blue test. **3)% Attached MG63 cells permm^2 cultured by 48hrs**.

Discussion

The work presented in this chapter sought to develop a protein-based ChG biomaterial hydrogel cross-linked with PA, with nonlinear tuneable mechanical properties for the investigation of the matrix stiffness influence on cell response. The effect of PA% and AT on the physical, chemical and mechanical properties of the ChG hydrogel substrates were characterised, and their effect on cell adherence and metabolic activity were also evaluated. All the experiments presented in this chapter aimed to provide a substrate hydrogel which favours cell adherence and growth to build up the understanding and investigation of how cells mechanosense stiffness differentials across hydrogels as a function of matrix thickness and substrate constrain boundaries – discussed in the next chapter.

ChG blends have been used in a wide range of biomedical applications [214-216]. However, they are unstable matrices and have rapid biodegradation rates; this instability has limited their applications as biomaterials for regenerative therapies. PA has been shown to be an effective cross-linker to stabilise these hydrogels, and the addition of an alkaline media (1M NaOH) to activate an additional pH dependant cross-linking reaction on these blends has been shown to enhance the stability and cell growth of the final formulation for these hydrogels (FM3 Table 4.1). The kinetic properties of these hydrogels i.e., swelling and stability in water is a function of PA content and surface alkaline treatment. Decreasing as the PA content increases in a nonlinear relation, the hydrophilicity of this blend has been shown to improve significantly as PA is introduced to the hydrogels, but gradually starts decreasing as PA content increases over a concentration of 2.5%; this effect is diminished by the surface alkaline treatment, which improves hydrophilicity for all the investigated combinations. Mechanical properties of the blends were enhanced by the addition of PA: the

compression modulus of the hydrogel increased as a function of the PA content and this effect was magnified by the surface alkaline treatment of the samples. The inner architecture of the samples was another property that was also affected by PA%, pore size and porosity, which decreased as the concentration of the cross-linker increased. The addition of PA to pure ChG decreased its crystallinity, which gradually increased as PA content was increased over 2.5%, cell growth was also seen to be higher on cells plated on ChG_2.5%. Alkaline-treated hydrogels with 0.1M NaOH was the highest, this combination showed a suitable performance for the general aims of this project, therefore was the one chosen to be used in subsequent experiments.

The first goal of this chapter was the development of this ChG_PA protein-based hydrogel which supports cell growth and cell adhesion and exhibited suitable kinetics, chemical and mechanical properties. An initial formulation was adjusted from that described by Kim et al. [206] for the fabrication of thin films, this formulation polymer Ch:G ratio (4:7) was shown to be very viscous for the needs of this study; several trials were made until a ratio of 3% (1:1) showed favourable viscosity for micro-pipetting, however increases in cell number were low, changes in colour of culturing media led to the conclusion that the acidity of the blend was leaching to the surface, therefore buffer solutions were added to the blend (PBS+HEPES). It was also observed that the method described by Kim et al. [206] for thin films did not work for thick hydrogels which showed a liquid centre; the addition of a coagulant media (1M NaOH) suggested by Ng et al.[222] for ChG blends allows the solution to go into a secondary pH-dependent process of cross-linking, and solves the hydrogel curing issue on thick hydrogels without apparent changes in the blend viscosity. This final formulation showed also high cell growth compared to TCP (FM3, Figure 4.3, Table 4.1) and was therefore the one used

to evaluate the effect of PA cross-linking concentration on the physical, mechanical, chemical and biological properties of these hydrogels.

The observations of this study showed that pore size and porosity of these hydrogels were a function of PA concentration (Figure 4.4), with pore size and porosity decreasing as PA concentration increased. Kang at al. [276] have reported that concentration of cross-linker is indirectly proportional to the pore size of the hydrogels. His group showed that as cross-linker content increases pores become smaller, this phenomena has also proved to have an effect on the hydrogel mechanical properties [127]. In this regard, Peppas and Khademhosseini et. al. [54, 256] respectively demonstrated that the degree of porosity has a substantial effect on the mechanical properties of the hydrogel, with the stiffness of the scaffold decreasing as porosity increases, and the mechanical characteristics varying greatly with fluid flux caused by deformation added on cell culture applications [277]. Observations were also made in this study where the mechanical properties of the hydrogel (compressive modulus) increased as PA content increased (Figure 4.13). Furthermore, it has been reported that a denser surface leads to a higher mechanical apparent stiffness sensed by cultured cells, especially for *in vitro* cell culture, where the property interactions of the engineered tissue are to be considered [278]. Another study done by Hayman et al. [279] has demonstrated that cell shape can be a potent regulator of growth and differentiation; the same study reported that cells have the ability to sense micro and even nanoscale geometric cues from their microenvironment and adapt morphologically to them. The Hayman group also stated that surface topography and porosity among other microenvironment cues may affect differences in molecular cell conformation. For example, neurite development from neurogenically-differentiated stem cells was significantly enhanced when grown on highly porous polystyrene hydrogels [279]. These substrate properties

have shown to have a significant effect on cell function[5]. As reported by Kang et al. [280] cross-linking density, hydrogel porosity, and hydrogel stiffness can be adjusted as correlated properties, and their correlation may have an effect on changes in cell morphology and differentiation [5, 279].

Kinetic properties of these hydrogels were also affected by PA concentration; it was found that the swelling ratio of pure chitosan-gelatin ChG hydrogels was higher at all the different pH solutions used (pH 4, pH 7 and pH10) than those hydrogels cross-linked with PA, and the swelling ability of these hydrogels was further decreased when samples surfaces were alkaline treated (Figure 4.7 and 4.8). These observations suggest that the presence of PA and the neutralization of the hydrogel surface enhance the stability of the sample sizes and shapes. This effect, hydrogel swelling being a function of cross-linking content, has been reported in literature previously [230, 267, 281, 282]. For example, Bigi et al. [283] reported that cross-linking provides a significant reduction of the swelling of gelatin hydrogels cross-linked with genipin. Kim et al. [206] showed a decrease in swelling on ChG films cross-linked with PA compared to those not cross-linked, and Ng et al. [222] showed that the addition of 1M NaOH to ChG blends improved the stability of the hydrogels. The stability of this hydrogel in water complies with the swelling ability of the ChG_PA hydrogels; it was observed that the cross-linked hydrogels ChG_PA produced notable increases in the stability of the hydrogels in water at pH4, pH 7 and pH10, and this characteristic was further enhanced when the hydrogel was alkaline-treated with 0.1M NaOH (Figure 4.5 and 4.6). This ability of ChG stability to be enhanced by the introduction of a cross-linking agent and especially the ability of PA to stabilised these blends has been previously reported in other studies [214, 238, 284]. This is probably because the surface of the ChG hydrogel became more hydrophobic as PA content is increased, in agreement with Hagerman et al. [285] who

postulate that one of the mechanisms for interaction between PA and proteins occurs by hydrogen-bonding interactions or hydrophobic interactions. Hagerman et al. [286] also reported that the interactions between PA and collagen can be disrupted by detergents or hydrogen bond-weakening solvents; this suggests that PA and proteins, such, gelatin complex formation, involves primarily hydrogen-bonding between the protein amide and the polyphenolic hydroxyl. On the other hand, the alkaline treatment with 1M NaOH may contribute to the changes of water content by converting polymer hydrophilic chain between chitosan and gelatin, resulting in more stability in the aqueous state [287]. Another important observation of these experiments was the significant increase on weight losses of the hydrogels sunk in low-pH aqueous solutions, which might be due to the hydrolysis of amide and ester linkages, which are formed when these blends are cross-linked with PA [206], which breaks in the acid state [284]. It was also observed that the degree of swelling and stability in water of this blend cross-linked with PA was dependent on pH values in the aqueous solution, in agreement with Liu and Wang et al. [288, 289] who respectively demonstrated that the introduction of polyphenolic extracts as cross-linker for polysaccharides showed pH-sensitive properties, due to their abundant anthocyanin content, with solution colour change from red to purple and finally grey, when the pH value increased from an acidic to an alkaline state – behaviour also being observed on chitosan-gelatin ChG blends once cross-linked with PA (data not shown). This pH-sensitive characteristic is favourable for a wide range of biomedical applications such as forming valves that are sensitive to a change in pH, or in systems that can release a compound when the pH is changed, or as pH sensors [284, 289]. It has been observed in other studies that the reduction of swelling experienced after the matrix is cross-linked is also related to the structure of the matrix, such as the pore size, the amount of the pores, and the wall thickness [290]; this is confirmed by the

significant decrease of the water content (Figure 4.9) and pore size and porosity (Figure 4.4) of the ChG hydrogels cross-linked with PA. Also, it is noteworthy that there is a threshold related to the efficacy of the PA as cross-linker, since at 5 PA% in an acidic solution (pH4), this blend showed a significantly low stability (Figure 4.5 and 4.6) which suggests a weak cross-linking binding between the amide and amino groups in gelatin and chitosan respectively, since both polymers becomes soluble at pH below 4.7 when not cross-linked. Based on these findings it is suggested that the kinetics of these blends is not a continuous process.

The gelation ability of this hydrogel at room temperature can be explained by the gelling nature of the biopolymers used, the presence of 1M NaOH in the blend as a coagulation agent (Figure 4.3), and the addition of the PA as cross-linker (Figure 4.10). Gelatin and chitosan are considered 'smart polymers, that means their kinetic behaviour is controlled by their microenvironment; this means these hydrogels respond to the conditions of their environment such as changes in temperature or pH, for example a gelatin solution with a concentration more than 1(w/w)% will increase its viscosity drastically when cooled to 35-40°C, and form a hydrogel when cooled further [291]. On the other hand, it has been reported that the introduction of a base such as 1M NaOH to chitosan solutions will favours chitosan to gel at room temperature [292, 293]. Furthermore, in a diluted acid solution (pH < 6.0) the amino groups of chitosan will be protonated, responsible for their solubility once the polymer chains undergo repulsion forces and remain in solution; an increase on the pH of the solution to physiological conditions by the addition of an alkaline character as 1M NaOH (pKa 6.7 at 25 °C) will caused chitosan to solidify [293]. PA modification is another factor that contributes to the gel formation of these blends. The introduction of PA initiates the cross-linking of soluble, polymers in the blend, speeding up gel formation as PA content increases [242,

294], all of the above explaining the observed hydrogel blend precipitation at room temperature and the gelation time to decrease as PA concentration increases (Figure 4.10). Further observations of these experiments showed that the introduction of PA to ChG blends improved the hydrophilicity of these substrates however, this property decreased as the PA concentration was increased (Figure 4.11A). This behaviour may be explained due to what has been reported in previous studies: the introduction of PA to these blends causes the formation of a denser structure, which will prevent moisture permeation as PA% increase [242, 295]. This is also explained by He et al. [295], who reported that the hydrogen-bonding formation leads the cross-linking of the amine groups such as those in gelatin to bond with proanthocyanidin, and in turn the hydrophobicity of the hydrogel increasing due to the hydrophilic groups of both components binding together, creating these denser structures. Interestingly, the nonlinear increase on hydrophilicity observed in samples cross-linked with PA was diminished by the alkaline treatment of these surfaces; these hydrogels showed to be hydrophilic with an average WCA of ~40° for hydrogels under 3.0 PA% (Figure 4.11B). Furthermore, this improvement in hydrophilicity caused by the alkaline treatment was not observed on samples not PA cross-linked (pure ChG), suggesting a reaction between PA and 0.1M NaOH which improves hydrophilicity of the hydrogel even when hydrophobicity of this blend has been reported previously [295, 296]. This decrease in contact angle as PA was introduced to these blends compared with pure ChG was reported by Kim et al. [206], demonstrating that the interaction between the positively-charged amino acids of chitosan with negative moieties of gelatin was stabilised by PA particles resulting in the reorientation of the hydrophobic amino acid chains [297], making the alkaline treatment with NaOH effective to improve hydrophilicity and the electrostatic attraction of surfaces [298]. 0.1M NaOH acts then as a hydrophilic surface

neutralizer conditioner to improve protein adsorption and cell attachment, which has proved to be greater on hydrophilic surfaces treated with different materials and methods including alkaline treatment with 1M NaOH [299]. Contact angle measurements have demonstrated that the hydrophilicity of pure ChG hydrogels can be tuned in a systematic way by adjusting PA content, which can be advantageous for the hydrogel to become suitable for a wide range of biomedical usages, such as systems for the release of entrapped cells, drugs or growth factors [300]. Furthermore, hydrophilic positive-charged hydrogels such as ChG cross-linked with PA showed higher increases in cell number than uncharged hydrogels. It is also noteworthy that cells prefer a positively-charged scaffold surface for attachment due to electrostatic interactions [301]. These results were confirmed by the observations made on the hydrogel surface chemical characterization using XPS (Figure 4.15), which shows the change in surface elemental compositions. Alkaline untreated ChG hydrogels surface is composed of 64% carbon and 21% oxygen. For the alkaline-treated ChG_PA hydrogel, the surface elemental composition changes to a more oxidized one, as PA content increases, achieving 60% carbon and 24% oxygen at the highest PA concentration (5.0PA%). These results demonstrate the power of 1M NaOH to quickly break up the ester bonds within the polymer chains and expose hydrophilic functional groups, as stated previously [302, 303].

Compression modulus of ChG cross-linked with PA hydrogels was found to increase directly proportional to the Proanthocyanidin content. This trend was amplified by the surface alkaline treatment (Figure 4.13). It has been demonstrated that introducing stiff chitosan into non-linear elastic gelatin increases its tensile strength because of strong interactions between chitosan and gelatin, but compromises flexibility of the matrix because this interactions enhances the stiffness of the matrix, however reduces

elongation at break point [206]. Noteworthy chitosan-gelatin ChG blends cross-linked with PA are strong but not brittle. This is because PA has proved to have the ability to promote elasticity and flexibility when it combines with polymers [191]. As expected, the introduction of PA into the chitosan-gelatin ChG-based hydrogels results in a significant improvement of the mechanical stiffness, which showed an outstanding increase as the PA concentration increases as previously reported [191, 296]. These results demonstrate that the cross-linking ability of PA can be used to improve the mechanical properties of chitosan-gelatin ChG biomaterials just as reported in various related studies [304-306].

XRD patterns (Figure 4.14) for the pure ChG hydrogel showed the characteristic peaks of these polymers, however they were reduced compared to their individual pure states [195, 307]. Several researchers documented the typical peaks of both chitosan and gelatin weakened after being prepared into blend hydrogels, which could be explained by the formation of strong intermolecular interactions between chitosan and gelatin that destroyed their close packing for the formation of regular crystallites [221, 308, 309]. Furthermore, when the PA was incorporated into ChG hydrogels, the diffraction peak intensity of the composite hydrogel at 8.1°, 11.3° and 18.1° decreased, and then the peaks gradually increased – this is in accordance with Tan et al., who suggest this might be caused by the incorporation of the polyphenol, which hindered the formation of ordered hydrogel structures due to the interactions between the extract and polymer – in this case, chitosan [310]. A similar behaviour was observed by Wang et al. [289] who incorporated black soybean seed extract into chitosan-based hydrogels. Likewise, Pérez-Córdoba et al. found the intensity of the crystalline peak at 10° decreases and then gradually increased after incorporating plant-derived

active polyphenol compounds into chitosan-gelatin blends [99]. This decrease on crystallinity as chitosan-gelatin chains became more loosely packed by introducing PA explains the observed increase on stiffness as PA content was increased for this hydrogel. The observed wider peaks of a more amorphous structure are consistent with Kim at al. [206], who found that PA increases stiffness but also flexibility of a ChG_PA cross-linked hydrogel. The XRD patterns were in accordance with the mechanical test results where PA introduction increased compressive modulus.

In addition, cell response studies (Figure 4.18-4.21) showed that increases in cell number and adherence were governed by PA content and surface alkaline treatment, these data are in good agreement with the results reported by Y. Lin and Y. Wang [311, 312] respectively, which demonstrated cell increases in cell number and adhesion will be strongly linked to matrix stiffness and wettability of their substrate. The number of attached and spread cells was observed to be different among the hydrogels of different PA% concentrations; NIH 3T3 and MG63 on ChG_2.5% hydrogels area showed to be more spread compared with the other two combinations (1.0 and 5.0%) and provided an increase in cell number like that observed on TCP. Contrary to what was expected, the stiffer hydrogel ChG_5.0% was the combination that performed more poorly (Figure 4.18 A a) to d), and Figure 4.19 A a) to d)). This results are in good agreement with the observations made on WCA results that showed ChG_5.0 PA% having a lower hydrophilicity factor that has proved to diminish protein adsorption, cell adherence and spreading [313]. Therefore, it is very likely that the observed effect is caused partly by the changes in wettability, in particular the increase of contact angles as the amount of cross-linker is increased. Furthermore, the sessile drop technique is not ideal for hydrogels, as the sample needs to be blotted and the method suffers from

dehydration effects – however it helps to differentiate among hydrogel combinations, if further exploration regarding cell response needs to be carried out in the future. Along with wettability, stiffness changes as a result of PA content variations can affect the cell-material interaction at the single cell level [1]. According Ingber et al. [9], the adhesion of cells to a material with specific stiffness triggers signalling cascades, allowing translation of extracellular mechanical cues into intracellular events. These dynamic interactions between cell and matrix control several cell behaviours such as spreading, migration and proliferation [314]. Notably, after 3 days of incubation, all cells on the 4 different sample combinations were attached (not visible round cells, cells not spread on the hydrogel surface). However, differences on cell growth were still evident for both cell lines a week after incubation (Figure 4.18 C a-d and 4.19 C a-d), supporting the hypostasis of wettability and stiffness of the matrix playing a determining role on increases in cell number and morphology changes. The observations reported in these studies partly explain the observed changes in morphology seen in this study for both cell lines (MG63 and 3T3); cells showed a more spread flatter and larger area on ChG_2.5% ~0.111MPa stiff hydrogels compared to the round and small shapes observed on cells when seeded on ChG_1.0% ~0.004MPa soft hydrogels, contrary to what was expected, cells on the stiffest hydrogels (ChG_5.0% ~0.396MPa) did not show a more spread morphology, neither a larger size compared to ChG_2.5%. These results might be linked to the fact that among all the diverse effects of PA content on these blends, it also increases hydrophobicity of the blends as PA content increases. Therefore, these observations can lead to the conclusion that effect of stiffness on cell spreading can be overridden by the hydrophobicity of the hydrogels. This study confirms what other reports have shown: compressive modulus of the hydrogel is a function of cross-linker concentration [24, 315]. The results of this study show that as

cross-linker concentration was increased, stronger substrates were produced. It can be observed that the effect of hydrogel cross-linker concentration on mechanical properties correlates to cell response to some extent, since this effect applied as PA content increased until a PA concentration of 2.5%; additionally, the alkaline treatment of the surfaces of these hydrogels improved cell spreading and the increases in cell number suggesting cell response on these hydrogels is a joint response derived from a diverse number of cues. Controlling the extent of cross-linking on hydrogels is a widely used practice to alter the mechanical properties of substrates in mechanobiology studies [100, 316], however the results of these study showed that along with stiffness, other essential cell-material cues are affected as well such as wettability of the hydrogels, therefore the decoupling of the influence of stiffness on cell response can be difficult using this approach.

Regarding the wettability of the hydrogels, it is important to note that although it showed to be affected by the extent of the cross-linking, this result can only be used to differentiate among samples of different cross-linking concentrations, since the measuring technique used in this study sessile drop [317] suffers from critical limitations once complex biocompatible cues of the hydrogel aim to be evaluated; the hydrogels were evaluated in the dry state which is not what the cells will experience when cultured in water [318, 319]. Therefore, if the aim of further studies is to evaluate the hydrogel wettability influence on cell response, a different technique may be suggested, such as the captive bubble technique, where an air bubble is released in contact with a solid which is immersed in a liquid; this technique is advantageous in that there is minimal preparation required and evaporation effects are minimised [319, 320], which may

better mimic what cells experience once seeded on the wet hydrogels immersed in growth media.

Conclusion

The studies on the structure and properties of the chitosan-gelatin ChG hydrogels cross-linked by PA can lead to the following conclusions. The hydrogen-bond interaction among polymers and the cross-linker and the secondary pH dependant cross-linking are mainly responsible for the stabilization of chitosan-gelatin ChG blends by PA. In comparison with pure ChG, the hydrophilicity of the ChG _PA was significantly improved, however this gap between pure and cross-linked samples decreases as PA content was increased. This effect was reduced when the surface of the hydrogels was alkaline-treated with sodium hydroxide 0.1M NaOH, which improved hydrophilicity significantly. The cross-linking process used interconnected the polymer chains and enhanced the mechanical stability of the hydrogel, by altering the density of the cross-links in the hydrogel; the porous structure was tuned, and the degree of swelling was adjusted, this effect was assumed to be caused because the modification of ChG with PA led to a denser network structure. The degree of cross-links used also affected the crystallinity of the structure, chemistry of the surface, elasticity of the bulk, gelation time and the insolubility of the polymer. Whilst small amounts of cross-linker resulted in viscous hydrogels with long gelation times, able to flow freely, they also led to the hydrogels becoming soluble in solvents and having low stability. Conversely, too high a degree of cross-linking resulted in stiff but fragile hydrogels.

Using Proanthocyanidins as biomaterials showed non-toxicity and increased in cell number, because they provide preferable places for the proliferation of cells. The mechanical properties of the hydrogel, surface chemistry and surface charge of hydrogels were also shown to play a significant role in cell adhesion and cell number.

Therefore, finding an alternative in which the mechanical properties as perceived by the cells varies without altering those significant cues can lead to a more accurate analysis of the cell response to the mechanical properties of their microenvironment alone. Furthermore, the ChG_PA hydrogel showed to be pH-sensitive, exhibiting reversibility and rather rapid response in swelling, water content and stability to pH changes. The results clearly suggested that the PA cross-linked ChG hydrogel could hold a wide range of uses in the biomedical field as environmental pH conditions altered biomaterials. These results are of significance for the development of new cross-linkers and design of chitosan-gelatin ChG biomaterials.

CHAPTER

5

Effect of Matrix Apparent Stiffness on Cell Behaviour

5. Effect of Matrix Apparent Stiffness on Cell Behaviour

Introduction

The aim of this chapter was to test the hypothesis that human mesenchymal hMSCs cells can sense and differentiate between hydrogels of different apparent stiffness. To achieve this aim, the influence on the cell response of three cell lineages (MG63, NIH 3T3 and hMSCs) to hydrogels constrained by the walls of TCP and of varied thickness was investigated.

The cell-material interaction is a complex phenomenon that has been widely studied from many different perspectives, including those relevant to the fields of Biology, Chemistry, Physics, and Engineering. An important aspect of biomaterial fabrication that has recently begun growing in recognition is the mechanical properties of the biomaterial in relation to cell-matrix interactions. Cells have complex intracellular mechanisms that allow them to mechanosense their material environment [19, 26, 27, 321]. Regardless of this, several aspects of the molecular and mechanical control of mechanosensing are not yet fully comprehended or are still controversial [9, 321]. Engineered biomedical systems in which the mechanical properties of the substrate used can be controlled are useful to understand how biophysical properties contribute to specific cell behaviours and to elucidate the pathways behind the variety of processes affected by the cells' ability to sense and respond to the rigidity of their surroundings.

One of the most common methods of investigating mechanotransduction is the culture of cells on substrates of controllable mechanical properties. It has been shown that a change in substrate stiffness can affect anchorage-dependent cell behaviour in a variety of ways including proliferation, migration, and differentiation among others [28, 29, 185, 321-323]. Hydrogels, highly swollen insoluble networks with controllable

mechanical integrity and structural similarities to the native ECM are reliable substrates for tissue growth, and the study of the influence of mechanotransduction on cell behaviour [324]. Several approaches have been developed in order to alter the stiffness of these highly-swollen, insoluble networks for *in vitro* cell culture applications, primarily by altering the hydrogel elastic intrinsic modulus [126]. Although it has been suggested that this approach results in differences of porosity, variations in the surface chemistry, surface energy and surface binding of ECM proteins; cues that may also have an effect on what cells detect [10, 17, 97].

It is important to note that the stiffness that a cell senses is a combination of both the intrinsic elastic modulus of the material and the material's physical geometry, as demonstrated in the literature [13, 17, 102]. Therefore, an alternative technique of altering the mechanical stiffness of hydrogels, without necessarily changing the substrate concentration, cross-linking density, or polymerization synthesis, is to alter the hydrogel thickness, as the dimensions, shape, or boundary conditions affect the hydrogel's apparent stiffness.

Phenotypic variations have been observed in individual cells on hydrogels of differing thicknesses firmly adhered to an underlying support of higher rigidity, such as glass or TCP [13, 17, 192, 246]. These studies show cell area to be a function of thickness, where the cell spread area will remain rounded on soft PAAm (e.g. ~2-8 KPa) above a 'critical thickness' while spreading gradually as the hydrogel gets thinner, even though the intrinsic Young's modulus of the hydrogel remains the same [180]. The 'critical thickness' has been calculated and proved for synthetic hydrogels such as PAAm to be in the range of few microns (~10μm) [13] depending on: the number of cells, the displacements, the size of the cells, and the dimensions of the focal adhesions [17, 185, 325].

In addition, the effect of substrate thickness on cell response has been also proved to be affected by the structure of the substrate in question [180]. Unlike the previously described synthetic materials that have linear elasticity and homogeneous structure, many ECM polymers (i.e., fibrin, collagen, actin cytoskeleton, etc.) are fibrillar and have nonlinear elasticity, thus undergo strain-hardening effect. It has been proved that deformation stress forces exerted by cells travel greater distances on these substrates [185]. Leong et al. [192] showed underlying rigid coverslips to influence cell spreading area and morphology on fibrous collagen hydrogels of up to1440μm thick. The greater propagation of mechanical cues has been accredited to the fibrous nature of biological substrates; specifically, it has been proposed that cell-induced forces travel through those fibres, and so over much longer distances than on synthetic materials [186]. Therefore, synthetic hydrogel might not be representative enough in predicting cellular response to matrix stiffness *in vivo*.

The aim of this chapter was to generate a greater understanding of the influence of hydrogel modulus, constrain boundaries and thickness on the apparent stiffness experienced by fibroblast NIH 3T3, osteoblast like MG63 and human mesenchymal stem hMSCs cells, and its effect on cell differentiation using mesenchymal stem cells hMSCs. Tissue culture well plates were used and subsequently, coated with the ChG_2.5% (Formulation Method (FM) 3 Table 4.1) of controlled thicknesses and known bulk Young's modulus (~111KPa). The ChG_PA was chosen because of the favourable properties as substrate for cell culture reported in Chapter 4. Cells were cultured on flat-shaped ChG_PA hydrogels of varied thickness, ranging from 0.2mm to 6.0mm; the physical, chemical and mechanical properties of these hydrogels were characterised as a function of the hydrogel thickness, while cell spread area, alkaline phosphatase (ALP) activity and Osteocalcin expression were used as indicators of cell differentiation of

hMSCs. Cell seeding density was varied to also investigate the effect of cell density on cell growth, and differentiation to elucidate the role of cell density on the apparent stiffness sensing and cell differentiation.

Results

Hydrogel of varied thickness characterization

Thickness controlled by hydrogel volume

In order to attempt to vary the thickness of ChG_PA hydrogel samples, the ChG_PA hydrogel (Formulation Method 3 FM3, Table 4.1) was poured in 24 cell culture well-plates (1.98cm^2 surface area), while the volume of the hydrogel was varied (Eq. 3.1) before measuring the thickness using light microscopy (Chapter 3 pp 80). Hydrogel thickness was found to increase gradually with ChG_PA volume (Figure 5.1).

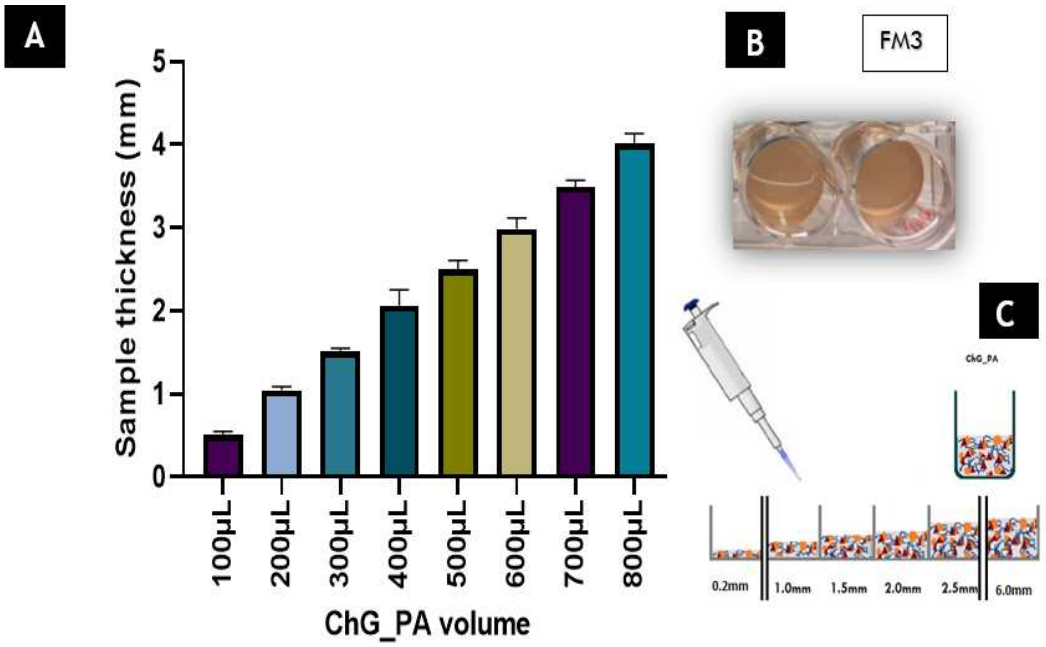

Figure 5. 1 Substrate thickness varies in proportion to the volume of ChG_PA hydrogel used. A Substrate thicknesses were measured using face contrast images and the aid of ImageJ software. Data is express as mean ± SEM **B** ChG_PA 2.5% hydrogel synthesis using FM3 from chapter 4 at different volumes (thickness). **C** Image showing hydrogel cast on 48 tissue culture plastic well plate.

Porosity

Cryo FIB SEM micrographs of the visible milled face of GCH hydrogel samples fabricated at different thicknesses were investigated and are shown in Figure 5.2.A - D, the obtained pore size as well as porosity are summarized in Table 5.1. Hydrogel samples exhibit numerous micropores uniformly distributed through the substrates. The interconnected and porous structures could be seen in all fabricated samples. No significant differences in the pore shape, wall thickness and size were found among the samples of different thickness. The statistical analysis showed no statistical significance among pore size and variability among samples of different thicknesses (Figure 5.2. E and F). Changes in sample thicknesses do not affect pore structure, variation, or size, as seen on Table 5.1 and Figure 5.2.

Table 5. 1. Porosity properties of hydrogel samples of different thicknesses.

Samples thickness	Pore size (µm)	Porosity (area %)
1.0 mm	0.2500 ±0.059	49%
3.0 mm	0.2426 ±0.055	45%
4.0 mm	0.2389±0.064	46%

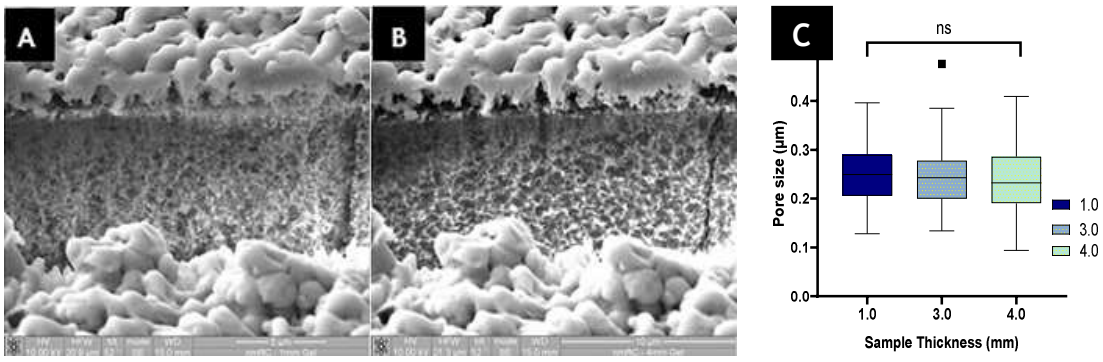

Figure 5. 2 Effect of sample thickness on matrix morphology. FIB-Scanning electron micrograph of Cross-sectional gelatin-chitosan hydrogel discs crosslinked at 2.5% PA and varying thickness from 1.0mm (A), to 4.0mm (B). The porous size is not significantly different after increasing the sample thickness from 1.0mm to 4.0mm (D). The data were expressed as mean ± SEM.

Water contact angle ChG_PA hydrogels of different thickness.

In order to explore the correlation between the Proanthocyanidin (PA) cross-linked chitosan-gelatin (ChG) hydrogels of a range of thicknesses and its surface energy, the hydrophobic-hydrophilic properties of these ChG_PA hydrogels have been examined using the water contact angle (WCA) technique as a function of the sample thickness (Figure 5.3). Figure 5.3A ChG_PA shows that the sample are highly hydrophilic (WCA ~31° Figure 5.3B) as previously reported (Figure 4.12). These properties showed not to be affected by the alteration of sample thickness. According to the results of this study, (Figure 5.3A) the changes in WCA due to modifications on sample thickness are not significant. It can be concluded that changing the samples thicknesses do not affect WCA, so the wettability should remain constant across all the samples.

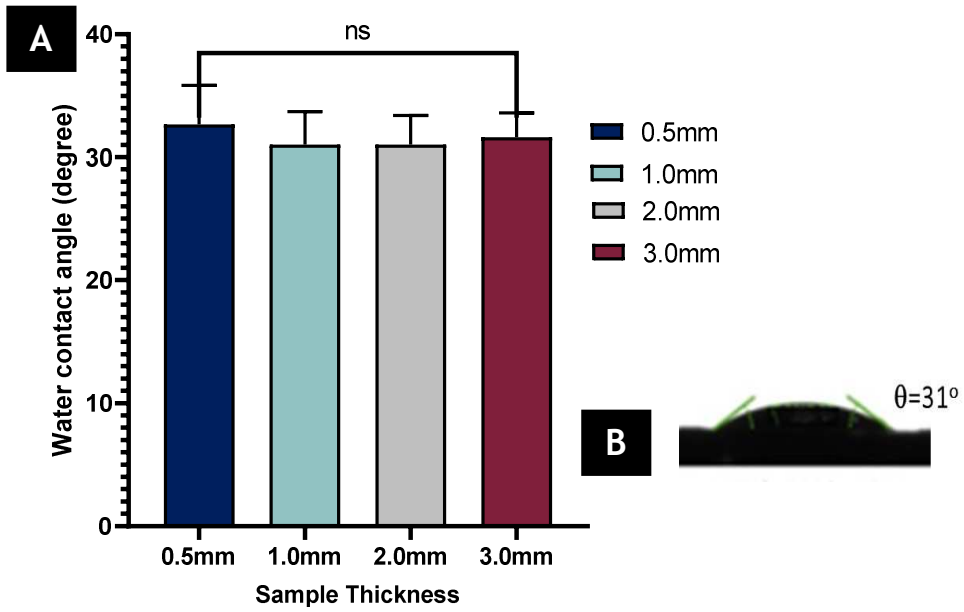

Figure 5. 3 Effect of sample thickness on WCA. **A** water contact angle (WCA) of chitosan-gelatin (ChG) cross-linked with Proanthocyanidin (PA) hydrogels as a function of varying thickness from 0.5mm to 4.0mm. The WCA did not significantly vary by altering sample thicknesses. The wettability of the samples is not a function of the sample thickness. The data were expressed as mean ± SEM.**B** Graphical illustration of the ~31° average WCA.

X-ray diffraction (XRD)

The XRD pattern of the chitosan-gelatin ChG hydrogels cross-linked with 2.5% of PA showed two broad peaks at 2θ = 11.0° and 21.0°, corresponding to the semi crystalline nature of chitosan observed in Chapter 4 (Figure 4.14). PA significantly decreased the intensity of the XRD peaks making the blend mostly amorphous. In this experiment the influence of sample thickness on the chemical properties of the bulk was also investigated, ChG_PA samples of thickness ranging from 0.5 to 4.0mm (Figure 5.4A-E) were produced and scanned (Chapter 3 pp 90). Figure 5.4 shows that all the hydrogels produced a diffraction pattern of an amorphous phase. Displaying an amorphous hump at 11° 2 θ, and a second amorphous hump less prominent at 2θ 21°. However, the intensity of the XRD hump at 2 θ 21° became slightly higher with increases in thickness (Figure 5.4A-E), suggesting an effect caused by the greater amount of material in thicker sample however this effect did not alter the amorphous state of the Proanthocyanidin cross-linked chitosan-gelatin ChG_PA blend. It can be seen (Figure 5.4F) that altering the thickness of the hydrogel samples does not alter the crystallinity of the bulk sample.

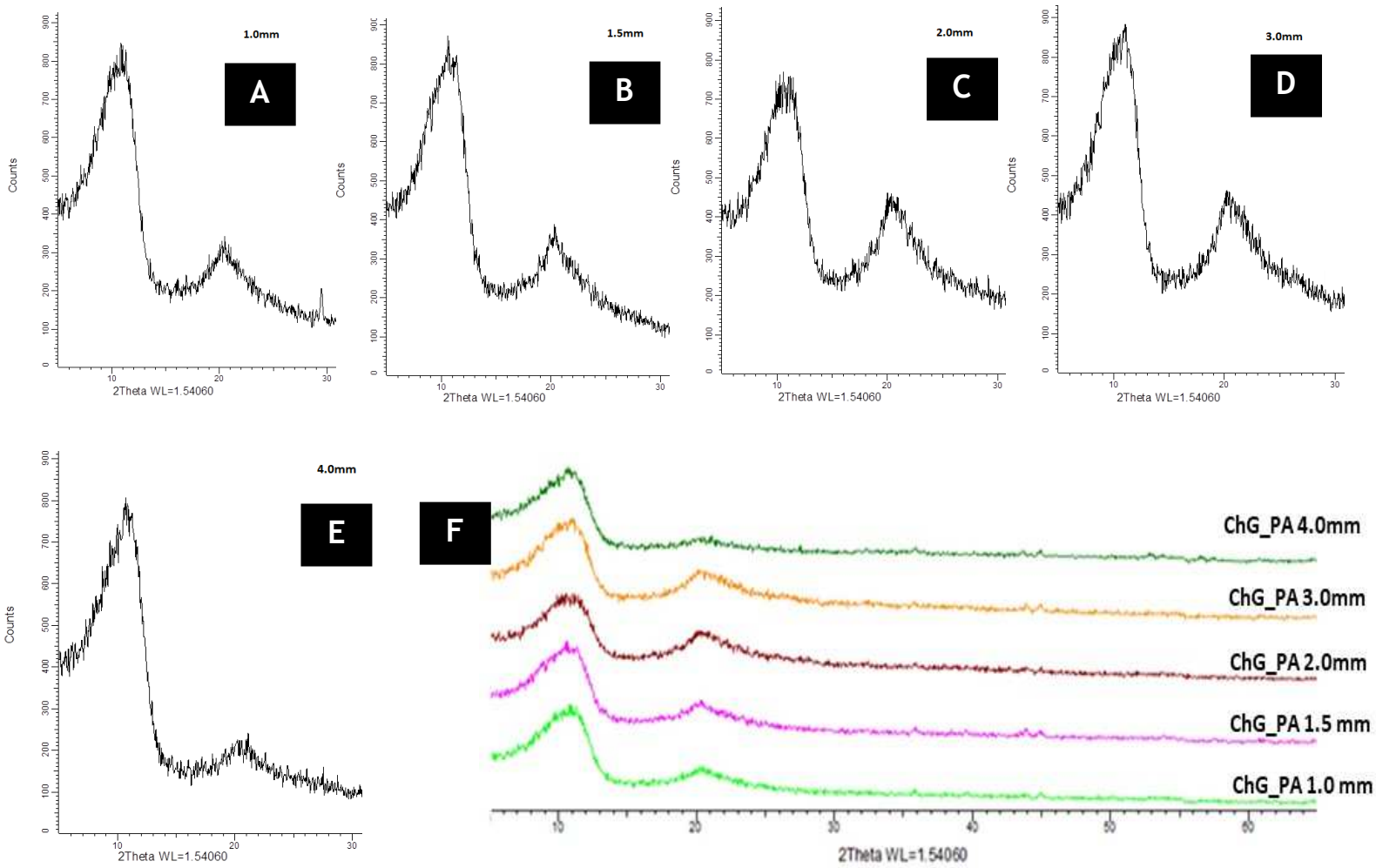

Figure 5. 4. XRD patterns of chitosan-gelatin hydrogels cross-linked by 2.5% Proanthocyanidins and A 1.0mm, **B** 1.5mm **B** 2.0mm, **C** 2.0mm **D** 3.0mm, **E** 4.0mm thick. **F** Overall view of the hydrogel's patterns. Altering sample thickness does not interfere with the bulk chemistry.

X-ray photoelectron spectroscopy (XPS)

Figure. 5.4 shows the qualitative XPS spectra of samples in a range of thicknesses (1.0-6.0mm) produced by a chitosan-gelatin ChG cross-linked with 2.5% PA and neutralised with NaOH. All the ChG_PA hydrogels have presented 4 main elements as shown in Figure 5.5A. The binding energies are 285.0 eV for C, 531.0 eV for O, 1072 eV for Na and 402 eV corresponding to nitrogen. The results of this study show that apart from the predominant C, at which the peaks expanded, and its intensity increased as the thickness of the samples increased, the remaining elements do not show significant atomic concentration% change (Table 5.5) among samples when the thickness of the specimen is altered. The presence of carbon could have originated from surface contamination, which is commonly reported and caused by unavoidable hydrocarbon contamination, adsorbing spontaneously from ambient air onto the surface [326, 327], and that in this case such contamination will increase in thicker samples, which will need longer periods of air-dry exposure in order to dry out and be tested. This result suggests chemical homogeneity among samples surfaces regardless of sample thickness.

A

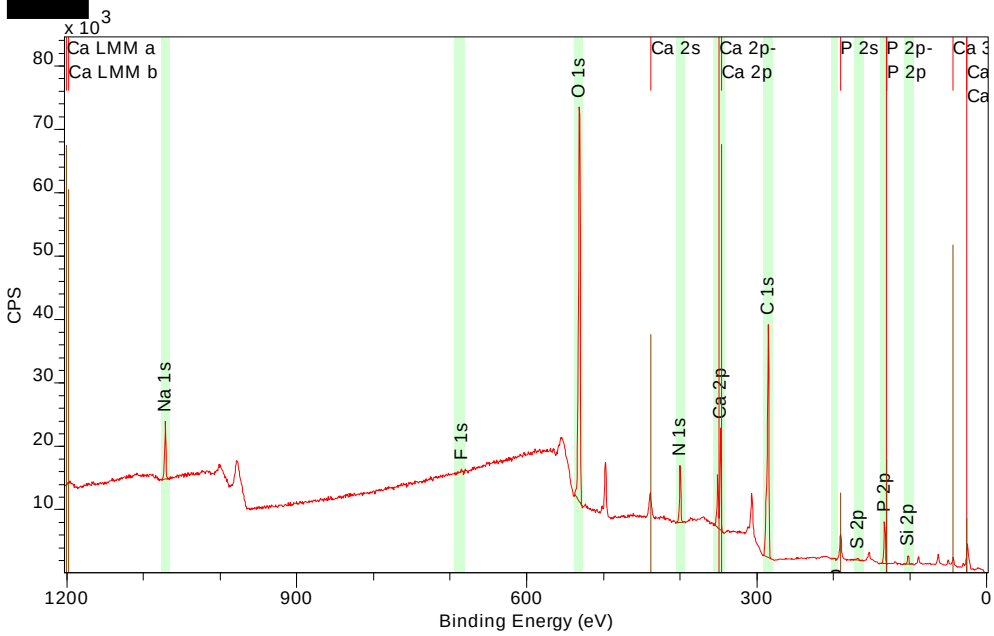

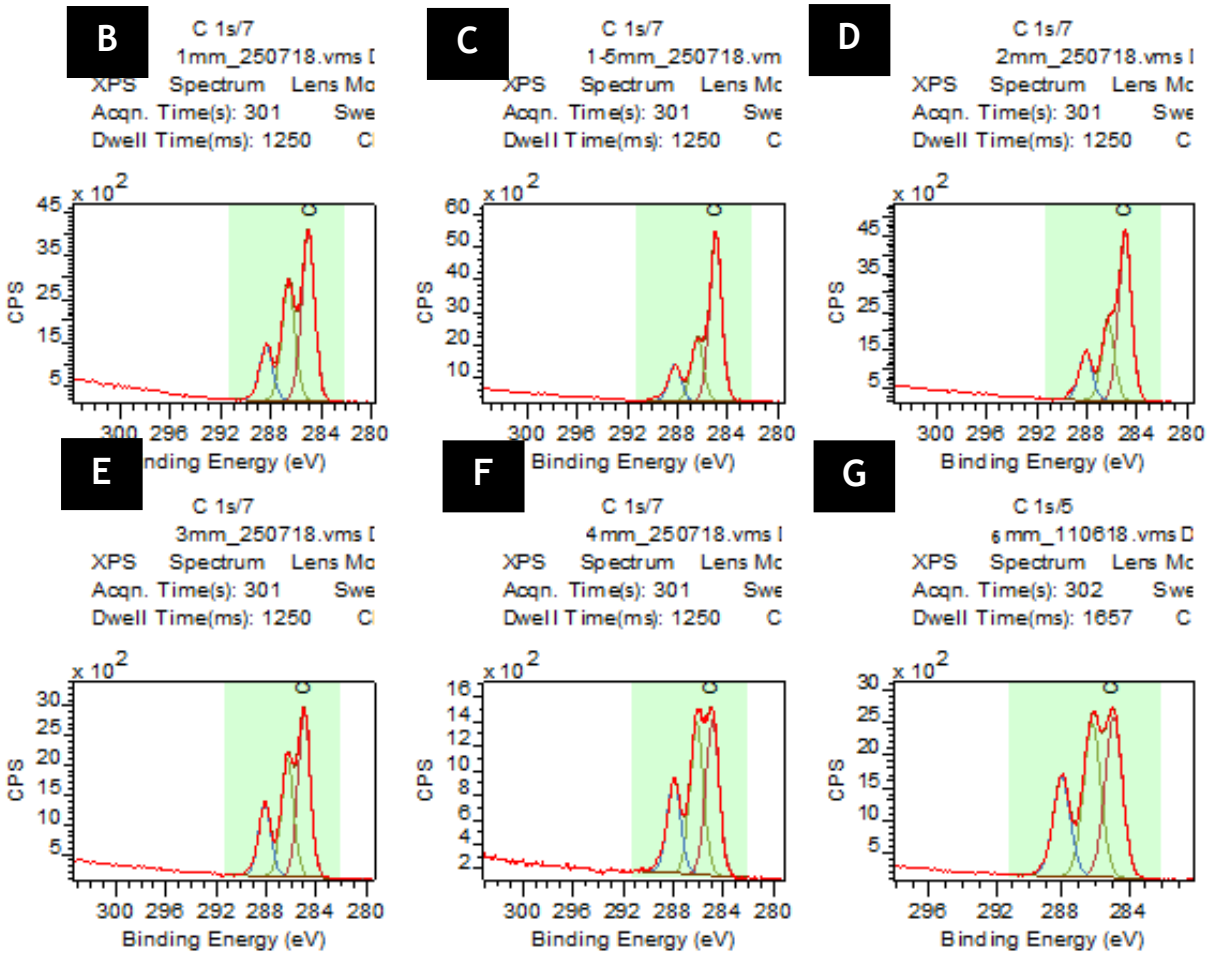

Figure 5. 5 XPS of chitosan-gelatin hydrogels cross-linked by 2.5% Proanthocyanidins of different thickness. **A** All samples showed the 4 main peaks previously reported in chapter 4 XPS with the variation of the C peak which show a thickness dependence behaviour **B** 1.0mm, **C** 1.5mm **D** 2.0mm, **E** 3.0mm **F** 4.0mm, **G** 6.0mm thick.

Hydrogel apparent stiffness as a function of sample thickness

The results of the apparent stiffness measurements of the ChG_PA hydrogels of varying thickness using atomic force microscopy (AFM) can be seen in Figure 5.6., which shows a pronounced effect of the hydrogel thickness on the apparent stiffness of the hydrogels, with thinner hydrogels showing significantly greater values of the elastic modulus when the hydrogel thickness is 500µm (287±7.8 KPa). It is noteworthy that for thicker hydrogels the mean measured stiffness was not significantly different compared to that obtained from the 3.0mm (~2.1 ± 0.3KPa) thick specimens. Figure 5.6B shows that the apparent stiffness of the hydrogel is a function of the sample thickness of the curve of its correlation, this correlation fits a one-phase exponential decay curve function with an R^2=0.9339. Table 5.2 provides a summary of the apparent stiffness to thickness.

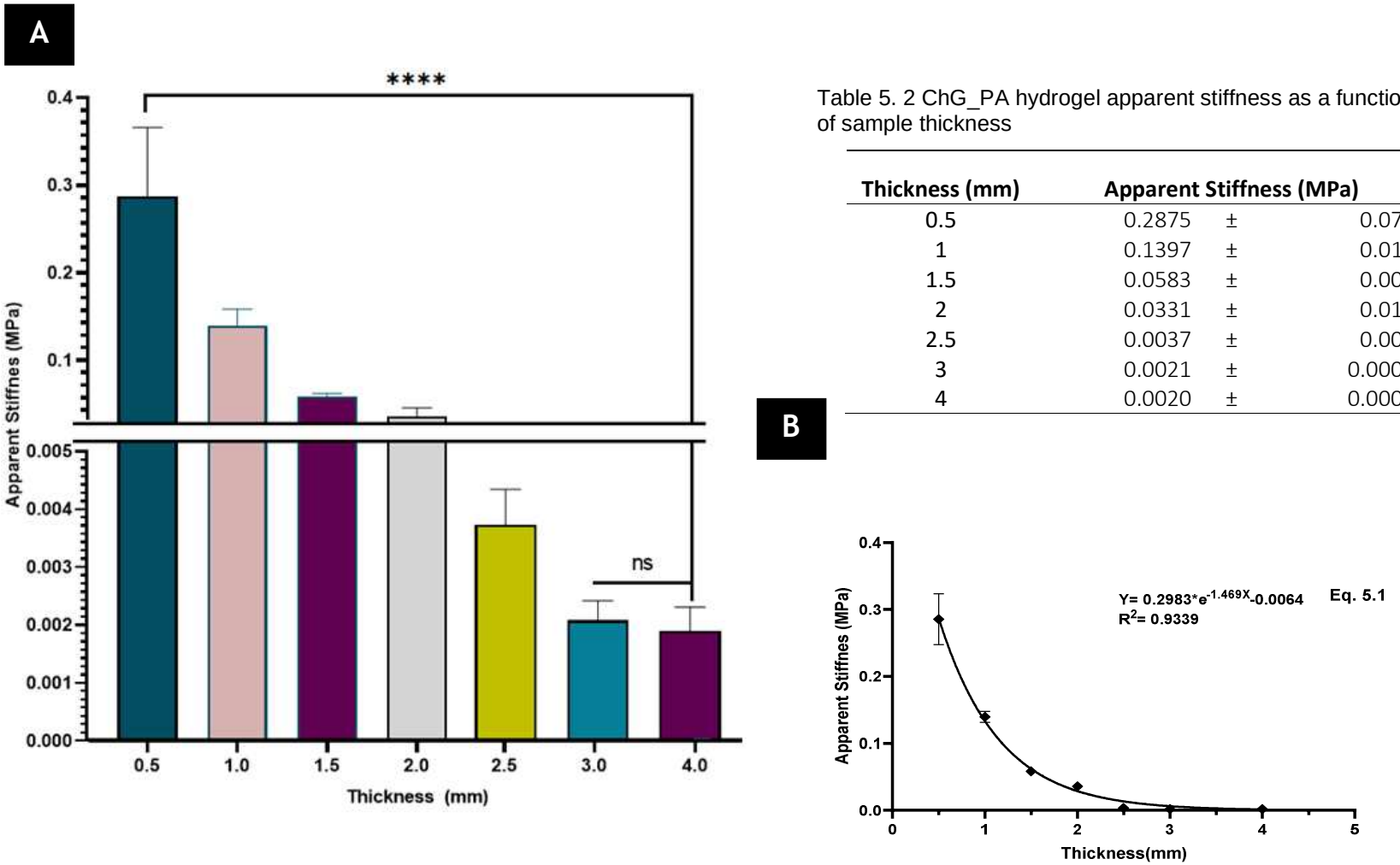

Table 5. 2 ChG_PA hydrogel apparent stiffness as a function of sample thickness

Thickness (mm)	Apparent Stiffness (MPa)		
0.5	0.2875	±	0.078
1	0.1397	±	0.019
1.5	0.0583	±	0.004
2	0.0331	±	0.010
2.5	0.0037	±	0.002
3	0.0021	±	0.0003
4	0.0020	±	0.0004

Figure 5. 6 Hydrogel stiffness A Apparent stiffness of hydrogel in the range of thickness 0.5 to 4.0mm, please be aware that the graph manages two scales for explanatory purpose. **B** Nonlinear fit curve. The data were expressed as mean ± SEM.

Cell response

Cytotoxicity

To evaluate the cytotoxicity of leached materials coming out of the ChG_PA of different thickness, the different cell lines used in this study (human mesenchymal stem cells hMSC, osteoblast-like MG63 and fibroblast NIH 3T3) were grown to a confluent monolayer in tissue-culture dishes. The growth media was aspirated and replenished to provide a resting confluent cell layer. The hydrogels and positive controls were soaked in media for 24hrs. Growth media was aspirated from tissue-culture dishes and replaced with test and fresh media. Tissue-culture dishes were incubated for 48hrs, and metabolic activity and morphological changes were examined under a microscope.

The metabolic activity results (Figure 5.7) do not show significant differences among the experimental groups in relation to positive control (TCP) and test control groups. Metabolic activity of all groups shows no cytotoxicity after 48hrs.

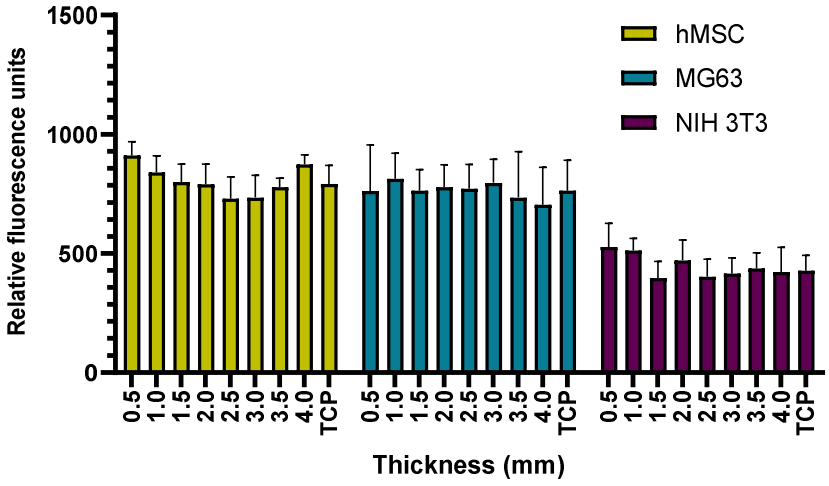

Figure 5. 7 Cytotoxicity of cells seeded on chitosan-gelatin ChG_PA hydrogels cast at different thickness, cells were cultured, and Alamar Blue test performed after 48hrs. Results expressed in relative fluorescence units for hMSC's, MG63 and NIH-3T3**.** Data is presented as mean±SEM.

The effect of matrix tension on cell response

Figure 5.8 shows NIH 3T3 cells cultured on TCP (Figure 5.8Aa,d,g B) and on chitosan-gelatin ChG_ PA, divided in two groups. Group I samples made of hydrogels firmly attached to TCP (Figure 5.8Ab,l,h B), Group II hydrogels cast and peeled off out of glass (Figure 5.8Ac,f,i C) to investigate the effect of matrix tension as a function of boundary constraints on cell number and cell morphology. The metabolic activity results carried at different timepoints (48, 72, and 96h) of their incubation (Figure 5.8D) showed that NIH 3T3 on group I, cells cultured on cast hydrogels, showed signs of spreading after 48hrs (Figure 5.8Ab) to be fully spread after 96hrs, however confluency showed to be lower compared to TCP which showed full confluency of cells after 48hrs (Figure 5.8Aa) and higher increases in cell number (Figure 5.8Aa to 5.8Ai D). Fibroblast NIH 3T3 cells in these tense stiff substrates (TCP) developed processes within the first 24hrs (image not shown). For group II cells were seeded on detached hydrogels in order to evaluate the effect of unconstrained substrates on cell morphology and metabolic activity (Figure 5.8A c,f,i D). After 48hrs, culture cells showed few cells to be attached (Figure 5.8C), in the following 24 hrs the totality of the cells were complete round cells (Figure 5.8Ai).

Cell metabolic activity (figure 5.8D) shows the effect of mechanical unloading matrices on cell morphology and adhesion, 1.0mm thick attached hydrogels (AS~139KPa) show significantly higher increase in cell number compared to the unconstrained hydrogels from days 1 to 5. While cell metabolic activity increased for TCP and cast hydrogels, a significant reduction in cell metabolic activity was observed for unconstrained samples suggesting possible cell apoptosis.

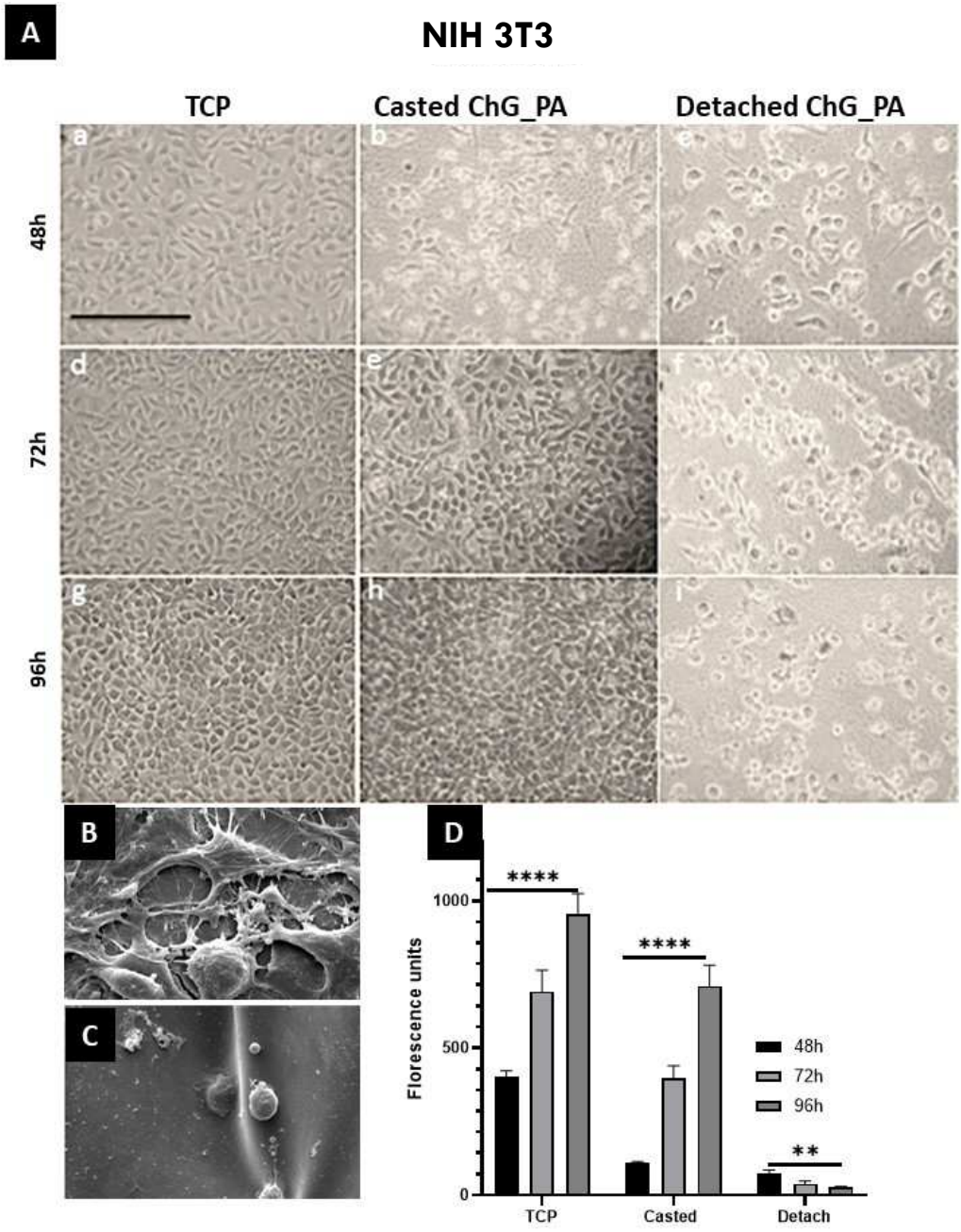

Figure 5. 8 Transferred chitosan-gelatin hydrogel experimental results for NIH 3T3 cell line; bar = **100µm A|** a, d, g) Cells cultured on 48 cell culture well plates at 48, 96, and 120h after being seeded b, e, h) Cells cultured on 3 cm^2 chitosan-gelatin hydrogels detached cut and transferred to 6 cell culture well plates at 48, 96, and 120h after being seeded c, f, i) Cells cultured on 3 cm^2 chitosan-gelatin hydrogels detached cut and transferred to cell culture well bioreactor at 48, 96, 120h after being seeded and at 24, 72, 96 hrs after dynamic cell culture was started; j) Cell viability test Alamar blue at 48,72,96 and 120 culture hours. **B|** SEM image of individual cells on transferred chitosan-gelatin hydrogel. **C|** SEM image of individual cells on transferred chitosan-gelatin hydrogel

Osteoblast-like MG63, also considered an anchorage-dependent cell line, show similar behaviour on 1.0mm cast and detached ChG_PA hydrogels to that observed for the fibroblast cell line. Results of this experiment can be analysed in Figure 5.9, in contrast to fibroblast, this cell line is shown to be much more sensitive to the instability and compliance of their culture matrices. Cells cultured on cast hydrogels increase in cell number and spread after 96hrs of culture (Figure 5.9Ah,D) but couldn't get close in % of confluence to those cells seeded on TCP (Figure 5.9Ag, h, j). Cells seeded on the unconstrained hydrogel responded at much slower pace (Figure 5.9A c,f,i D) compared to cast samples. SEM images (Figure 5.9B, C) show the characteristic round morphology of MG63 cells on unconstrained culture ChG_PA hydrogels and the well spread and flat morphology of samples seeded on constrained hydrogels.

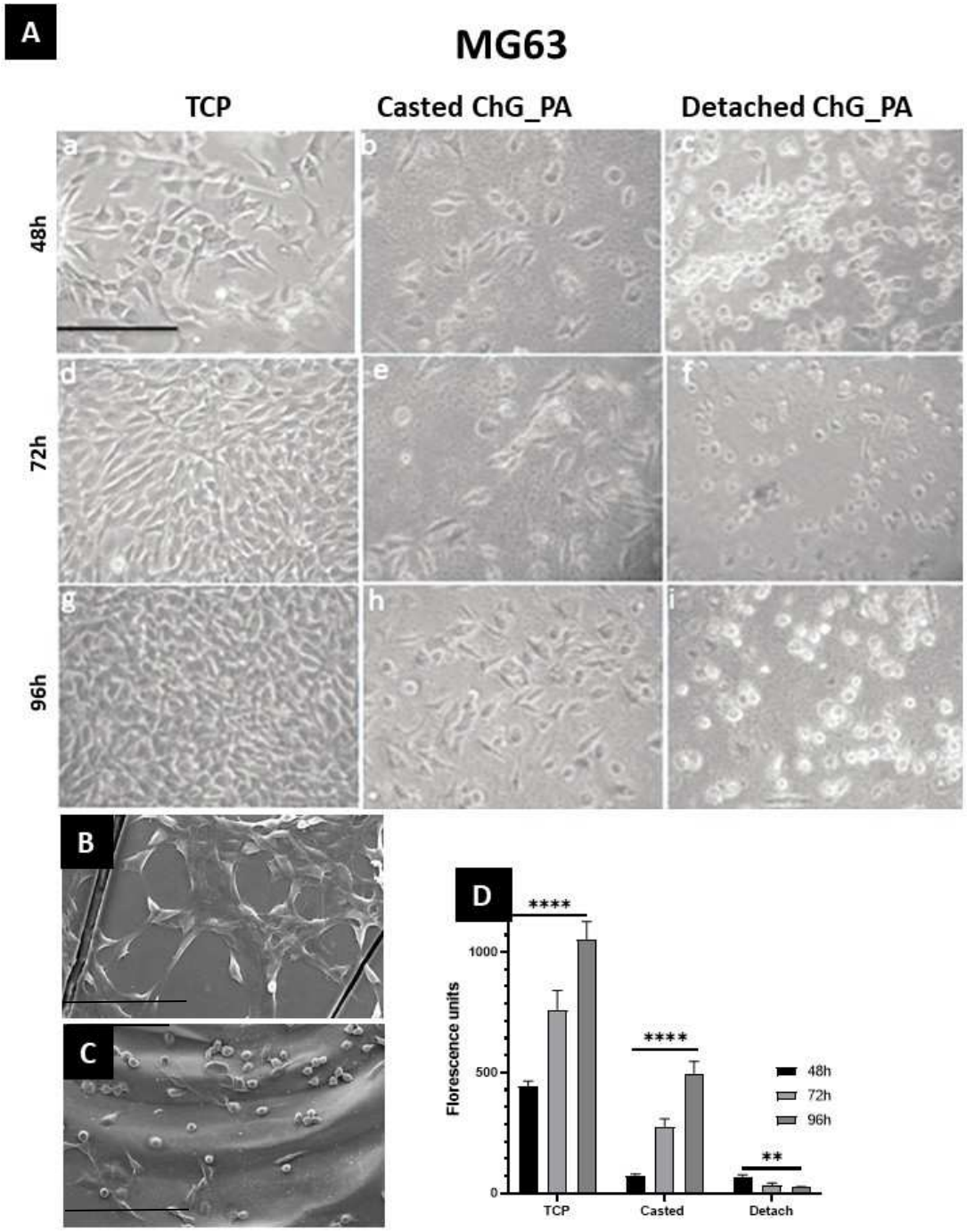

Figure 5. 9 Transferred chitosan-gelatin hydrogel experimental results for MG63 cell line; bar ____= 100µm a, d, g) Cells cultured on 48 cell culture well plates at 48, 96, and 120hrs after being seeded b, e, h) Cells cultured on 3 cm^2 chitosan-gelatin hydrogels detached cut and transferred to 6 cell culture well plates at 48, 96, and 120hrs after being seeded c, f, i) Cells cultured on 3 cm^2 chitosan-gelatin hydrogels detached cut and transferred to cell culture well bioreactor at 48, 96, 120hrs after being seeded and at 24, 72, 96 hrs after dynamic cell culture was started; j) Cell viability test Alamar blue at 48,72,96 and 120 culture hours. k) SEM image of individual cells on transferred chitosan-gelatin hydrogel.

Effects of substrate stiffness on cell number

The preceding experiments (Figure 5.10 and 5.11) showed that the cells used in this study do not increase in cell number on instable loose matrices. Therefore, a hydrogel firmly attached to the bottom and walls of TCP could be a favourable tool to study cell response to variations on the ChG_PA apparent stiffness (AS) *in vivo*.

Metabolic activity

MG63 osteoblast-like cells were cultured on ChG_PA hydrogels cast on TCP at a range of different thicknesses for a period of 21 days. It can be observed (Figure 5.10A) that cells cultured on thick hydrogels (thickness >1.5mm AS > ~58KPa) had relatively little expansion over the first 14-day period, then increased to show significant differences at the 21-day period. Thicker hydrogels over 3.0mm (AS >~2.1KPa) did not show significant change in cell number for the whole extent of the experiment; up to 1.5mm (AS ~58KPa) thick cell number consistently increased over time until the end of the experiment at day 21. The 1.0mm (AS > ~139KPa) hydrogel exhibited increased metabolic activity from each timepoint up until 7-day period in, and then back again at day 21. The 0.5mm (AS ~287KPa) hydrogel showed higher metabolic activity compared to the rest of the samples, reaching its peak at 14 days, and showing no significant decrease after 21-day period. TCP displays a similar trend to 1.5mm (AS ~58KPa) to 0.5mm (AS ~287KPa) with a peak around the 14-day period which slowly declines at later timepoints. From 3-day period and onwards, there was a strong difference between metabolic activity on the 2.0mm (AS ~33KPa) and the 0.5mm (AS ~287KPa) thick hydrogel.

In order to investigate the effect of matrix stiffness in different cell lines, its influence on an additional cell line was investigated. NIH 3T3 fibroblast cells were cultured on ChG_PA hydrogels of thicknesses ranging from 0.5 (AS ~287KPa) to 4.0mm (AS

~2KPa), to determine their effects on cell number. These cells were also cultured for a 21-day period before the samples were prepared for further assays (Figure 5.11B). Different from the MG63 cells, 3T3 cells appear to be able to successfully increase in cell number on all the different hydrogels produced for this study. Despite there being a trend for higher metabolic activity values on the thinner hydrogels, 3T3 relative fluorescence values do not appear to be as strongly affected when compared to trends seen in MG-63 cells. Figure 5.8B shows that cells grown on 2mm (AS ~33KPa) hydrogels onwards appear to display a peak fluorescence value by day 14 leading to a slight decrease in florescence units by day 21indicatiating confluence and contact inhibition. The remaining samples continue to give increased fluorescence values up to day 21, indicating a continuous increase of cellular metabolic activity. TCP peaked at day 14, and readings did not decrease until the end of the experiment at day 21. There is a significant difference between metabolic activity values measured on the TCP controls compared to hydrogels over 1.0mm (AS ~139KPa) thick. Samples of different thickness showed significant difference in metabolic activity between them, i.e., 1.5mm (AS ~58KPa) vs 2.5mm (AS ~4KPa) by 14-day period the significance was stronger on samples between 0.5 (AS ~287KPa) to 2mm (AS ~33KPa) thick hydrogels.

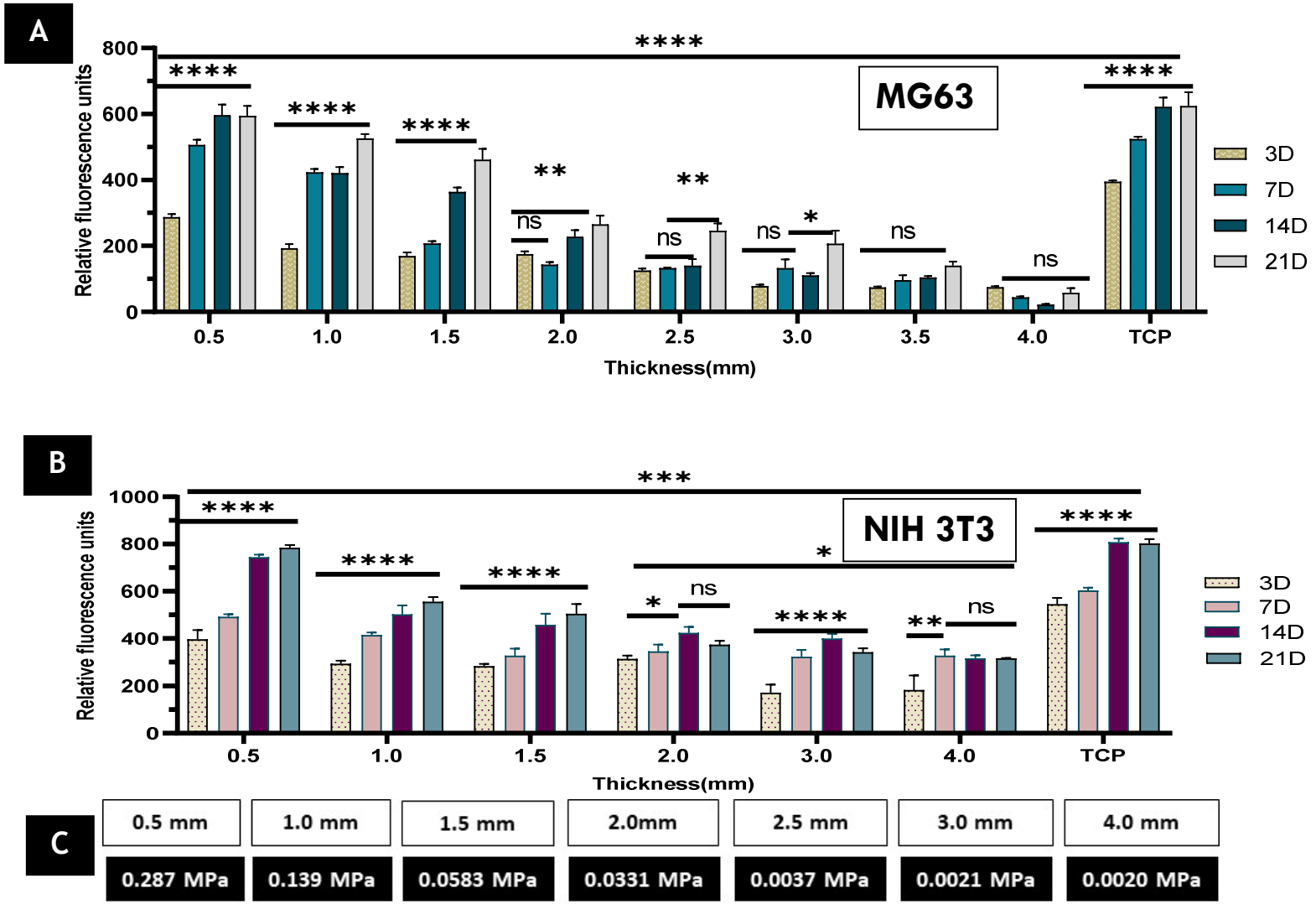

Figure 5. 10 Results of Alamar blue assay on A MG-63 cells. **B** NIH 3T3, cells. The assays were performed on samples seeded onto hydrogels of each thickness and measured at various timepoints. **C** Thickness to apparent stiffness guide. Data was expressed as mean±SEM.

Hoechst 33258 DNA assay

The DNA assay was performed to support the evidence provided by the Alamar Blue assays to elucidate the influence of the hydrogel's stiffness for each cell line cell number. DNA assays were conducted at 14-day, 21-day and 28-day timepoints.

It can be seen from Figure 5.11A, that MG63 cells by 14-day period showed a similar trend to the one seen from the Alamar Blue results. The difference among samples is significant for hydrogels over 2.0mm (AS >~33KPa) thick, a trend on thicker hydrogels can be observed but the difference at this timepoint is not significant. Values ranged from ~0. 1µg/ml for samples over 2.0mm (AS >~33KPa) thick hydrogels to 1.1µg/ml on the stiffest hydrogel 0.5mm (AS ~287KPa) hydrogel. DNA values significantly increased over time on all samples over 2.0mm thick (AS >~33KPa). For the positive control, the trend was more akin to that observed on the Alamar blue results in which the 21-day measurement was as high then for the 28-day timepoint. Values for TCP match those seen on thin hydrogels (0.5mm AS ~287KPa). By the 28-day period there are significant differences between the concentrations from the hydrogel samples and TCP and among all hydrogel samples up to 3.0mm (AS >~2.1KPa)

In a similar fashion MG63 results, the fibroblast NIH3T3 cells cultured on the ChG_PA hydrogel of different thickness exhibited a trend to favour stiffer hydrogels. However, the trend is not as strong as the one observed for MG63, 3T3 are shown to increase in cell number in soft hydrogel as well for hydrogels up to 3.0mm (AS ~2.1KPa) thick (Figure 5.11B). A similar trend was observed on hydrogels thinner than 3.0mm (AS >~2.1KPa), shown to have fast increase in cell number up to 21-day period and reaching their peak for samples 1.0mm (AS ~139KPa) and 2.0 (AS ~33KPa) and slowing down for the other samples. The DNA results showed a consistency the Alamar Blue assay for 3T3 cells which indicated that cell numbers were still increasing by 21-

day timepoint. By the 14-day period, the values between the TCP controls and both 0.5mm (AS~287KPa) and 2.0mm (AS ~33KPa) hydrogels were found to be statistically significant. By the end of the experiment changes in DNA concentrations are seen to vary significantly with hydrogel thickness and in comparison, to TCP.

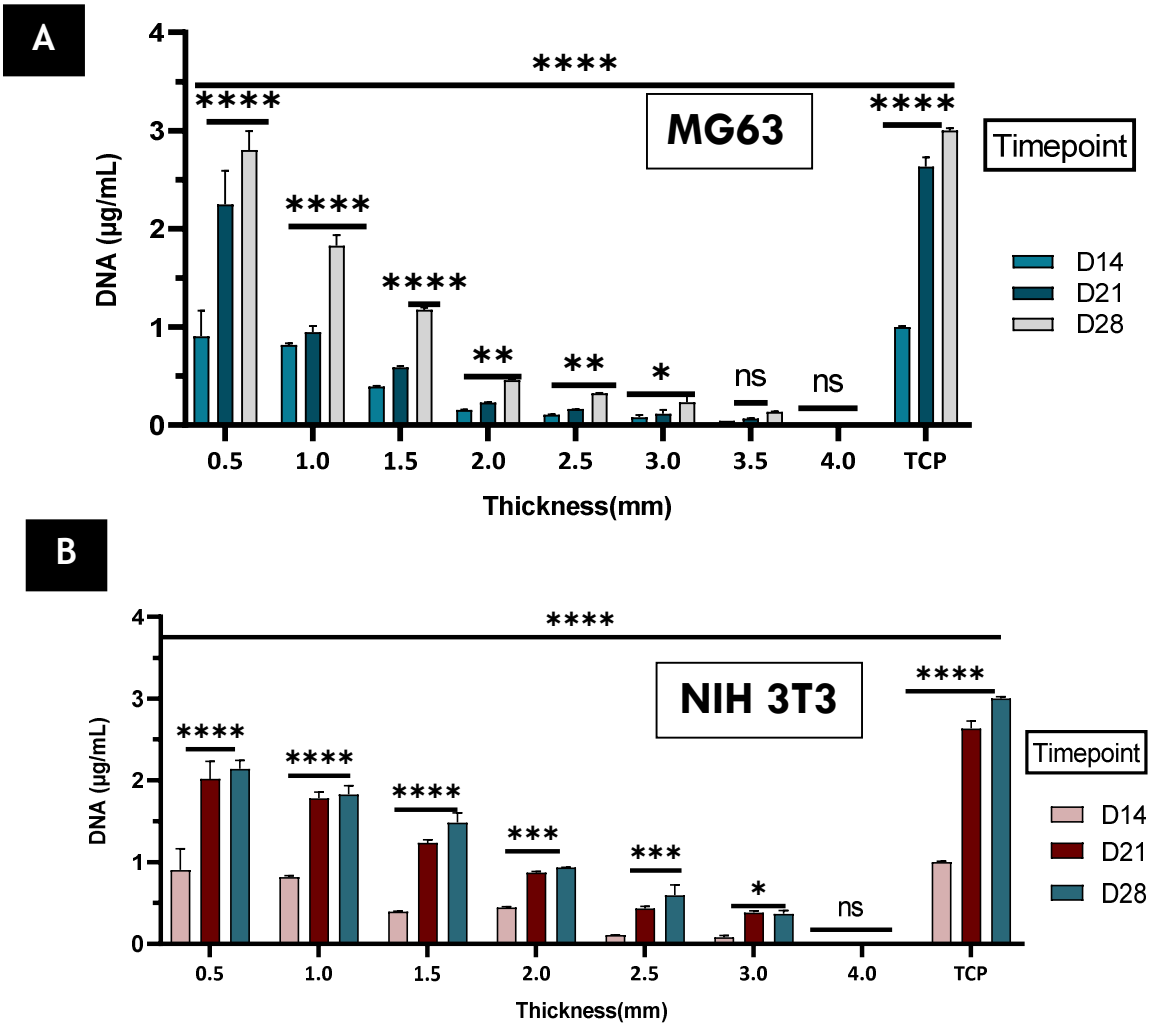

Figure 5. 11 Results of DNA content on A MG-63 cells. **B** NIH 3T3, cells. The assays were performed on samples seeded onto hydrogels of each thickness and measured at 14, 21 and 28 days after seeding. Data is expressed as mean±SEM.

Effects of substrate stiffness on cell morphology

To test the effect of substrate apparent stiffness on single cell spreading, MG63 and 3T3 cells were seeded on ChG_PA hydrogels of different thicknesses. Figures 5.12 and 5.13 show the morphological cell differences between hydrogels of different apparent stiffness for both cell lines MG63 (Figure 5.12) and 3T3 (Figure 5.13).

Phase contrast images of MG63 grown on ChG_PA hydrogels of varying thicknesses, after 24, 48, 72 and 120h of culture are shown in Figure 5.12A. Cells seeded on thin hydrogels (0.5mm AS~287KPa) showed a flattened morphology fully attached and spread after 24hrs of incubation. This characteristic was observed to change as the thickness of the substrate was increased (1mm, AS~58KPa and 2.5 mm, AS ~3.7KPa), leading to a rounder spherical shape for those cells seeded on substrates of higher thickness and lower stiffness (Figure 5.12Aa-b, B, C). At the end of 7 days of culture, increase in cell number was found to be higher on the thinnest hydrogel when compared to the thickest with no cell spread uniformly on these hydrogels compared to thick hydrogels. The formation of cell aggregates was observed on softer hydrogels, and morphology, number and size showed to change as thickness of the substrate was varied (Figure 5.9A h,i,l).

Contrary to MG63, which showed perceptible morphological differences between groups for the whole extent of the experiment, fibroblast showed morphological difference only until confluence was achieved; before then a similar trend as seen on MG63 could be seen cells were flat and spread on stiff substrates and rounded but, not spherical on soft ones (Figure 5.12Aa-b B-C). After confluence was achieved, no appreciable difference could be observed among groups (Figure 5.12. j, k, m, n). MG63 showed a higher predilection for stiffer substrates contrary to fibroblast NIH 3T3, which kept their round shape longer (76 hrs) on softer materials and formed dense

cell aggregates for the duration of cell culture. This trend was not observed for 3T3, which at all timepoints kept a uniform flat monolayer of spread cells as collective morphology and no cell aggregates of dense rounded cells were found.

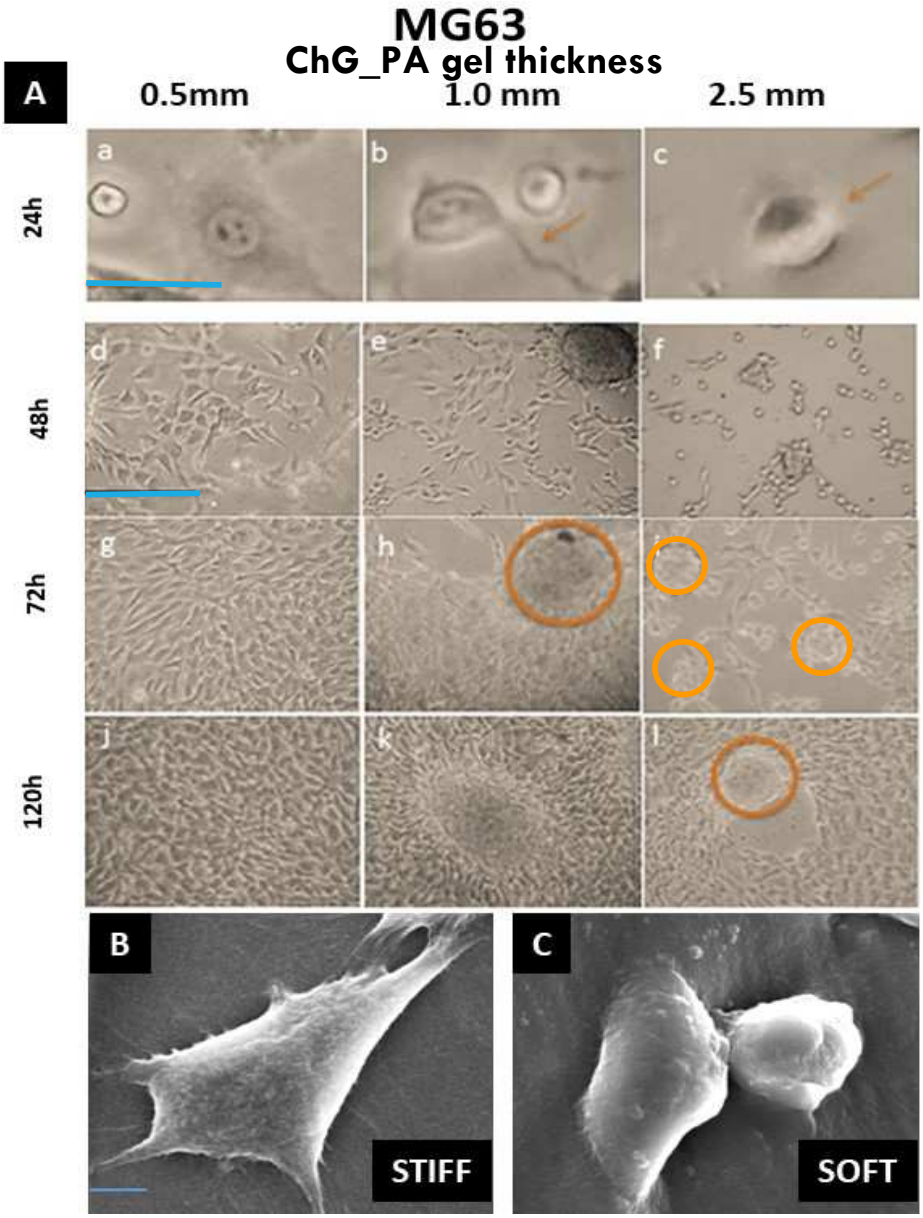

Figure 5. 12 MG63 cell line morphology changes as response to hydrogel apparent stiffness; bar = 10µm ▬ bar = 100µm **A| a, d, g, j)** Cells cultured on 0.5mm thick hydrogels; **b, e, h, k)** Cells cultured on 1.0mm thick hydrogels **c, f, i, l)** Cells cultured on 2.5mm thick hydrogels at 24, 48, 72, and 120h of incubation; small orange arrows show the cell process formations, as orange circles point at the formation of cell aggregates as they appear on soft substrates **B|** SEM image of cells on 0.5mm (AS ~287KPa) thick hydrogel **C|** SEM image of cultured cells on 2.5mm(AS ~3.7KPa) thick sample.

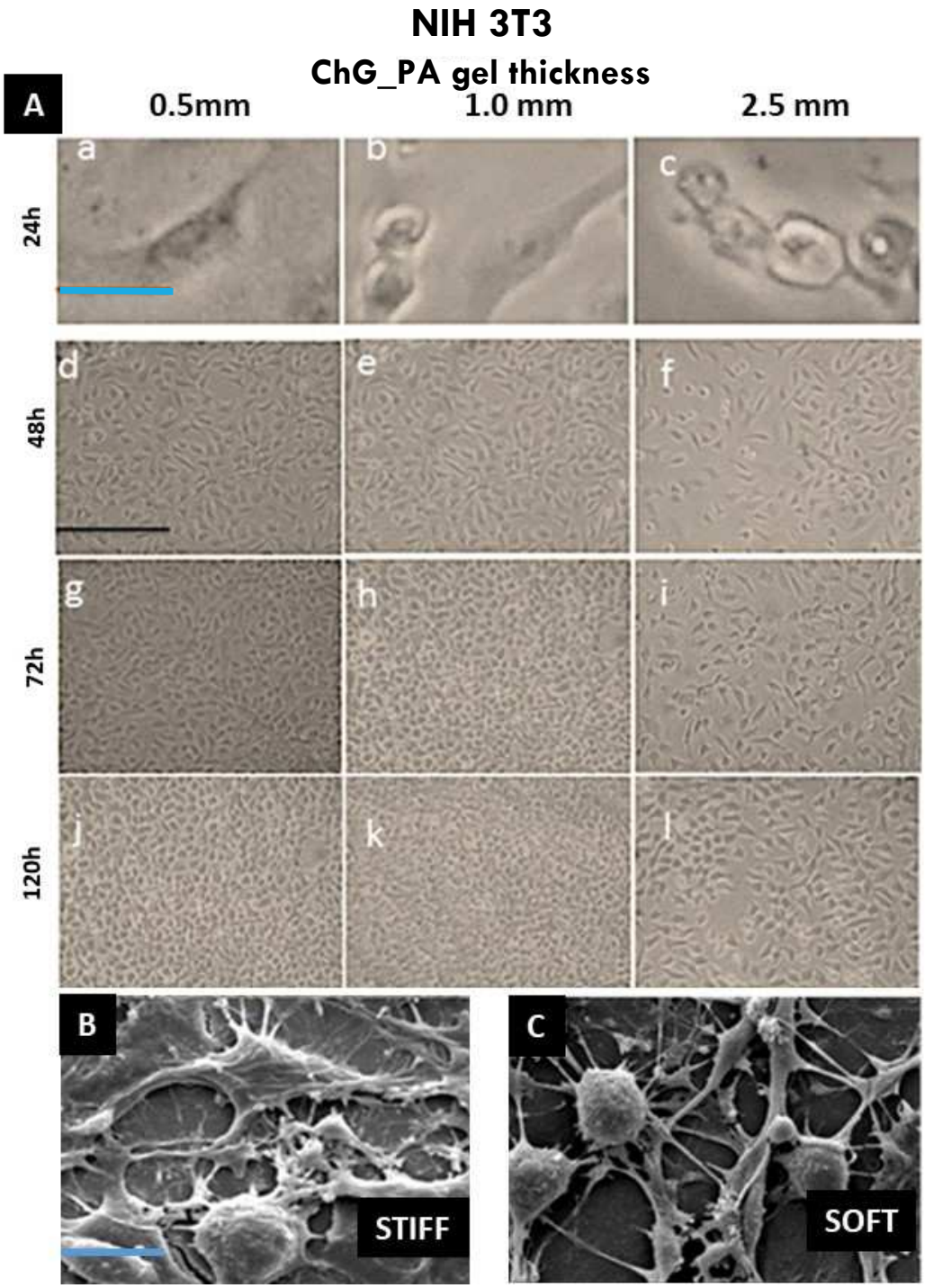

Figure 5. 13 NIH 3T3 cell line morphology changes as response to hydrogel apparent stiffness; bar = 10μm ▬ bar = 100μm **A| a, d, g, j)** Cells cultured on 0.5mm thick hydrogels; **b, e, h, k)** Cells cultured on 1.0mm thick hydrogels **c, f, i, l)** Cells cultured on 2.5mm thick (AS~3.7KPa) hydrogels at 24, 48, 72, and 120h of incubation; **B|** SEM image of cells on 0.5mm thick (AS ~287KPa) hydrogel **C|** SEM image of cultured cells on 2.5mm thick sample.

Effects of substrate stiffness on human mesenchymal stem cell hMSC

hMCS cells were seeded at two different cell densities: low density (Low_SD= 250 cells/cm$^{2)}$ and high density (High_SD=2500 cells/cm^2) to evaluate the effect of apparent stiffness sensing on differentiation.

Observing effects of substrate stiffness on short term cell attachment.

The short-term cell attachment of hMSC as a function of hydrogel apparent stiffness can be seen on Figure 5.14. To generate quantitative results for these images, cell morphology was grouped into 3 different types, each describing different stages on the cell attachment process (Figure 5.14B).

Type 1 cells display a circular morphology and appear to be sitting on the surface of the hydrogel substrate and do not appear to have formed surface adhesion.

Type 2 cells are beginning to move away from a circular morphology and are beginning to elongate and extend lamellipodia, indicating that they are beginning to adhere and spread on the surface.

Type 3 cells have substantially elongated and developed a much 'flatter' morphology as they have begun to spread across the surface of the substrate.

Each sample image was analysed based on the previously described categorization, and percentage values of each type per thickness and timepoint were plotted and presented in Figure 5.14C from which it can be observed that 2 hours after seeding, the stiffer 1mm hydrogel had a higher number of cells with a morphology indicative of early attachment to the substrate. On the 2mm hydrogel (AS ~33KPa), 93% of cells were found to be type 1 by the 2-hour timepoint; compared to only 51% of cells being categorized as type 1 on the 1mm hydrogel (AS~139KPa). This trend became more acute for the 6-hour sample, with the 1.0mm (AS~139KPa) hydrogels having only 20%

of their cell population being categorised as type 1- and 2-mm hydrogels having still 75% cells on the type 1 category, indicating significant difference as a function of sample thickness and time.

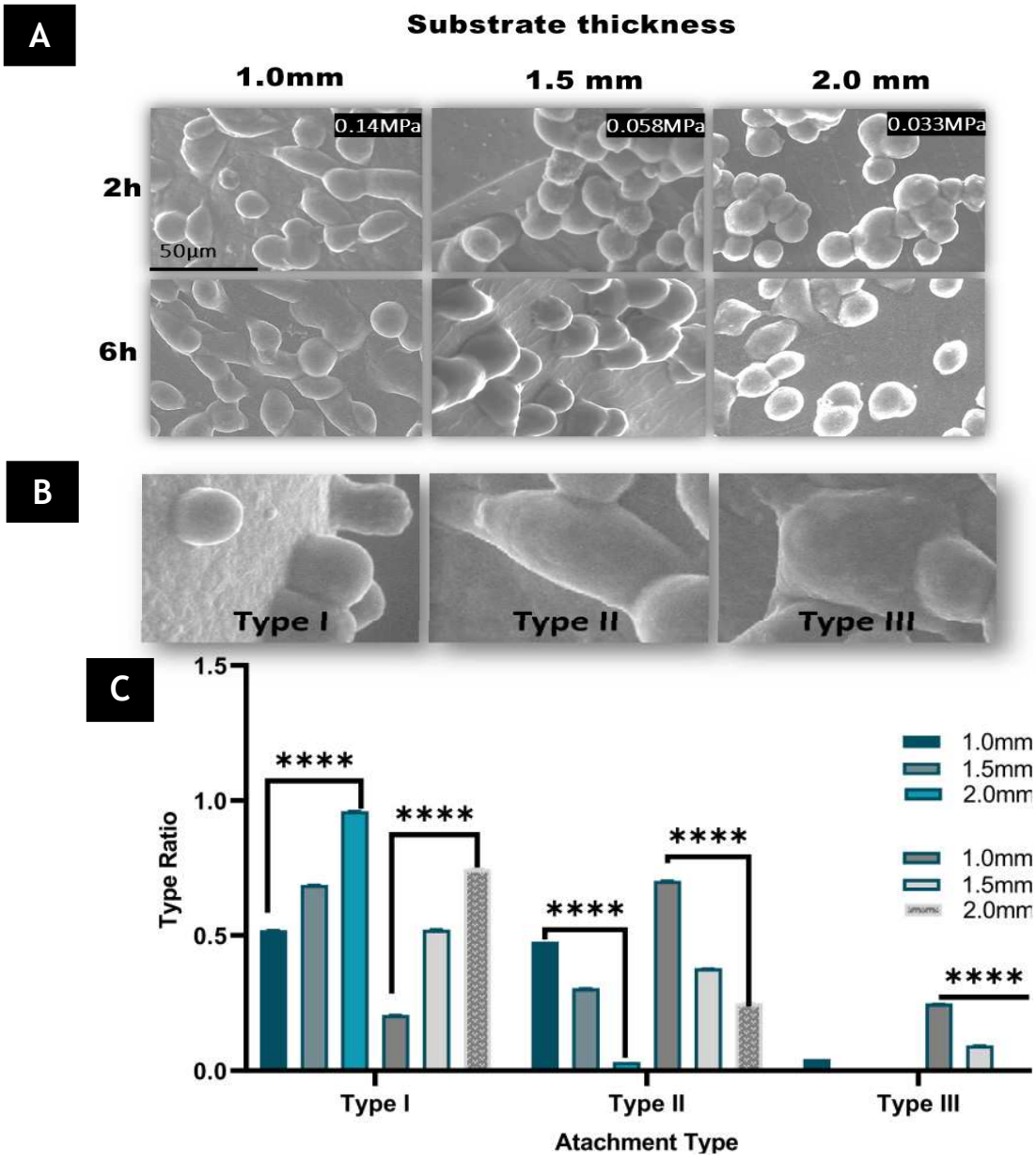

Figure 5. 14 Cell attachment observation. A Cell response the different cell morphology types that were categorised to quantify attachment and adhesion of hMSCs to hydrogel samples. B ESEM images showing the categorized cell types, **type i** represents the cells which have only just adhere and not began to spread along the surface, **type ii** indicates cells that have just started spreading and **type iii** denotes the cells with the most spread morphology indicating full adhesion to the surface. **C** Graphical representation of cell adherence ratios.

Cell viability studies

Metabolic activity

hMSCs were cultured on ChG_PA hydrogels of varying thickness for periods of up to 42 days. Alamar blue tests were carried out on days 3, 7, 14, 21,28,35 and 42 of their incubation to measure the increase in cell number over extended lengths of time.

It can be observed (Figure 5.15A) that samples seeded at low cell seeding density (Low_SD) had little expansion over the first 3 and 7-day period of culture and no significant differences could be detected. It is after 14-day period when significant expansion on thinner (0.5mm AS~287KPa and 1.0mm AS~139KPa) hydrogels was observed, compared to thicker hydrogels (over 2.0mm AS >>~33KPa) which showed no significant expansion. Significant growth for the majority of the samples was achieved by day 28 of culture when expansion was significant between timepoints and samples over 2.5mm thick (AS >~3.7KPa) and a significant increase in metabolic activity similar to that one observed for MG63 was observed on thinner, stiffer hydrogels (over 1.5mm, AS >~058MPa), hMSCs showed strong preference for stiffer substrates as MG63, however hMSCs were more responsive to thicker hydrogels (2.5mm thick AS~4KPa) compared to MG63 (2.0mm AS ~33KPa). In most samples peaked at day 35 of culture and then started to decrease. Thicker hydrogels (over 3.0mm thick AS >~2.1KPa) did not show significant changes in cell number for the whole extent of the experiment. Cells growing on TCP showed similar increase in cell number to those on the 0.5mm (AS ~287KPa) thick hydrogels, however they showed significant differences between them after 7 days of incubation, and a faster increase in cell number, reaching their peak at day 21.

For cells seeded at a higher cell density (High _SD), from Figure 5.15B, these hydrogels also had low metabolic activity over the first 3 and 7-day period of culture. However, compared to what was observed on the Low_SD group for the thinner hydrogels (0.5 AS ~287KPa, 1.0 AS ~139KPa- and 1.5-mm AS ~58KPa thick hydrogels), significant differences were observed compared to soft, thick hydrogels (3mm AS ~2.1KPa). By the 14-day period, the preference of this cell line for stiffer substrates was marked compared to soft hydrogels over 2.5mm thick (AS ~3.7KPa). Significant increase in metabolic activity for the majority of the samples was achieved by day 28 of culture compere to day 21 and below, when maximum metabolic activity was achieved for all the samples except for those on soft =<3.0mm thick (AS ~2.1KPa) samples, for which cells did not show sensitivity for the whole extent of the experiment for cells seeded at low density. Most of these samples also peaked at day 35 of culture, and then started to decrease. Thicker hydrogels over 3.5mm (AS> ~2.1KPa) did not show a significant change in cell number for the whole extent of the experiment. Cells growing on TCP showed to increase in cell number similarly to the 0.5mm (AS ~287KPa) thick hydrogels, but showed significant difference from the first week, and a faster increase in cell number reaching their peak at day 28, a week earlier then the low cell density group.

DNA Content

Pico Green DNA assays were conducted, as an indicator of MSC absolute cell number via correlating DNA content with relative metabolic activity to give an estimate of relative cell numbers. This test was also important to allow ALP and mineral deposition data to be normalised to DNA content. Since low seeding-densities were used, DNA content in cultures was higher after 21 days and 28 days of culture. Cell numbers were generally higher for higher cell seeding-density samples.

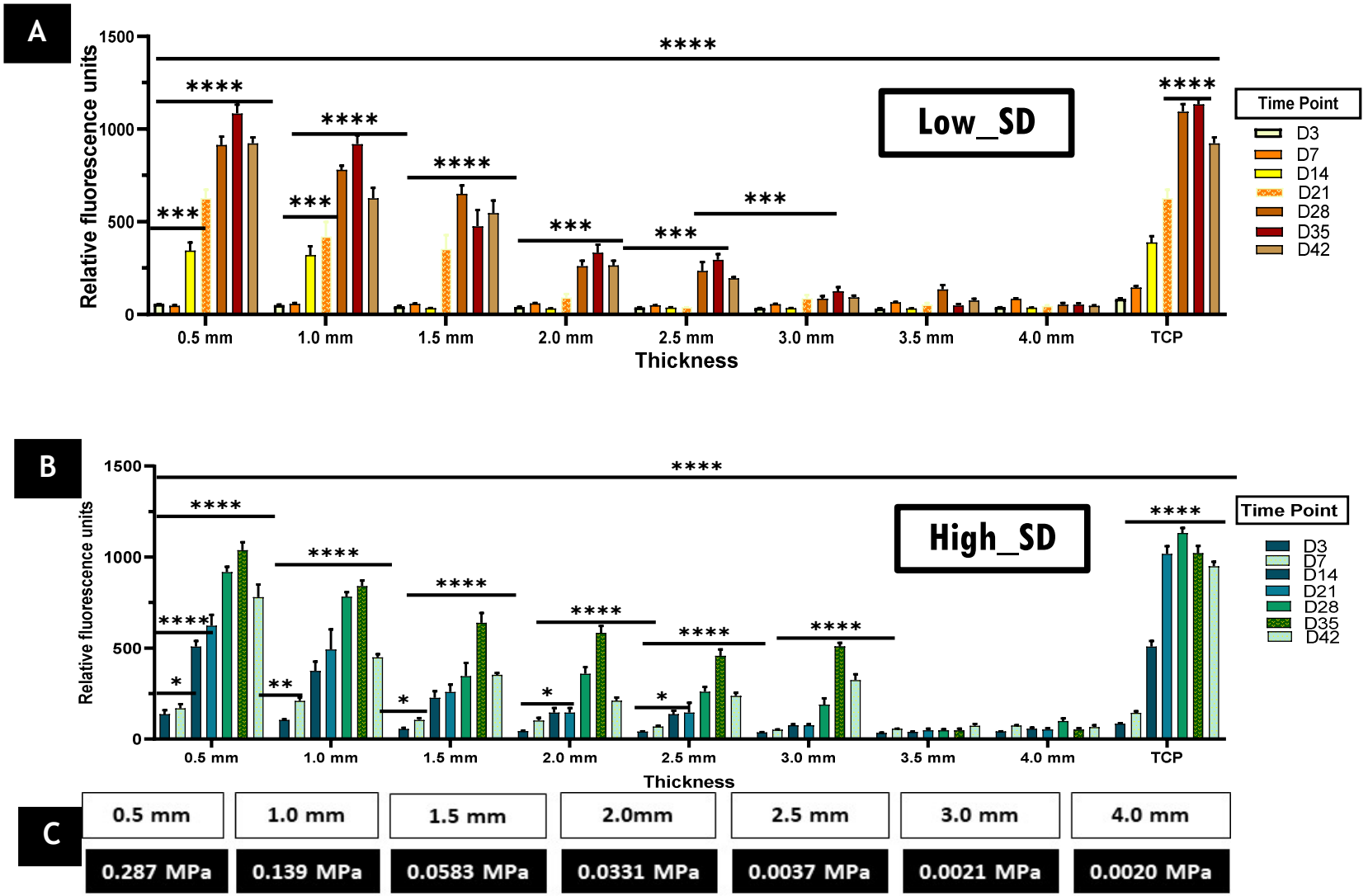

Figure 5. 15 Results of Alamar blue assay hMSC's A Low cell seeding density (Low_SD 250 c/cm^2 cell density). **B** High cell seeding density (High_SD 2500 c/cm^2 cell density). The assays were performed on samples seeded onto hydrogels of each thickness and measured at various timepoints. **C** Thickness to apparent stiffness guide. Data is express as mean ±SEM

DNA tests were conducted at 21-day, 28-day and 35-day timepoints using hMSC. Low_SD samples (Figure 5.16A) showed growth as response to sample thickness, significant differences between samples and TCP were seen by day 21 of culture. At this timepoint, DNA content can be observed for 0.5mm (AS ~287KPa), 1.0mm (AS ~139KPa) and the positive control TCP, with values ranging from 0.25µg/ml to 0.35µg/ml, and the difference on DNA content compared to soft, thick hydrogels was found to be significant. DNA values keep significantly increasing over time for stiffer samples (<1.0mm AS ~139KPa) only until the 21-day period, compared to soft hydrogels (>1.5mm AS ~58KPa), yet by day 28 of culture, DNA content on these stiff hydrogels reached their peak, ranging from 0.01µg/ml to 0.98µg/ml and were significantly different compared to samples over 3mm (AS ~2.1KPa) thick. DNA content for thicker samples (3.5mm AS ~2KPa and 4.0mm AS ~2KPa) remained without significant differences among themselves at diffe0rent timepoints and between thickness over 3.5mm (AS ~2KPa) thick, throughout the extent of the experiment.

As seen on Low_SD hydrogels, hMSC also increase in cell number as a function of sample thickness on High_SD hydrogels (Figure 5.16B), for this sample the same trend was observed in which significant differences between samples over 1.0mm (AS ~139KPa) thick and TCP were observed compared to thick hydrogels over 2.0mm thick (AS ~33KPa). By day 21 of culture, DNA content differences were seen on samples 0.5mm (AS ~287KPa), 1.0mm (AS ~139KPa) and the TCP, with values ranging from 0.25µg/ml to 0.35µg/ml, no significant DNA concentration was detected for the thicker samples compared to stiff hydrogels over 1.0mm (AS ~139KPa) thick until day 28 of culture, when DNA content was significantly different for samples over 3mm thick. DNA content for thicker samples (3.5mm and 4.0mm, AS ~2KPa) was detected at day 28, but showed no significance between timepoints and hydrogels.

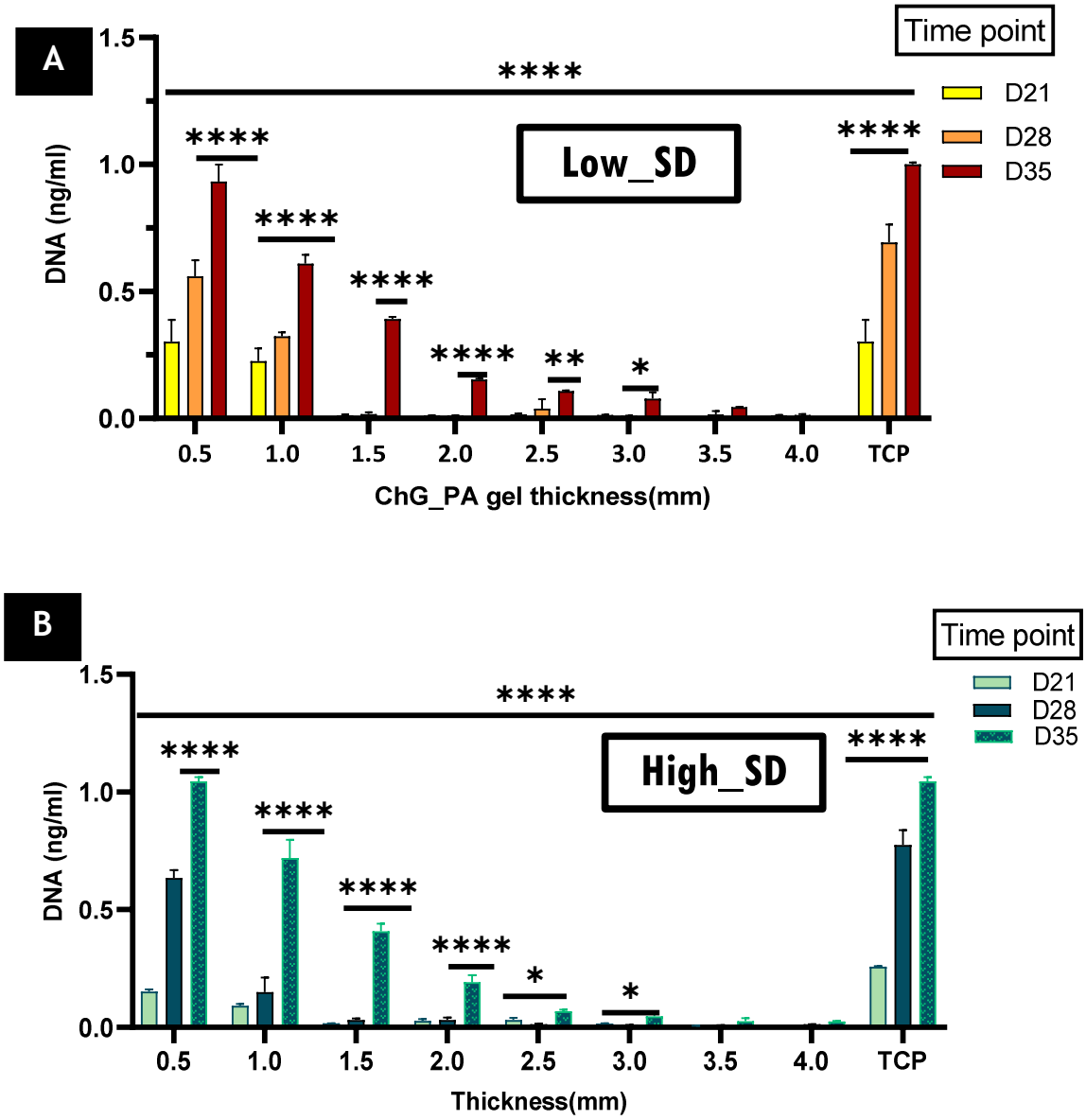

Figure 5. 16 Pico green DNA Test quantifies hMSC's DNA content A Low cell seeding density (Low_SD 250 c/cm^2 cell density). **B** High cell seeding density (High_SD 2500 c/cm^2 cell density). The assays were performed on samples seeded onto hydrogels of each thickness and measured at various timepoints.

Morphological changes

Single cell area

The preceding experiments (Figure 5.15 and 5.16) showed hMSC response to changes in apparent stiffness due to changes in hydrogel thickness. This led to the hypothesis that these cells would be able to sense changes in stiffness through soft hydrogels due to the firm attachment of the hydrogel to an underlying stiffer material and rearrange their inner structure, therefore. To test this hypothesis, hMSC cells at different cell densities (Low_SD and High_SD) were seeded on ChG_PA hydrogels cast on TCP of varying thickness (0.5-4.0mm, AS ~287KPa to 2KPa). The results (Figure 5.17) showed that cells detect and respond to changes in the apparent sample stiffness. There was an increase in cell area on stiff hydrogels (287.5 KPa: 4873± 314μm$^{2)}$ compared with soft ones (4KPa: 435± 36μm^2). The maximum area was reached on 0.5mm thick hydrogel (AS~287 KPa) and was like the area on TCP which has a Young's modulus of approximately 10MPa. Table 5.3 shows a summary area versus thickness. The decrease in cell area can be described using an empirical relationship as a function of thickness. This relationship between single cell-spread area and hydrogel thickness was well described by an exponential model ($Y = (Yo - Y\infty)e^{-Kx} + Y\infty$) with a value for $\ln 2/k$ (the elasticity at which a cell reach half of its maximum spreading and to half-life in an exponential decay function – referred in similar studies as 'tactile half-depth' [22]) equal to 1.44mm, and an $R^2 = 0.972$). This half-maximal response ($\ln 2/k$) value of 1.44mm corresponds to a tactile half-depth equivalent to the ~3.4μm value reported previously for marrow stromal cells on synthetic soft PAAm (E 9KPa) [13]. Indicating that a non-linear fibrillar biomaterial, such as the ChG_PA hydrogel used in this study, can substantially amplify the transmission of stress forces and therefore the depth at which cells sense an underlying rigid material.

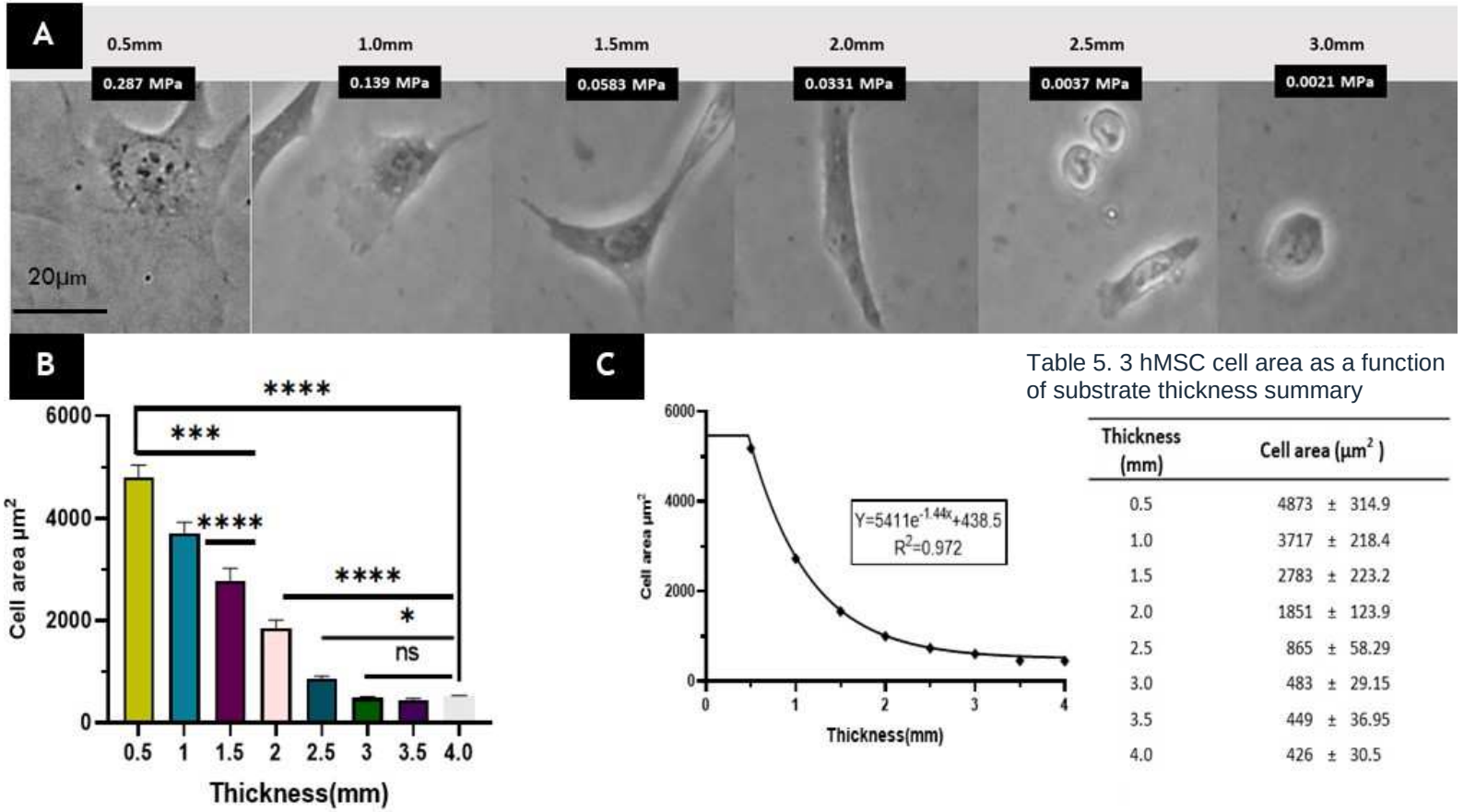

Table 5. 3 hMSC cell area as a function of substrate thickness summary

Thickness (mm)	Cell area (µm²)
0.5	4873 ± 314.9
1.0	3717 ± 218.4
1.5	2783 ± 223.2
2.0	1851 ± 123.9
2.5	865 ± 58.29
3.0	483 ± 29.15
3.5	449 ± 36.95
4.0	426 ± 30.5

Figure 5. 17 Cell spreading area is affected by the depth at which cells sense an underling stiffer substrate. A hMSC cells were cultured on ChG_PA hydrogel. Cells were imaged after 96 h in culture. **B** Mean cell area decreased asymptotically as thickness increased to a threshold of ~3.0mm. The data were fitted to an exponential model (R^2 = 0.972, with a half-maximal response (ln2/k) at 1.44mm). Data presented as mean ± SEM.

Cell orientation

It was of interest for this study to investigate whether matrix stiffness had any influence on the cell orientation angle, as this is a predictor of cell durotaxis [92]. Human mesenchymal stem cells were seeded on ChG_PA hydrogels of varying thickness, and images after 72hrs were taken and analysed. No significant differences between samples were detected for samples over 3mm thick (AS ~2.1KPa). The shape of the orientation angle distribution of each group shows a random distribution of cell orientation; no dependent relationship between cell angle orientation and thickness was found. The orientation angle of the round cells on soft hydrogels (3.0mm thick, AS ~2.1KPa) showed to have an orientation average of 15°. This result leads to the conclusion that cells seeded on substrates of uniform apparent stiffness will not show preference for a particular orientation.

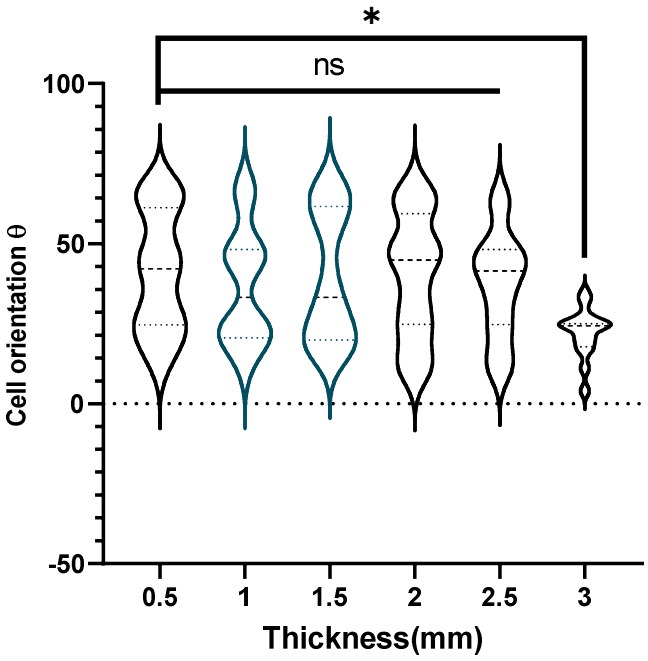

Figure 5. 18 Cell orientation angle sample distribution. No significant correlation was found among orientation angle and substrate stiffness (R^2=0.043).

The effect of substrate thickness on cell aggregates stiffness sensing

The previous experiments showed that single hMSC cells could mechanosense substrate stiffness through changes in the geometry of the material (thickness) (Figure 5.14-5.17). It was also shown that the formation of MG63 clusters increased as a function of substrate thickness (Figure 5.11). Therefore, a decrease in substrate thickness was expected to increase the local stiffness that the cell experiences and to induce an increase in colony spreading.

To determine substrate thickness effect on colony morphology, ChG_PA hydrogels of varying thicknesses were prepared and hMSC cells seeded at different cell densities and after 5 days in culture, the cell clusters were imaged, it was observed that cells formed larger spread-areas on thin hydrogels than on the thick ones as was observed for single cell experiments (Figure 5.17). Cell aggregate morphology was observed to be also dependent on hydrogel thickness (Figure 5.19). On thin (~0.5mm, AS ~287KPa) ChG_PA hydrogels, the cell clusters appeared spread, and each cell within the aggregates was clearly distinguishable. In contrast, on thick (~3.0mm, AS ~2.1KPa) hydrogels, colonies appeared rounded and densely packed. It was also observed that cell colony formation was dependent on both the substrate thickness and the cell seeding density and that there is a threshold for its appearance, linked to these two restrictions.

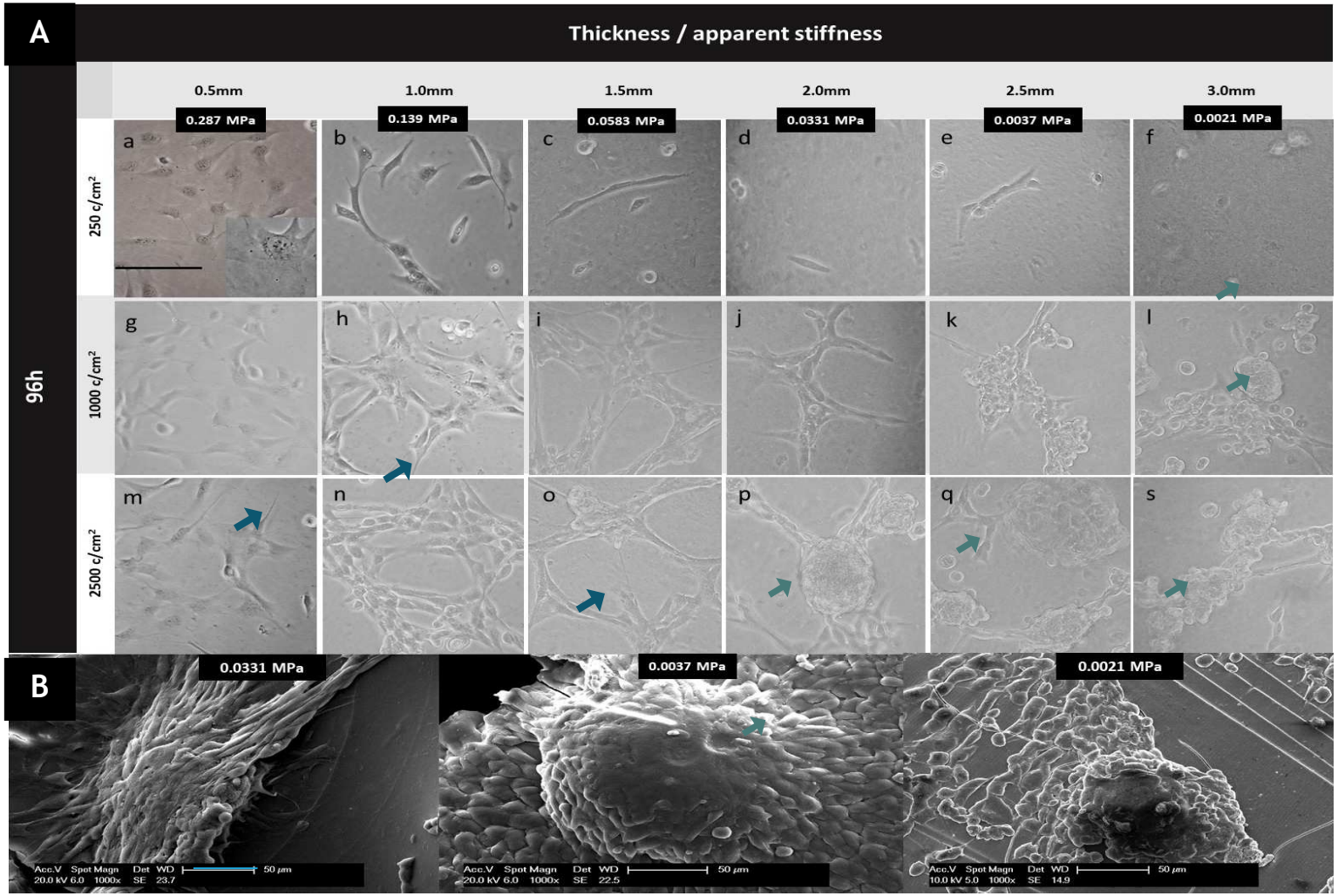

Figure 5. 19 The effect of cell seeding density and substrate stiffness on hMSC cells colony formation. A The phase contrasts images show hMSCs will group on dense packed colony formations as a function of population size and substrate stiffness. (Pointed by green arrows). As stiffness, increased cells displayed a fusiform shape with evident formation of filopodia-like structure (blue arrow). Scale bar__: 100 µm scale bar__ :20µm **B** SEM images of hMSC colonies on substrates of different stiffness.

Effects of substrate stiffness on hMSC osteogenic differentiation

To determine the influence of matrix stiffness on the differentiation of hMSCs, cells were seeded on ChG_PA hydrogels of varying thickness (0.5mm to 4.0mm) at two different cell densities: 250 cells/cm^2 (Low_SD) and 25000 cells/cm^2 (High_SD) for 21-, 28-, and 35-day timepoints. Two osteogenic markers ALP and osteocalcin were assessed in cells to determine hMSCs osteogenic differentiation.

ALP expression

It can be observed (Figure 5.20A) that samples seeded at low cell seeding density (Low_SD) on substrates of different thicknesses showed ALP activity over the first 21days of culture. Thin stiff substrates (0.5mm AS~287KPa and 1.0mm AS~139KPa) hydrogels and TCP (Young's modulus ~10MPa) achieved their highest levels of the marker expression at 21days timepoint. Significant differences were observed on ALP activity on these stiff surfaces compared to the rest of the hydrogels tested at this timepoint (21 days), ALP activity was significantly lower on hydrogels below 1.5mm (AS~58KPa) thick and no significant variations were detected between these medium to soft gels (AS<~58KPa). No significant differences were observed between day 21 and day 28 for most of the samples, except for the 1.0mm thick hydrogel, which expressed a significant reduction compared to the previous 21days timepoint, and the 2.0mm thick hydrogel which showed a significant increased ALP activity, compared to the 21 days timepoint. However, significant reductions of ALP activity were observed for stiff thin samples (0.5mm and 1.0mm) and TCP by day 35 of culture compared to samples at 28 days of culture. Samples over 2.5mm (AS < ~3.7KPa) thick, did not show significant variations on ALP activity during this experiment.

For cells seeded at a higher cell density (High _SD) it can be seen (Figure 5.20B) that by day 21of culture, ALP activity on the 1.0mm thick (AS ~139KPa) hydrogels was

significantly high compared to the rest of the hydrogels and TCP. By day 28 of culture a significant increase on the ALP activity, compared to the ALP activity observed at 21 days timepoint, was observed on most of the hydrogels (except for the 1.0mm AS ~58KPa, 2.0 mm AS~ 33KPa thick samples and thicker hydrogels over >3.0mm AS <~2.1KPa). Except for 1.0mm (AS ~58KPa) and 2.0mm (AS ~33KPa) thick hydrogels, the rest of the hydrogels over the AS threshold (AS~2.1 KPa) maximum ALP activity was reached at day 28 of culture– for the 1.0mm thick hydrogel (AS~139 KPa) maximum ALP was observed at timepoint day 21 of culture, and for 2.0mm thick hydrogel (AS~33 KPa) at timepoint day 35. Significant decrease in ALP activity was reported for all substrates, except for samples 2.0mm thick (AS~33KPa), which, as mentioned, expressed their maximum ALP activity by this timepoint; for samples over the ~AS threshold AS ~2.1KPa, 3.5mm and 4.0mm (AS<~2KPa), however, no significant variations were observed along the length of the experiment. The results for ALP activity on samples of different seeding densities also showed significant differences, suggesting that ALP activity is a combined cell-cell interaction, matrix-stiffness dependent function.

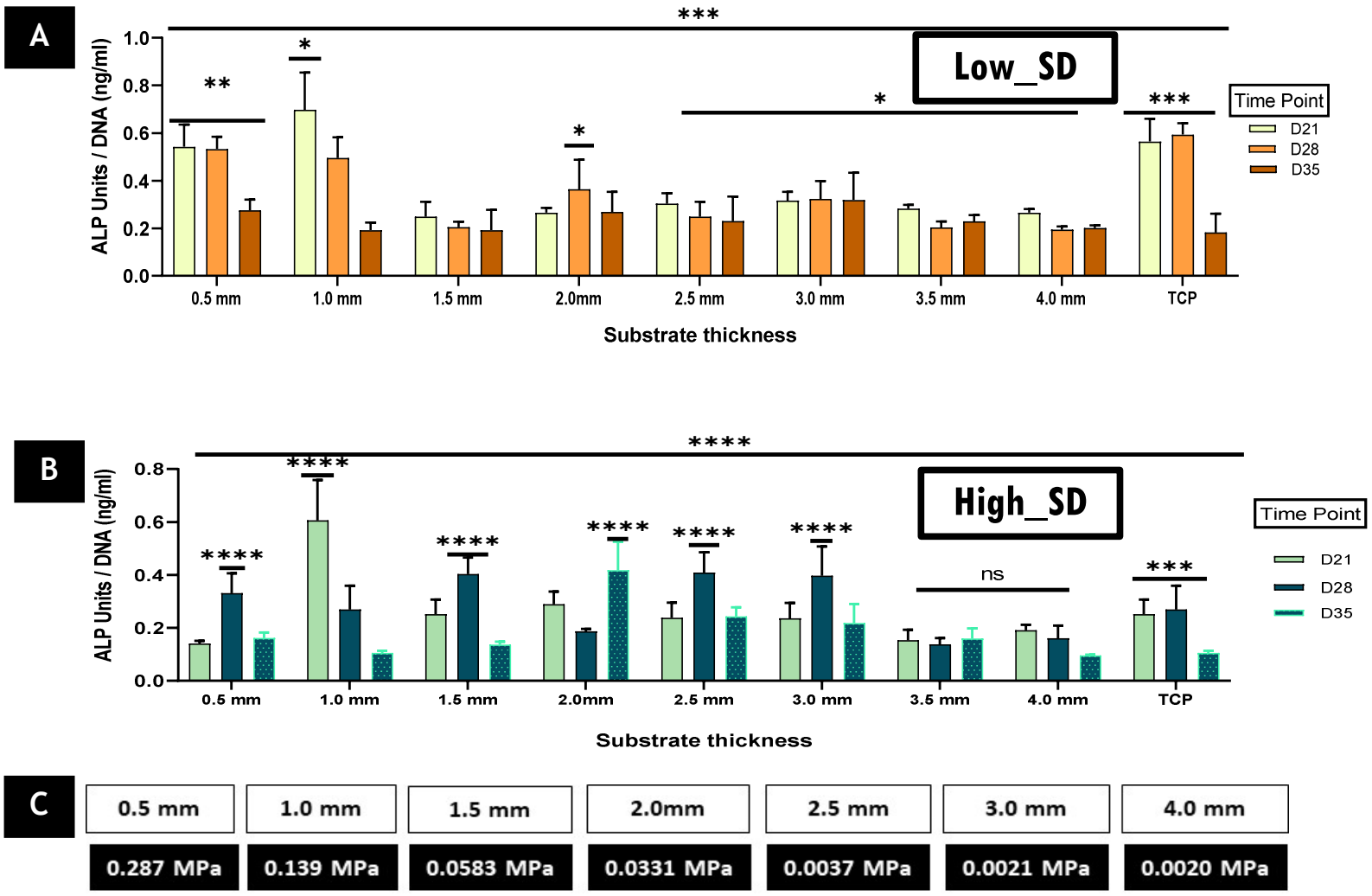

Figure 5. 20 Results of ALP expression assay of hMSC's A Low cell seeding density (Low_SD 250 c/cm^2 cell density). **B** High cell seeding density (High_SD 2500 c/cm^2 cell density). The assays were performed on samples seeded onto hydrogels of each thickness and measured at various timepoints. Florescence unites where normalized with DNA content. Data is shown as group mean ± SEM **C** Thickness to apparent stiffness guide.

Osteocalcin expression

Figure 5.21A shows the osteocalcin expression for hMSCs seeded on hydrogels of different thickness at low cell seeding density (Low_SD). Osteocalcin expression was seen to be significantly higher at 21day of culture on thin stiff hydrogels of 0.5mm thick (AS~287KPa) and TCP (Y'sM ~10MPa) compared to the rest; Two mm and 3 mm thick hydrogels (AS ~33 to ~2KPa) were seen to have higher osteocalcin expression levels compared to thicker (3.5mm -4.0mm, AS~2 KPa) hydrogels, however, differences showed no significance. Except for hydrogels 2.5mm thick (~3.7 KPa), the osteocalcin expression was observed to decrease for all the other samples after day 28.

Figure 5.21B shows the osteocalcin expression for hMSCs seeded on hydrogels of different thickness at high cell seeding density (High_SD). hMSCs seeded at high cell showed osteocalcin expression on all samples from day 21 of culture. Stiffer samples (0.5mm to 2.0mm thick; AS ~287-33KPa) and TCP (~10MPa) presented higher significant levels of this marker from day 21, the thinnest stiff samples (0.5mm, AS ~287KPa) and TCP showed their peak at this timepoint. Thicker samples (3.5mm and 4.0mm AS ~2KPa) showed significant lower levels of the marker compared to stiffer samples (over 3.0mm thick; AS~2.1KPa) but also peaked at day 21 of culture. By day 28 of culture, expression of osteocalcin decreased in all the samples except for 1.0mm and 1.5mm (AS~139KPa and ~58KPa), for which samples osteocalcin expression increased, on the latter the increase was shown to be significant.

The difference between cell seeding densities (Low_SD and High_SD) showed significant differences for samples over 1.0mm (AS~139KPa) for both timepoints, suggesting that the expression of the osteocalcin marker is an interrelated function of sample thickness and cell numbers. Collectively, these results suggest that culture on AS ~258KPa–~58 KPa better facilitate hMSCs to differentiate into osteoblasts.

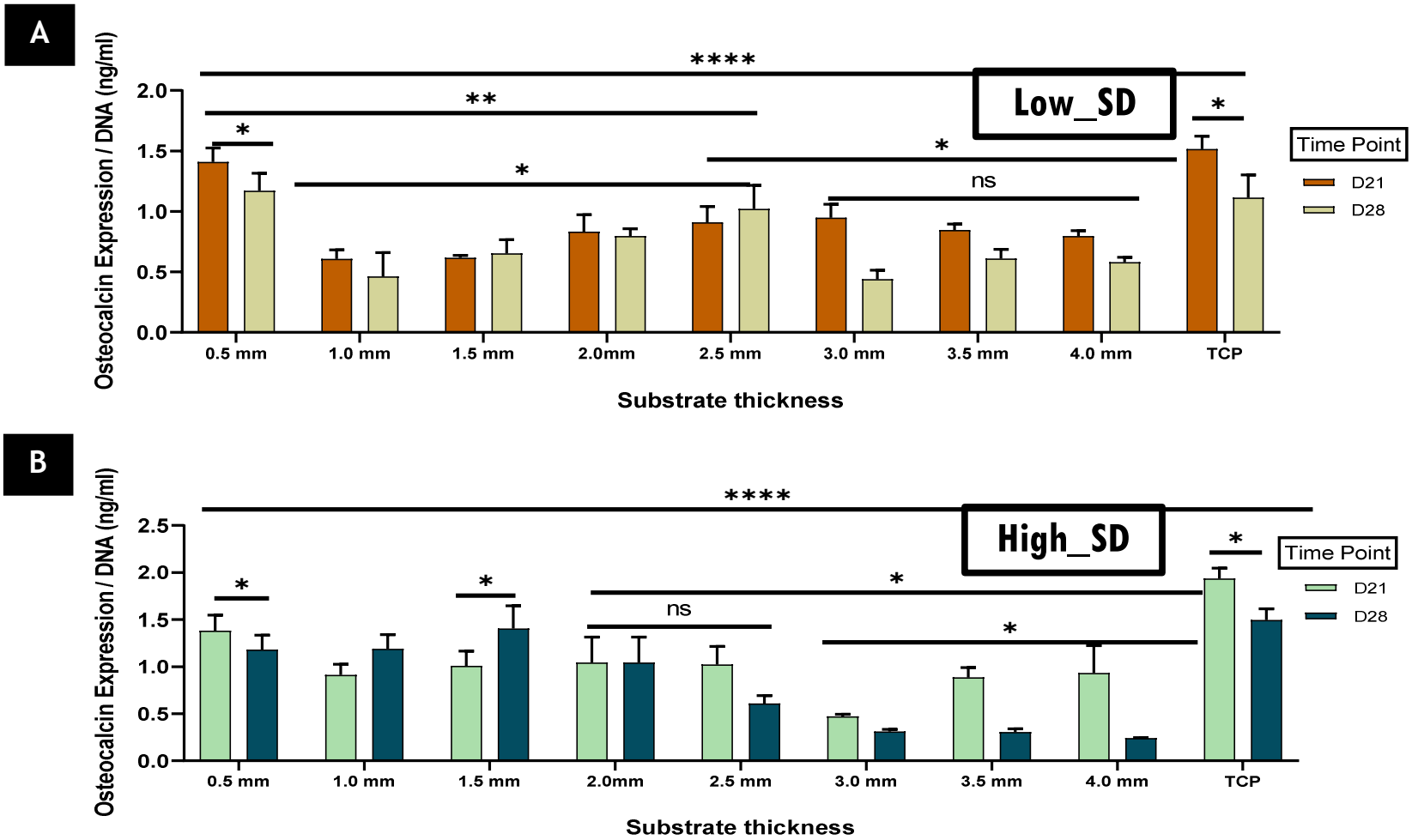

Figure 5. 21 Results of Osteocalcin expression assay of hMSC's A Low cell seeding density (Low_SD 250 c/cm^2 cell density). **B** High cell seeding density (High_SD 2500 c/cm^2 cell density). The assays were performed on samples seeded onto hydrogels of each thickness and measured at various timepoints. Florescence unites where normalized with DNA content. Data is shown as group mean ± SEM.

Discussion

The work presented in this chapter sought to elucidate the effect of mechanical properties of the ChG_PA on cell response, characterising the effect of matrix tension and thickness on cell behaviour. The physical, chemical and mechanical properties of the ChG_PA hydrogel of different thickness were investigated, aiming to decouple the effect of apparent stiffness from other cell microenvironmental cues, such as surface chemistry or sample architecture (porosity) on the cell response. The next chapter will investigate how cells mechanosense stiffness gradients across their ECM as a function of matrix apparent stiffness, discussed in the next chapter.

It was found that constraining the ChG_PA to a specific shape (48 tissue culture plastic well plate) and varying the volume, thus the thickness of these hydrogels, was an effective method to alter the hydrogel apparent stiffness. This method showed that varying the thickness of the substrates does not affect the internal architecture, wettability chemistry of the surface, or crystallinity of the ChG_PA hydrogels. Moreover, it was observed that the apparent stiffness of the ChG_PA hydrogel is a nonlinear function of its thickness, and that the apparent stiffness of these hydrogels is amplified by their fibrous nature as protein-based biopolymers, compared to similar applications using synthetic elastic linear hydrogels. Furthermore, MG63 and NIH 3T3 cells showed to be significantly sensitive to the resistance tension offered by constrained hydrogels cast in TCP, compared to relaxed unconstrained hydrogels. Finally, MG63, NIH 3T3 and hMSCs were shown to sense and respond to changes in the apparent stiffness of their culture matrix.

Previous research has shown that varying the stiffness of the underlying substrate matrix can lead to significant changes in the way cells proliferate and differentiate [1, 13, 74]. A common approach for investigating the influence of matrix stiffness on cell response is

by modifying the mechanical properties of mechanically linear soft hydrogels by photo-polymerization, or varying the cross-linker concentrations [126, 328]. However, these modifications to alter the stiffness of these substrates also have been demonstrated to alter their chemical, physical and physiological properties, making the interpretation of the results confusing, and the decoupling of the matrix stiffness effect difficult. This phenomenon was observed in Chapter 4, where the PA concentration of ChG hydrogels was varied resulting in alterations in matrix stiffness, but also affecting other cues such as wettability, porosity and chemistry of their surfaces; all these cues have been shown to influence cell-material response. The alternative used in this study to overcome these limitations, instead of varying the hydrogel Young's modulus, was in varying the stiffness that the cells sense when interacting with the hydrogel, the hydrogel apparent stiffness. It was found in this chapter that constraining the hydrogel to a specific shape (tissue culture plastic 48 well plates) and then varying the volume of the hydrogel was an effective technique to achieve consistent repeatable variations in the hydrogel apparent stiffness (Figure 5.1, 5.6). One of the concerns of these study was to decouple the influence of apparent stiffness on cell response from other material cues, which could obscure the interpretation of results. Therefore, it was hypothesised that varying the thickness of the constrained ChG_PA hydrogels to alter the apparent stiffness sense by the cells does not alter other important properties linked to cell-material interaction cues, e.g., porosity or surface chemistry. To prove this hypothesis, TCWPs were used and subsequently coated with ChG_PA cross-linked hydrogels of controlled thicknesses and known bulk Young's modulus (~111KPa). Therefore, the surface of these substrates was made of the same material with the same cross-linker density and mesh size; yet the distance from the construct surface to the underlaying TCP surface varied between hydrogels of different thickness. These hydrogels were then characterised as function of

their thickness. The observations of this study demonstrated that porosity, wettability, surface chemistry and bulk crystallinity are not altered by hydrogel thickness (Figure 5.2-5.5). Therefore, it can be concluded that the observations on mechanical properties and cell response on the ChG_PA hydrogels presented in this chapter were not affected by variations in other material cues, e.g., wettability or pore size.

It was found in the experiments presented in this chapter that the apparent stiffness of the hydrogel was altered when sample thickness was varied. In these experiments, it was observed that the apparent stiffness of the substrates decreased exponentially as the thickness of the hydrogel increased (Figure5.6), compliant with other studies in the present literature, which state that thickness of the compliant hydrogels determines the effective mechanical properties which the cells will sense [13, 185, 192, 246, 329].

For the first part of the cell experimental work, the impact of mechanical strain of the cell culture matrix on cell response was evaluated, and two different cell lines NIH 3T3 (fibroblast), MG63 (osteoblast-like) were seeded on the unconstrained and TCP-cast constrained ChG_PA hydrogels of 0.4mm thick hydrogels. The findings of this study are consistent with previous literature; the matrix constrain boundaries play a critical role for cell survival. The observations from this experiment indicate that release of mechanical load changes cell shape and reduces cell metabolic activity for both cell lines. Cells cultured on unconstrained hydrogels showed significant reductions in cell metabolic activity, compared to those cultured on hydrogels constrained by the well plate. This may be attributed to low mechanical matrix resistance strain offered to the cultured cells, since it has been demonstrated that the presence of mechanical load is critical to preserve the continuous remodelling of osteoblast-like constructs [330]. Fibroblasts are

another example which divide very little and undergo apoptosis when cultured in transferred matrices [331].

Once the importance of the hydrogel mechanical strain was understood, the hypothesis was tested that varying the thickness of ChG_PA hydrogel samples may affect the apparent stiffness that cells can sense. For this set of experiments, tissue culture 48 well plates were used and subsequently coated with ChG_PA cross-linked hydrogels of controlled thicknesses and known bulk Young's modulus (~111 KPa). These experiments also allowed early understanding of the effect of a range of apparent stiffnesses on different cell lines. Three cell lines were used (NIH 3T3, MG63 and hMSCs) which according to the literature present stiffness-dependent behaviour [332, 333]. Cells were seeded on hydrogel samples of thicknesses ranging from 0.5mm to 4.0mm thick (AS~287KPa to ~2KPa). On soft ChG_PA hydrogels (~3 KPa) MG63 cells did not spread and adopted a round morphology, while on stiff hydrogels (AS>~139KPa) they spread and adopted a spindle-shape morphology (Figure 5.12Aa and 5.13Aa, 5.17). Engler et al. [64] have shown that changes in matrix stiffness lead MSCs to respond by changing their morphology and phenotype. In this context, the MG63 increase in cell number and spreading data supports some of their findings. These cells were shown to favour stiffer hydrogels (AS >58KPa) over soft ones (AS <33KPa). They spread (Figure 5.12, 5.17) and increase in cell number (Figure 5.10A, 5.11A, 5.15 and 5.16) faster on thin stiff hydrogels (AS >139KPa) than on softer ones (AS >~4KPa), showing little increase in cell number and a round shape on the thicker substrates (Figure5.12Ac, C, 5.17), compared to stiff surfaces (AS >139KPa) on which the cell metabolic activity as well as DNA content was higher, and cells showed a flatter more spread morphology (Figure5.12Aa, B 5.16). Also observed on MG63 cells was a tendency to form packed

dense cell aggregates as stiffness of the hydrogel decreased (AS <~33KPa); once formed, these cell groups maintained their condensed packed morphology throughout the length of the experiment (Figure5.12Ah, i, l, Figure 5.19). This behaviour was shown to correlate to substrate stiffness, as the lower the stiffness (AS ~33KPa to ~2KPa), the higher the number of these clusters (Figure5.12Ai, 5.19). These results are consistent with previous studies reported by Tusan et al. [22] that showed that PAAm hydrogels of varying elasticity and apparent stiffness (nominal stiffness 0.5 to 40 KPa) of softer materials (E 0.5KPa, 100-200μm thick, AS ~3KPa) compared to stiff ones (E 40 KPa, 10-20μm thick, AS ~40KPa) support the formation of dense packed groups of MG63 cells, showing the ability of cell aggregates to sense the mechanical properties of their matrices, demonstrating that the hydrogel stiffness within the expected KPa range can influence the cell morphology, increase in cell number, and differentiation of osteoblast-like cells [64, 334].

Fibroblasts seeded on hydrogels of high stiffness began (AS>58KPa) to spread and increase in cell number rapidly compared to soft ones (AS<~3.7KPa) (Figure 5.10B and 5.13). These cells showed a stiffness dependence response, also adopting a round morphology as the substrate apparent stiffness decreased (Figure 5.10Ac). This behaviour was diminished as the increase in cell number occurred (Figure 5.10A). This may suggest possible cell matrix deposition, which in turn will increase the whole construct stiffness to that which cells favour, as suggested in the literature [335]. However, it is still unclear if such behaviour is a result of the change on the stiffness or a natural response of the cells to its microenvironment [336]. Another explanation for this behaviour is the effect of cell aggregate formation. It has been postulated that the addition of the cells' forces increases the deformation forces applied on the matrix by

cell aggregates, resulting in forces traveling longer distances in the X, Y and Z axis [22]. More experimentation is needed to clarify this. The observations for 3T3 cells support what has been established in previous studies [333]. NIH 3T3 cells display the ability to detect the stiffness of their context environment, and to adjust their morphology and increase in cell number rates correspondingly. These cells showed elevated lamellipodial protrusions when seeded on soft, thick hydrogels (AS <~4KPa) (Figure 5.13Ab,c). In this cell group, no morphological differences among samples of different apparent stiffness were observed once this group reached confluence. This was in agreement with Yeung et al. [32], who observed that differences in morphology due to variations in substrate stiffness became indistinguishable once a monolayer of 3T3 fibroblast and other epithelia-like cells were formed. The collective results of these experiments support what other groups have reported: cells on thick substrates with low apparent stiffness (i.e. AS > ~4KPa) exhibit smaller size and less-developed actin stress fibre, due to the lack of reactive forces upon cell probing compared to those plated on stiff surfaces [102]. Cellular behaviours, including cell morphology, and increase in cell number rate have been observed in this section of the study to change on NIH 3T3 and MG63. These results demonstrated the ability of both cell lines to recognize difference among sample apparent stiffness as a function of hydrogel thicknesses, in which thin hydrogel exposed cells to higher apparent stiffness (AS>~58KPa) than thick hydrogels (AS<~4KPa). Therefore, cells apply traction force and respond to the generated resistance from substrate, which forms a feedback loop until they reach equilibrium [18]. In the case of thin hydrogels, they give rise to higher resistance upon cell contraction and exhibit higher effective modulus that supports a series of cell activities [192]. However, for thick hydrogel, there is no offered resistance by the substrate, forcing the cell to enter a quiescent state (Figure 5.22), which explains the round shape observed in both cell lines

used in this study seeded on thick hydrogel. As a result, the thick hydrogel demonstrated lower effective modulus which inhibits not just proliferation but a series of cell activities [192]. Even when MG63 and NIH 3T3 both showed to be responsive to the apparent stiffness of the hydrogel, significant differences in proliferation and visible differences in morphology were detected between cell lines. This observation supports what Yeung et al. postulated: stiffness of the surface to which cells adhere can deeply influence the response of adhered cells; however these mechanical effects will vary accordingly to cell type [32], i.e. a softer material (AS <~4KPa) compared to stiff one (AS >139KPa) supports the formation of dense packed groups of MG63 cells but not NIH 3T3.

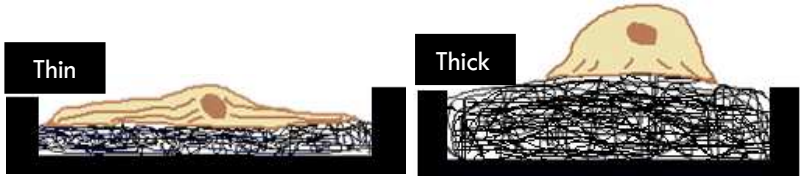

Figure 5. 22 Cells sense hydrogel thickness. The cartoon displays the difference in resistance that a cell experiences by pulling (contracting) an equivalent amount of material on **thin** and **thick** hydrogels of equal elastic modulus and then adopting a shape that matches those forces.

Once the ChG_PA hydrogel's apparent stiffness was tested by MG63 and NIH 3T3 cells, its influence was analysed on the cell number, attachment and morphology of hMSCs. To test this, a group of experiments was conducted using hMSCs as a cell source, different cell seeding densities (Low_SD and High_SD), and tissue cultured 48 well plates coated with ChG_PA hydrogels of different thickness (ranging from 0.5mm to 4.0mm). hMSCs increase in cell number rate showed to be affected by the stiffness and cell-cell constant (Figure 5.15 and 5.16). Cells on the Low_SD group showed significant higher increase in cell number compared to softer hydrogels on hydrogels of medium (~33 KPa, ~2.0mm) to high (>~139KPa, >~1.0mm thick) stiffness. Furthermore, this range increased for cells in the High_SD group, which increase in cell number showed to

be significantly responsive from hydrogels as soft as ~3 KPa (>~3.0mm thick). These results comply with several other studies that show proliferation of multiple cell lines to be dependent on an optimal substrate stiffness. For example fibroblasts [333] and smooth muscle cells [322] grow better on stiff (~45KPa) substrates, while neural stem cells proliferate most quickly on substrates of medium stiffness (~10KPa) [337], and the influence of cell-cell contact can override the effect of substrate stiffness under specific conditions [105]. The observations of the presented study showed that hMSCs will prefer stiff substrates up to ~100 KPa, also the cells respond over a stiffness of ~3KPa, and under this rigidity cells did not show to proliferate. Supporting this observation is the work of Park et al. [74] whose previous experiment showed that hMSCs proliferated better at ~3 and ~15 KPa compared to those on soft 1 KPa substrate. They reported significant decrease in the proliferation rate on soft substrate, whereas no significant difference was observed between 3 and 15 KPa. Significant differences on hMSCs sensitivity to apparent stiffness measured by increases in cell number rates were observed on cells seeding at high densities (25000 cells/cm^2) compared to those seeding at low density (250 cells/cm^2). High cell seeding density increase in cell number rates showed to be more sensitive to changes in apparent stiffness and showed to increase in cell number on soft hydrogels over 2.5 mm thick (AS>~ 3.7KPa) (however at a slower rate compared to stiff hydrogels). Tusan et al. [22] demonstrated that aggregate cell size influences the colony ability of sense apparent stiffness. They demonstrated cell aggregates can sense more deeply into hydrogel substrates than individual cells, reporting that MG63 cells can detect an underlying stiffer substrate through a compliant- PAAm hydrogel up to a thickness of 6.8μm, whereas MG63 cell aggregates can still sense it up to a deepness of ~108μm. Thus, aggregates of cells are more responsive to apparent stiffness. The observations presented in this thesis support

these findings; the relationship between stiffness and increases in cell number rate follows a nonlinear relationship and a high number of immediate neighbouring cells and increasing stiffness enhances hMSC increase in cell number. Furthermore, collective cell behaviour (Figure 5.19) showed that hMSCs formed these dense-packed groups of cells or colonies on soft hydrogels under ~3.7KPa or 2.5mm thick (Figure 5.19Af, k, l, q, s), whereas on stiff surfaces over ~58 KPa, cells increase in number and spread apart from each other till they reach confluency (Figure 5.19Ab, h); yet even after this, the cell perimeter can still be visibly distinguished (Figure 5.19Ai). it is noteworthy that these dense aggregates seem to be also a function of cell numbers per sample, since the higher the seeding density, the stiffer the threshold for its formation appeared to be. For example, for low cell seeding densities under 1000 cells/cm2, they appear only on hydrogels under ~3.7 KPa stiff (2.5mm thick); while as cell seeding density increased, this threshold was found on stiffer surfaces around ~33PKa stiff (2.0mm thick Figure 5.19Ap). Douezan et al. [338] found that murine sarcoma (S-180) aggregates on soft substrates below the single cell threshold elastic modulus of ~8 KPa neither spread nor attached, but remained densely packed in an aggregate form. The observations of this study found the threshold elastic modulus for hMSCs cell aggregates formation for the low-density groups to be around ~3.7KPa (2.5mm). Furthermore, this group observed on a substrate with an elastic modulus of ~7.4 KPa that single cells still spread, whereas a dense-packed aggregate did not. Thus, the group postulated that the critical modulus for the aggregate formation is slightly larger than the one for single cells, because the cells lose the ability to firmly attach to the surface as the stiffness of their matrix decreases, and this inability is amplified by increasing neighbouring cell numbers attaching and exerting pulling forces into each other. The findings of this study suggest that cell aggregate formation is a joint relationship between matrix stiffness and cell

number, as the higher the number of cells in the aggregate, the higher the resistance force needed to be offered by the substrate to keep the aggregate firmly attached to the surface of this substrate (Figure 5.19B).

Another important finding of this study was the extent of ChG_PA hydrogel thickness up to which hMSCs showed to be responsive. Compared to results presented using synthetic homogeneous linear substrates, the reported depth at which single cells started to sense the underlying rigid support through the fibrous nonlinear ChG_PA hydrogel was amplified. Whereas studies on linear PAAm and similar synthetic hydrogels reported cells to be sensitive to substrate thickness up to a 'critical thickness' (called also mechanosensing length) in the microns scale [13, 18, 64], Buxboim et al.[13] reported hMSCs to have a tactile half-depth (the elasticity at which a cell reaches half of its maximum spreading) of ~3.4μm and a critical thickness of 10 μm on soft PAAm hydrogels (nominal stiffness ~1KPa) and a critical thickness of 20μm for stiffer PAAm hydrogels (nominal stiffness~10KPa). The results presented in this study reported considerably higher critical thickness and tactile half-depth (3000μm and 1440μm); one may assume that the difference is only a function of the hydrogel nominal stiffness, which for the hydrogels used in this study was 111KPa. However, the reported tactile half depth of the 1KPa PAAm is 400 times smaller than that of the 111KPa ChG_PA used in this study which is not explained by a linear relationship. Another explanation is provided by previous studies that have shown that the fibrous, nonlinear elasticity of the ECM allows stress transmission to travel further distances [186], as do nonlinear-hydrogels that emulate the nonlinear elasticity of the ECM like collagen hydrogels [192]. Collagen and fibrin hydrogels [185] enable adherence dependant cells to sense depths over the microns scale greater than those of linear synthetic hydrogels. Moreover Mullen et al. [246] proved that cells' spreading area significantly increased when cultured on

soft fibrous collagen hydrogels (1KPa) compared to stiff PAAm (~38KPa) hydrogels; their finite element simulations predicted that the equivalent shear stiffness of a fibre-reinforced soft hydrogel is significantly greater than that of a non-fibrous hydrogel. It was also shown that, by cross-linking these fibrous hydrogels, the fibre concentration and the effective stiffness experience by the cells increased compared to less fibrous ones. Therefore, the observations presented in this section add another layer of evidence, demonstrating the importance of the material internal structure in the apparent stiffness sensing phenomenon; cells are capable of detecting stiff substrates underneath thicker fibrous hydrogels compared to linear homogeneous synthetic ones [185]. Figure 5.23 shows a representation of how the fibrous nature of the protein-based ChA_PA might amplify the contractile forces applied by the anchorage-dependent cell.

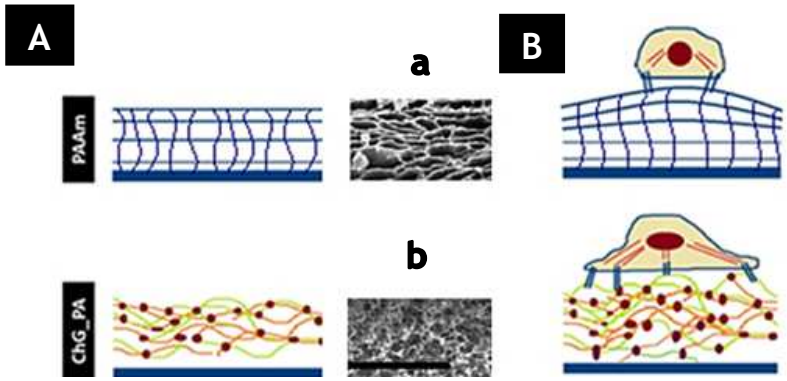

Figure 5. 23 Illustration showing the effect of cell contractile forces on linear synthetic PAAm hydrogels vs nonlinear ChG_PA hydrogels – before (**A**) and after (**B**). The dense interconnected mesh nature of the ChG_PA (**A.b**) compared to the uniform layered structure of PAAm (**A.a**) perhaps amplifies the contractile forces exerted by the cells plated on the surface. SEM images of PAAm are reproduced [187] and the ChG_PA hydrogel used in this study (scale bar 100µm).

Cell polarization is a phenomenon that has been linked to cell orientation on the cell migration process [82]. In this study it was detected that cells showed a cell elongated polarized morphology with two distant ends on medium-stiff hydrogels (AS ~33-3.7KPa) (Figure 5.19), however it was proved that the average orientation of cells on

uniform hydrogels was not a function of the matrix apparent stiffness (Figure 5.20). Cells showed a polarized morphology, but their alignment was random, with no significant peak on any specific direction angle; therefore, cells were distributed approximately equally among all possible directions.

In addition, cell-spreading area has been reported to be an indicator of the differentiation stage of hMSCs, with osteogenic differentiation found to correlate with an increase on cell area [339, 340]. In agreement with previous studies, the observation of this study showed that osteogenic differentiation of MSCs preferentially occurred on stiffer substrates (over ~58KPa), coinciding with the stiffness range where the cell-spreading area was reported to be higher (Figure 5.20 5.21). This is consistent with previous studies [10, 65, 114, 246, 341]. The expression of these markers, however, were also observed on samples ranging from ~3.7KPa to ~33 KPa, yet the differences on the marker expression were not as significant between them as for the stiffer samples (AS~287KPa to 58KPa), in agreement with Hwang et al. [341], who proved that the hMSCs elastic module threshold for osteogenic differentiation of hMSCs was between 4.47KPa and 2.8KPa. Moreover, the observations also showed the osteogenic response of hMSCs to be a combined relationship between the stiffness of the hydrogel and the amount of immediate neighbouring cells. This combined effect was shown to be more significant for the expression of the Osteocalcin marker, which showed higher expression and no significant difference for samples over AS~58KPa, compared to the low seeding density group which show a strong preference for the AS~258KPa. This is in agreement with Mao et al. [249], who proved that the interplay of both mechanical and cell-cell contact cues were significant for the osteogenic response of MSCs, demonstrating that single MSCs produced little ALP, regardless of the modulus of their substrate. However,

on hydrogels with elastic modulus over ~22 KPa, only cells in direct cell-cell contact produced significant amounts of ALP on ~22 KPa hydrogels compared to single cells on the same stiffness.

Conclusion

This study suggests that altering the ChG_PA hydrogel thickness has a significant effect on the hydrogel apparent stiffness without altering other cell-material interaction features. The apparent stiffness of these hydrogels was seen to be a nonlinear function of the hydrogel thickness, decreasing exponentially as the thickness of the material increased up to 3.0mm (AS ~2.1KPa). This characteristic allowed the investigation of the cell response to a wide range of hydrogels in the physiological-like stiffness scale. It was also observed that the apparent stiffness of the hydrogels is amplified by the hydrogel fibrous nature compared to similar applications using synthetic elastic linear hydrogels, where changes in apparent stiffness are not observed on hydrogels over a few µm thick. NIH 3T3, MG63 and hMSC cell number and morphology were shown to be influenced by changes in the hydrogel apparent stiffness; however, these cell responses varied according to the cell line. It was also shown that apparent stiffness and cell-cell interactions both strongly influence the hMSC response, showing significant differences between single and collective cell behaviour, and that together, cell-cell interaction and apparent stiffness determine osteogenic differentiation.

CHAPTER

6

Human Mesenchymal Stem Cell's (hMSC) Response to Non-linear Stiffness Gradient.

6. Human Mesenchymal Stem Cell's (hMSC) Response to Non-linear Stiffness Gradient

Introduction

The main aim of this chapter was to test the hypothesis that hMSCs can sense and differentiate between apparent stiffness gradients. To achieve this aim, the influence of two ChG_PA stepparent stiffness gradients defined as θ8° and θ12° were investigated.

A number of studies have recently highlighted the importance of the mechanical cues of the cell microenvironment in regulating cell behaviour for tissue development, homeostasis, and pathological process [19, 66, 89, 106, 116]. The stiffness of the native ECM is highly variable, ranging from the Pa to GPa scale, e.g. 0.5-1 KPa for Fat [44] and ~10 GPa for bone [342, 343]. Moreover biological tissues are mechanically inhomogeneous, particularly during cell growth and migration[46]. These variations can be found at the physiological scale (variations within tissues 1 Pa/μm) [77], at the soft-hard tissue interface (e.g., stiffness gradient at bone–cartilage interface 100 Pa/μm) [44], and those stiffness variations can be produced during pathological processes (e.g., on cancer tumour progression and myocardial infarction ~10 Pa/μm) [78, 79]. Many efforts have been made to achieve the *in vivo* ECM-like stiffness of a variety of tissues. However, the majority of the approaches to alter matrix stiffness are performed on substrates with approximated suitable and homogeneous stiffness, which results in many limitations in the understanding of the in vivo ECM stiffness impact[34, 98]. Such limitations include the inability to identify an optimal stiffness value for appropriate cell behaviour, and to investigate durotaxis since this occurs as response to local stiffness. Therefore, an effective and versatile approach to surpass these limitations is to

fabricate stiffness gradients instead of cell-cultured constructs with uniform substrate stiffness.

Various techniques to fabricate stiffness gradients *in vitro* have been explored, including manipulation of physical cross-linking[93] repeated freeze-thaw methods [344] and photo-polymerization [345]. However, all require significant technical background, such as material science knowledge, highly specialized equipment, or are remarkably expensive; also they are limited by the minimum possible shear modulus, which is usually in the pascal scale[94]; the steepness of the gradient, which is often shallow [96], and the simplicity of the stiffness gradients, which are usually linear [84].

Therefore, having a simple method to fabricate stiffness gradients, that more closely resemble the inhomogeneous structure and nonlinear elasticity of the ECM while keeping the surface and bulk chemistry along the stiffness gradient intact, is desirable to elucidate their specific effect on cell mechanotransduction.

In this chapter it was sought to investigate the response of hMSCs to hydrogels that mimic natural tissue stiffness variations from natural variations in soft tissue (physiological ~2.5 Pa/μm), to soft-hard tissue interface variations (tissue interface >~100 Pa/μm). Wedge-shape hydrogels were fabricated varying the thickness of the ChG_PA hydrogel, therefore the distance between the hydrogel surface and the attached underlying stiffer substrate surface varied across the samples, using two different steepness across the final substrate (8°, 12°). Such gradient surfaces possess a range of stiffness ~2 – 619 KPa and ~2-530 KPa respectively, and an assortment of stiffness gradient variations coexist at different locations in the same gradient sample. Using the chitosan-gelatin hydrogel cross-linked with 2.5% (w/w) Proanthocyanidins (ChG_PA) developed in Chapter 4 (Table 4.1 Formulation Method 3), gradients were produced of

nonlinear stiffness and different steepness (Figure 3.4) to create continuous changes in the stiffness gradient, in such a way as to produce reproducible gradient complexes. Correlation between MSC, morphological cues change, durotactic response, cell differentiation, cell population size and stiffness gradient were investigated.

Results

Stiffness gradient hydrogel development: the wedge approach

The first goal of this chapter was to identify a method to fabricate ChG_PA gradient hydrogels with nonlinear stiffness profile, capable of reproducing a variety of relevant biologically stiffness gradients ranging from the tissue interface to physiological tissue variations (Figure 6.1) passing across the stiffness gradient threshold for durotaxis of the MSCs (~8.7 to 2.9 Pa/μm) reported by Hadden and Vincent et al. respectively [76, 94].

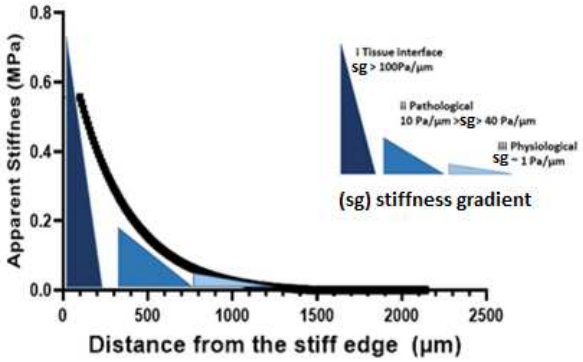

Figure 6. 1 Schematic representation of i hard-tissue interface **tissue interface**, **ii** variations in disease **pathological**, and **iii** natural variation within soft tissue **physiological** stiffness gradient (SG) used in this study.

Briefly, 6 food grade stainless-steel culture well plate holders (Figure 3.4A) with variable tilt angle were designed and fabricated (Figure 3.4 B). The aim for these holders was to facilitate the fabrication of thickness gradients by constraining the tissue culture well plate at a specific gradient, for hydrogel casting, setting and incubation of

cell culture in periods of 5 to 35 days. This was to ensure the fidelity of the thickness gradient throughout the length of each experiment, while the surface of the samples always remained planar, avoiding the variation caused by the influence of gravity (Figure 3.4.C).

To investigate the influence of the stiffness gradient on cell response, 3 of these holders were tilted at 8° and the other 3 tilted at 12° (Figure 3.4 B, D), and samples are referred to as either θ8° or θ12° later in this study. Different well plate sizes were tested (24, 12, 6); because of the needs of this study regarding sample size per timepoint and total culture area the size that better suited the experiment was the 12 well plate. The ChG_PA hydrogel samples formed a wedge like sample with a planar surface and all their other faces firmly adhered to the surface and walls of the 12 well plate, therefore it subsequently served as a constraint for the hydrogel samples and facilitated cell culture; the system yielded 3 X12 (2.54cm^2) samples per gradient per experiment.

Sample shape characterization: Thickness controlled by ChG_PA volume

To attempt to vary the thickness of ChG_PA hydrogel gradient across the distance of the sample, the volume of the hydrogel and the steepness were varied for each gradient (Eq. 3.2) and once sample set the thickness of each gradient was measured using light microscope cross-section images of the gradient hydrogel and the ImageJ software (Chapter 3 pp80). Hydrogel thickness was found to increase in a linear fashion as a function of distance from the vertex of acute angle of the sample (Figure 6.2) and sample gradient θ, thickness from the tissue culture plastic surface to hydrogel surface showed to be higher for steeper samples (θ12°) compere to shallowness (θ8°). Table 6.1. shows a summary distance vs thickness and a schematic representation of it.

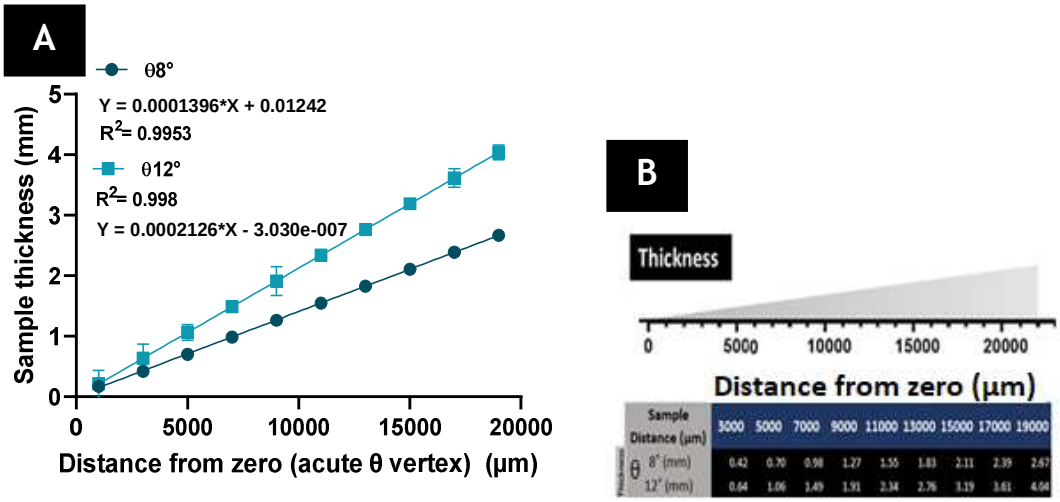

Figure 6. 2 Substrate thickness varies in proportion to the sample gradient. **A** Substrate thicknesses were measured using light microscope images and the ImageJ software. The error bars represent the SE of the mean for the measurements (n=10) on each sample(n=12). B **Correlation guide** gradient location to sample thickness for both θ8˚ and θ12˚.

Mechanical properties: stiffness gradient profile

In order to determine whether there is any variation in apparent mechanical properties across the hydrogel stiffness gradient and between samples of different gradients, AFM was used to measure the apparent stiffness of the θ8˚ and θ12˚ hydrogel gradients. Figure 6. 3A shows the apparent stiffness of the hydrogels as a function of gradient and gradient sample thickness. It was found that there is a pronounced effect of the hydrogel thickness, with hydrogels showing significantly larger values of apparent stiffness when the hydrogel distance from zero was short and thickness low (200µm thick for the θ8˚ ~503.78 KPa and for the θ12˚~405 KPa). It is noteworthy that, as shown in Chapter 5, the thick end of the sample where thickness of the hydrogel is over 3000µm the mean measured modulus was not significantly different to that obtained from the 3000µm thick regions (2.67 ± 0.3 KPa), showing to be an apparent stiffness threshold point. For θ8˚ was reported to be at ~21000µm distance from the sample zero (~ 2951µm thick, AS~2.87KPa), and closer to zero for the steeper θ12˚ ~15000µm

(apparent stiffness threshold at ~3000µm thick AS~2.67KPa). Figure 6.3B shows the correlation between the apparent stiffness of the gradient and location (sample thickness) follows a nonlinear relationship for both gradients (θ8˚ and θ12˚) a curve that fits well that of an exponential decay function with an R^2=0.96 for the θ8˚ and for the θ12˚ R^2=0.98, this means the apparent stiffness will be a function and varied according to sample gradient (θ8˚ and θ12˚) and location. Figure 6.3C shows a schematic guide of the gradient distance and apparent stiffness. Table 6.1shows a cross-reference summary distance vs stiffness per location.

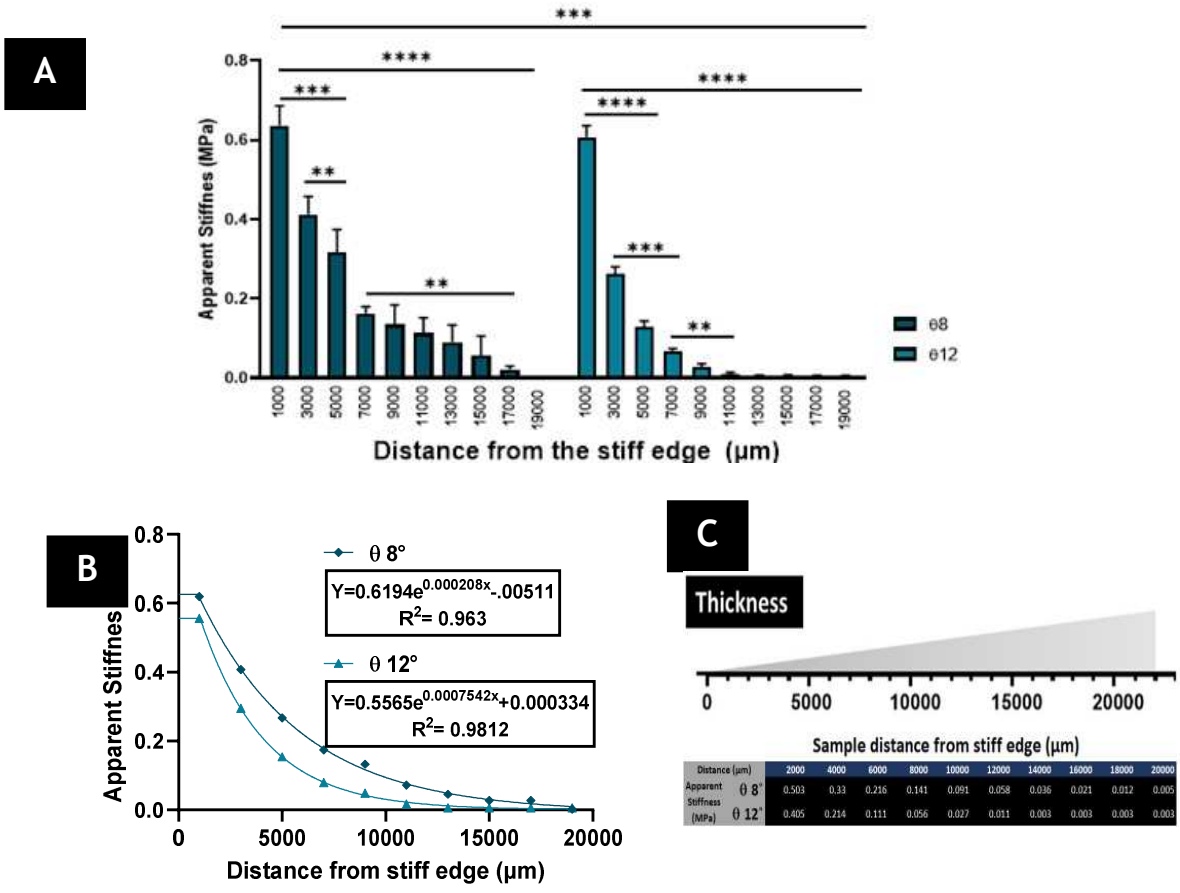

Figure 6. 3 Substrate stiffness varies in proportion to the sample gradient. **A** Apparent stiffness of hydrogel for gradients θ8˚ and θ12˚. **B** Nonlinear fit curve and equation for both gradients. The data were expressed as average ± SEM. **C** Correlation guide gradient location to apparent stiffness for both θ8˚ and θ12˚.

Stiffness gradient

Figure 6.4A shows the sample gradient (θ8° and θ12°) affects the apparent stiffness rate of change by unit of length or stiffness gradient (Pa/µm calculated from the hydrogels apparent stiffness profile Figure 6.3) and that this will be a function of sample gradient and sample apparent stiffness. This change or stiffness gradient showed to be significantly different for gradients θ8° compared to samples of gradient θ12°. ChG_PA hydrogel has a nonlinear apparent stiffness profile so does a nonlinear stiffness gradient, therefor stiffness gradient is as function of location on the sample which showed to be also significantly different between gradient θ8° and θ12°. The θ8° rate of change (gradient) showed to change (Figure 6.4C) across the sample, starting at the soft-hard tissue interface stiffness gradient (~104 Pa/µm, AS~504 KPa at 2000µm from the gradient origin), and gradually decreasing until reach the soft tissue physiological scale gradient (~2.3 Pa/µm, AS~ 2.6KPa at 20000µm from the gradient origin) at the far thick end of the sample. Twelve degrees gradients were shown to have a steeper stiffness gradient profile compared to gradient θ8°. They reported the steepest changes, also at the range of the hard-soft tissue interface, on the thinner section of the gradient (~126 Pa/µm AS~ 405 KPa at 2000µm from the gradient origin), however this gradient holds the shallowest gradients also, those relevant to physiological soft tissue stiffness changes, and starting from about the centre of the sample all the way to its end (~2.9 Pa/µm AS~ 2KPa at 14000µm from the gradient origin Figure 6.4D). Figure 6.4B shows a schematic representation of the gradient distance to stiffness gradient. Refer to Table 6.1 for a summary distance versus stiffness and stiffness gradient at different sample locations.

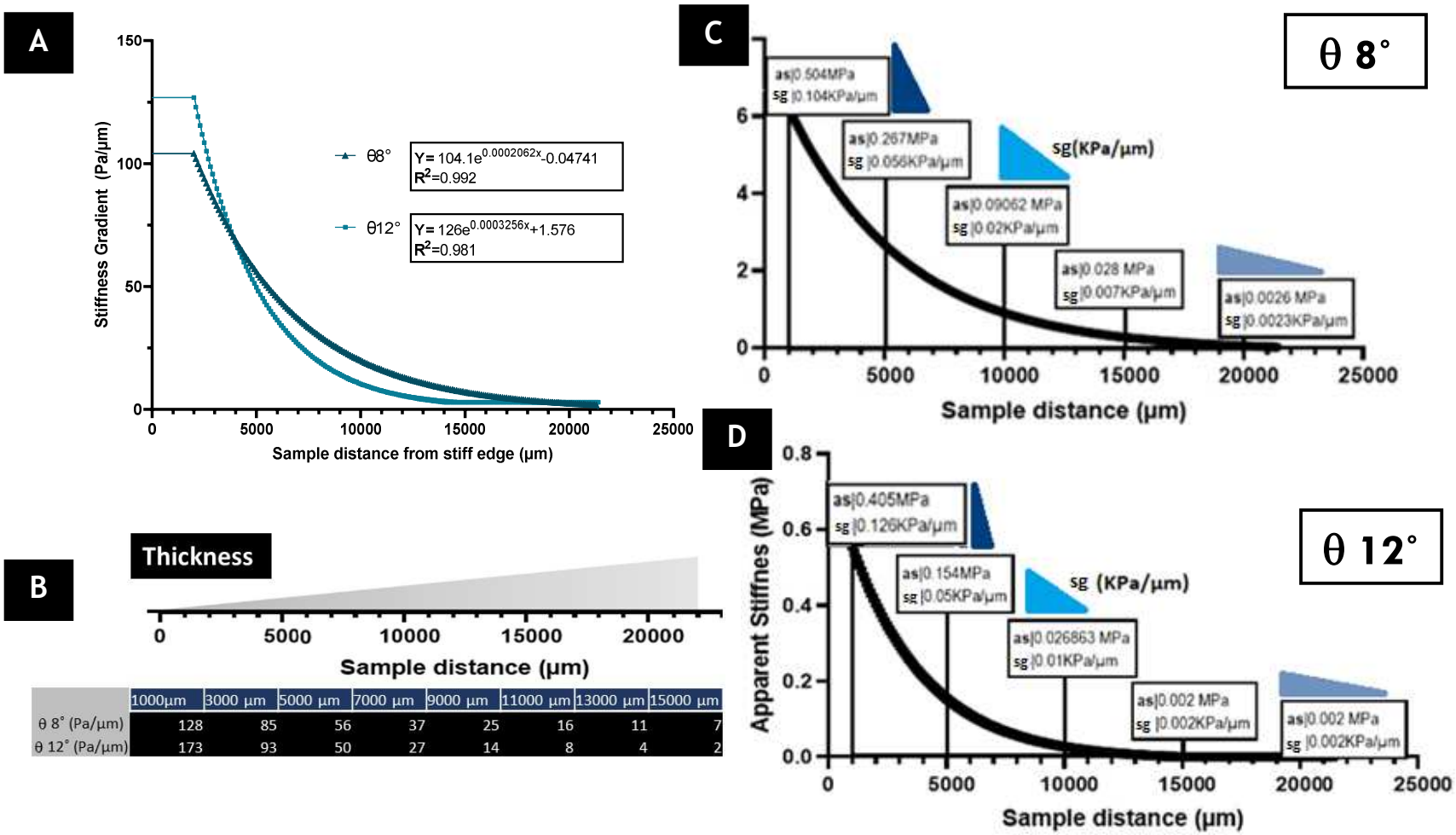

	1000µm	3000 µm	5000 µm	7000 µm	9000 µm	11000 µm	13000 µm	15000 µm
θ 8° (Pa/µm)	128	85	56	37	25	16	11	7
θ 12° (Pa/µm)	173	93	50	27	14	8	4	2

Figure 6. 4 Stiffness gradient A stiffness gradients (Pa/µm) θ8˚ and θ12˚, and nonlinear fit curve equations**. B** Correlation guide gradient location to stiffness for both θ 8˚ and θ12˚. **C** Graphical representation of stiffness to gradient stiffness for θ8˚. **D** graphical representation of stiffness to gradient stiffness for θ8˚, x axis represents gradient location from the stiff (0µm) to the soft (20X10^{3}µm) end.

Table 6. 1 Tabulated summary of stiffness range vs stiffness gradient as a function of sample location.

Distance (µm)	Thickness (mm)		Apparent Stiffness (MPa)		Stiffness Gradient (Pa/µm)	
	θ8˚	θ12˚	θ8˚	θ12˚	θ8˚	θ12˚
2000	0.281	0.425	0.503	0.405	104.13	126.78
4000	0.562	0.85	0.33	0.214	68.9	67.9
6000	0.843	1.275	0.216	0.111	45.6	36.36
8000	1.124	1.7	0.141	0.056	30.17	19.47
10000	1.405	2.126	0.091	0.027	19.97	10.43
12000	1.686	2.551	0.058	0.011	13.21	5.58
14000	1.968	2.976	0.036	0.003	8.74	2.99
16000	2.249	3.401	0.021	0.003	5.79*	2.9*
18000	2.53	3.826	0.012	0.003	2.83	2.9*
20000	2.811	4.251	0.005	0.003	2.53*	2.90*

*The apparent stiffness threshold has been highlighted in blue for the θ8˚ gradient and in grey for the θ12˚ gradient.

Cell viability studies

Metabolic activity

hMSCs were cultured on ChG_PA hydrogels (Figure 6.5) of varying gradients (shallow θ**8**˚ and steep θ**12**˚**)** divided in two groups per each gradient of two different cell seeding densities (250 c/cm^2 **LD** and 1000 c/cm^2 **HD**). This stiffness gradients have a stiff and an opposite soft end, this study hypothesis hMSCs will migrate from the soft compliant regions following the direction of the stiff end on these (shallow θ**8**˚ and steep θ**12**˚) gradients, according to what has been reported in previous studies [34, 306]. To prove this hypothesis, it was sought to determine whether differing ECM rigidities regulates the increases in cell number of hSMCs. To evaluate this assumption, initial cell seeding was carried on the soft end of each sample only, and cell culture was carried out for a 21-day period. For analysis hydrogel samples were divided into 4 regions as described in p70 and Alamar blue tests were carried out to measure relative cell number on days 3, 14 and 21 of their incubation, to measure variations in cell number at four different fixed location a cross the gradients in such a way that location 4 is the softest gradient region and 1the most rigid.

Figure 6.5A shows hMSCs seeded on shallow gradients (θ 8˚); it can be observed that by the day-3 of culture, for both groups (LD and HD) most of the cells are concentrated at the soft end of the sample at region 4 (~AS 13KPa and SG 5.8 Pa/μm), with no significant variation in metabolic activity among the other regions of the gradient. It is after a 14-day period when a shift in cell concentration can be observed, for the LD group cell concentration of 70% ~were on location 1 (~AS 416KPa and SG 86.5Pa/μm) and 2 (~AS 201 KPa and SG 44.45Pa/μm), for the HD group a ~50% of cells were on region 1. By this timepoint no significant expansion was observed for the

other regions. A significant bimodal distribution between soft and stiff ends on these gradients was observed in both groups (LD and HD) by day 21 of culture, the higher expansion was observed on both ends location 1 and 4. With cell metabolic activity significant higher for region 1 compared to sample centre, however, a significant difference was observed for region 4 also compared to the central region of these hydrogels. No expansion or significant differences were observed at this timepoint for the central regions in this gradient. A significant difference in expansion was reported between LD and HD group for timepoints 14- and 21-days period on the central regions.

From Figure 6.5B hMSCs cells seeded on steeper gradients θ12˚, by day 3 of culture most cells (~40%) of both groups are at the thick end of the sample at region 4 (~AS 3KPa and SG 2.9 Pa/µm) showing a significant difference in metabolic activity compared to the other regions, as seen for gradient θ8˚. By day 14 of culture, cell metabolic activity distribution on these hydrogels reorganised all the way across the other end of the gradient samples with a 50% of the cells of the HD group and 40% of the LD group samples on the stiffer region of the gradient region 1(~AS 309 KPa and SG 97.35 Pa/µm). A ~25% of the activity was observed on region 2 (~AS 69 KPa and SG 39.15 Pa/µm) and a significant decrease on cell metabolic activity for both groups on region 4 was observed, compared to day 3. By day 21 of culture cell metabolic activity was significant higher at region 1 for both groups, with lower but significant cell metabolic activity at region 2 compared to softer regions (3 ~AS 7 KPa and SG 10 Pa/µm and 4 ~AS 3KPa and SG 2.9 Pa/µm).

Both groups at gradient θ12˚ showed to be significant different compared to θ8˚showing a significantly higher preference for stiffer regions across the gradient.

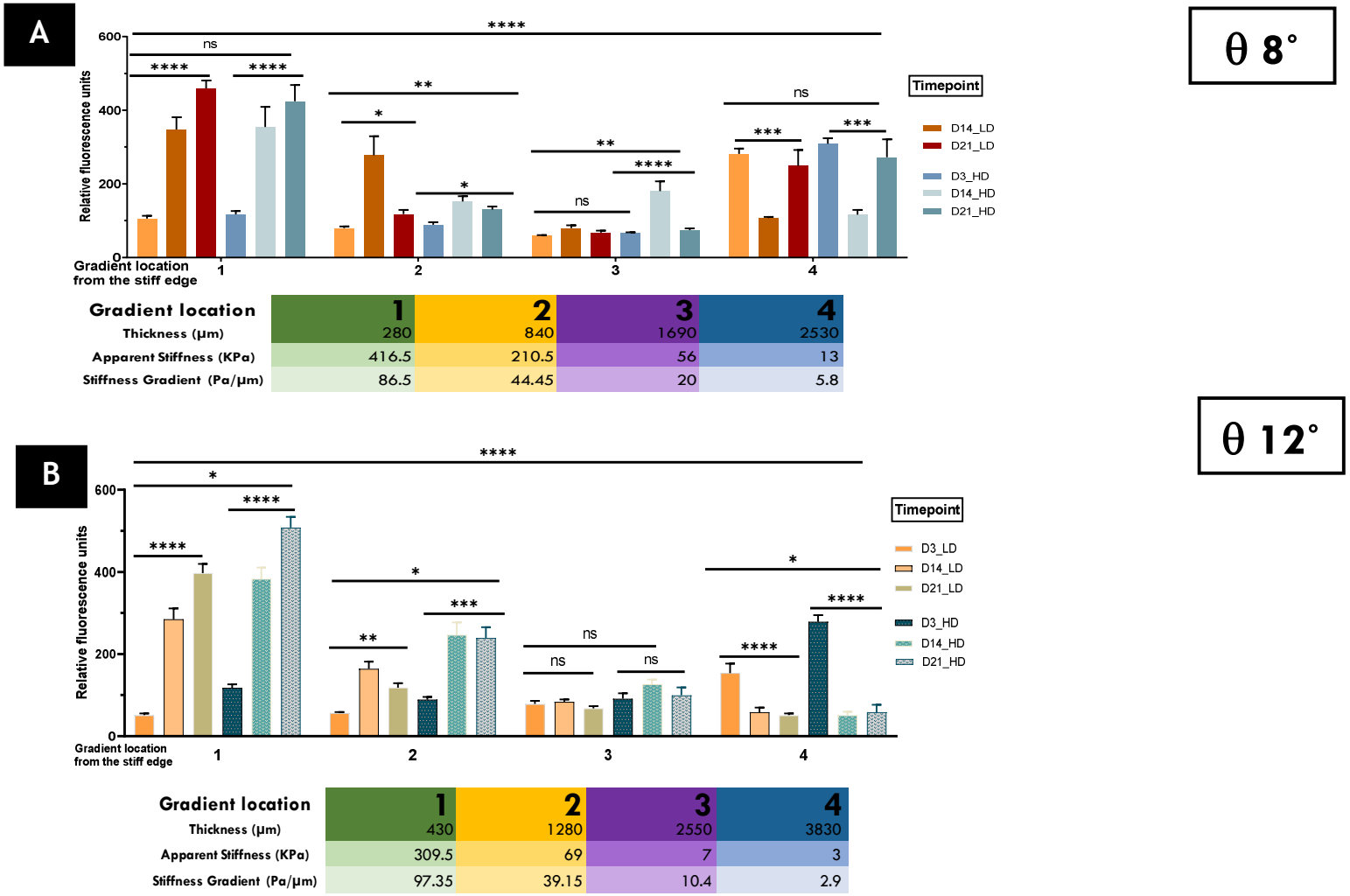

Figure 6. 5 Results of Alamar blue assay which quantifies cell metabolism on hMSC's A Gradient θ8˚ low (**LD)** 250 c/cm^2 and high (**HD**) 1000 c/cm^2 cell seeding density. **B** Gradient θ12˚ LD 250 c/cm^2 and HD 1000 c/cm^2 cell density. Samples were divided in four regions and the assays were performed on each and repeated at various timepoints. The data were expressed as average ± SEM

DNA Content

Pico Green DNA assays were conducted, as an indicator of hMSC increase in cell number via correlating DNA content with relative cell numbers. This test was also important to allow ALP and mineral deposition data to be normalised to well contents. Since low seeding densities were used, DNA content in cultures was sensitive enough just after 14-days and 21-days culture period. Also, cell numbers were generally higher for higher cell seeding density samples. DNA tests were conducted at 14-day and 21-days timepoints using hMSC. Samples seeded on the shallow gradient θ 8° (Figure 6.6A) showed to follow the same trend as that one seen on the metabolic activity assessment. Cells favour the stiffest regions of the hydrogel. The stiffest region presents the highest cell density at every single point and for both seeding densities. However, some significant activity can be observed at the centre of these samples where DNA content significantly decreased for both seeding densities compared to region 1(~AS 416KPa and SG 86.5Pa/μm) and 4 (~AS 13 KPa and SG 5.8Pa/μm)., After region 1 the second highest cell density was observed at the very soft end of these gradients (region 4), which is consistent with the metabolic activity results presented in the previous section which also showed a bipolar cell activity distribution..

As can be observed on the steeper gradient θ 12°, by day 14 of cultured 80% of the total cell on the samples were concentrated in the stiffest region of these gradients 1 (~AS 309 KPa and SG 97.35 Pa/μm) and the remaining 20% was gradually distributed among the other 3 regions. No significant difference was observed among different cell densities. Significant difference was found between samples of different steepness gradients. See Figure 6.6C for a correlation gradient location apparent stiffness.

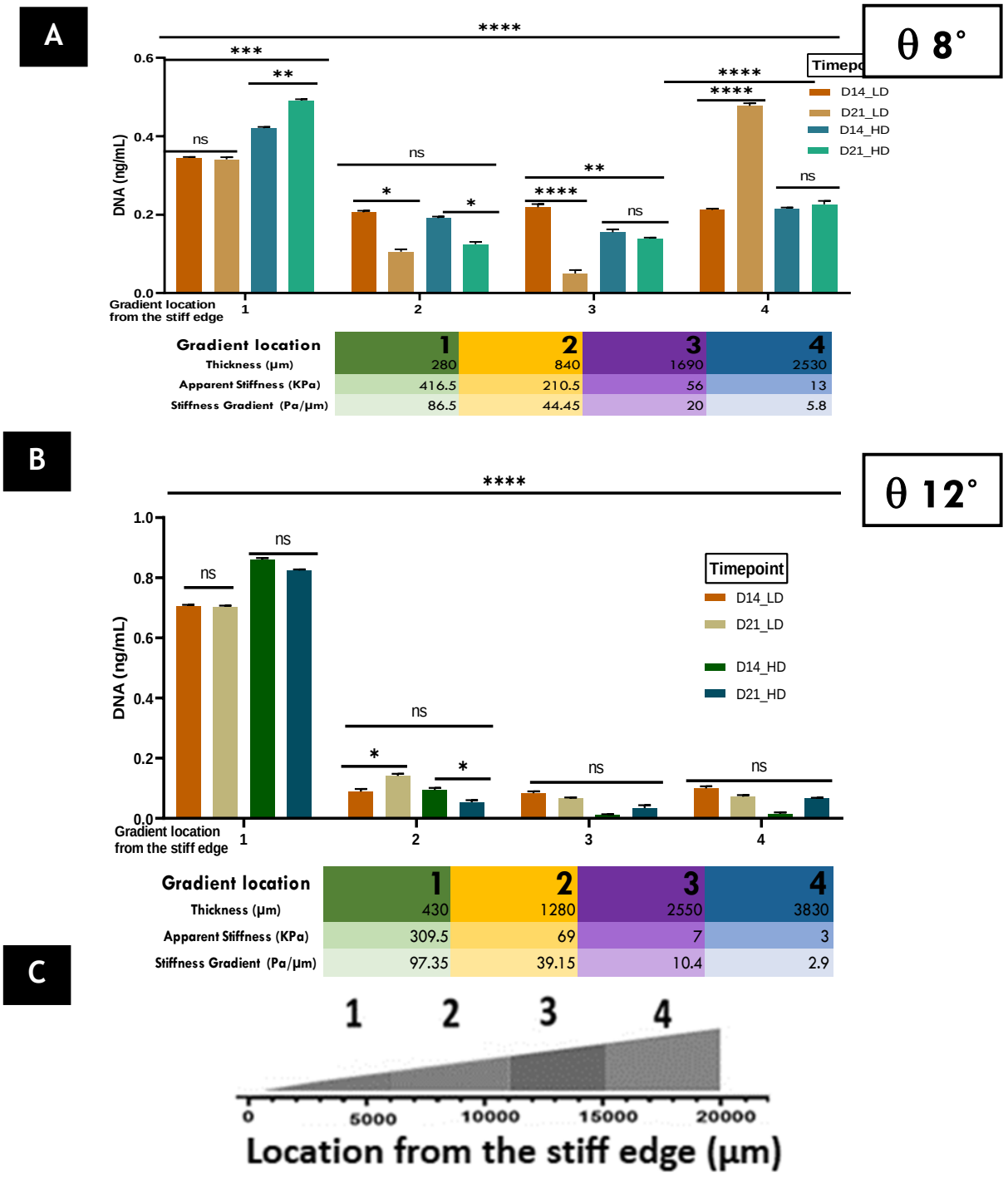

Figure 6. 6 Results of Picogreen assay which quantified hMSC's DNA content A Gradient θ8˚ at low LD 250 c/cm2 and high HD 1000 c/cm2 cell seeding density. **B** Gradient θ12˚ LD 250 c/cm2 and HD 1000 c/cm2 cell density. Samples were divided in four regions and the assays were perform on each and repeated at various timepoints. The data were expressed as average ± SEM **C**. Schematic guide of gradient location.

hMSCs cell morphology is sensitive to stiffness gradients and stiffness gradient ratio of change

To investigate the influence of the ChG_ PA stiffness gradient (SG) on cell morphology, hMSCs were cultured on the ChG_PA gradient hydrogels of different steepness (θ8° and θ12°). Cells were seeded at a low density (250 cells/cm^2) and cultured for 5 days before analysis.

The observations of this studies (Figure 6.7-6.12) suggest that a stiffer region where the stiffness gradient is higher (SG>~100 Pa/μm) may interact more strongly with the hMSCs shape than that of the soft, and shallower stiffness gradient end (SG < 3 Pa/μm). Quantitatively, cells cultured on the shallow regions of the gradients (SG < 10 Pa/μm), where stiffness is also low, showed distinct morphologic phenotypes as compared to those cultured on the steeper sections of the gradient hydrogel (>25 Pa/μm).

The results of this study indicate that individual hMSCs assumed a variety of cell shapes according to the mechanical properties of the ChG_PA, suggesting that hMSCs adapt their morphology to their matrix mechanical stiffness profile in a variety of different ways. See Figure 6.7 for a landscape of morphological differences at different gradients (θ8° and θ12°) and stiffness gradient locations. Full correlation thickness apparent stiffness, stiffness gradient and cell descriptor can be seen on Table 6.3.

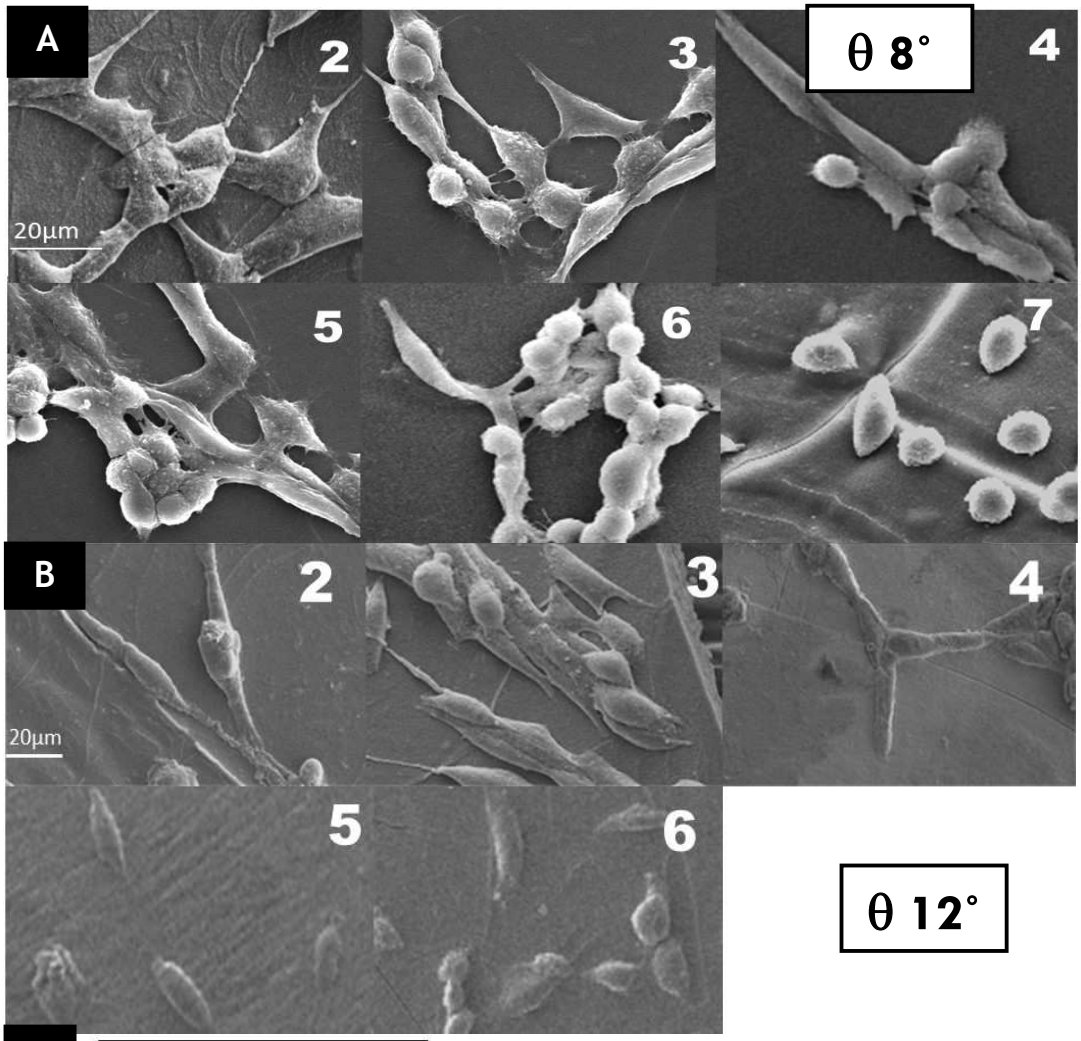

a)

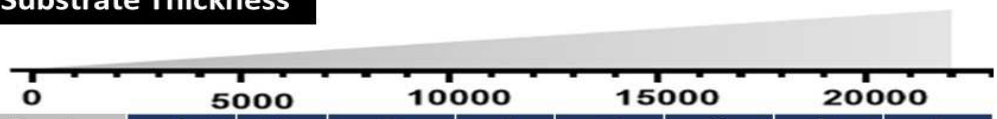

Region	1	2	3	4	5	6	7	8
Location (µm)	1000µm	3000µm	5000µm	7000µm	9000µm	11000µm	13000µm	15000µm
θ 8° (Pa/µm)	128	85	56	37	25	16	11	7
θ 12° (Pa/µm)	173	93	50	27	14	8	4	2

b)

Distance (µm)		2000	4000	6000	8000	10000	12000	14000	16000	18000
Apparent Stiffness (MPa)	θ 8°	0.503	0.33	0.216	0.141	0.091	0.058	0.036	0.021	0.012
	θ 12°	0.405	0.214	0.111	0.056	0.027	0.011	0.003	0.003	0.003

Figure 6. 7 Cell morphology observations. SEM images showing hMSCs plated at **A** across the **θ8**˚ stiffness gradient (locations 2-7) **B** On **θ12**˚ stiffness gradient (locations 2-6); analysed at day 5 of cultured. hMSCs showed a variety of morphologies as a function of the ratio of change of the stiffness gradient from highly elongated and aligned closer to the 90˚ cells on the steeper sections to fully rounded on the shallow low stiffness gradient end. **C** Graphical representation of the stiffness gradient and a cross-reference table of the **a)** stiffness gradient and b) apparent stiffness as function of gradient location and gradient θ for both the θ8˚ and θ12˚ gradient.

Cell area

hMSCs area on both gradient hydrogels (Figure 6.8) was observed to express significant differences as a function of the stiffness gradient (Pa/μm) and steepness (gradient θ), with a higher surface area on medium stiffness gradients (SG 10 Pa/μm to 40Pa/μm) particularly for the θ 8° on which the regions in this pathological stiffness gradient range (AS 180KPa to 50KPa) are more distributed across the hydrogel sample, Figure 6.8A shows significant difference in cell spread area in the central regions of the hydrogel. However, when the area on the steeper end of both gradient substrates was reduced, cells showed a more elongated slim shape as the stiffness and stiffness gradient of the hydrogel increased, which reached the tissue interface scale (SG>100 Pa/μm, AS θ 8°>416KPa, θ 12°>310KPa), although no significant differences were observed across these regions. Whereas significant reductions in spreading area were observed as the stiffness gradient approached the physiological scale with shallow stiffness gradients for both gradients (SG <3 Pa/μm, AS θ 8°<5KPa, θ 12°<3KPa), with an average cell area of 656.5±73μm^2 and 571±63μm^2 for gradients θ8° and θ12°, respectively.

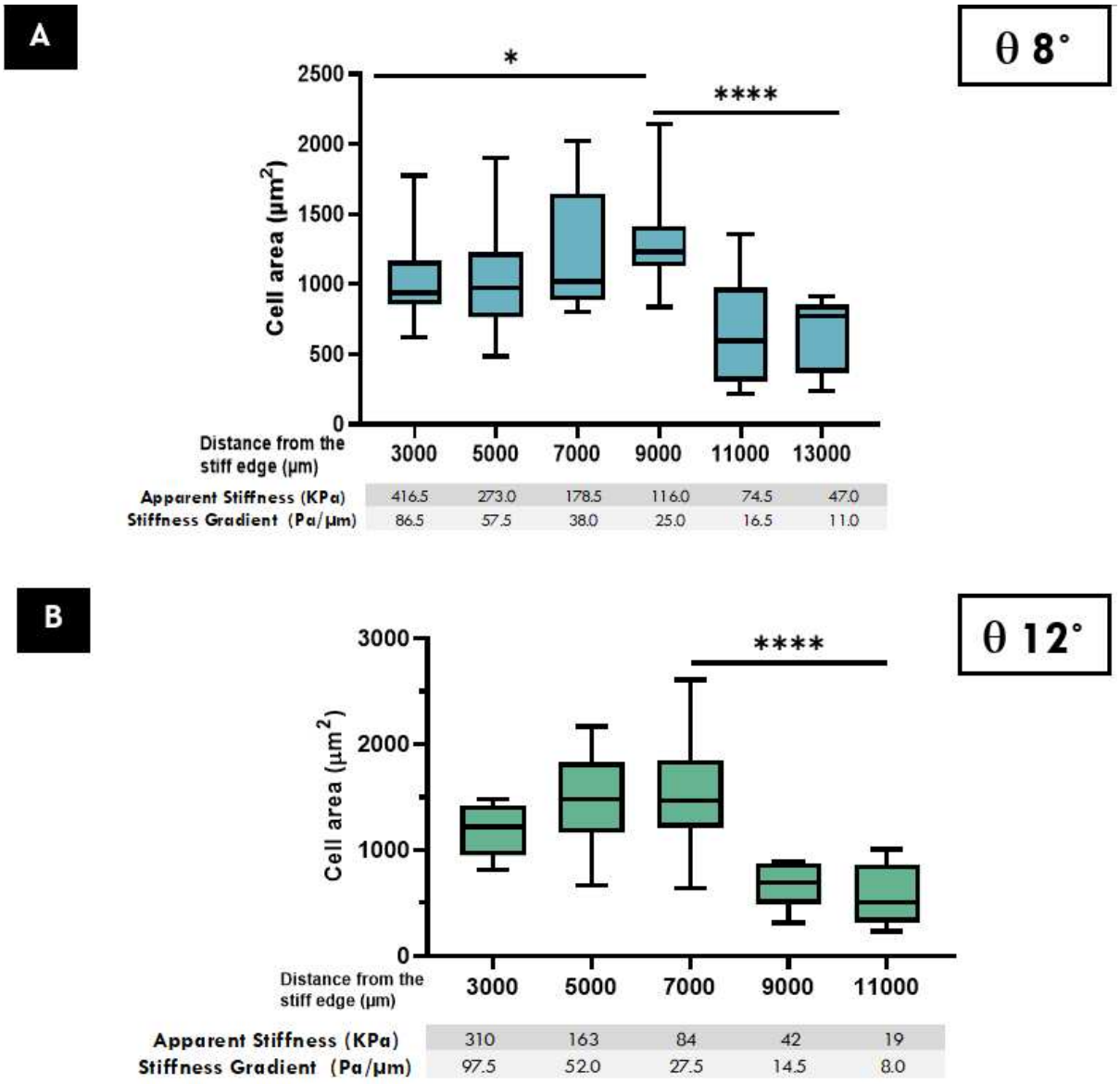

Figure 6. 8 hMSC cell area distributions across the A θ8˚ gradient **B** θ12˚ gradient, across the gradient from the thin stiff end represented by 3000μm to the thicker, softer regions at 11000μm. Statistical significance was assessed using one-way ANOVA test. Data presented as box ± whiskers (Tukey) (n = 10 single cells per field of view).

Cell orientation θ

In the previous chapter it was reported that the average orientation of cells on uniform hydrogels was not a function of apparent stiffness (Figure 5.15). However, as can be

seen in Figure 6.9 and 6.10, cells on gradient hydrogels aligned in the direction of the gradient (θ=90°). This alignment strengthened as the stiffness gradient increased (Figure 6.10B θ 12° ~gradient location 3000μm SG >97 Pa/μm, AS >301KPa). On these nonlinear gradients as stiffness gradient increased, the fraction of cells oriented against the gradient (orientation 0–40°) decreased and the portion oriented in the direction of the gradient (orientation angles of 60°-90°) significantly increased. This significance showed to be stronger for steeper gradients (θ 12°) where the stiffness gradient at the steepest regions is over 120 Pa/μm and AS ~405KPa. However, cell orientation highly depended on stiffness gradient only, not on absolute stiffness: correlation studies of orientation angles for both systems (θ8°, and θ12°) versus apparent stiffness for both gradient hydrogels showed to be uncorrelated (R^2 = 0.4982 orientation angle as function of stiffness data no shown), while scatter plots of cell orientation angle versus stiffness gradient (Figure 6.10A, B) showed a strong correlation (R^2 = 0.7757, for θ 8°, R^2 = 0.9993, for θ 12°) higher for the steeper gradient system. It is noteworthy that for both systems there was shown to be a stiffness gradient threshold around (TG~5 Pa/μm AS θ 8°<21KPa, θ 12°<11KPa) coinciding with the durotactic threshold range of 8.2 to 2.9 Pa/μm reported by Hadden and Vincent et al. [76, 94]; below that point no orientation could be found and cells showed a no polarized morphology. [80]

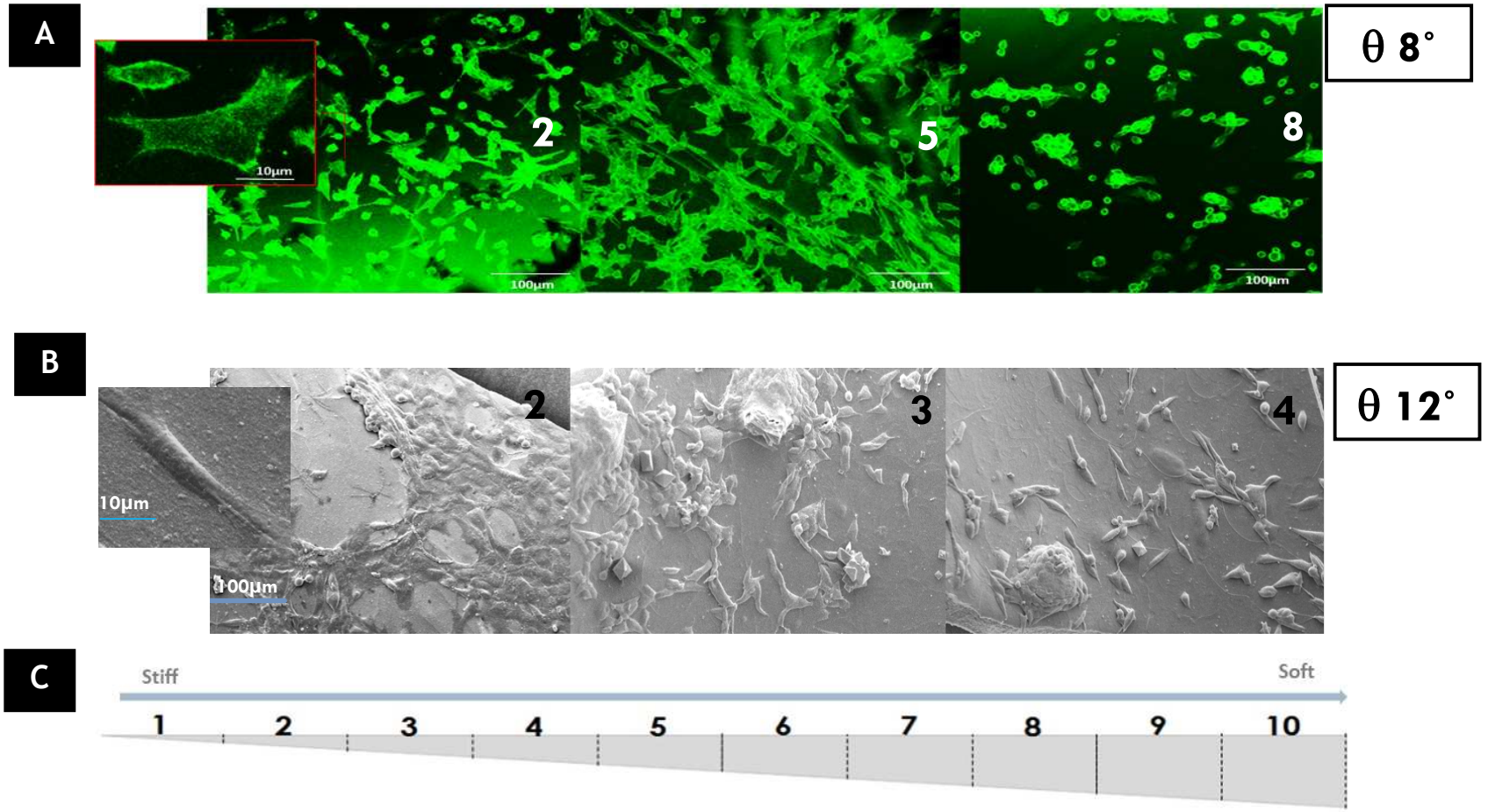

Figure 6. 9 hMSC cell orientation θ across the A θ 8˚ gradient confocal microscopy images of θ8˚gradient, at stiff end 2, centre 5 and soft end 8 of the gradient at day 5 of cultured, hMSCs morphology show higher cell polarity and alignment signs in the gradient direction (90˚) as the stiffness gradient increased (centre to the stiff surface of the gradient); some few signs of morphology polarization and alignment could also be observed at the soft end of this gradient (A8)**.B** θ12˚ gradient SEM images of θ8˚gradient, at the stiff end 2, 3, and centre 4 of the gradient at day 5 of cultured, hMSCs morphology showed higher cell polarity and alignment signs in the gradient direction (90˚) as the stiffness gradient increased (centre to the stiff surface of the gradient). **C** Schematic representation of the stiffness gradient locations.

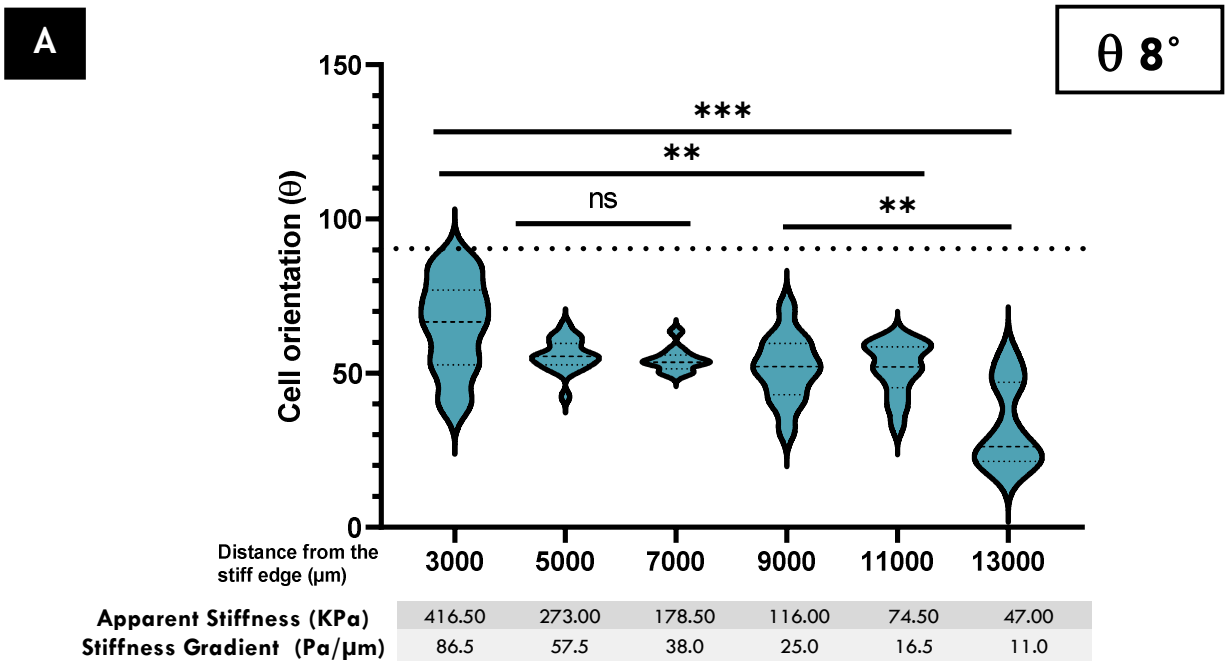

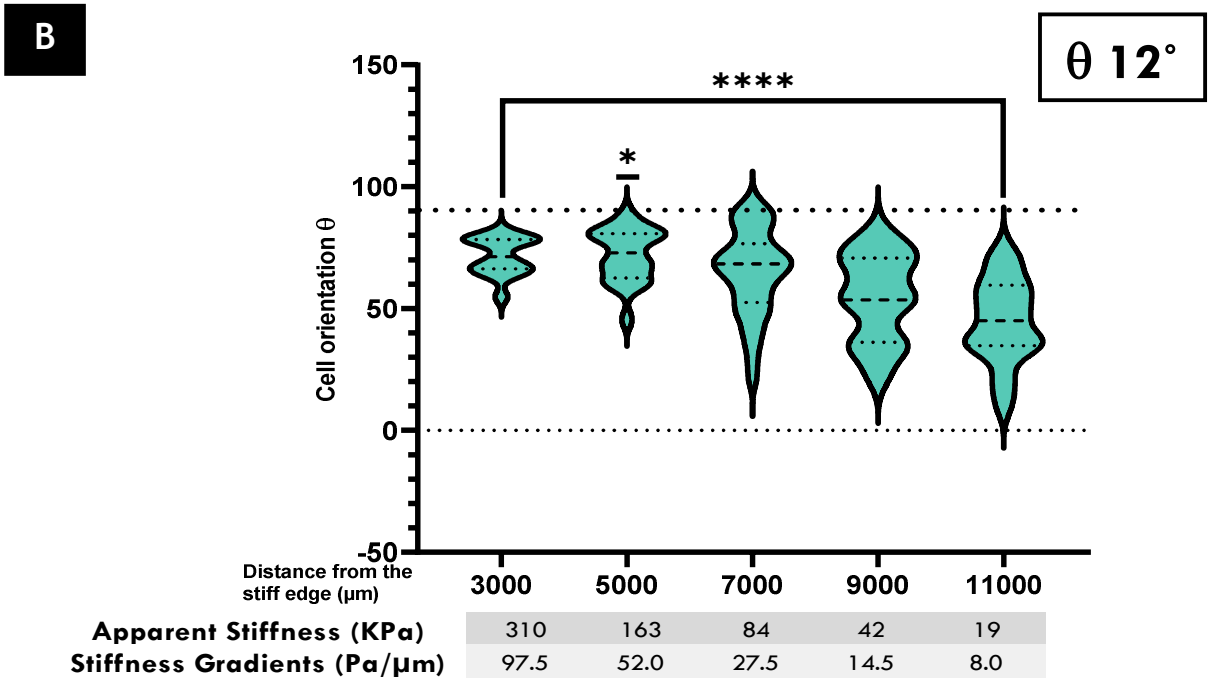

Figure 6. 10 hMSC cell orientation q across the A θ 8˚ gradient **B** θ 12˚ gradient. Statistical significance was assessed using one-way ANOVA test. Data presented as a violin plot (n = 10 single cells per field of view).

Cell circularity

The reported changes in cell morphology also correlated with changes in cell circularity for hMSCs cultured on both θ8° and θ12°, as can be observed in Figure 6.11A and B. Cells found on the steeper regions of both gradients (SG >~100Pa/μm AS θ 8°>500 KPa, θ 12°>405 KPa) presented a slim elongated-like shape, with circularity ratios significantly lower compared with those of the shape of hMSCs on the shallow end (SG <~10 Pa/μm AS θ 8°<~40 KPa, θ 12°<~27 KPa) of both gradients. These have circularity ratios approaching one (Figure 6.7A7, B6). Cell circularity of hMSCs varied significantly as a function of the stiffness gradient. Significant increases in circularity were observed as the stiffness gradient decreased and became close to a physiological range (>10 Pa/μm Figure 6.13A, B), showing a more rounded shape and shape variability for both gradients θ 8° and θ12°. It can be observed that this variation in shape, however, is stronger for cells plated on θ8° gradients, although the difference showed not to be significant. The cell circularity significantly decreased as stiffness gradient and stiffness gradient differential increased, exhibiting the lowest mean cell circularity value on the steepest regions (126 Pa/μm AS >405KPa) of the θ12° gradient (0.2107 ± 0.013 Figure 6.11B), presenting a slim elongated shape and a reduced variation in circularity compared to those cells on the shallow regions of the sample (SG< 10 Pa/μm AS θ 8°<~40 KPa, θ 12°<~27 KPa), which rounded up significantly, exhibiting means of 0.6476± 0.045 and 0.695 ± 0.041 on gradients θ8° and θ12°respectively (see Figure 6.7A and B for the broad spectrum of different morphologies), suggesting the presence of a stiffness gradient threshold below which cells adopt a rounded circular morphology with less cell adhesion processes (~10 Pa/μm).

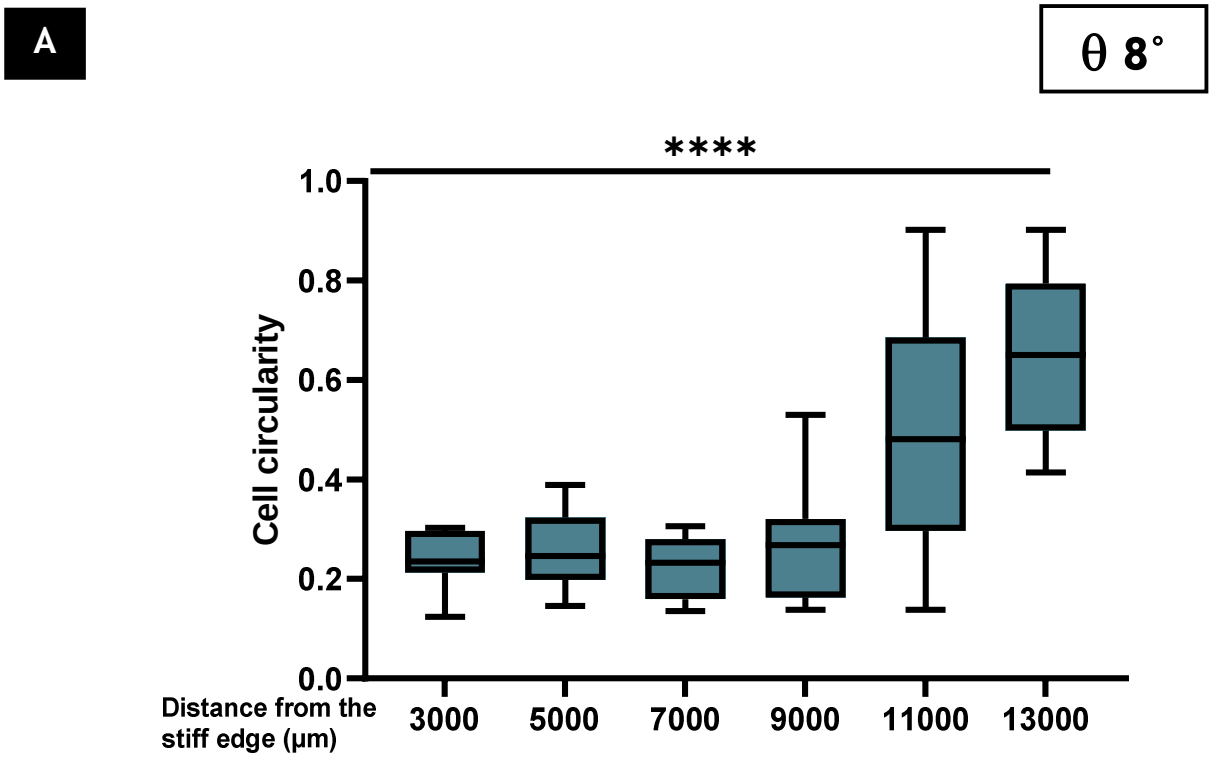

Apparent Stiffness (KPa)	416.50	273.00	178.50	116.00	74.50	47.00
Stiffness Gradients	86.5	57.5	38.0	25.0	16.5	11.0

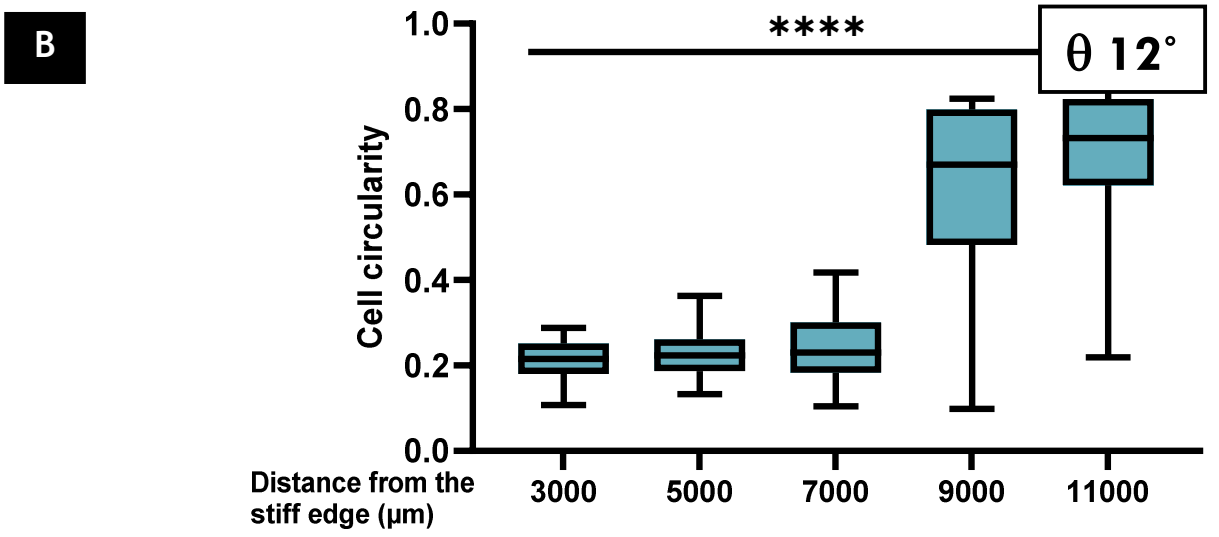

Apparent Stiffness (KPa)	310	163	84	42	19
Stiffness Gradients (Pa/µm)	97.5	52.0	27.5	14.5	8.0

Figure 6. 11 hMSC cell circularity across the A θ 8˚ gradient **B** θ12˚ gradient. Statistical significance was assessed using one-way ANOVA test. Data presented as box ± whiskers (Tukey) (n = 10 single cells per field of view).

Cell aspect ratio

As observed on Figure 6.8, the major shape mode for hMSCs on stiffness gradients with stiffness gradient over 25 Pa/μm (AS θ 8°~120 KPa, θ 12°~80 KPa) was a polarized elongated shape, as reported previously for stiffness gradients in this variation range [34], whereas the softer the gradient region, the smaller the cell aspect ratio (Figure 6.7 and 6.12A, B). It can be observed that the aspect ratio of cells decreased significantly as the stiffness gradient became lower (>10 Pa/μm, AS θ 8°<~40 KPa, θ 12°<~27 KPa) and the substrate softer (Figure 6.12A, B), showing a significant lower cell elongation and elongation variability on shallow softer gradient regions. The cell aspect ratio increased with increasing on stiffness gradient and stiffness gradient differential, exhibiting the highest mean aspect ratio on the steepest regions (126 Pa/μm AS>405 KPa) of the θ12° gradient 8.0 ± 0.10 (Figure 6.12B), and an elongated lamellipodium and broad variety in shape (Figure 6.7A2-4 and B2-5). – whereas those observed on the gradient shallow ends of both θ8° and θ12° (SG<10 Pa/μm) were rounded with a significant decrease in aspect ratio which exhibited means of 1.43 ± 0.126 and 1.72 ± 0.11 on gradients θ8° and θ12°, (Figure 6.7A7 and B6) respectively, and low variability in shape. These results (Figure 6.12A and B) showed significant differences on aspect ratio through the gradient and the variety on stiffness gradient, mostly increasing as the stiffness gradient did so. The stiffness gradient and the physical gradient (θ8° and θ12°), both parameters showed to be significant factors to control hMSC polarized morphology variations, steeper gradient (θ12°) showed higher aspect ratios and the lower variability in shape along the gradient.

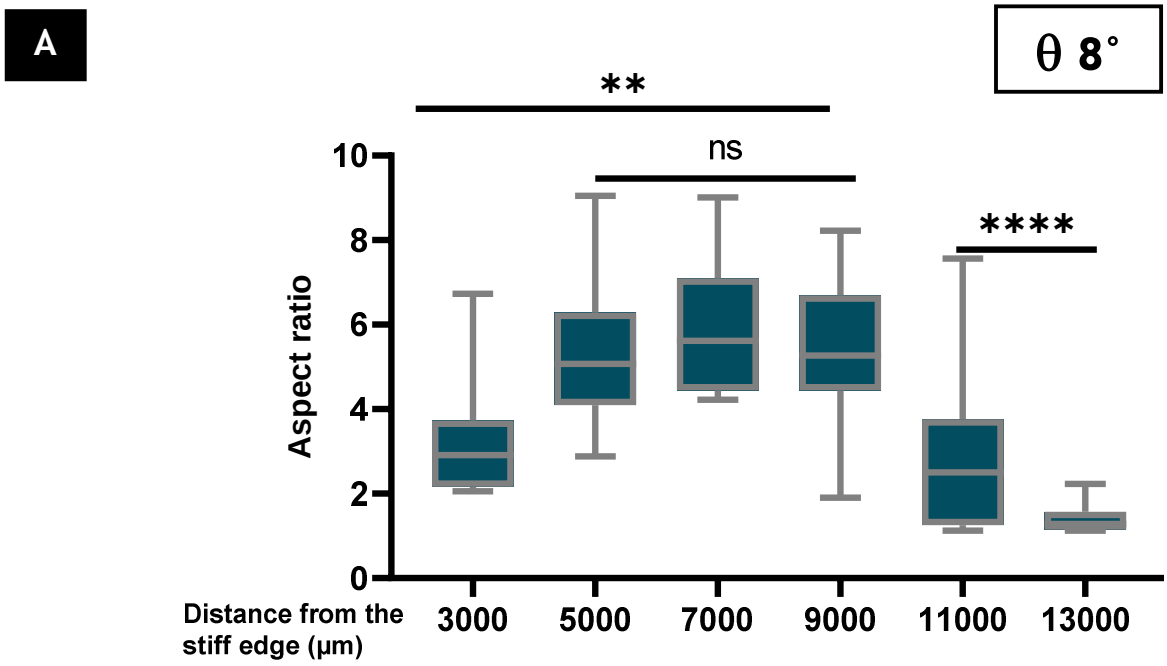

Apparent Stiffness (KPa)	416.50	273.00	178.50	116.00	74.50	47
Stiffness Gradients (Pa/µm)	86.5	57.5	38.0	25.0	16.5	11

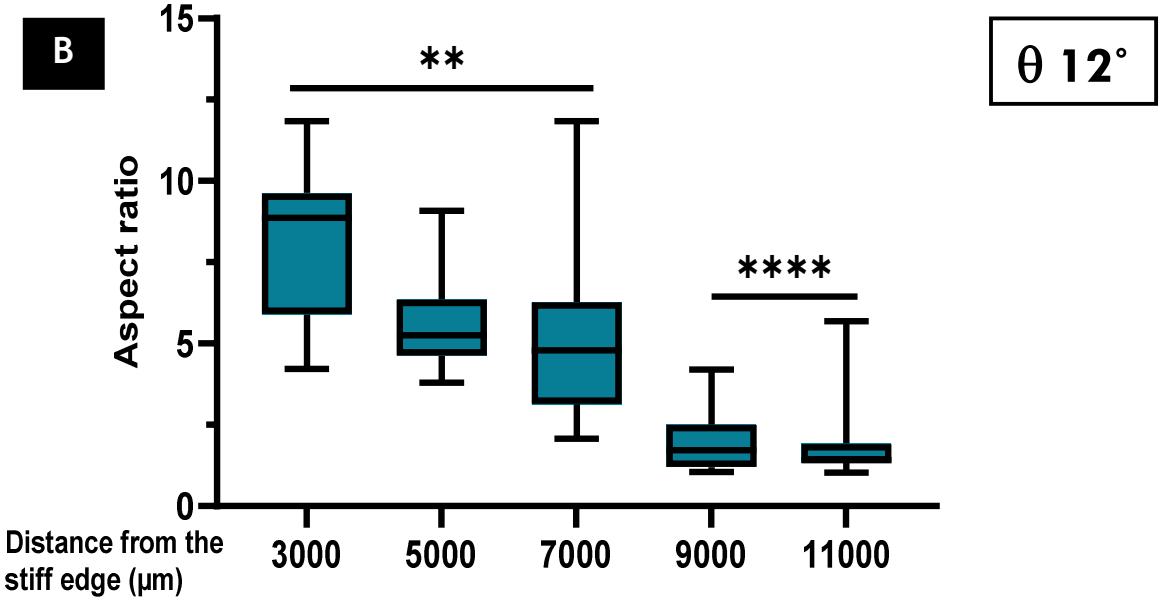

Apparent Stiffness (KPa)	310	163	84	42	19
Stiffness Gradients (Pa/µm)	97.5	52.0	27.5	14.5	8.0

Figure 6. 12 hMSC Aspect ratio at A θ 8˚ gradient; **B** θ12˚ gradient. Statistical significance was assessed using one-way ANOVA test. Data presented as box ± whiskers (Tukey) (n = 10 single cells per field of view).

Table 6. 2 Tabulated summary of morphology changes as a function of stiffness gradient and gradient angle (θ).

Region	Distance from the stiff edge (μm)	θ	Apparent Stiffness (MPa)			Stiffness Gradient (Pa/μm)			hMSCs morphological assessment			
			Max	Min	Range	Max	Min	Range	Cell area (μm)	Cell orientation (θ)	Aspect ratio	Circularity
1	3000	8°	0.503	0.330	0.17	104	69	35	1003 ± 63.05	65.66 ± 3.91	3.373 ± 0.46	0.2415 ± 0.015
		12°	0.405	0.214	0.19	127	68	59	1201 ± 95.39	71.56 ± 2.02	8.072 ± 0.77	0.2107 ± 0.014
2	5000	8°	0.330	0.216	0.11	69	46	23	1039 ± 83.57	55.84 ± 1.13	5.286 ± 0.36	0.2608 ± 0.016
		12°	0.214	0.111	0.10	68	36	32	1475 ± 100.2	71.99 ± 2.39	5.636 ± 0.35	0.2272 ± 0.013
3	7000	8°	0.216	0.141	0.08	46	30	15	1216 ± 125	54.3 ± 1.09	5.827 ± 0.45	0.2249 ± 0.018
		12°	0.111	0.056	0.05	36	19	17	1496 ± 87.4	64.83 ± 3.17	5.208 ± 0.47	0.2408 ± 0.016
4	9000	8°	0.141	0.091	0.05	30	20	10	1281 ± 97.36	51.67 ± 3.09	5.345 ± 0.52	0.269 ± 0.032
		12°	0.056	0.027	0.03	19	10	9	648.7 ± 64.67	54.45 ± 5.00	1.964 ± 0.31	0.614 ± 0.073
5	11000	8°	0.091	0.058	0.03	20	13	7	667.4 ± 100.5	51.49 ± 2.16	2.964 ± 0.51	0.4994 ± 0.061
		12°	0.027	0.011	0.02	10	6	5	571 ± 63.66	44.72 ± 3.76	1.782 ± 0.24	0.695 ± 0.042
6	13000	8°	0.058	0.036	0.02	13	9	4	656.5 ± 73.26	32.55 ± 3.95	1.423 ± 0.11	0.6476 ± 0.045
		12°	0.011	0.003	0.01	6	3	3	-	-	-	-

Migration Studies

hMSCs were seeded on the soft end of each gradient (θ12° and θ8°) at a low density (250 cells/cm^2) in order to minimize cell to cell contact and adhesion and the traction forces transmitted to adjacent cells. After seeding they were shown to have a uniform even spatial distribution at the thick end of the gradient where they were originally seeded. After 5 and 9 days of culture, cell density (cells/cm^2) showed to double between the stiffest and softest regions of the hydrogel (Figure 6.13C and 6.14B) for both gradient systems (θ8° and θ12°). Yet most of the visible cells across both gradients showed some sort of spread and have cytoskeletal processes even in the thicker locations of both gradient hydrogels (θ12° Figure 6.13B and θ8° 6.14A) also showed by the increase in cell number –assessed and reported previously (Figure 6.7 and 6.8)– cells reached local confluency at the stiffer regions from day 7 to 9 on steeper gradients (θ 12°), which correlates with the cell viability assessment. By day 14, the stiffer regions of these hydrogels were fully confluent however the other regions showed poor increase in cell number, and no cells at all from the centre to the soft edge of the sample, the experiment for this group (θ 12° Figure 6.14B) was terminated at day 14 after the 80% of the cells were on the stiffer location. Local confluency at the stiffer regions of the shallow gradients (θ 8°) showed up later (Figure 6.13C), starting from day 14 onward, cells were still individually studied until day 21 of culture when this experiment ended. Spatial distribution on this gradient hydrogel was more evenly scattered from the centre to the stiffest end of the gradient. hMSCs spatial scattering on the θ 8°-gradient steadily progress from a uniform distribution across the soft end of the gradient hydrogel to became locally confluent from the centre to the stiff end of these gradients by day 21. These results correlate with the cell viability assessment that shows

steeper gradients to rapidly shift its spatial cell distribution from thick, soft regions to thin stiff ones within a period of 14 days when the 80% of their DNA content could be found at the stiffest regions of these samples only, whereas θ 8˚ gradients present a more spread cell spatial distribution across the gradient. Figure 6.7 and 6.9 show SEM images of hMSCs on gradient θ12˚ and θ8˚at 5-culture day period.

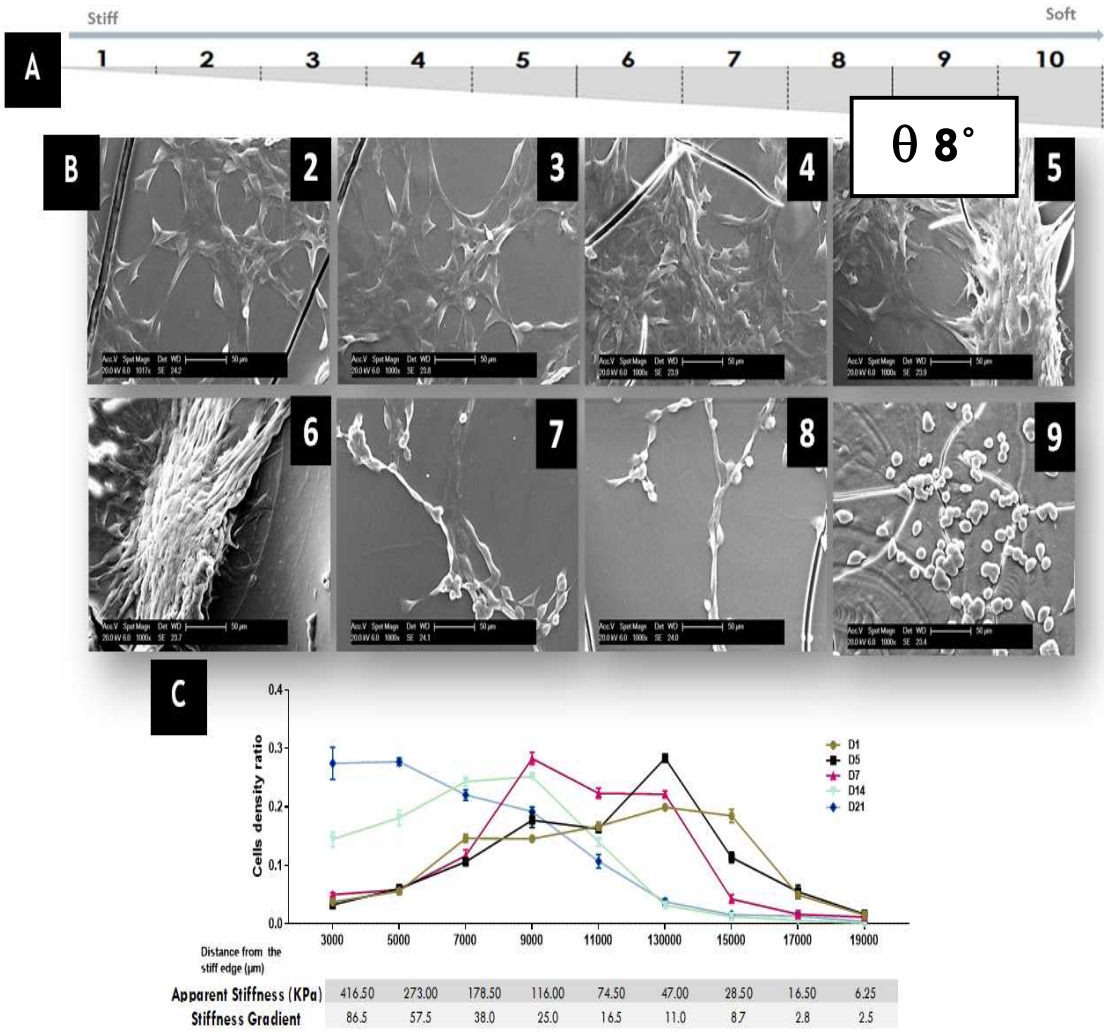

Figure 6. 13 hMSC Distribution of hMSCs ratio along the stiffness gradient A SEM images of hMSCs distribution across the stiffness gradient θ8˚ with stiffness gradient ranging from 104 Pa/µm to 2.9Pa/µm and apparent stiffness from 500KPa to 10KPa **B** hMSCs cell number ratio across the θ8˚ gradient at different timepoints. Data presented as location cell density ratio mean ± SE (n = ~200 cells per sample).

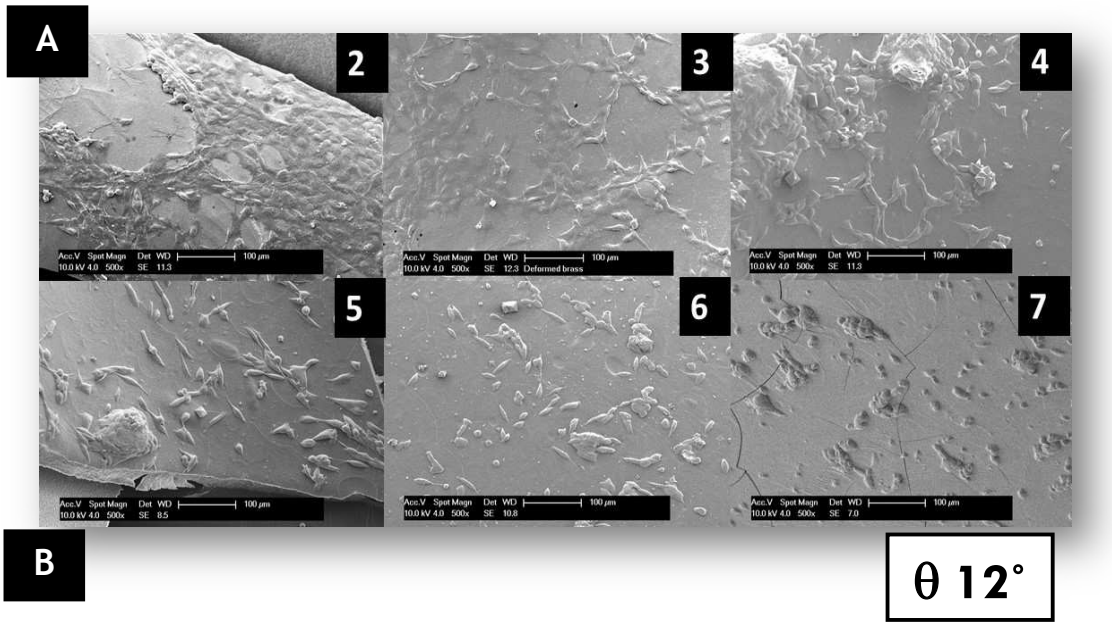

Apparent Stiffness (KPa)	310	163	84	42	19	7	3	3
Stiffness Gradient (Pa/µm)	97.5	52.0	27.5	14.5	8.0	4.5	3.0	2.9

Figure 6. 14 hMSC Distribution of hMSCs ratio along the stiffness gradient A SEM images of hMSCs distribution across the stiffness gradient θ12˚ with stiffness gradient ranging from 126 Pa/µm to 2.9Pa/µm and apparent stiffness from 400KPa to 3KPa **B** hMSCs cell number ratio across the θ12˚ gradient at different timepoints. Data presented as location cell density mean ratio ± SE (n = ~200 cells per sample).

Effects of stiffness gradient on human mesenchymal stem cell hMSC

Osteogenic differentiation

In order to estimate the influence of the gradient θ and the stiffness gradient on the osteogenic differentiation of hMSCs, cells were seeded on ChG_PA gradient hydrogels of two different angles (θ8˚ and θ12˚) and at two different cell densities 250 cells/cm^2 (LD) and 1000 cells/cm^2 (HD) for 14 and 21days. Samples were divided in 4 regions horizontal to the direction of the gradient (Figure 6.15) for location related analysis. Refer to Table 6.3 for full description of each gradient region. Osteogenic markers ALP and Osteocalcin were assessed in cells and normalised by cell number (DNA content) to determine hMSCs osteogenic differentiation.

Table 6. 3 Tabulated summary of apparent stiffness (AS) and stiffness gradient (SG) as a function of gradient location (region).

Gradient location	Distance from the stiff edge (µm)		θ	Thickness (mm)		Apparent Stiffness (MPa)		Stiffness Gradient (Pa/µm)	
1	2000	6500	θ8˚	0.28	0.56	0.503	0.330	104.1	68.9
			θ12˚	0.43	0.85	0.405	0.214	126.8	67.9
2	6500	11000	θ8˚	0.84	1.41	0.330	0.091	68.9	20.0
			θ12˚	1.28	2.13	0.111	0.027	67.9	10.4
3	11000	15500	θ8˚	1.69	2.25	0.091	0.021	20.0	5.8*
			θ12˚	2.55	3.40	0.011	0.003	10.4	2.9*
4	15500	20000	θ8˚	2.53	2.81	0.021	0.005	5.8	2.53*
			θ12˚	3.83	4.25	0.003	0.003	2.9	2.90*

*The apparent stiffness durotactic threshold (GT) has been highlighted in blue for both the θ8˚ and the θ12˚ gradient.

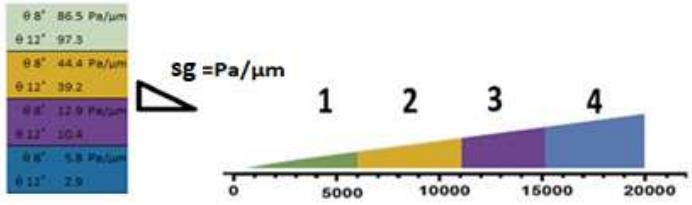

Figure 6. 15 Stiffness gradient corresponding to gradient locations schematic guide.

ALP activity

Figure 6.16A shows the ALP activity of hMSCs seeded on θ8° gradients at different cell seeding densities. It can be seen that the activity of the osteogenic ALP marker increased from the shallow gradient region coinciding with the reported durotactic threshold (GT) (~8.2 to 2.9 Pa/μm) [76, 94] to the steep gradient hydrogel regions with the highest activity occurring on region 1 with a SG in the range of ~104.1 to 68.9 Pa/μm AS 503 to 330 KPa (region 1 for the θ8° in Table 6.3), for both seeding densities, however significant higher for the HD group at both timepoints, not significant differences where observed for cells found on location 2 (SG ~68.9-20.0 Pa/μm AS ~330 to 91KPa) comparing timepoints or cell seeding densities, whereas significant differences were observed in location 3 when comparing timepoints (SG~20.0-5.8 Pa/μm AS~91 to 21KPa) on which hMSCs in group LD showed significant increased on ALP activity compared to cells on the HD group on the same gradient location. The results analysis also showed that the shallowest ChG_PA θ 8°region (SG~5.8Pa/μm, AS <~21KPa location 4 for the θ8° in Table 6.3), yield significantly high levels of ALP activity compared with cells in the centre regions of the gradient. This gradient seems to be divided by the durotactic threshold introduced in the literature (8.2 to 2.9 Pa/μm) [76], showing higher levels of ALP activity as the stiffness gradient increases over the GT and therefore sample location apparent stiffness. Dual significant variations (Increases and reductions) depending on stiffness gradient range were also observed between cell seeding density groups (LD and HD) suggesting that cell density plays a role in stiffness gradient-based osteogenic differentiation.

It can be observed from Figure 6.16B a partly similar trend on steeper gradients (θ12°) to the one seen on the shallow gradient (θ8°). For both cell seeding groups (LD and HD)

it was observed that hMSCs on these steep (θ12°) gradients increased the ALP activity in an exponential fashion as SG increased, also from the durotactic GT region (SG~2.9Pa/μm AS 11 to 3 KPa Region 3 for the θ12° gradient in Table 6.3) to the steeper gradient hydrogel regions with the highest activity occurring on region 1 with SG in the range of ~126.8-67.9 Pa/μm and AS 405 to 214 KPa (region 1 for the θ12° in Table 6.3), however for these gradients no significant variation on ALP activity was observed beyond the durotactic threshold, suggesting the observed ALP activity significant increased on the stiff end with a strong SG (126.8-67.9 Pa/μm) compared to the centre of the sample with thick weak SG (10.4-2.9 Pa/μm) is a joint effect of apparent stiffness- stiffness gradient, and the stiffness gradient differential resulting from the gradient tilt angle.

Significant variations in ALP activity were reported for regions 1 and 2 also, when compared as a function of cell seeding density (LD and HD) suggesting, the cell density plays a role in stiffness gradient-based osteogenic differentiation for steeper gradients as well. Osteogenic differentiation as a function of gradient angle showed to be also significant hMSCs showed to prefer stiffer regions better on steeper gradients.

Osteocalcin expression

It can be observed (Figure 6.17A) that osteocalcin expression of hMSCs seeded on θ8° gradients at different cell seeding densities (HD and LD) increased from the shallow gradient region coinciding, as seen for ALP activity, with the reported durotactic threshold (8.2 to 2.9 Pa/μm) [76, 94] to the steep gradient hydrogel regions with the highest expression occurring on region 1 with a stiffness gradient in the range of ~104.1 to 68.9 Pa/μm AS 503 to 330 KPa (Region 1 for the θ8° in Table 6.3), for both seeding densities, however significantly higher for the HD group at 21 day

timepoint, no significant variations at the other timepoints were observed among the other samples in this region. There was osteocalcin expression present in region 2 (68.9-20.0 Pa/μm AS ~330 to 91KPa) however, no significant variation in osteocalcin expression were observed for these groups. Significantly higher osteocalcin expression for both timepoints were observed for cells in the LD groups compared with osteocalcin expression to the HD group of hMSCs founded on region 3 (SG 20.0-5.8 Pa/μm AS 91to 21KPa). The results also showed that the shallowest ChG_PA θ 8˚region (~5.8-2.53Pa/μm AS <21KPa region 4 for the θ8˚ in Table 6.3), presents significant high levels of osteocalcin expression compared with cells in the centre regions of this gradient. The osteocalcin expression seems to be also divided (as that of ALP) by the durotactic threshold (~8.2 to 2.9 Pa/μm) hMSCs expressing higher levels of osteocalcin as the stiffness gradient increases and therefore substrate stiffness above the durotactic threshold only.

Figure 6.17B shows the osteocalcin marker expression of hMSCs on steep gradients (θ12˚) to increase from the soft to stiff hydrogel sections with the highest expression occurring on region 1 (SG range of~126.8 to 67.9 Pa/μm AS 405 to 214 KPa), followed by a lower but significant osteocalcin expression on region 2 (SG range of of~67.9 to 10.4 Pa/μm and AS 111 to 27 KPa). As for osteocalcin expression no significant variations compared to stiffer regions were observed on regions below the durotactic threshold. Except for the HD group on the steep region 1which showed a timepoint-dependent significant change, the osteocalcin expression was higher at 14-day period compared to 21-day period, no significant differences were observed as a result of time on the other regions, whereas osteocalcin expression as a function of cell seeding density showed to be significant, osteocalcin expression for LD showed to be

significantly lower compared to HD. Together, these results suggest differentiation of hMSCs into osteoblasts is an interconnected effect of stiffness gradient, cell seeding densities, the stiffness gradient differential resulting from the gradient tilt angle and also the durotactic threshold on stiffness gradient-based systems.

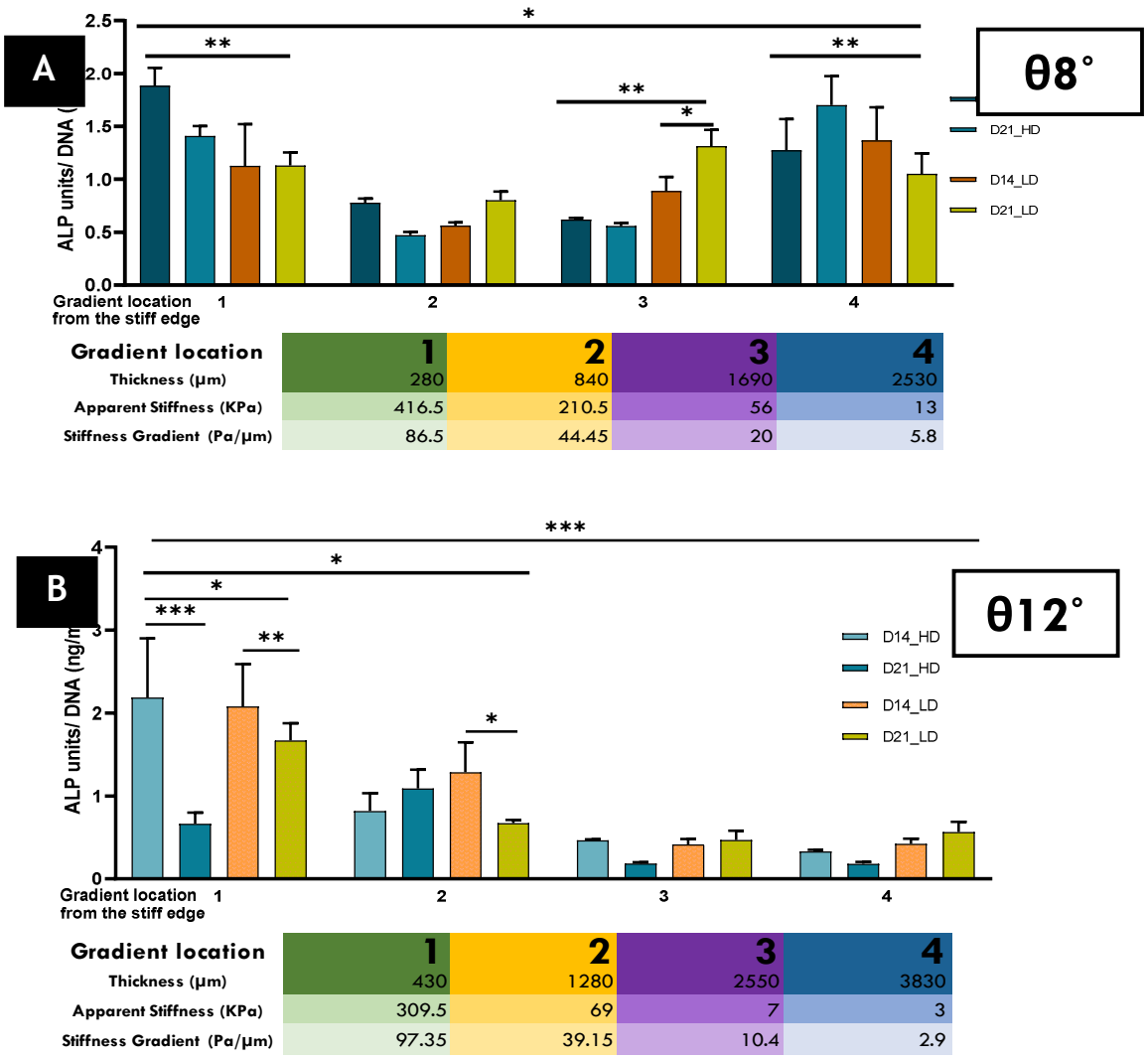

Figure 6. 16 Results of ALP activity assay of hMSC's A θ8˚ stiffness gradient at low 250 c/cm^2 cell seeding density (**LD**) and High 2500 c/cm^2 cell seeding density (**HD**) B θ12˚. The assays were performed on samples seeded onto hydrogels of each thickness and measured at various timepoints. Florescence unites where normalized with DNA content. Data is shown as group mean ± SEM (n=9).

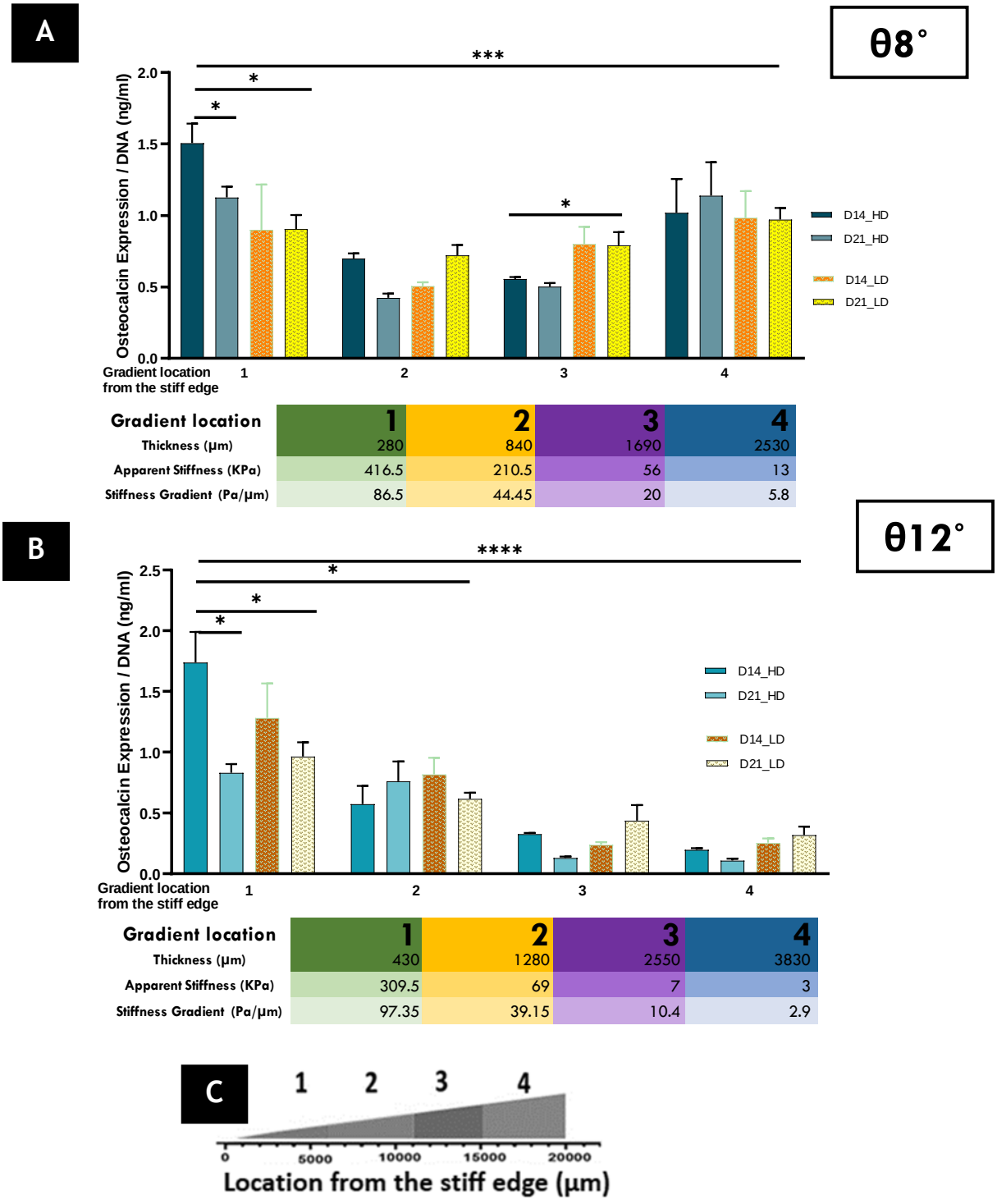

Figure 6. 17 Results of Osteocalcin expression assay of hMSC's on A θ8˚ stiffness gradient at low 250 c/cm^2 cell seeding density (**LD**) and High 2500 c/cm^2 cell seeding density (**HD**) B θ12˚. The assays were performed on samples seeded onto hydrogels of each thickness and measured at various timepoints. Florescence unites where normalized with DNA content. Data is shown as group mean ± SEM (n=9).

Discussion

It was found in this study that protein-based hydrogels with a nonlinear mechanical profile help to reproduce a range of different stiffness gradients, i.e. stiffness change per unit of length, facilitating the fabrication of, soft-hard tissue Interfaces (SG >100Pa/μm), pathological (40Pa/μm>SG> 10 Pa/μm) and soft tissue physiological (SG< 10 Pa/μm) gradients on the same single sample, therefore, contractile hMSCs encounter those different gradients as a spatial function while they interact and travelled across one single sample. This characteristic led to the appreciation of another feature of these gradients: the differential on stiffness gradient, i.e., the change in stiffness gradient per unit of length, which together with stiffness gradient (change in apparent stiffness per unit of length) and absolute apparent stiffness showed to be deterministic on hMSCs response. To assess the influence of this differential in stiffness gradient on hMSC behaviour, gradients of two overall different steepness were fabricated, a simple system was developed to fabricate complex stiffness gradient hydrogels which emulate the inhomogeneous nonlinear mechanical profile of the native ECM, comprising in a single sample the biological relevant stiffness gradients a cell may encounter in living tissue, above and below the durotactic threshold, achieving variations in stiffness by manipulating the ChG_PA hydrogel thickness, which from the previous chapter showed to be an effective technique to alter the apparent stiffness that cells can sense, making it possible to study durotactic behaviour in hMSCs cells as well as cell behaviour below the durotactic threshold, offering the possibility to identify optimal stiffness values for a wide range of biological phenomenon, without the confusing effect of variations on the architecture or chemistry of the sample surface or the durotactic effect (when analysing cells below the durotactic threshold). This system aimed to recapitulate the wide stiffness gradient possibilities in the hMSCs niche on a single

sample, for an accessible way to study mechanotransduction in a more physiological-like environment.

Wedge shaped ChG_PA hydrogels with thickness variations across the sample, showed to be an effective technique to fabricate stiffness gradients by varying the apparent stiffness across the sample. Due to the nonlinear elastic nature of the ChG_PA hydrogels, comprising different stiffness gradients in a single sample is possible, this stiffness gradient variations will be a function of ChG_PA thickness and gradient tilt angle, hMSCs showed to sense and increase in cell number, migrate and differentiate as response to changes in the stiffness gradient and the differential in stiffness gradient of ChG_PA hydrogels.

Here hMSCs were presented with the developed ChG_PA gradients hydrogels and showed that entire population of cells will preferentially accumulate on stiffer hydrogel regions over the hMSC durotactic threshold (estimated to be 2.9 Pa/μm to 8.2Pa/μm) [76]. Apparent stiffness hydrogel gradients of two different steepness, ($\theta 8^{o}$ or $\theta 12^{o}$) were fabricated and their mechanical properties characterised. The mechanical profile of these gradients showed to fit a nonlinear exponential decay function of thickness (Figure 6.3) on which thickness was itself a function of the gradient steepness, i.e., $\theta 8^{o}$ or $\theta 12^{o}$. Compliant with previous observations in this project (Figure 5.6) which demonstrated that altering the thickness of ChG_PA of known Young's modulus (111KPa) firmly adhered to a more rigid underlying material altered the apparent stiffness of the hydrogel in a nonlinear manner and in accordance to Rudnicki et al. [185] that showed collagen and fibrin hydrogels apparent stiffness increase consistently with a decreased on thickness displaying the characteristic nonlinear mechanical profile of biological materials. The distribution of the mechanical profile of each gradient was

shown to be significantly different (Figure 6.3). The shallower gradient ($\theta 8^{o}$) showed a distributed mechanical profile across the whole gradient hydrogel with steady shallow increases in stiffness between regions as the thickness decreased, whereas these changes on stiffness between regions were greater for the steeper gradient ($\theta 12^{o}$), and occurring from the centre to the stiff end of the gradient only (where these changes were all significantly different compared to each other), from the centre to the soft end changes in stiffness were little and non-significant. The stiffness gradient as a function of gradient steepness showed a similar profile to the one seen in the apparent stiffness (Figure 6.4) the stiffness gradient was spatially distributed in each gradient hydrogel containing each of the 3 biologically relevant gradients. In shallow gradients θ8°, stiffness gradient apparent stiffness ranges showed to be more spatially distributed across the effective length of the gradient, showing shallow changes in stiffness gradient from below and over the durotactic threshold that has been estimated for hMSCs to be between 2.9 Pa/μm to 8.2Pa/μm [76]. The steeper gradient $\theta 12^{o}$ showed stronger variation between locations from the centre of the sample to the stiff/steeper edge, with most of the area under its stiffness gradient curve (Figure 6.4) concentrated between the tissue interface stiffness gradient (~>100Pa/μm, AS ~302 KPa) and the upper limit of the pathological stiffness gradient (~40Pa/μm AS~111KPa). The physiological stiffness gradient range in these gradients was significantly smaller compared to the steeper regions and showed no differential stiffness gradient change over 2.9Pa/μm (AS ~3KPa). The observations of these experiments suggested that variations in the gradient steepness ($\theta 8^{o}$ and $\theta 12^{o}$) of the gradient not only change the stiffness gradient profile, but also the rate of change at which these differences on stiffness gradient spatially appear. hMSCs seeded on both gradients showed a spatial/temporal

reorganization of their distribution, from being mainly concentrated at the soft edge, where they were seeded originally at 3-day period culture, to have reorganised themselves into showing a predominant preference for the stiffer edge of both gradients by the 14-day period (Figure 6.7 and 6.8). However, cell distribution between samples showed to be significantly different, on the shallow gradient ($\theta 8^{o}$) the distribution of hMSCs showed to be bimodal (Figure 6.7A and 6.8A) with its highest peak being localised at the stiff edge of gradient and the smaller at the opposite soft edge of these gradients. A possible explanation to these observations is that a durotactic threshold is localised in this soft region of the gradient, from below which hMSCs do not experience a durotactic response therefore become trapped in the shallow regions of these gradients where the stiffness gradient is below 5.79 Pa/μm (~AS 21KPa), consistent with the findings of Hadden et al. [94], who developed stiffness gradient above and below the hMSC durotactic threshold (over 8.2 Pa/μm and below 2.9 Pa/μm) and observed a similar response cells found on the regions below the durotactic threshold moved indistinctly over the x and y axis of the sample, thus no orientation in the direction of the gradient was found. Therefore, it can be assumed that the durotactic threshold for hMSCs in theses gradients can be found below ~5.79 Pa/μm where the apparent stiffness is >21kPa. Conversely for hMSC on steeper gradients ($\theta 12^{o}$), the preference for stiff regions over 70 kPa/μm (AS ~214KPa) stiffness gradient was stronger similar to that observed by Sunyer et al. [98] who fabricated stiffness gradients of different individual stiffness gradients (ranging from ~68 to ~114KPa/μm) and found that cells will favour the stiff edges of the steeper gradients, with the majority of the cells concentrated on this region (Figure 6.7B and 6.8B), preference that was significantly amplified by a high cell seeding density compared to low seeding

densities, as reported by Sunyer et al. [109], who have demonstrated that cell collective systems are more effective at responding to environmental stiffness gradients than their isolated constituents. It was also observed that the cell number distribution for these gradients differ to the one seen on $\theta 8^{o}$samples. This distribution was seen to be unimodal in the direction of the stiff edge, showing also that aggregates of cells on these gradients do not become trapped, suggesting that the durotactic threshold in these gradients is below ~2.9 Pa/KPa (AS 3KPa) therefore smaller than the one found on the $\theta 8^{o}$. These observations suggested the idea that hMSCs are not just able to sense the stiffness gradient of their surroundings but also the acceleration at which this stiffness gradient change and the apparent stiffness (i.e., differential of the stiffness gradient).

hMSCs spread area, aspect ratio and circularity displayed spatial-dependant changes on both gradients. It was observed that while cell spread area (Figure 6.8) did not show significant differences between gradient locations over the durotactic threshold, on uniform stiffness substrates in Chapter 5 (Figure 5.17) cell spread area significantly varied with apparent stiffness, i.e. the degree of cell spreading increased with increasing stiffness, cell spread area on gradients showed significant differences extend as a function of absolute stiffness but compared to uniform apparent stiffness hydrogels, the magnitude of spreading area on gradients was smaller. That can be explained by the fact that whereas on uniform stiffness substrates, cell area was mostly spread and flattened in all directions with some polarization observed on stiff hydrogels (Figure 5.17), cells on gradients hydrogels (above the durotactic threshold) showed a dominant elongated shape (with aspect ratios over ~5 and circularity below ~0.2), over the durotactic threshold ($\theta 8^{o}$ ~5.79Pa/μm, AS ~21KPa; $\theta 12^{o}$ 2.9Pa/μm, AS~3 KPa). Cell morphology was mostly polarized and polarized as a function of their stiffness gradient

on both, i.e., θ8°, θ12° (Figure 6.7), it was noted also that significant differences exist between gradients (θ8°, θ12°) hMSCs on gradient θ12° showed visible more elongated shapes and significantly higher aspect ratio and lower circularity compere to those observed on the shallow gradient (θ8°). These findings are in partial agreement with Isenberg et al.[92] who reported that Vascular Smooth Muscle Cells (VSMCs) growing on PDMS hydrogels functionalised with type I collagen of uniform stiffness with moduli ranging from 5 to 80 KPa and gradients of 20Pa/μm (AS 0.93 to 41.7 KPa) and 40Pa/μm (AS 4.64 to 80.1 KPa) cells presented spread areas dependant on absolute modulus, with more spread areas on stiff substrates compared to soft and cell polarized morphology being predominant for cells seeded on both gradients without significant differences among them; in their study this response showed to be a function of the gradient, but not stiffness gradient – probably because the group has the limitation of only being able to assess 2 different stiffness gradients (20Pa/μm, AS 0.93 to 41.7 KPa) and 40Pa/μm AS 4.64 to 80.1 KPa) independently, whereas on the nonlinear gradients all the possible stiffness gradients (from ~2.9 Pa/μm to ~100Pa/μm) coexist together on the same sample (**AS** θ8° 5 to 503 KPa; θ12° 3 to 405 KPa). These observations support the idea that hMSCs response is also constricted by a third and fourth factor on this nonlinear stiffness gradient besides stiffness gradient: **the differential of stiffness gradient and apparent stiffness range.**

This stiffness gradients possess a stiff and an opposite soft edge, it has been hypothesised that hMSCs will migrate from the soft complaint regions follow the direction of the stiff edge on those gradients, according to what has been reported in previous studies. To prove this hypothesis, hMSC alignment (Figure 6.9 and 6.12) and spatial cell concentration over time (Figure 6.13 and 6.14) for both gradients were

characterised. The findings of these experiments showed that hMSCs orientate themselves in the direction of the gradient in a stiffness gradient-dependant manner (Figure 6.9), with cells showing stronger alignment in the gradient direction as stiffness gradient increased over the ~40Pa/μm (AS 4.64 to 80.1 KPa) for both gradients (Figure 6.10). Significant variances on orientation angle among regions from the soft to stiff edge were observed on shallow gradients $\theta 8^{o}$ (Figure 6.10A), contrary to what was observed on steeper gradients, where orientation in the direction of the gradient was stronger and significant differences were mainly observed between the stiffest and the softer edge of the sample (Figure 6.10B). It is also worth noticing in this regard that according to findings in Chapter 5, this phenomenon was seen not to be a function of apparent stiffness (Figure5.18) confirming that cell orientation depended only on stiffness gradient, not on absolute apparent stiffness. Another study that shows similarities with the findings seen in these experiments are the observations made by Hadden et al. [94], who showed that human adipose-derived stem cells (hASCs) on gradients with stiffness gradient above (8.2Pa/μm) and below (2.9Pa/μm) their average cell speed was similar; however, when the cell speed was divided into components either perpendicular to or parallel to the gradient direction (x and y, respectively), the steeper gradient (8.2 Pa/μm) exhibited significantly higher **y** velocities, indicating orientation toward the stiffer region. Similar observations were reported by Isenberg et al. [92], in their study the average orientation of VSMCs on uniform hydrogels was close to zero, therefore not a function of modulus, while cells on gradient hydrogels of 20Pa/μm (AS 0.93 to 41.7 KPa) and 40Pa/μm (AS 4.64 to 80.1 KPa) aligned on average in the direction of the gradient and this alignment strengthened as the stiffness gradient increased. They hypothesized this phenomenon is the result of mechanical noise, by drawing the parallel with chemotaxis by seeing

micron- or submicron-scale variations in substrate stiffness as mechanical 'noise': that cells on shallow gradients of stiffness with stiffness magnitudes in the scale of the mechanical noise would appear to exhibit random behaviour or confusion, mistaking the mechanical noise as a given direction and losing track of the imposed gradient, whereas cells on steeper gradients, which provide a higher signal/noise ratio, would be influenced primarily by the imposed gradient itself, rather than by mechanical fluctuations. Further observations of this study showed that hMSC migration over the durotactic threshold ($\theta 8^{o}$ GS~5.79Pa/μm AS ~21KPa $\theta 12^{o}$ GS ~2.9Pa/μm AS~3KPa) for both gradients are independent of local hydrogel stiffness magnitude, i.e., regardless of what the stiffness is where the cell is within the gradient, it continuously migrates towards the stiffer edge. In this study, it was observed that cells on the steeper gradient $\theta 12^{o}$ reorganised themselves in the stiff direction faster (9 days to reach the stiff end), whereas for hMSCs plated on the shallow gradients $\theta 8^{o}$ took longer (14 days to reach the stiff edge). Several previous studies on stiffness gradients have stated that stiffness gradient, in this case the differential of stiffness gradient, dictates cell migration speed [76, 80, 92, 177]. A limitation observed in these studies was the fact that with the available method (cell density analysis) proliferation couldn't be disassociated from cell density since cell proliferation wasn't inhibited, therefore cell density reorganisation might be a combined effect of migration and proliferation. Hadden et al.[94] overcome this limitation by using time-lapse microscopy, and tagging and tracing single cells towards the stiffness gradients used in their study confirming cells will migrate towards the stiffest edge of the gradients, with cell speed correlating to the stiffness gradient steepness. With this approach, further data can be gathered such as speed, orientation,

and morphological changes at every different region of the gradient for every tagged cell. Figure 6.18 shows an example of how Hadden group analysed their data.

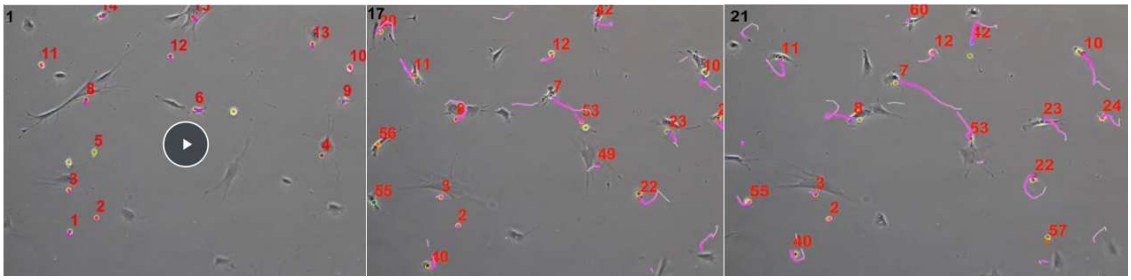

Figure 6. 18 Time-lapse live cell imaging of hASC migration on 12/12% cells were traced using automated tracking software a spot-detection algorithm in conjunction with an optimal Bayes multiobject tracking algorithm and cells were detected from each image using a spot-detection algorithm with adaptive wavelet threshold. (Shown in numbers and colour overlay) adapted from [94].

Differentiations studies (Figure 6.16 and 6.17) for both gradients showed osteogenic activity significantly present on the stiff edge of the samples, consistent with other studies that have proved that on stiffness gradients over the durotactic threshold cells will preferentially differentiate into osteogenic linages on the stiff regions [34, 344].

Shallow gradients ($\theta 8^{\circ}$) showed a bimodal distribution (6.16A, 6.17A) with ALP activity and Osteocalcin expression peaks at both opposite edges over the stiffness gradient above ~70Pa/µm (AS 503 to 330KPa) on the stiff edge and below the observed durotatic threshold of ~5.79Pa/µm (AS >~21KPa) of the gradient. A possible explanation for this observation is that cells on location below GT (~5.79Pa/µm, AS >~21KPa) get trapped under the durotactic threshold where apparent stiffness is still suitable for cell function, forming the dense packed colonies observed in Chapter 5 (Figure 5.19) and ending changing the effective stiffness that cells can sense on top [45] encouraging osteogenic differentiation. hMSCs at the centre of these gradients (stiffness gradient ~70Pa/µm to ~20Pa/µm, AS 330 to 91KPa, location 2; and ~20Pa/µm to 5.79Pa/µm, AS 91KPa to 21KPa location 3) osteogenic activity show a stronger cell

density-spatial dependence with low seeding density showing a significant higher ALP activity and Osteocalcin expression compared to high cell density and response shown to be stronger for both markers for the central locations of the gradient (location 3 compared to 2 Table 6.3). A possible explanation for this phenomenon is what has been previously reported by Tusan et al. [349]: the sum of cell aggregates contractile forces is higher, therefore these forces travel deeper inside the soft hydrogel than single cells, allowing aggregates to interrogate deeper for changes in mechanical properties of their surroundings, making them more susceptible to the enforced gradient. which may encourage them to migrate instead to stay and differentiate, whereas single cells lack that extra incentive, therefore they are more susceptible to mechanical noise, making it easier for them to go into differentiation instead of migrating. Steeper gradients $\theta 12^{o}$ (Figure 6.14B, and 6.15B) showed a lower durotactic threshold 2.9Pa/μm (AS ~3KPa) and not a bimodal distribution on cell differentiation, showing osteogenic differentiation strongly concentrated on the stiff edge of the samples independently of cell density, in agreement with previous research that has shown that cells above the durotactic threshold will favour stiffer regions of the gradient for osteogenic differentiation [147, 350].

Conclusion

The majority of biological phenomena inside the body are to some extent affected by mechanical forces: from soft brain to hard bone, a wide variety of stiffness and stiffness gradients can be found in living tissue, these mechanical variances have been seen to influence important biological process such as stem cell differentiation [29], cancer spread and progression [19] and homeostasis[38]. Together, cell spatial redistribution and lineage specification data presented in this study suggest that

hMSCs on gradient hydrogels go into durotaxis and then differentiate. The data also suggests that these responses are determined by the absolute stiffness, stiffness gradient, stiffness gradient differential, and cell-cell interaction. This emphasizes the importance of ECM mechanical properties as fundamental regulators of stem cell fate and demonstrates that known variation in these properties can have a profound effect on undifferentiated stem cell behaviours. The stiffness gradient system developed and presented in this section showed that a fibrous protein-based hydrogel with a nonlinear mechanical profile can allow the production of a range of different stiffness gradients, from soft-hard tissue interfaces to soft tissue variations in the tissue homeostasis state, allowing the continuous change of stiffness gradient through the gradient hydrogel; therefore cells can be subjected to a variety of ranges as they travel across the gradient sample, facilitating the elucidation of critical cell response, such as durotactic thresholds, or stiffness-sensing thresholds, demonstrating the importance of the implications of these studies for hMSC biology generally, and for single-cell and cell-cell mechanobiology analysis platforms. Furthermore, the stiffness gradient system developed and presented in this section is a simple option to fabricate complex stiffness gradients in a reproducible and consistent manner, without the need of sophisticated equipment or special reagents. Moreover, this system allows the investigation of a wide range of mechanical-induced cues on a single sample and, because the steepness of the gradient in this technology is easily adjusted, it can be adapted to fit a limitless variety of biological conditions or disease processes, therefore shallow slopes below durotactic thresholds can isolate absolute stiffness and enable the study of more subtle cell responses without the confusing effect of durotactic responses, and steeper slopes over the durotactic threshold can help to elucidate the pathways behind durotactic responses.

CHAPTER

7

Bioreactor Development for the Investigation of the Combine effect of Flow-induced Shear and ChG_PA Apparent Stiffness on hMSC Response, Limitations and Guidance for Future Work

7. Bioreactor Development for the Investigation of the Combine effect of Flow-induced Shear and ChG_PA Apparent Stiffness on hMSC Response, Limitations and Guidance for Future Work

Introduction

The aim of this chapter was to provide a foundation for a future full validation of the hypothesis that human mesenchymal hMSCs can respond and differentiate while influenced by static and dynamic mechanical stimulation cues interplaying simultaneously. A custom-made parallel flow bioreactor was developed, and early testing was carried out with the aim of facilitating the study of the combined effect of both apparent stiffness and shear stress.

hMSCs have a critical role for tissue homeostasis and repair: they can exit and migrate out from their niche to damaged tissue or tissue that needs to be remodelled and repaired. Once they arrive at the new location, they undergo tissue-specific commitment and differentiation [351, 352]. This makes tissue repair and tissue remodelling a promising field for hMSCs applications [353]. This ability of hMSCs to migrate and locate themselves in the place of injury have been widely investigated. However, most of these cell migration studies have evaluated cell movement under static culture conditions and have primarily tested the effects of biochemical cell-migration-driving factors in a process known as chemotaxis [107, 354]. There is growing recognition other cues besides chemokine gradients, such as static and dynamic mechanical signals or electric fields, also have a critical role in how a cell interacts with its microenvironment and migrates [177, 355, 356]. For example, hMSCs will make use of the shear flow provided by the cardiovascular system or the pressure gradients generated by natural body motion resulting in interstitial fluid-flow to get to the place of injury. In this regard,

fluid-flow stimulation of hMSCs has been widely used for fundamental research and for the expansion and conditioning of cells for tissue engineering and regenerative medicine [77, 117, 118, 124]. Fluid-flow applications are good alternatives to take advantage of biomimetic flows to control cell responses *in vitro*. Basically, cells subjected to fluid-flow shear stress interpret these mechanical cues as triggers for biochemical responses – the previously described mechanotransduction process [125]. Ongoing research in the field has shown that flow controls a wide range of hMSC responses [122, 357, 358].

Macro 2D fluid-flow cell culture devices have been extensively used to examine the cell response to flow and its influence on triggering mechanotransduction pathways. Parallel plate flow chambers are common devices used in these applications, mainly because its flow profiles are easy to characterize with simple fluid mechanic formulas, allowing the design of devices with precise flow profile features that have the benefit of reproducibility offered by these applications [359]. Therefore, strong correlation of cell response to shear stress effect can be attained. These applications are suitable for the development of numerical simulation when combined effects need to be elucidated. For example, Salvi et at. [360] have developed a model to identify flow profiles depending on cell confluence, cell height, and substrate nano-topographies. Some of the main drawbacks of these devices include: their limited ability to mimic the physiological microflow environments of native in situ conditions; they typically rely on glass slides as the culture surface, which limits the formation of biomimicking mechanically complex microenvironment, and they usually hold a few test slides at a time, all of which are under the same flow conditions. Testing multiple conditions is therefore a time-consuming task.

In addition to migration, stem cells are exposed to numerous chemical and biophysical stimuli, which serves to guide the homing process and facilitate tissue repair [355]. The role of mechanical cues such as the influence of shear stress on stem cell migration is still poorly understood, particularly compared with chemotactic homing. Yuan et al. and Riel et al. respectively demonstrated that a crawling migration mode characterized MSCs under shear stress forces [176, 361]. It has also been reported that fluid-flow is a strong regulator of MSCs with the migration path efficiency being affected by increasing shear and that hMSCs will preferably orientate in the flow direction [355, 361].

Previous findings in this study have demonstrated that variations in substrate mechanical properties strongly influence cell number, migration and differential hMSCs responses as a function of the matrix apparent stiffness scale. For example, hMSC early adhesion and increase in cell number are significantly greater on stiff hydrogels (~100KPa) than on soft (~2KPa) hydrogels. This demonstrates that hMSCs cells preferentially adhere to and grow on specific stiffness ranges. Also, it was found that substrate apparent stiffness influences ALP activity and osteocalcin expression on hMSCs. These data suggest that substrate stiffness is an important mediator of initial cell adhesion, increase in cell number, and differentiation of hMSCs. This cell response to substrate apparent stiffness might alter the sensitivity of cells to other biophysical signals. This query led to develop the hypothesis that a combination of biophysical signals and substrate apparent stiffness would result in variations on the apparent shear stress effects. However, it is possible that the culture of cells on substrates of known apparent stiffness alters the shear stress to which the cells are exposed rather than affecting the cell's sensitivity to shear stress. To address this, hMSCs were cultured under various conditions including apparent stiffness variations. To answer the hypothesis postulated above a modular parallel flow

chamber device was designed and fabricated which tries to address the drawbacks listed previously and on which the apparent stiffness of the culture matrix was altered thus cells were subjected to fluid flow-induced shear alongside substrate apparent stiffness.

Results

Bioreactor design development

A modular parallel flow bioreactor system was designed and developed to be used in this study. The final design and a previous prototype are both variation from a version used for 3D cell culturing, in which the media perfuses from bottom to top and passes through a 3D construct (Figure 7.1a, b). Several alternatives were tested in order to be able to use the device for 2D constructs (either for thick hydrogels or free floating-hydrogel films), some adjustments to the original design were made until a redesigned module that can hold 2D constructs was achieved, making use of most of the infrastructure for the 3D scaffolds design, the parallel flow module interchange with the perfusion module to allow both uses. The chamber layer, (Interior layer from previous design Figure 7.1c) was replaced by a bottom layer with a casting well in which hydrogel can be cast, or a free-floating hydrogel film could be placed (Figure 7.1f) and the inlets and outlets for each culture chamber are on the upper layer (Figure 7.1d).

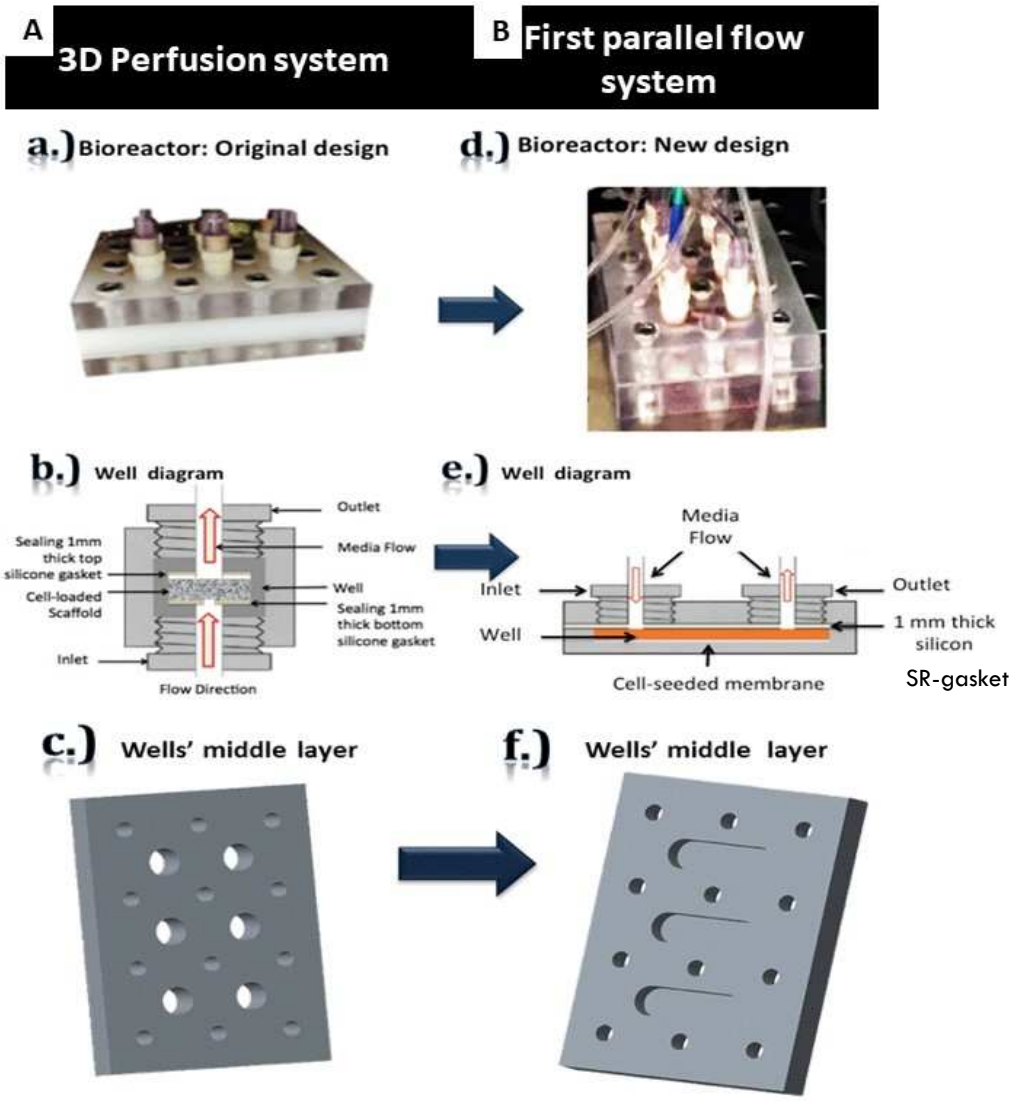

Figure 7. 1 Bioreactor A BEFORE and B AFTER diagram. a) Polycarbonate-UHMWPE bioreactor version b) Flow culture well diagram. the diagram illustrates the design of the flow chamber in the perfusion system. The previous design comprises 6 of these wells, permitting the culture of six samples at the same time with individual liquid flow for each one. The well with the scaffold is sealed in place by two silicone gaskets above and below the well layer. This five-part assembly (polycarbonate layer-silicone rubber (SR) gasket-UHMWPE layer-silicone membrane-polycarbonate layer) perfectly support 3D constructs culturing **c) UHMWPE wells layer d) Bioreactor new version for 2D dynamic cell culture e) Flow culture newest version well diagram.** The diagram illustrates the design of the flow chamber in the new perfusion system version. The design comprises 3 of these wells, permitting the culture of 3 samples at the same time with individual liquid flow for each one. The well layer is sealed in place with the upper layer by silicone gaskets and fasted by Plexiglas screws. This is 3-part assembly polycarbonate layer-silicone gasket- polycarbonate layer. **f) Polycarbonate wells layer** the main addition to previous design is this layer which looks to be at the same time a casting mould for 2D constructs in order to offer proper tension for cell viability and increases in cell number.

The first prototype comprised 2 modular blocks to allow the investigation of different cell linages or timepoints in the same run (Figure 7.2A). Each device comprised 2 exterior layers made from 12mm width polycarbonate sheet and a 1mm thick silicone rubber (SR) gasket to ensure no leaking. The device has 3 3cm^2 area, 5mm deep, 1.5cm^3 volume culturing chambers (Figure 7.1G), the upper exterior layer has an inlet and an outlet arranged in a rectangular format (Figure 7.2B, F). The design provided a uniform flow distribution over the hydrogel surface (Figure 7.2B). The whole closed loop comprised also 2 media reservoirs, one for each bioreactor block (Figure. 3.11a) a multi-channel peristaltic pump (Watson-Marlow 2500s, Figure. 3.11b) and interconnecting tubing (Figure. 3.11a) polymer ferrules, silicone tubes, tubing with lure endings, all biological inert materials which interconnect components exposed to the media in the system. For the study, culture media was pumped continuously through the chamber, at 0.093ml/min, for up to 7 days (Figure. 3.11). The entire system was kept in a 100% humidity atmosphere in a NuAire HEPA-filtered CO^2 incubator (Figure 3.11). Gaseous exchange is achieved as media returns to the reservoir, droplets of media drop through an air gap between the return line and the media in the reservoir (Figure. 3.11a). For both systems, culturing media was recirculating, and its quality validated after the experiment. The total media in the parallel flow system was 50ml. In order to sustain media condition in each system, media were replaced every 3 days. Samples were evaluated after seeding (0-day period cell seeded for 2 h), before going into dynamic culture (1-day period just before placement in the bioreactor) and after samples were separately taken out of the bioreactors at different timepoints, day 3, and 5, for cell viability, morphological change and increase in cell number.

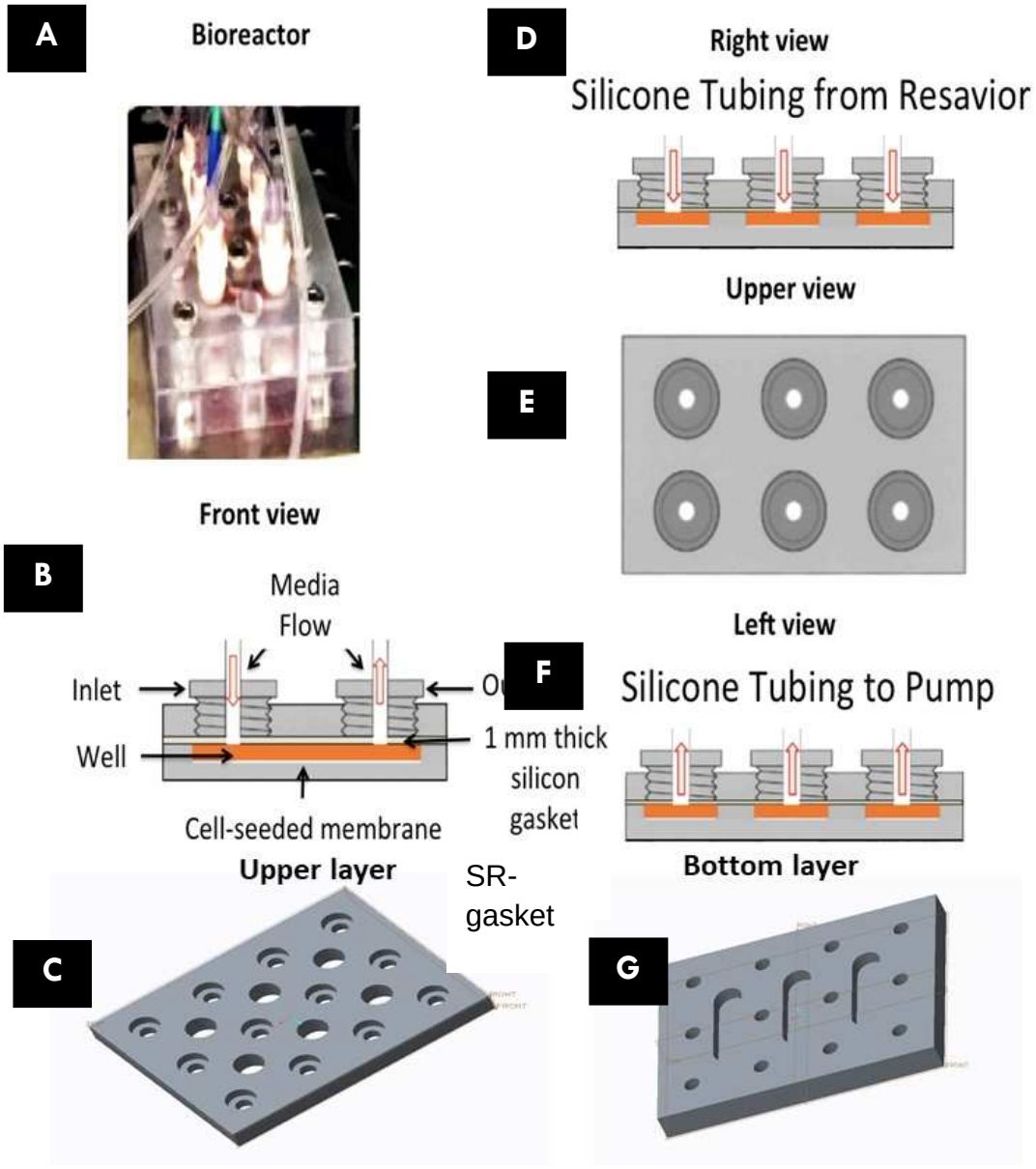

Figure 7. 2 Parallel flow chamber system prototype 1 block diagram. A Polycarbonate 2-layer bioreactor device B Flow culture well diagram. The diagram illustrates the design of the flow chamber in the parallel flow system. Each bioreactor has 3 of these wells, allowing the culture of 3 samples at the same time with individual liquid flow to each one. The well with the scaffold is sealed in place by a 1mm thick SR gasket. This 3-part assembly (polycarbonate layer-SR gasket, polycarbonate layer) is held in place by a Plexiglas screw. Silicone interconnecting tubing is fastening to each of these flow culture chambers coming from the media reservoir and going out to the peristaltic pump. **C Bioreactor upper external layer D Bioreactor side cross-sectional right diagram view. E Bioreactor upper view F left diagram view. G Bioreactor bottom external layer.**

Results presented on Figure 7.3 A-C shows the validation of parallel flow chamber redesign **prototype 1**. The system was assessed based on increases in cell number and cell morphology when possible. Cell metabolic activity of MG63 cells seeded on free floating ChG_PA hydrogel culture under dynamic conditions (Figure 7.3 A and C) showed a gradual decreased on cell number from day 3 to day 5 of culture period (Figure 7.3A), changes in morphology were also observed cells rounded up as time progressed (Figure 7.3 C). Cells seeded on thick hydrogels and subjected to shear-induced forces shoed very small increase in cell number and did not show significant cell number changes through time (Figure 7.3B).

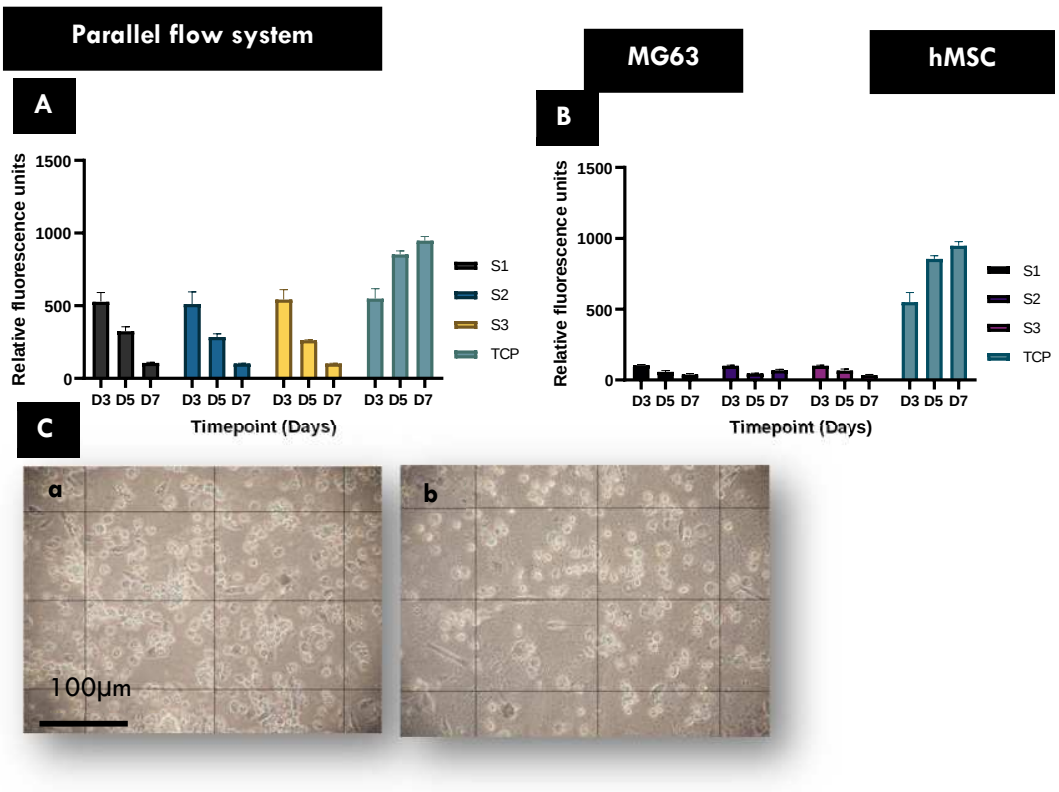

Figure 7. 3 Cell response to parallel flow prototype 1 A MG63 response to free floating ChG_PA hydrogel film **B** MG63 cell response to 5000µm thick ChG_PA hydrogels subjected to shear stress at a flow rate of 0.016ml/min and TCP was used as a control. Data is represented as mean ± SEM **C** micrographs of MG63 seeded on free floating ChG_PA hydrogels and cultured under dynamic flow conditions at **a** day 3 and **b** day 5 of culture. Cast samples were too thick to be analysed under light microscopy.

Parallel flow chamber bioreactor optimization.

It was observed that cells cultured on free floating hydrogels subjected to shear stress forces underwent what suggested and apoptotic response and cells on the 5.0mm thick ChG_PA hydrogel did not increase in cell number at all after the findings made in this project these result are explain by the high preferences that anchorage dependant cells show for tense constrain matrices (Figure 5.8, 9) and how they favour and increase in cell number on thin stiff hydrogels (Figure 5.12, 13,15,16) in the optimization phase of the parallel flow developmental process these and other previous findings were incorporated to generate a more robust design.

In order to address the drawbacks of prototype 1 an optimized alternative was designed; the goal for this device was to provide a suitable flexible culturing chamber for cell to attach and increase in cell number in 2D with the capacity of being subjected shear-induced forces. The culture chamber for this device should provide enough support and appropriate constrain to the hydrogels, also following on the light of previous findings it was suggested to incorporate step stiffness variations to the culturing chambers in order to investigate the combine effect between fluid flow-induced forces and matrix stiffness. The final design comprised 2 exterior layers made from 12mm width polycarbonate sheet and a culture block, comprised of 7 (GoodFellow – Silicone elastomer sheets 6x1mm, 1x0.6mm), SR gasket which work as a culturing chamber and as sealant for the whole system. The culture block has (Figure 7.4) 3, 3.0 cm^2 area, 0.6, 1.6 and 2.6mm thick ChG_PA hydrogels (Figure 7.4 F) and a 0.3cm^2 flow channel, culturing chambers (Figure 7.4E). Before achieving the final mentioned dimensions for the culturing chamber trials were performed to optimise them specially those for the flow channel cross-sectional area since high levels of pressure inside the chamber were observed initially, when the flow channel cross-sectional area was 0.1cm^2 against the

.19cm^2 of the feeding tubing leading to acceleration of flow inside the chamber and leakages at different points in the devise. The channel cross-sectional area was adjusted adding height to the channel using 1mm thick layers of SR gaskets (the setup of the device is described in Chapter 3 Figure 3.11).

Parallel flow culture construct chamber development

The development of the culturing chamber in this device relies on the findings made in this project knowing that the apparent stiffness experienced by the cells does not only depends on the materials Young's modulus but in the boundary conditions and dimensions of its culturing matrix, and that a more rigid material can be detected through a soft compliant hydrogel layer on top. A layer by layer approached that comprised these findings was designed to fabricate cell-seeding constructs of 3 different apparent stiffness per devise by varying the thickness of a ChG_PA hydrogel of known Young's modulus (0.11MPa). This approach used 4 SR membranes of different thickness (1x0.6mm, 3x1.0mm) (Figure 7.5A) with the perforations in the shape of the perimeter of the substrate (Figure 7.5A 2-4) the four layers are assembled one on top of the other in a fixed order (Figure 7.5A from 1 to 4) to create the 3D shape of each of the 3 final constructs (Figure 7.5B) with three different thickness (Figure 7.5C) to create a descending stairs-like casting mould for the ChG_PA hydrogel.

Parallel flow media flow channel development.

To allow media to pass through the culturing chamber a flow channel was designed, following the same concept used in previous section (Figure 7.5A). A layer-by-layer approach was used: 3 SR membranes of 1.0mm thick (Figure 7.6A) with a perforation in an oval-like shape (Figure 7.6A) were assembled together and placed on top of the culturing chamber module (Figure 7.6B) to create a channel which allow media to flow and bath uniformity the surface of each of the hydrogel substrates individually (Figure

7.6C). The complete assembly sequence from end to beginning can be seen on Figure 7.7. Increase in cell number studies were used to validate, cell density, flow channel dimensions and flow rate (data no shown).

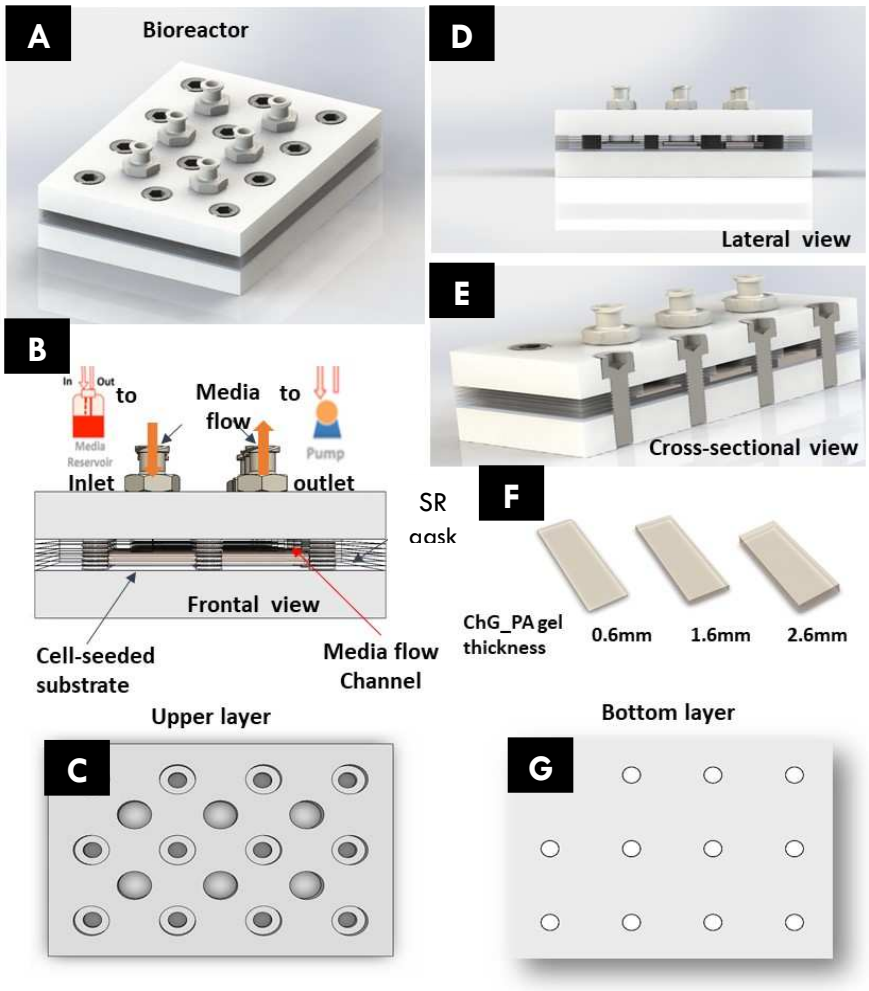

Figure 7. 4 Parallel flow chamber with cell-culture of varying apparent stiffness block diagram. A Polycarbonate 2-layer + culture chamber bioreactor device B Flow culture well diagram. The diagram illustrates the design of the flow chamber in the parallel flow system. 3 of these wells are contented in each bioreactor, allowing the culture of 3 samples at the same time this samples are cast at three different thicknesses on pre-cut SR mould of 0.6mm, 1.6mm and 2.6mm depth part of the culture chamber, this chamber is sealed in place by 3 1mm thick SR gasket with a pre-cut slot for media flow for individual liquid flow to each sample. This 3-part assembly (polycarbonate layer-SR culture clock, polycarbonate layer) is held in place by a Plexiglas screw. Silicone interconnecting tubing is fastening to each of these flow culture chambers coming from the media reservoir and going out to the peristaltic pump. **C Bioreactor upper external layer D Bioreactor side view render. E Bioreactor cross-sectional of the system inside. F Bioreactor ChG_PA hydrogel samples of different apparent stiffness. G Bioreactor bottom external layer.**

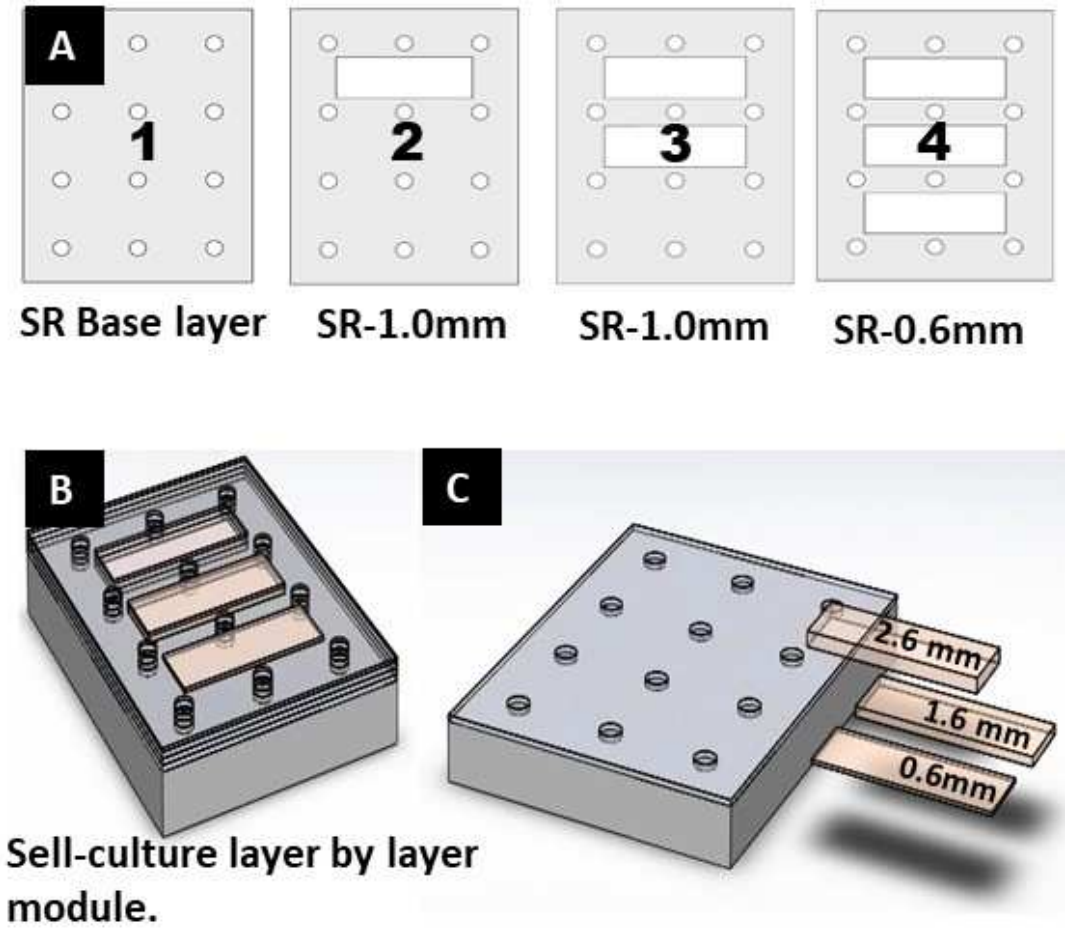

Figure 7. 5 Parallel flow chamber bioreactor cell-culture module diagram. A Cell-culture module the diagram illustrates the design of the cell-culture module of the parallel flow system. It comprises 4 SR layers assemble as follow. **From bottom to top, 1** a base 1.0mm layer that serves as a support and the stiff subtract cell will sense through the ChG_PA hydrogel, **2** a second 1.0mm thick SR layer with a perforation in the top end, **3** a third 1.0mm SR layer with 2 perforation one at the top and a second in the centre, **4** and a fourth 0.6mm thick SR layer with three perforations, top, centre and bottom. **B ChG_PA cast on the assembled module. D Bioreactor ChG_PA hydrogel samples of different thickness (0.6, 1.6,2.6mm).**

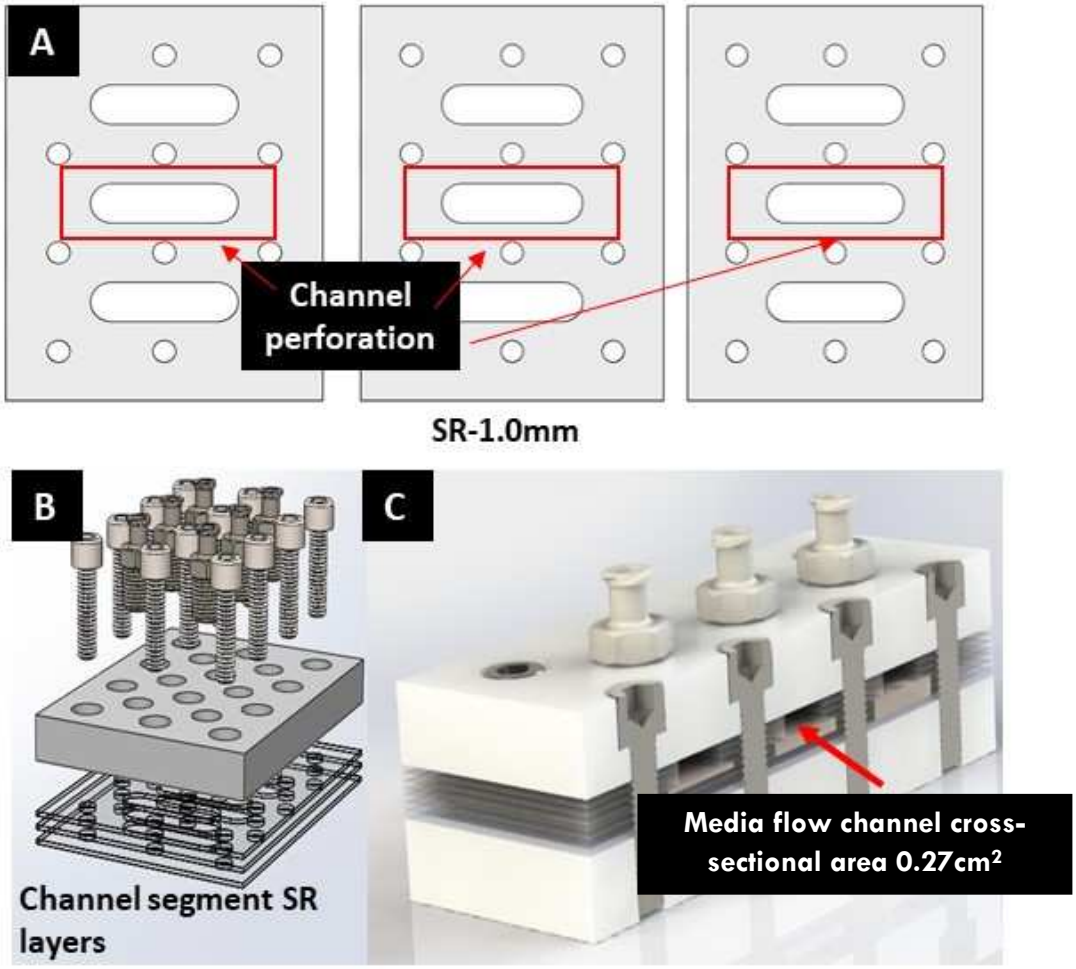

Figure 7. 6 Parallel flow chamber bioreactor media flow representation A Cell-culture channel parts the diagram illustrates the design of the device flow channel module. It comprises 3 equal 1.0mm SR layers with three perforation in an oval shape at the top centre and bottom of each membrane assemble and creating a channel for media to pass through on top of each culturing chamber. **B The flow channer module assembly. D Cross- sectional image of the assembled devise showing the three flow media channels of 0.27cm^2 cross-sectional area each.**

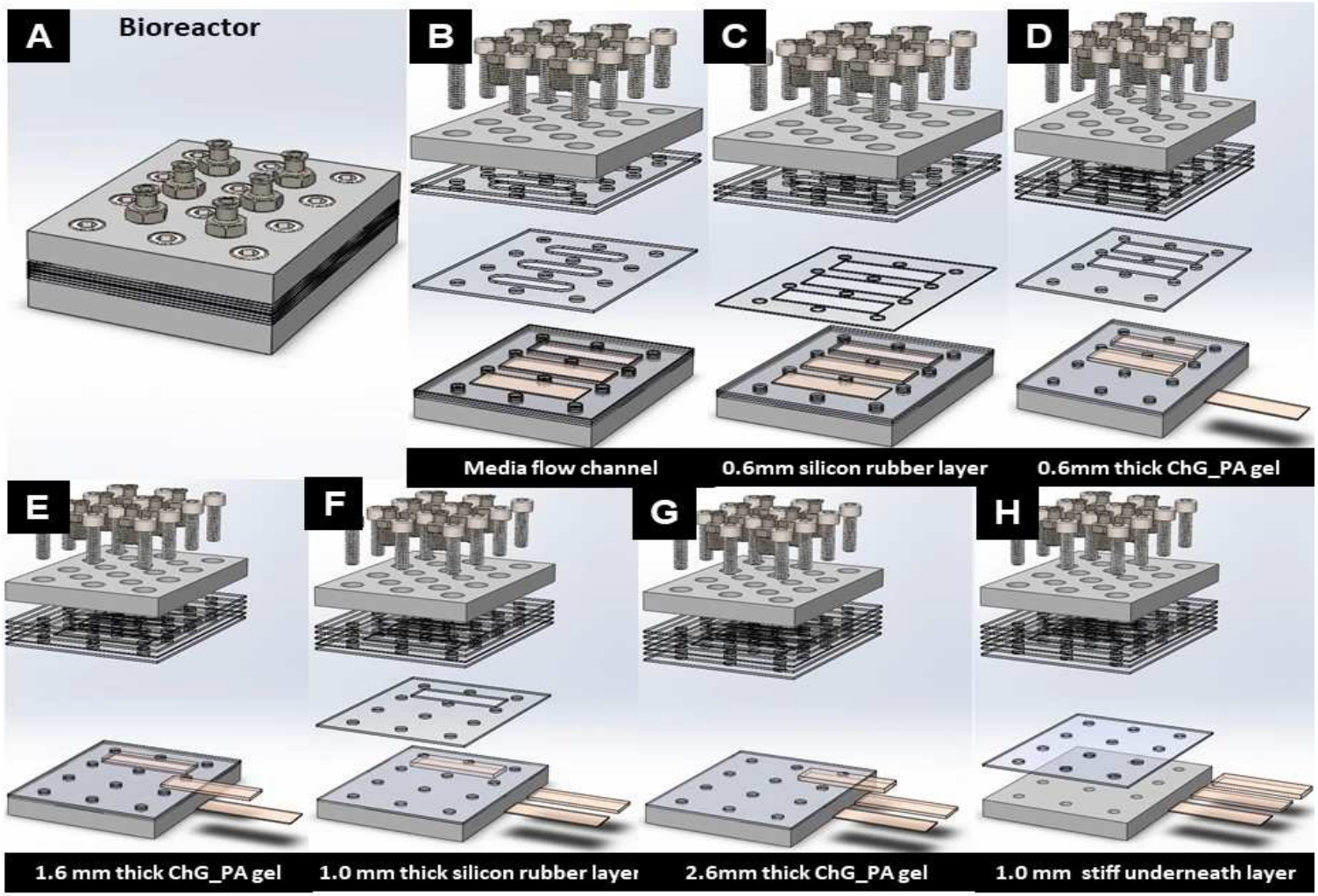

Figure 7. 7 Parallel flow chamber bioreactor assembling diagram from assembled to parts A Assembled culturing block. B 6 lure, 12 screws, the polycarbonate top layer and de flow channel up apart revelling the cell-culture module, **C** the 0.6mm SR layer coming out realising the 0.6mm thick ChG_PA hydrogel, **D** 1.0mm thick SR layer coming out **E** realising the 1.6mm thick ChG_PA hydrogel **F** the second 1.0mm thick SR layer coming apart **G** releasing the 2.6mm thick ChG_PA hydrogel **H** at this point all the substrates have been released and the base layer can be removed from the bottom polycarbonate layer.

Shear force inside the culturing chamber calculation

These experiments characterize the influence of dynamic forces on the response of anchorage dependent cells, especially the influence of shear stress. Following the development of the system the shear force exerting on cells by the flow of media, mathematical formulations were calculated. Media flow in the experiment was assumed to be laminar and the pressure gradient constant as the flow rate is relatively low. The cross-section of the cell culture well channel is illustrated below (Figure 7.8).

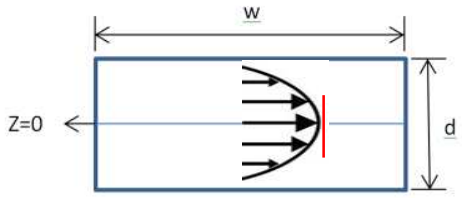

Figure 7. 8 cross-section illustration of the media flow channel

The area of the cross section:

$$A = width\ (w) \times depth\ (d)$$

Shear force between the plates (constant):

$$\tau = -\mu \frac{d^2v}{dz^2} \quad \text{Eq 7.1}$$

Mean velocity of media flow:

$$\bar{v} = \frac{q}{wd}$$

Taking integration of equation (7.1) to obtain the expression of velocity:

$$\frac{d^2v}{dz^2} = -\frac{\tau}{\mu}$$

$$\frac{dv}{dz} = \int -\frac{\tau}{\mu} dz = \frac{-\tau}{\mu} z + A$$

$$v = \int \left(\frac{\tau}{\mu} z + A\right) dz = \frac{-\tau}{2\mu} z^2 + Az + B \text{ Eq 7.2}$$

Defining z=0 as the centre of the channel (i.e., walls are at $\frac{\pm d}{2}$), from no slip condition at walls:

$$z = \pm \frac{d}{2} \; v = 0$$

Substituting the values into equation (7.2):

$$\frac{-\tau}{8\mu} d^2 + A\frac{d}{2} + B = 0$$

$$\frac{-\tau}{8\mu} d^2 - A\frac{d}{2} + B = 0$$

$A = 0$ and $B = \frac{\tau}{8\mu} d^2$

$$v = \frac{\tau}{8\mu}(d^2 - 4z^2) \text{ Eq 7.3}$$

From the flow rate, q:

$$q = vA = w \int_{-d/2}^{d/2} \frac{\tau}{8\mu}(d^2 - 4z^2)\, dz = \frac{w\tau}{8\mu}\left[d^2 z - \frac{4z^3}{3}\right]_{z=-d/2}^{z=d/2} = \frac{w\tau}{8\mu} \times \frac{2d^3}{3} = \frac{w\tau d^3}{12\mu}$$

$$\tau = \frac{12\mu q}{w d^3} \text{ Eq 7.4}$$

Therefore, the shear force acting on cells was:

$q = 0.016 ml/min$

$w = 10 mm$

$d = 3 mm$

$\mu = 1.002 \times 10^{-3} N\, s/m^2$

$$\tau = \frac{12 \times 1.002 \times 10^{-3} \times 0.00026 \times 10^{-3}}{0.01 \times 0.003^3}$$

$$\tau = 1.157\ dyne/cm^2$$

Mechanical properties: Construct apparent stiffness

After validating the hydrogel thickness following the thickness measuring method described in chapter 3 (pp 87), the constructs mechanical stiffness was calculated from the apparent stiffness curve obtain in chapter 5 (Figure 5.1) by interpolation. Figure 7.9 demonstrates a pronounced effect of the hydrogel thickness, with hydrogels showing significantly larger values of the elastic modulus for the thin hydrogel (0.6mm thick for ~213 KPa) and this will decrease as the samples get thicker (1.6mm ~44KPa) reaching the 1-digit scale in the KPa range for the thickest sample (2.6mm ~5KPa).

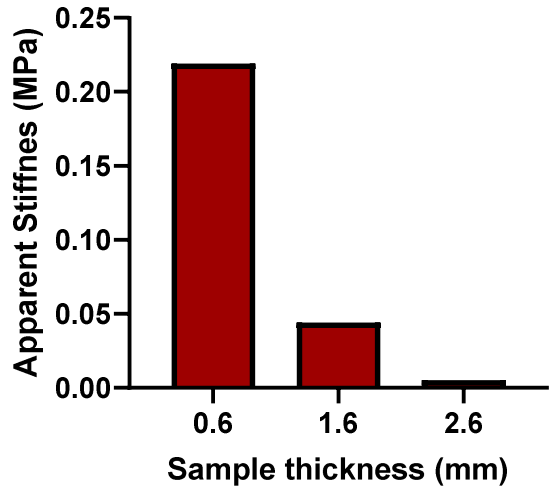

Figure 7. 9 Samples approximations of the ChG_PA bioreactor cell culturing hydrogels, apparent stiffness interpolated from results in chapter 5 (Figure 5.6).

Effects of shear stress on cell response

The preceding experiments (Chapters 5 and 6) showed that the hMSCs favour stiffer matrices to increase in cell number on static flow conditions. In this study, the combined influence of the matrix's apparent stiffness and shear stress will be investigated by assessing cell response to the mechanical properties of the hMSCs microenvironment *in vivo*.

Cell viability studies: Metabolic activity

hMSCs were cultured under dynamic conditions (under laminal flow stimuli) on ChG_PA hydrogels cast on SR of different thicknesses (0.6mm, 1.6mm, 2.6mm) for a period of 9 days and 14 days. Alamar blue tests were carried out on days 0, 9, 14 of their incubation to measure cell viability and to determine increase in cell number over time (please note that day 0 represent 3 days after seeding 2 hours before the dynamic stimuli begun). It can be observed (Figure 7.10) that cells at day 0 of their cultured period, showed an even distribution among the samples, for the 3 different thickness, showing no preference in location (start, centre and end, in the direction of the media flow). It can also be seen that cells significantly prefer the thinnest hydrogel compared to the thick and thickest samples which showed small increase in cell number in a thickness dependant manner. By day 9, a significant population redistribution could be observed among the start, centre, and end of all three samples of different thicknesses. At least 80% of all the metabolic activity of the sample was concentrated at the end of the sample, where the media flow exited the system. This distributional change showed to be more pronounced for thicker samples, although there was only three samples and therefore no statistical evidence could be provided to support this. No differences in the shape of the cell distribution were seen after a 14-day period and relative fluorescence were comparable to values from the previous timepoint for the stiffest substrate, although for the soft and thick substrates (1.6 and 2.6mm) the changes in cell number between timepoints showed to be

significant.

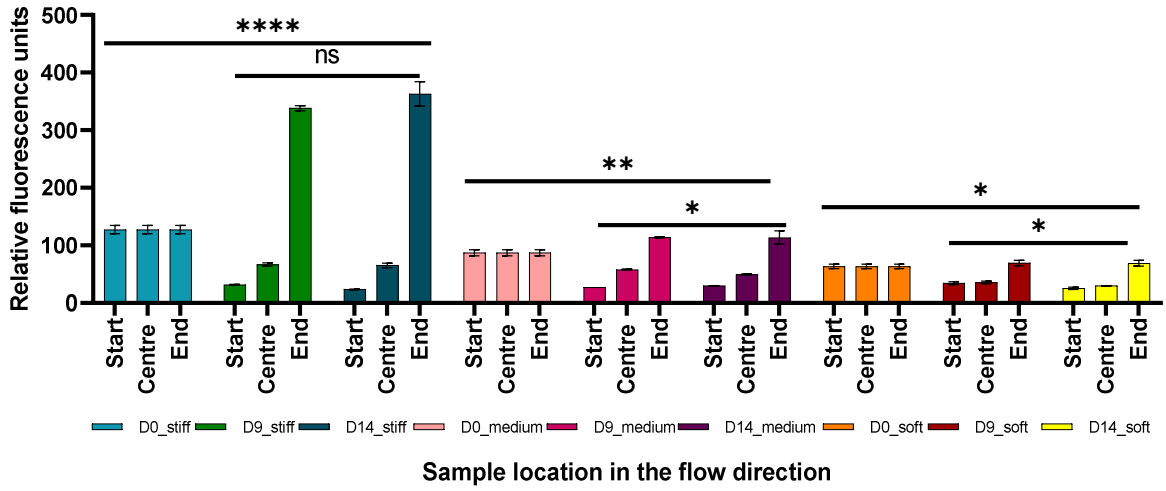

Figure 7. 10 Results of Alamar blue assay on hMSC's seeded on samples of different thickness (0.6~Stiff, 1.6 ~Medium and 2.6~Softmm thick) at three different timepoints 0, 9 and 14-day period (D0, D9 and D14 correspondingly) and from different location on the sample start, centre and end taking as a reference the direction of the media flow. The data were expressed as mean ± SEM

hMSC morphological changes

Single cell area

The preceding experiments in chapter 5 (Figure 5.17) showed that the morphology of hMSC changes as a response to the apparent stiffness due to changes on hydrogel thickness. Chapter 6 showed that the changes in shape can also be controlled by a stiffness gradient forcing the cell to elongate as a response of the changes in apparent stiffness experienced along the gradient profile. Therefore, it has been hypothesised that these cells will be able to sense changes in stiffness through soft hydrogels due to the firm attachment to an underling stiffer material SR and as response to the flow-induced shear force and rearrange their inner structure, therefore. To test this hypothesis hMSC cells were seeded on ChG_PA hydrogels of varying thickness (0.6,1.6, 2.6mm) and subjected to a shear stress flow of 1.157 dyne/cm^2 for a 9-day period.

The results (Figure 7.11) showed that cells changed shape as a function of the matrix apparent stiffness. There was a significant increase in cell spreading on stiff hydrogels (~213 KPa: 1055± 67μm$^{2)}$ compared to the softest (0.005 MPa: 573 ± 67μm^2). However, significant differences were not observed for the stiff substrate compared to the medium stiff one (44KPa: 897±50μm^2).

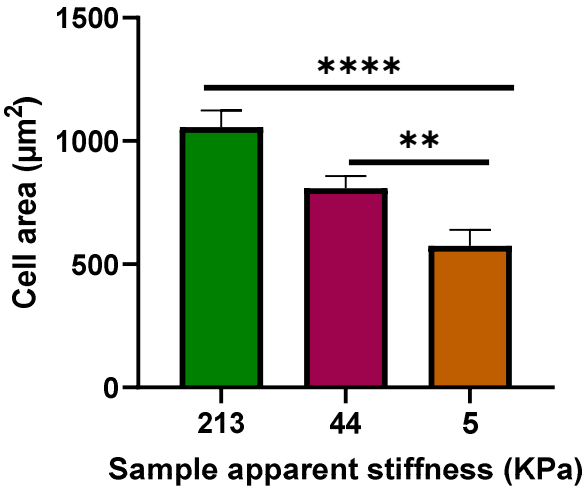

Figure 7. 11 hMSCs spreading area as a response to apparent stiffness and shear stress the data were expressed as mean ± SEM

Shape descriptors

As observed in Figure 7.12A, the shape mode for hMSCs under dynamic conditions (subjected to flow-induced shear) on ChG_PA, independent of its apparent stiffness, was a polarized elongated shape in the aspect ratio range of 3 to 15. No significant differences were observed between the stiff and the medium ChG_PA hydrogel whereas the soft hydrogel was shown to have a slightly smaller aspect ratio (compared to medium and stiff) and a wider variation. The circularity assessment (Figure 7.12B) followed the same trend with a mean for all the samples of around ~0.2. No significant differences were detected between the stiff and medium ChG_PA hydrogel, whereas the circularity of the cells plated on the soft hydrogel showed to be

significantly different, with a mean just above 0.2, but a wider variation and range compared to the other two samples.

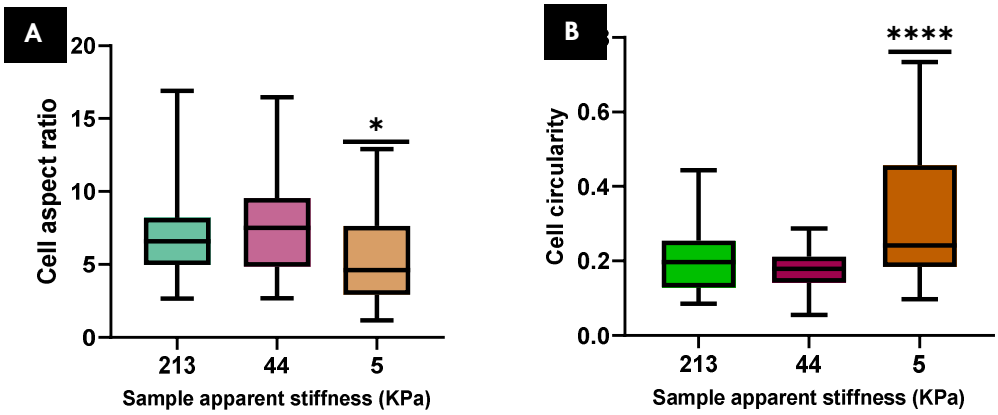

Figure 7. 12 hMSCs shape descriptors of cells seeded on substrates of different apparent stiffness subjected to flow-induced shear A cell aspect ratio **B** cell circularity. Data presented as a box ± whiskers plot (n = 10 single cells per field of view, 3 fields of view per sample).

Cell orientation θ

In Chapter 5 it was reported that the average orientation of hMSCs on uniform apparent stiffness hydrogels was random, with no detected preference for a specific orientation, thus it was found not to be a function of modulus (Figure 5.15). However, as can be seen in Figure 7.13, cells subjected to flow-induced shear and seeded on ChG_PA of uniform apparent stiffness, showed a strong preference to aligning themselves on the 0° direction, whereas significant differences between samples of different apparent stiffness were not found, leading to formulate the assumption that the strong cell alignment on the 0° direction corresponds to the cell response to the flow-induced shear (going in the same 0° direction).

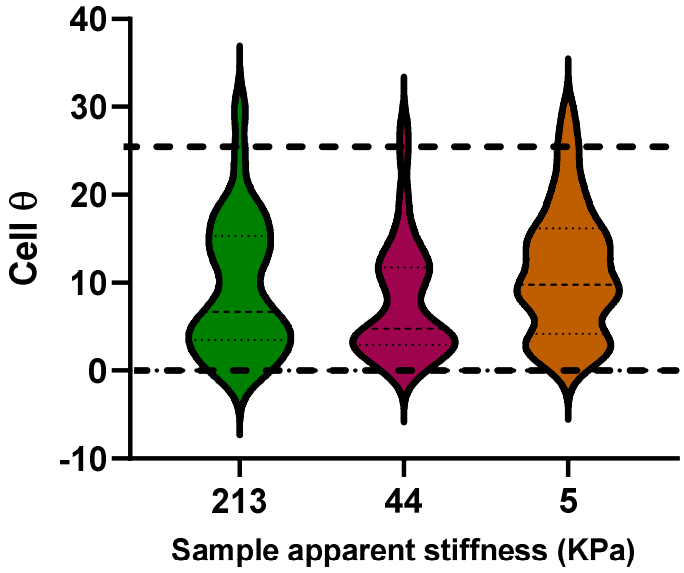

Figure 7. 13 hMSC cell orientation q across samples of different apparent stiffness subjected to flow-induced shear. The dashed lines point at the θ range (0-25°) where the data was found, cells showed a strong affinity for the direction of the flow. Data presented as a violin plot (n = 10 single cells per field of view, 3 fields of view per sample).

Cell spatial distribution

hMSCs were shown (Figure 7.14) to have a uniform even spatial distribution across every sample, no matter what thickness, three days after seeding just before going into dynamic culture (0-day period). This was corroborated by the cell viability studies which showed an even metabolic activity for these samples at 0-day period timepoint. After 9 and 14 days of culture, cell distribution (number of cells per region divided by total cells per sample) showed a significant spatial rearrangement compared to 0-day period. In this new distribution profile, many of the cells were found on the end of the sample (following the direction of the media flow); slight differences were observed between samples, related to the rate of change, which seemed to be steeper for the soft samples (Figure 7.14C) compared to the stiff ones (Figure 7.14B). Again, there was not sufficient samples to provide statistical evidence. A landscape of

the cell special distribution on the three different samples at 9-day period can be seen on Figure 7.15.

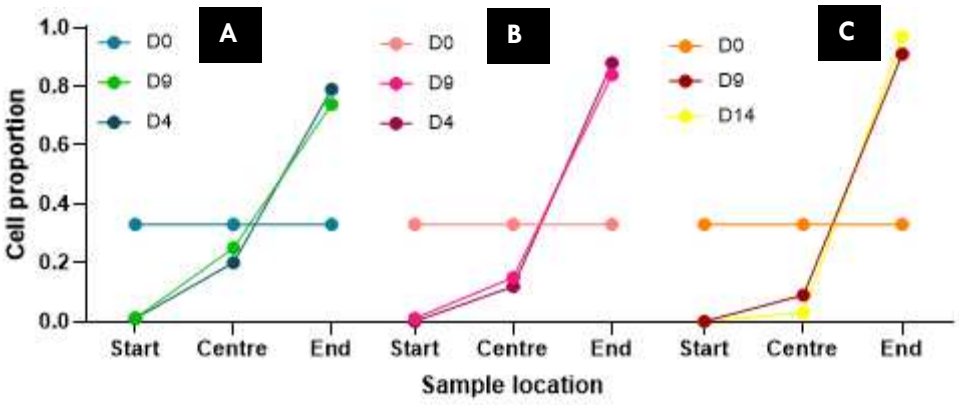

Figure 7. 14 Cell spatial distribution. Cell number proportion per location per sample hMSCs plated on **A** 0.6mm, ~213KPa ChG_PA hydrogel **B** 1.6mm, ~44KPa ChG_PA hydrogel **C** .6mm, ~2KPa ChG_PA hydrogel at different locations of the ChG_PA hydrogel samples (start**,** centre and end of the sample taking as a reference the direction of the flow) at 0,9 and 14-day period timepoints.

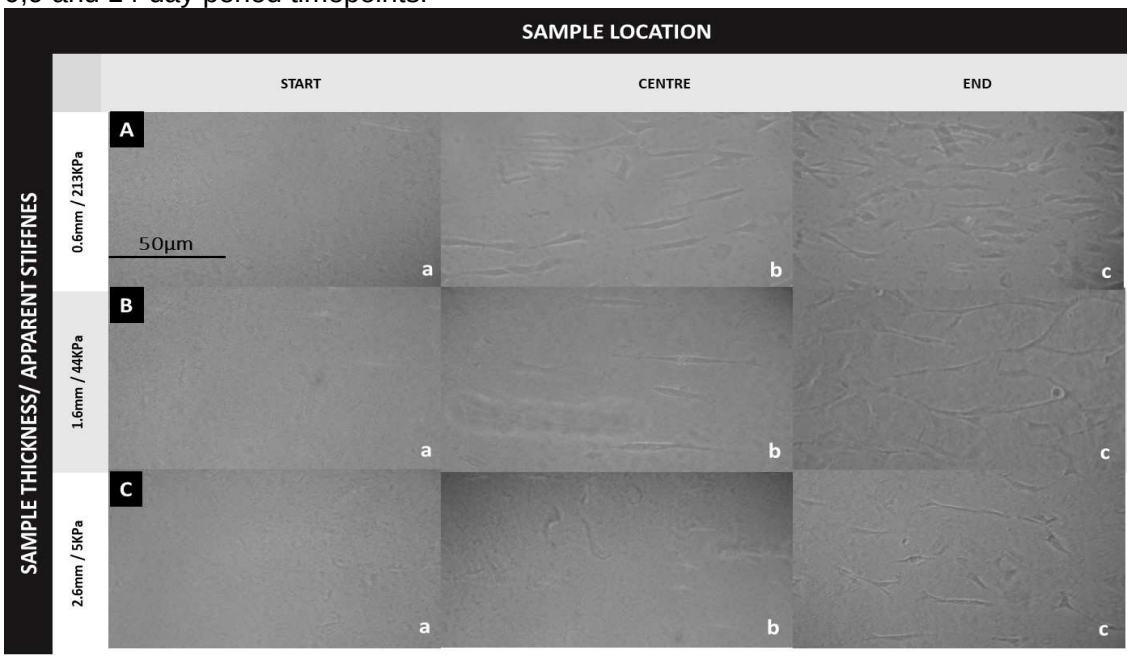

Figure 7. 15 Cell morphology observations and cell spatial distribution. Phase contrast images showing hMSCs at 9-day culture period on A 0.6mm, ~213KPa ChG hydrogel B 1.6mm, ~44KPa ChG_PA hydrogel C .6mm, ~2KPa ChG_PA hydrogel on a. start b. centre c. end of the sample taking as a reference the direction of the flow.

Discussion

The work presented in this chapter sought to provide initial insight and the early design of a tool to study the combined effect of mechanical properties of the ECM acting in parallel to the stimuli given by shear stress forces on cell response. Thus, the effect of apparent stiffness and flow-induced shear forces on cell response was characterised. Internal body fluid flow is an important regulator of the cell behaviour. The field of mechanobiology and its application to functional-tissue engineering is still in its early stages, therefore is providing opportunity for exploration. Many usages of fluid flow applications have been demonstrated, either by chemotransports or by the effect of shear stress; however, how this stimulus regulates stem function and fate is still not well understood. A parallel flow bioreactor for the culture in 2D of anchorage-dependent cells subjected to flow-induced shear was designed, and initial validation was carried on towards this chapter, resulting from the principles and learned lessons in previous stages of this project.

Prototype I proved not to be flexible enough to accommodate hydrogels of different constraint characteristics and thickness, making validation difficult of the combined effect of the hydrogel apparent stiffness plus flow-induced shear. MG63 cell number proved to be negatively affected by flow-induced added instability given to an already instable free floating ChG_PA matrix. hMSC cell distribution plated on ChG_PA hydrogels of different apparent stiffness and subjected to flow-induced shear showed to spatially rearrange in the direction of the flow. Furthermore, it was observed that Laminar flow induced shear arrest, stopping hMSCs cells from proliferating. Another observation of this study was that hMSCs showed signs of being directed in the direction of the flow-induced shear.

This study explores two related hypotheses: a) hMSCs respond to the mechanical stimulation given by flow-induced shear, and b) and that this effect can be altered by the rigidity of the matrix to which cells adhered. The results of this study present early observations can be further explored to fully prove the validity of these hypotheses and suggested that the response of cell-seeded constructs will be strongly affected by the cell culture conditions *in vitro*.

For the early trials with flow-induced stress an initial version of the current device was manufactured (for identification purposes, called in this study prototype 1). For these initial attempts, MG63 cells were seeded on both thin hydrogels free-floating on a culture chamber part of the culturing module of the device and on thick hydrogels (5.0mm) cast in the same chamber, which were the two options possible to test in this design. The results of these initial trials were consistent with what was observed in Chapter 5 (Figure 5.9): MG63 did not increase in cell number on free-floated unconstrained substrates (in agreement with the literature), which demonstrated that mechanical adhesion plays a critical role for cell survival, cell number and morphological control of anchorage-dependent cell lines. Decreasing ECM's adhesive properties will decrease its ability to resist cell-generated tensile forces, and this will reduce cytoskeletal tension and inhibit G1 progression, preventing S-phase entry and thus proliferation [362]. Grinnell et al. [331] showed that fibroblasts cultured in transferred matrices divide very little and undergo apoptosis. The observations indicate that release of mechanical load changes cell shape and activates an apoptotic response, and mechanical unloading effects are dependent on the degree of stress released from the matrix. Transferred free-floating matrix cells cultured under dynamic conditions showed pronounced apoptosis (Figure 7.3A, C) compared to what was observed on culturing in

static conditions (Figure 5.9). This may be attributed to shear stress, which provides further movement to the already unstable free-floating matrix, as well as shear-induced removal of poorly attached cells. The second attempt was to cast the hydrogel using the culturing chamber as a casting mould, resulting in thick 5.0mm hydrogels (Figure 7.3B). MG63 were seeded on those substrates and then subjected to flow-induced stress. The results showed poor cell response; cells showed very low viability at 3-day culture period just before being brought under dynamic conditions, and low to nil proliferation after being subjected to the dynamic flow-induced stress. These results agree with the findings presented in Chapter 5 (Figure 5.10), which showed that MG63 does not proliferate or respond when plated on ChG_PA of thickness over the 3.0mm thick. In addition, soft substrates offer poor conditions for cells to spread and adhere – also shown for the results of this project (Figure 5.19) – making the cells more susceptible to shear-induced removal of poorly attached cells. The findings of these early attempts led to a full redesign of the culturing parallel flow system; the new designs integrated some of the findings obtained in previous experiments, sought to provide high flexibility to assist in the elucidation of unknown or not yet well-characterised mechanobiology pathways. This approach, different to the traditional 2D microfluid systems on plastic/glass cell culture matrices, uses ChG_PA hydrogels as a culturing substrate, providing a more physiological-like environment. It is made by SR layers of different thickness piled on top of each other, which creates a system in which hydrogels of different thicknesses are cast directly on the device. The cell culture module of the device allowed the substrate to be fully always constrained by the equipment, reducing the variation provided by the instability of unconstrained matrices. This is in agreement with literature that has found that boundary conditions of the substrate strongly altered how the cells experience the mechanical properties of their microenvironment [363], and

addressing the instability offered by the free-floating hydrogel constructs from prototype 1 (Figure 7.3A,C). This system allows the production of ChG_PA hydrogel samples of different thicknesses, in the range of what was observed to be responsive for hMSCs (0.6mm, 1.6mm and 2.6mm) allowing the study of the combined effect resulting from the parallel stimulation provided by the mechanical properties of the matrix and the flow-induced shear (Figure 7.5 and 7.7). Looking to provide physiological shear stress condition to hMSCs (proved by Kashial et al. to be between 1 and 25 dynes/cm^2 for this cell line [364]), Eq. 7.3 was used to calculate the cross-sectional area of the flow-media channel to attain the minimal physiological shear stress (1 dyn/cm^2). Layers of SR were added to meet this requirement. From this point, all other variations in shear stress can be achieved controlling the media flow mechanically with the peristaltic pump (Watson-Marlow 2500s) used in this study.

Following with the validation of the new design, hMSCs seeded on each of the three different ChG_PA hydrogel samples showed to be viable and evenly distributed across the entire construct (Figure 7.10, 7.14) 0-day period timepoint, not making any distinction for any specific region on the ChG_PA different hydrogels. hMSC cell viability showed to be significantly higher on stiff hydrogels (0.6mm thick) in compliance with other findings of this project (Figure 5.15A) which demonstrated that cells could sense a stiffer material, in this case SR, through a firmly adhered soft hydrogel. The degree at which cells can sense will by a function of the thickness of the compliant hydrogel. Khatiwa and Engler et al. [64, 334] respectively have demonstrated that the extracellular matrix stiffness within the expected KPa range can influence the cell morphology, proliferation, and differentiation of cells. Once cells were subjected to mechanical stimuli in the form of flow-induced shear, the spatial distribution of the cell

metabolic activity was observed to be strongly affected. The cells metabolic activity showed a spatial redistribution showing a high concentration of metabolic activity at the end of each ChG_PA hydrogels in the direction of the flow, and this trend showed to be stronger on thicker hydrogels. This response is in good agreement with the cell distribution results of this study, which showed that cells strongly align themselves in the 0^{o} direction (Figure 7.13) corresponding to the direction of the fluid-flow (0°). This effect was shown not to be dependent on substrate apparent stiffness, leading to the conclusion that cell alignment orientation is function of the flow-induced shear direction. These results are also aligned to the results observed for the spatial redistribution analysis of the hMSC number, which showed the concentration of cell per analyse region (start, middle and end in the direction of the flow) to be redistributed in the direction of the flow (Figure 7.14 and 7.15). The same trend was observed in this analysis: the change rate in cell concentration was stronger for soft substrates (Figure 7.14), however data analysis did not show the differences between soft and stiff hydrogels to be significant. In this regard a larger sample size will be needed to detect a significant difference. These results are in agreement with previous research, which has proved that MSCs under shear reorganise themselves in the direction of fluid-flow [176, 365], and that attachment of hMSCs on softer substrates showed to be not as strong as on stiff matrices [29], making cells plated on soft substrates under flow-induced shear more susceptible to the effect of shear stress. This effect is comparable to the findings of Saxena et al. [26], who reported that on chemotactic gradients, a faster chemotaxis of MSCs plated on soft substrates compared to those plated on stiff ones was observed, therefore a soft matrix may amplify the effect of these forces on cell behaviour. Overall proliferation independently of the substrate apparent stiffness showed not to change through time. This phenomenon is in agreement with what has been reported previously,

that steady 2D laminar flow inducing shear stress in the relevant physiological scale provokes MSCs cell cycle arrest and inhibits apoptosis [130]. This phenomenon has proved to be useful to decouple the effect of shear stress from proliferation, as reported by Kreke et al. [366], who showed the phenomenon serves to preserve the stem cell progenitor pool after proliferation and migration. Therefore, it may be useful to elucidate mechanotransduction pathways without the confusing effects of cell growth. Another finding was the observed change on hMSCs morphology, which changed (Figure 7.15) compared to cells culture under static conditions (Figure 5.12, 5.13 and 5.17) as response to shear stress. Cells were elongated (Figure 7.13) and oriented in the direction of flow (Figure 7.15) after exposure to shear stress for nine days. hMSC spread area showed the same trend observed in previous studies of cells cultured on hydrogels of uniform apparent stiffness, large on stiff substrate and small on soft substrates. However, differently to the results reported on these studies (Figure 5.17), the cell spread area on the flow-induced shear experiments showed to be significantly smaller compared to cells cultured under static conditions (Figure 7.11 vs 5.17). These results may suggest a strong effect of flow-induced shear on cell shape. This is in agreement with Gao et al., who by using low flow-induced shear (10^{-5} dynes/cm^2 to 10^{-2} dynes/cm^2) showed that hMSC spread area under very low shear stress (10^{-5} dynes/cm$^{2)}$ presented a spread-flattened area compared to those under low shear stress (10^{-2} dynes/cm^2) which area was smaller and shape was more elongated. This proved a relationship between flow-induced shear and cell shape [367]. Dong et al. proved hMSC MSCs changed their morphology in response to shear stress and elongated shape, and to be aligned in the direction of flow after been subjected to shear stress for four days [368]. It was observed that the aspect ratio of the cells

increased, with a decrease on sample stiffness, suggesting that this effect is also magnified with a soft underling matrix that does not offer the best conditions for hMSC adherence.

Project limitations and remarks for future research

Important ground findings were investigated in the study presented in this chapter; however, it did face several challenges and there are limitations that can be addressed in future studies.

The initial design, called prototype I, accommodated 6 samples of a single thickness in two blocks, therefore comparison between thicknesses (apparent stiffness) was not possible, which was a matter of key interest for the overall objective of this thesis, to overcome this challenge, a chamber that accommodated samples of different thickness was developed and replaced the previous one. A limitation attached to it was that the chamber designed in this study offers only 1 sample per apparent stiffness per device with 2 devices available. Therefore, the results presented in this thesis are prelaminar since they lack statistical robustness and should be considered a guideline for future work only. A suggestion for future work would be to reduce sample surface area to accommodate a higher number of samples per block as to duplicate the number of blocks and run simultaneously, in order to generate multiple identical samples per combination for comparison in order to give the system the statistical robustness is lacking.

Another important limitation is that the current study only investigated the behaviour of two cell lines (MG63 and hMSC). Moreover, most of the results focused on a single transformed cell line (hMSC). Therefore, future studies will test if the results identified here are valid for many other cell types or only for the cell type used in this study.

Other studies showed that cells such as NIH3T3 cells [369], human epithelium cells [370], and primarily isolated keratinocytes [319] respond to the stiffness of their substrate, but not in the context of varying substrate thickness in the other hand cells such as vascular endothelial cells [177] and adipocytes like such as 3T3-L1[371, 372] have proved to respond to both stiffness of their substrate and fluid flow induced shear stress however not, at least to the knowledge of the author, simultaneously. It would be valuable to study and compare how epithelial cells such as vascular smooth tissue, skin keratinocytes or guts epithelium respond to material thickness and the mechanical stimulation provided by fluid flow and compared to the cell lines used in this experiment.

Other limitation was that the apparent stiffness of the hydrogels used in the experiments presented in these chapter where calculated using as a reference the results observed in pervious chapters, however the rigid supports beneath these soft hydrogels was of a different material therefore also merit individual investigation, for further research, the complete apparent stiffness profile of these hydrogels should be measured and analysed. Similarly to what was done in this research project, Kuo et al. [84] used bead soft hydrogels but also gradient stepped hydrogels to show both the effect of thickness on single cell spreading and migration toward the stiffer regions. It would be interesting to study how hMSCs or other stem cell types, respond to the effect of changes in substrate apparent stiffness due to the variations in thickness (gradient), combined to the effect of shear induced stress due to the fluid-flow provided by the system.

Furthermore fluid-flow-induced shear stress can be used to control stem cell osteogenesis by activating mechanosensitive differentiation pathways as reported previously, fluid-flow induces stem cell osteogenesis exposed by an increase in alkaline phosphatase

(ALP) activity, gene expression of markers of osteoblastic differentiation, mineralized matrix deposition, and release of growth factors [116, 373]. Another study showed that subjecting MSCs to fluid flow-induce forces *in vitro* encouraged the expression of (BMP)-2 a bone morphogenetic protein a crucial growth factor that assists in the bone remodelling process *in vivo* [374]. This mechanosensitive osteogenesis response observed on stem cell has been found to be significantly sensitive to the components of fluid-flow such as shear stress scale as well as profile whether flow is steady, oscillatory, or intermittent, and frequency [116, 123, 375]. Particularly important is the role of flow rate for mechanotransduction studies, which increased the expression of β1 integrin, a key focal adhesion protein, which likely modified cell sensing of dynamic flow shear [376]. It would be valuable, using the technology developed in this chapter, to carry up studies that focus on the differentiation potential of hMSCs once exposed to the effect of apparent matrix stiffness and shear stress simultaneously.

Conclusion

It can be concluded that the developed parallel flow culturing system design supports cell culture and can serve as a start point for more extensive studies, having the ability to reproduce results under the same culturing conditions, and for this reason it can safely be used in further research. It has been demonstrated that flow-induced culture may favour cells viability on ChG_PA hydrogels of different apparent stiffness under shear stress conditions. This system allowed cells to be subjected simultaneously or individually to both dynamic and static mechanical stimuli and investigated the various behaviours of hMSCs in response to flow-induced shear conditions. It was demonstrated that cell reorganised themselves in the direction of the flow and suggested that the device can be a useful and reliable tool in the elucidation of hMSCs mechanotrasduction pathways that are still poorly understood. The layer by layer cell culture module of this device

facilitates the production of multiple samples at different dimensions (by simply adding or taking away, or changing the thickness of SR layers) and the flexibility to vary the flow-induced shear level – by changing the flow channel dimension (which cross-sectional area can be modified by changing the mount or thickness of SR) and peristaltic pump flow rate – provides an attractive platform for mimicking a physiologically relevant mechanical environment for hMSC *in vitro,* and allows for the study of mechanobiology in other types of cells as well.

Appendix

Glossary

AA/AM	Antibiotics-antimycotics
AS	Apparent Stiffness
AT	Alkaline treatment with NaOH
Ch	Chitosan
ChG	Chitosan-gelatin hydrogel
ChG_PA	Chitosan-gelatin hydrogel cross-linked with Proanthocyanidins
CSK	Cytoskeleton
Col I	Type I collagen
Col II	Type II collagen
COPS 5	Sensor protein involved in the activation of copper resistance gene
DMEM	Dulbecco's modified minimum essential medium
ECM	Extracellular matrix
FA	Focal adhesion
FAK	Focal adhesion kinase
G	Gelatin
GAG	Glycosaminoglycan
GA	Glutaraldehyde
SG	Stiffness Gradient
GT	Gradient threshold
sGAG	Sulphated glycosaminoglycan
HEPES	A zwitterionic organic chemical buffering agent
hMSC	Human mesenchymal stem cell
HyA	Hyaluronic acid
IC	Intra cellular
IMS	Industrial methylated spirit
MG63	Osteoblast-like

MHC	Major histocompatibility complex
MSC	Mesenchymal stem cell
mRNA	messenger ribonucleic acid
Myc	A regulator gene that codes for a transcription factor; it plays a role in cell cycle progression, apoptosis, and cellular transformation
NEAA	Nonessential amino acids
NIH 3T3	Cell CultureSwiss fibroblasts
NPM1	Nucleophosmin Protein
PA	Proanthocyanidin
PAAm	Polyacrylamide
PBS	Phosphate buffered saline suspension
PDMS	Polydimethylsiloxane
PEG	Poly(ethylene glycol)
PEGDA	Poly(ethylene glycol) diacrylate
PEGDE	Poly(ethylene glycol) diglycidyl ether
PVA	Poly(vinyl alcohol)
RGD	Arginylglycylaspartic acid
SCs	Stem cells
SDW	Sterile distilled water
SM	Smooth muscle
SMC	Smooth muscle cell
SR	Silicone rubber
TAZ	Transcriptional regulator
TCP	Tissue Culture Plastic
TCWP	Tissue Culture Well Plates
TDSC	Tendon-Derived Stem Cells
UV	Ultraviolet light
VSMCs	Vascular Smooth Muscle Cells
YAP	Transcriptional regulator

List of Tables

List of Figures

References

1. Discher, D.E., P. Janmey, and Y.L. Wang, *Tissue cells feel and respond to the stiffness of their substrate.* Science, 2005. **310**(5751): p. 1139-1143.
2. Engler, A.J., et al., *Surface probe measurements of the elasticity of sectioned tissue, thin gels and polyelectrolyte multilayer films: Correlations between substrate stiffness and cell adhesion.* Surface Science, 2004. **570**(1-2): p. 142-154.
3. Zajac, A.L. and D.E. Discher, *Cell differentiation through tissue elasticity-coupled, myosin-driven remodeling.* Current Opinion in Cell Biology, 2008. **20**(6): p. 609-615.
4. Ruoslahti, E. and B. Öbrink, *Common Principles in Cell Adhesion.* Experimental Cell Research, 1996. **227**(1): p. 1-11.
5. Vogel, V. and M. Sheetz, *Local force and geometry sensing regulate cell functions.* Nat Rev Mol Cell Biol, 2006. **7**(4): p. 265-75.
6. Beningo, K.A., C.M. Lo, and Y.L. Wang, *Flexible polyacrylamide substrata for the analysis of mechanical interactions at cell-substratum adhesions*, in *Methods in Cell Biology*. 2002. p. 325-339.
7. Pelham, R.J. and Y.-l. Wang, *Cell locomotion and focal adhesions are regulated by substrate flexibility.* Proceedings of the National Academy of Sciences, 1997. **94**(25): p. 13661.
8. du Roure, O., et al., *Force mapping in epithelial cell migration.* Proceedings of the National Academy of Sciences of the United States of America, 2005. **102**(7): p. 2390.
9. Ingber, D.E., *Cellular mechanotransduction: putting all the pieces together again.* FASEB J, 2006. **20**(7): p. 811-27.
10. Trappmann, B., et al., *Extracellular-matrix tethering regulates stem-cell fate.* Nat Mater, 2012. **11**(7): p. 642-9.
11. Wang, Y., et al., *Substrate stiffness regulates the proliferation, migration, and differentiation of epidermal cells.* Burns, 2012. **38**(3): p. 414-420.
12. Pham, J.T., et al., *Guiding cell migration with microscale stiffness patterns and undulated surfaces.* Acta Biomaterialia, 2016. **38**: p. 106-115.
13. Buxboim, A., et al., *How deeply cells feel: methods for thin gels.* J Phys Condens Matter, 2010. **22**(19): p. 194116.
14. Sottile, V., A. Thomson, and J. McWhir, *In Vitro Osteogenic Differentiation of Human ES Cells.* Cloning and Stem Cells, 2003. **5**(2): p. 149-155.
15. Altman, G., et al., *Cell differentiation by mechanical stress.* The FASEB Journal, 2001. **16**(2): p. 270-272.
16. Tibbitt, M.W. and K.S. Anseth, *Hydrogels as extracellular matrix mimics for 3D cell culture.* Biotechnol Bioeng, 2009. **103**(4): p. 655-63.
17. Sen, S., A.J. Engler, and D.E. Discher, *Matrix Strains Induced by Cells: Computing How Far Cells Can Feel.* Cellular and Molecular Bioengineering, 2009. **2**(1): p. 39-48.
18. Maloney, J.M., et al., *Influence of finite thickness and stiffness on cellular adhesion-induced deformation of compliant substrata.* Physical Review E, 2008. **78**(4): p. 041923.
19. Unnikandam Veettil, S.R., et al., *Tuning surface functionalization and collagen gel thickness to regulate cancer cell migration.* Colloids and Surfaces B: Biointerfaces, 2019. **179**: p. 37-47.
20. Fletcher, D.A. and R.D. Mullins, *Cell mechanics and the cytoskeleton.* Nature, 2010. **463**(7280): p. 485-492.
21. Schwarz, U.S. and M.L. Gardel, *United we stand – integrating the actin cytoskeleton and cell–matrix adhesions in cellular mechanotransduction.* Journal of Cell Science, 2012. **125**(13): p. 3051.
22. Tusan, C.G., et al., *Collective Cell Behavior in Mechanosensing of Substrate Thickness.* Biophysical Journal, 2018. **114**(11): p. 2743-2755.
23. DuChez, B.J., et al., *Durotaxis by Human Cancer Cells.* Biophysical Journal, 2019. **116**(4): p. 670-683.
24. Haugh, M.G., et al., *Crosslinking and Mechanical Properties Significantly Influence Cell Attachment, Proliferation, and Migration Within Collagen Glycosaminoglycan Scaffolds.* Tissue Engineering Part A, 2010. **17**(9-10): p. 1201-1208.
25. Wang, H.-B., M. Dembo, and Y.-L. Wang, *Substrate flexibility regulates growth and apoptosis of normal but not transformed cells.* American Journal of Physiology-Cell Physiology, 2000. **279**(5): p. C1345-C1350.
26. Saxena, N., et al., *Matrix elasticity regulates mesenchymal stem cell chemotaxis.* Journal of Cell Science, 2018. **131**(7): p. jcs211391.
27. Lin, C., et al., *Matrix promote mesenchymal stromal cell migration with improved deformation via nuclear stiffness decrease.* Biomaterials, 2019. **217**: p. 119300.
28. Ehrbar, M., et al., *Elucidating the Role of Matrix Stiffness in 3D Cell Migration and Remodeling.* Biophysical Journal, 2011. **100**(2): p. 284-293.
29. Sun, M., et al., *Effects of Matrix Stiffness on the Morphology, Adhesion, Proliferation and Osteogenic Differentiation of Mesenchymal Stem Cells.* International journal of medical sciences, 2018. **15**(3): p. 257-268.
30. Feng, C.-h., Y.-c. Cheng, and P.-h.G. Chao, *The influence and interactions of substrate thickness, organization and dimensionality on cell morphology and migration.* Acta Biomaterialia, 2013. **9**(3): p. 5502-5510.

31. Moshayedi, P., et al., *Mechanosensitivity of astrocytes on optimized polyacrylamide gels analyzed by quantitative morphometry.* Journal of Physics: Condensed Matter, 2010. **22**(19): p. 194114.
32. Yeung, T., et al., *Effects of substrate stiffness on cell morphology, cytoskeletal structure, and adhesion.* Cell Motil Cytoskeleton, 2005. **60**(1): p. 24-34.
33. Pandamooz, S., et al., *Substrate stiffness affects the morphology and gene expression of epidermal neural crest stem cells in a short term culture.* Biotechnology and Bioengineering, 2019. **0**(ja).
34. Tse, J.R. and A.J. Engler, *Stiffness gradients mimicking in vivo tissue variation regulate mesenchymal stem cell fate.* PLoS One, 2011. **6**(1): p. e15978.
35. Swift, J., et al., *Nuclear Lamin-A Scales with Tissue Stiffness and Enhances Matrix-Directed Differentiation.* Science, 2013. **341**(6149): p. 1240104.
36. Buxboim, A., et al., *Matrix Elasticity Regulates Lamin-A,C Phosphorylation and Turnover with Feedback to Actomyosin.* Current Biology, 2014. **24**(16): p. 1909-1917.
37. Evans, N.D. and E. Gentleman, *The role of material structure and mechanical properties in cell–matrix interactions.* Journal of Materials Chemistry B, 2014. **2**(17): p. 2345-2356.
38. Handorf, A.M., et al., *Tissue stiffness dictates development, homeostasis, and disease progression.* Organogenesis, 2015. **11**(1): p. 1-15.
39. Wang, N., J.P. Butler, and D.E. Ingber, *Mechanotransduction across the cell surface and through the cytoskeleton.* Science, 1993. **260**(5111): p. 1124-1127.
40. Jaalouk, D.E. and J. Lammerding, *Mechanotransduction gone awry.* Nature Reviews Molecular Cell Biology, 2009. **10**(1): p. 63-73.
41. Guilak, F., et al., *Control of stem cell fate by physical interactions with the extracellular matrix.* Cell Stem Cell, 2009. **5**(1): p. 17-26.
42. Rosenfeld, D. and S. Levenberg, *Effect of Matrix Mechanical Forces and Geometry on Stem Cell Behavior*, in *Biology and Engineering of Stem Cell Niches*. 2017. p. 233-243.
43. Mohammadi, H. and C.A. McCulloch, *Impact of elastic and inelastic substrate behaviors on mechanosensation.* Soft Matter, 2014. **10**(3): p. 408-420.
44. Cox, T.R. and J.T. Erler, *Remodeling and homeostasis of the extracellular matrix: implications for fibrotic diseases and cancer.* Disease models & mechanisms, 2011. **4**(2): p. 165-178.
45. Barriga, E.H., et al., *Tissue stiffening coordinates morphogenesis by triggering collective cell migration in vivo.* Nature, 2018. **554**(7693): p. 523-527.
46. Al-Mayah, A., & Nafo, W. , *Mechanical Investigations of Biological Tissues Using Tensile Loading and Indentation.* , in *Biomechanics of Soft Tissues* 2018, CRC Press. p. (pp. 27–54). .
47. Rice, A. and A. del Rio Hernandez, *Chapter 4.2 - Biomechanics of cancer cells*, in *Bioengineering Innovative Solutions for Cancer*, S. Ladame and J.Y.H. Chang, Editors. 2020, Academic Press. p. 327-361.
48. Welch R., S.T., Pioquinto R, Leonard T,, *Transfection of Constitutively Active Mitogen-activated Protein/Extracellular Signal-regulated Kinase Kinase Confers Tumorigenic and Metastatic Potentials to NIH3T3 Cells, .* Cancer Res March, 2000. **15**(60).
49. Lin, C.Q. and M.J. Bissell, *Multi-faceted regulation of cell differentiation by extracellular matrix.* The FASEB Journal, 1993. **7**(9): p. 737-743.
50. Streuli, C., *Extracellular matrix remodelling and cellular differentiation.* Current Opinion in Cell Biology, 1999. **11**(5): p. 634-640.
51. Estes, B.T., J.M. Gimble, and F. Guilak, *Mechanical Signals as Regulators of Stem Cell Fate*, in *Current Topics in Developmental Biology*. 2004, Academic Press. p. 91-126.
52. Malone, A.M., R. Narain, and C.R. Jacobs, *Biomechanical regulation of mesenchymal stem and progenitor cells and the implications for regenerative medicine.* Current Opinion in Orthopaedics, 2005. **16**(5): p. 363-367.
53. Washburn NR, Y.K., Simon CG Jr, Kennedy SB, Amis EJ. , *High-throughput investigation of osteoblast response to polymer crystallinity: influence of nanometer-scale roughness on proliferation. Biomaterials. 2004;25(7-8):1215-24.* Biomaterials. , 2004. **25**((7-8)): p. 1215-24.
54. Wake MC, P.C.J., Mikos AG. , *Pore morphology effects on the fibrovascular tissue growth in porous polymer substrates. .* Cell Transplant. , 1994. **3**((4)): p. 339-43. .
55. Zeltinger J, S.J., Graham DA, Mueller R, Griffith LG. , *Effect of pore size and void fraction on cellular adhesion, proliferation, and matrix deposition. .* Tissue Eng., 2001;7(5):557-72. **7**((5)): p. 557-72.
56. Liu, W.F. and C.S. Chen, *Engineering biomaterials to control cell function.* Materials Today, 2005. **8**(12): p. 28-35.
57. d'Angelo, M., et al., *The Role of Stiffness in Cell Reprogramming: A Potential Role for Biomaterials in Inducing Tissue Regeneration.* Cells, 2019. **8**(9): p. 1036.
58. Ingber, D.E. and J. Folkman, *Mechanochemical switching between growth and differentiation during fibroblast growth factor-stimulated angiogenesis in vitro: role of extracellular matrix.* The Journal of Cell Biology, 1989. **109**(1): p. 317.
59. Folkman, J. and A. Moscona, *Role of cell shape in growth control.* Nature, 1978. **273**(5661): p. 345-349.
60. Ingber, D. and J. Jamieson, Gene Expression during Normal and Malignant Differentiation, 1985: p. 13-32.

61. Shamsan, G.A. and D.J. Odde, *Emerging technologies in mechanotransduction research.* Current Opinion in Chemical Biology, 2019. **53**: p. 125-130.
62. Lo, C.M., et al., *Cell movement is guided by the rigidity of the substrate.* Biophysical Journal, 2000. **79**(1): p. 144-152.
63. Shannon, J.M. and D.R. Pitelka, *The influence of cell shape on the induction of functional differentiation in mouse mammary cells in vitro.* In Vitro, 1981. **17**(11): p. 1016-1028.
64. Engler, A.J., et al., *Matrix elasticity directs stem cell lineage specification.* Cell, 2006. **126**(4): p. 677-89.
65. Rowlands, A.S., P.A. George, and J.J. Cooper-White, *Directing osteogenic and myogenic differentiation of MSCs: interplay of stiffness and adhesive ligand presentation.* Am J Physiol Cell Physiol, 2008. **295**(4): p. C1037-44.
66. Wells, R.G., *The role of matrix stiffness in regulating cell behavior.* Hepatology, 2008. **47**(4): p. 1394-400.
67. Pek, Y.S., A.C. Wan, and J.Y. Ying, *The effect of matrix stiffness on mesenchymal stem cell differentiation in a 3D thixotropic gel.* Biomaterials, 2010. **31**(3): p. 385-91.
68. Mason, B.N., J.P. Califano, and C.A. Reinhart-King, *Matrix stiffness: A regulator of cellular behavior and tissue formation*, in *Engineering Biomaterials for Regenerative Medicine: Novel Technologies for Clinical Applications*. 2012. p. 19-37.
69. Deroanne, C.F., C.M. Lapiere, and B.V. Nusgens, *In vitro tubulogenesis of endothelial cells by relaxation of the coupling extracellular matrix-cytoskeleton.* Cardiovascular Research, 2001. **49**(3): p. 647-658.
70. Engler, A.J., et al., *Myotubes differentiate optimally on substrates with tissue-like stiffness: Pathological implications for soft or stiff microenvironments.* Journal of Cell Biology, 2004. **166**(6): p. 877-887.
71. McKee, C.T., et al., *Indentation versus tensile measurements of Young's modulus for soft biological tissues.* Tissue engineering. Part B, Reviews, 2011. **17**(3): p. 155-164.
72. Hui, L., Zhang, J., Ding, X., Guo, X., & Jiang, X. , *Matrix stiffness regulates the proliferation, stemness and chemoresistance of laryngeal squamous cancer cells. .* International Journal of Oncology, , (2017). . **50,** : p. 1439-1447. .
73. Hong, H., et al., *Grayscale mask-assisted photochemical crosslinking for a dense collagen construct with stiffness gradient.* Journal of Biomedical Materials Research Part B: Applied Biomaterials, 2020. **108**(3): p. 1000-1009.
74. Park, J.S., et al., *The effect of matrix stiffness on the differentiation of mesenchymal stem cells in response to TGF-β.* Biomaterials, 2011. **32**(16): p. 3921-3930.
75. Vogel V, S.M., *Local force and geometry sensing regulate cell functions. .* Nat Rev Mol Cell Biol, 2006,. **7**: p. 265-275. .
76. Vincent, L.G., et al., *Mesenchymal stem cell durotaxis depends on substrate stiffness gradient strength.* Biotechnology Journal, 2013. **8**(4): p. 472-484.
77. Butcher, D.T., T. Alliston, and V.M. Weaver, *A tense situation: forcing tumour progression.* Nature Reviews Cancer, 2009. **9**(2): p. 108-122.
78. Berry, M.F., et al., *Mesenchymal stem cell injection after myocardial infarction improves myocardial compliance.* American Journal of Physiology-Heart and Circulatory Physiology, 2006. **290**(6): p. H2196-H2203.
79. DeLong, S.A., A.S. Gobin, and J.L. West, *Covalent immobilization of RGDS on hydrogel surfaces to direct cell alignment and migration.* J Control Release, 2005. **109**(1-3): p. 139-48.
80. Moriyama, K. and S. Kidoaki, *Cellular Durotaxis Revisited: Initial-Position-Dependent Determination of the Threshold Stiffness Gradient to Induce Durotaxis.* Langmuir, 2019. **35**(23): p. 7478-7486.
81. Majumdar, R., M. Sixt, and C.A. Parent, *New paradigms in the establishment and maintenance of gradients during directed cell migration.* Current Opinion in Cell Biology, 2014. **30**: p. 33-40.
82. Roca-Cusachs, P., R. Sunyer, and X. Trepat, *Mechanical guidance of cell migration: lessons from chemotaxis.* Curr Opin Cell Biol, 2013. **25**(5): p. 543-9.
83. Lo, C.-M., et al., *Cell Movement Is Guided by the Rigidity of the Substrate.* Biophysical Journal, 2000. **79**(1): p. 144-152.
84. Kuo, C.H.R., et al., *Complex stiffness gradient substrates for studying mechanotactic cell migration.* Advanced Materials, 2012. **24**(45): p. 6059-6064.
85. Kawano, T. and S. Kidoaki, *Elasticity boundary conditions required for cell mechanotaxis on microelastically-patterned gels.* Biomaterials, 2011. **32**(11): p. 2725-33.
86. Flanagan, L.A., et al., *Neurite branching on deformable substrates.* Neuroreport, 2002. **13**(18): p. 2411-5.
87. Liu, F., et al., *Feedback amplification of fibrosis through matrix stiffening and COX-2 suppression.* Journal of Cell Biology, 2010. **190**(4): p. 693-706.
88. Ulrich, T.A., E.M. de Juan Pardo, and S. Kumar, *The Mechanical Rigidity of the Extracellular Matrix Regulates the Structure, Motility, and Proliferation of Glioma Cells.* Cancer Research, 2009. **69**(10): p. 4167.
89. Wong, J.Y., et al., *Directed Movement of Vascular Smooth Muscle Cells on Gradient-Compliant Hydrogels.* Langmuir, 2003. **19**(5): p. 1908-1913.
90. Zaari, N., et al., *Photopolymerization in Microfluidic Gradient Generators: Microscale Control of Substrate Compliance to Manipulate Cell Response.* Advanced Materials, 2004. **16**(23-24): p. 2133-2137.

91. Kloxin, A.M., J.A. Benton, and K.S. Anseth, *In situ elasticity modulation with dynamic substrates to direct cell phenotype.* Biomaterials, 2010. **31**(1): p. 1-8.
92. Isenberg, B.C., et al., *Vascular Smooth Muscle Cell Durotaxis Depends on Substrate Stiffness Gradient Strength.* Biophysical Journal, 2009. **97**(5): p. 1313-1322.
93. Oh, S.H., et al., *Wide-range stiffness gradient PVA/HA hydrogel to investigate stem cell differentiation behavior.* Acta Biomaterialia, 2016. **35**: p. 23-31.
94. Hadden, W.J., et al., *Stem cell migration and mechanotransduction on linear stiffness gradient hydrogels.* Proc Natl Acad Sci U S A, 2017. **114**(22): p. 5647-5652.
95. Hartman, C.D., et al., *Vascular smooth muscle cell durotaxis depends on extracellular matrix composition.* Proceedings of the National Academy of Sciences, 2016. **113**(40): p. 11190.
96. Chao, P.H., S.C. Sheng, and W.R. Chang, *Micro-composite substrates for the study of cell-matrix mechanical interactions.* J Mech Behav Biomed Mater, 2014. **38**: p. 232-41.
97. Wen, J.H., et al., *Interplay of matrix stiffness and protein tethering in stem cell differentiation.* Nature Materials, 2014. **13**(10): p. 979-987.
98. Sunyer, R., et al., *Fabrication of hydrogels with steep stiffness gradients for studying cell mechanical response.* PLoS One, 2012. **7**(10): p. e46107.
99. Pérez-Córdoba, L.J., et al., *Physico-chemical, antimicrobial and antioxidant properties of gelatin-chitosan based films loaded with nanoemulsions encapsulating active compounds.* Food Hydrocolloids, 2018. **79**: p. 544-559.
100. Tse, J.R. and A.J. Engler, *Preparation of Hydrogel Substrates with Tunable Mechanical Properties.* Current Protocols in Cell Biology, 2010. **47**(1): p. 10.16.1-10.16.16.
101. Buxboim, A. and D.E. Discher, *Stem cells feel the difference.* Nat Methods, 2010. **7**(9): p. 695-7.
102. Lin, Y.-C., et al., *Mechanosensing of substrate thickness.* Physical Review E, 2010. **82**(4): p. 041918.
103. Tusan, N.D.E.C.G., *Extracellular Matrix Structure and Stem Cell Mechanosensing*, in *Mechanobiology*. 2017. p. 1-21.
104. Trepat, X., et al., *Physical forces during collective cell migration.* Nature Physics, 2009. **5**(6): p. 426-430.
105. Venugopal, B., et al., *Cell density overrides the effect of substrate stiffness on human mesenchymal stem cells' morphology and proliferation.* Biomaterials science, 2018. **6**(5): p. 1109-1119.
106. Zarkoob, H., et al., *Substrate Stiffness Affects Human Keratinocyte Colony Formation.* Cellular and Molecular Bioengineering, 2015. **8**(1): p. 32-50.
107. Haeger, A., et al., *Collective cell migration: guidance principles and hierarchies.* Trends in Cell Biology, 2015. **25**(9): p. 556-566.
108. Bianco, A., et al., *Two distinct modes of guidance signalling during collective migration of border cells.* Nature, 2007. **448**(7151): p. 362-365.
109. Sunyer, R., et al., *Collective cell durotaxis emerges from long-range intercellular force transmission.* Science, 2016. **353**(6304): p. 1157.
110. Wagenseil, J.E. and R.P. Mecham, *Vascular extracellular matrix and arterial mechanics.* Physiological reviews, 2009. **89**(3): p. 957-989.
111. Steward, R.L., et al., *Probing Cell Structure Responses Through a Shear and Stretching Mechanical Stimulation Technique.* Cell Biochemistry and Biophysics, 2010. **56**(2): p. 115-124.
112. Prodanov, L., et al., *Influence of nanostructural environment and fluid flow on osteoblast-like cell behavior: A model for cell-mechanics studies.* Acta Biomaterialia, 2013. **9**(5): p. 6653-6662.
113. Kshitiz, et al., *Control of stem cell fate and function by engineering physical microenvironments.* Integrative Biology, 2012. **4**(9): p. 1008-1018.
114. Castillo, A.B. and C.R. Jacobs, *Mesenchymal Stem Cell Mechanobiology.* Current Osteoporosis Reports, 2010. **8**(2): p. 98-104.
115. Delaine-Smith, R.M. and G.C. Reilly, *Mesenchymal stem cell responses to mechanical stimuli.* Muscles, ligaments and tendons journal, 2012. **2**(3): p. 169-180.
116. Yourek, G., et al., *Shear stress induces osteogenic differentiation of human mesenchymal stem cells.* Regenerative medicine, 2010. **5**(5): p. 713-724.
117. Galie, P.A., et al., *Application of multiple levels of fluid shear stress to endothelial cells plated on polyacrylamide gels.* Lab on a chip, 2015. **15**(4): p. 1205-1212.
118. Anneh Mohammad, G., et al., *Design and Validation of Perfusion Bioreactor with Low Shear Stress for Tissue Engineering.* Journal of Medical and Biological Engineering, 2013. **33**(2): p. 185-191.
119. Nieponice, A., et al., *Mechanical stimulation induces morphological and phenotypic changes in bone marrow-derived progenitor cells within a three-dimensional fibrin matrix.* Journal of Biomedical Materials Research Part A, 2007. **81A**(3): p. 523-530.
120. Shojaei, S., et al., *Effects of Mechanical and Chemical Stimuli on Differentiation of Human Adipose-Derived Stem Cells into Endothelial Cells.* The International Journal of Artificial Organs, 2013. **36**(9): p. 663-673.
121. Ravichandran, A., Y. Liu, and S.-H. Teoh, *Review: bioreactor design towards generation of relevant engineered tissues: focus on clinical translation.* Journal of Tissue Engineering and Regenerative Medicine, 2018. **12**(1): p. e7-e22.

122. Kim, J. and T. Ma, *Perfusion regulation of hMSC microenvironment and osteogenic differentiation in 3D scaffold.* Biotechnology and Bioengineering, 2012. **109**(1): p. 252-261.
123. Liu, L., et al., *Different effects of intermittent and continuous fluid shear stresses on osteogenic differentiation of human mesenchymal stem cells.* Biomechanics and Modeling in Mechanobiology, 2012. **11**(3): p. 391-401.
124. Leandro S. Gardel, L.A.S., Rui L. Reis, and Manuela E. Gomes, *Use of Perfusion Bioreactors and Large Animal Models for Long Bone Tissue Engineering.* Tissue Engineering Part B: Reviews, 2014. **20**(2): p. 126-146.
125. Conway, D.E. and M.A. Schwartz, *Flow-dependent cellular mechanotransduction in atherosclerosis.* Journal of Cell Science, 2013. **126**(22): p. 5101.
126. Li, L., J. Eyckmans, and C.S. Chen, *Designer biomaterials for mechanobiology.* Nature Materials, 2017. **16**(12): p. 1164-1168.
127. Denisin, A.K. and B.L. Pruitt, *Tuning the Range of Polyacrylamide Gel Stiffness for Mechanobiology Applications.* ACS Applied Materials & Interfaces, 2016. **8**(34): p. 21893-21902.
128. Kshitiz, et al., *Control of stem cell fate and function by engineering physical microenvironments.* Integrative biology : quantitative biosciences from nano to macro, 2012. **4**(9): p. 1008-1018.
129. Engler, A.J., et al., *Surface probe measurements of the elasticity of sectioned tissue, thin gels and polyelectrolyte multilayer films: Correlations between substrate stiffness and cell adhesion.* Surface Science, 2004. **570**(1): p. 142-154.
130. Luo, W., et al., *Laminar shear stress delivers cell cycle arrest and anti-apoptosis to mesenchymal stem cells.* Acta Biochim Biophys Sin (Shanghai), 2011. **43**(3): p. 210-6.
131. Wagers, A.J. and I.L. Weissman, *Plasticity of Adult Stem Cells.* Cell, 2004. **116**(5): p. 639-648.
132. Minguell, J.J., A. Erices, and P. Conget, *Mesenchymal Stem Cells.* Experimental Biology and Medicine, 2001. **226**(6): p. 507-520.
133. Jackson, L., et al., *Adult mesenchymal stem cells: differentiation potential and therapeutic applications.* J Postgrad Med, 2007. **53**(2): p. 121-7.
134. Caplan, A.I., *Mesenchymal stem cells.* Journal of Orthopaedic Research, 1991. **9**(5): p. 641-650.
135. Pittenger, M.F., et al., *Multilineage Potential of Adult Human Mesenchymal Stem Cells.* Science, 1999. **284**(5411): p. 143.
136. Jacobs, S.A., et al., *Immunological characteristics of human mesenchymal stem cells and multipotent adult progenitor cells.* Immunology and cell biology, 2013. **91**(1): p. 32-39.
137. Pittenger MF, M.A., Beck SC, Jaiswal RK, Douglas R, Mosca JD,, *Multilineage potential of adult human mesenchymal stem cells. .* 1999 Science 284(5411):143e7.
138. Baiguera, S., et al., *Mesenchymal stromal cells for tissue-engineered tissue and organ replacements.* Transpl Int, 2012. **25**(4): p. 369-82.
139. Caplan, A.I., *Why are MSCs therapeutic? New data: new insight.* The Journal of Pathology, 2009. **217**(2): p. 318-324.
140. Friedenstein AJ, P.-S.I., Petrakova KV. , *Osteogenesis in transplants of bone marrow cells. J.* Embryo Exp Morph, 1966. **16**(3): p. 381-390.
141. Jiang Y, J.B., Reinhardt RL, Schwartz RE, Keene CD, Ortiz-Gonzalez XR, Pluripotency of mesenchymal stem cells derived from adult marrow. Nature 2002;418(6893):41e9., *Pluripotency of mesenchymal stem cells derived from adult marrow.* Nature, 2002. **418**((6893)): p. 41-49.
142. Chiou, M., Y. Xu, and M.T. Longaker, *Mitogenic and chondrogenic effects of fibroblast growth factor-2 in adipose-derived mesenchymal cells.* Biochemical and Biophysical Research Communications, 2006. **343**(2): p. 644-652.
143. Suon S, J.H., Donaldson AE, Caterson EJ, Tuan RS, Deschennes G., *Transient differentiation of adult human bone marrow cells into neuron-like cells in culture.* Stem Cells Dev, 2004. **13**((6)): p. 625-35.
144. Tamagawa, T., et al., *Differentiation of mesenchymal cells derived from human amniotic membranes into hepatocyte-like cells in vitro.* Human Cell, 2007. **20**(3): p. 77-84.
145. P. Alexander, H.H., K. Clark and R. Tuan . *Mesenchymal Stem Cells in Musculoskeletal Tissue Engineering*, in *Principles of Tissue Engineering*, R. Lanza, Langer, R., and Vacanti, J., Editor., Academic Press: San Diego. p. 143-156.
146. Vazin, T. and D.V. Schaffer, *Engineering strategies to emulate the stem cell niche.* Trends in Biotechnology, 2010. **28**(3): p. 117-124.
147. Engler, A., Sen, S., Sweeney, H. & Discher, D. Matrix elasticity directs stem cell lineage specification., *Matrix elasticity directs stem cell lineage specification.* Cell, 2006. **126**: p. 677-689.
148. Pittenger Mark, F. and J. Martin Bradley, *Mesenchymal Stem Cells and Their Potential as Cardiac Therapeutics.* Circulation Research, 2004. **95**(1): p. 9-20.
149. Higuchi, A., et al., *Physical cues of biomaterials guide stem cell differentiation fate.* Chemical Reviews, 2013. **113**(5): p. 3297-3328.
150. Winer, J.P., S. Oake, and P.A. Janmey, *Non-Linear Elasticity of Extracellular Matrices Enables Contractile Cells to Communicate Local Position and Orientation.* PLOS ONE, 2009. **4**(7): p. e6382.
151. Timoshenko, S.P., *13.79 Felix Klein*, in *History of Strength of Materials - With a Brief Account of the History of Theory of Elasticity and Theory of Structures*. Dover Publications.

152. Mihai, L.A. and A. Goriely, *How to characterize a nonlinear elastic material? A review on nonlinear constitutive parameters in isotropic finite elasticity.* Proceedings of the Royal Society A: Mathematical, Physical and Engineering Sciences, 2017. **473**(2207): p. 20170607.
153. Storm, C., et al., *Nonlinear elasticity in biological gels.* Nature, 2005. **435**(7039): p. 191-194.
154. Özkaya, N. and M. Nordin, *Mechanical Properties of Biological Tissues*, in *Fundamentals of Biomechanics: Equilibrium, Motion, and Deformation*. 1999, Springer New York: New York, NY. p. 195-218.
155. Park, H., Park, K., Shalaby, W. , *Biodegradable Hydrogels for Drug Delivery.* CRC Press, 1993.
156. Jhon, M.S. and J.D. Andrade, *Water and hydrogels.* Journal of Biomedical Materials Research, 1973. **7**(6): p. 509-522.
157. Jeon, O., et al., *Mechanical properties and degradation behaviors of hyaluronic acid hydrogels cross-linked at various cross-linking densities.* Carbohydrate Polymers, 2007. **70**(3): p. 251-257.
158. Ingber, D., et al., *CHAPTER 2 - Mechanochemical Transduction across Extracellular Matrix and through the Cytoskeleton*, in *Physical Forces and the Mamilian Cell*, J.A. Frangos, Editor. 1993, Academic Press: Boston. p. 61-79.
159. Sundelacruz, S. and D.L. Kaplan, *Stem cell- and scaffold-based tissue engineering approaches to osteochondral regenerative medicine.* Seminars in Cell & Developmental Biology, 2009. **20**(6): p. 646-655.
160. Kretlow, J.D. and A.G. Mikos, *From material to tissue: Biomaterial development, scaffold fabrication, and tissue engineering.* AIChE Journal, 2008. **54**(12): p. 3048-3067.
161. Eyckmans, J., et al., *A Hitchhiker's Guide to Mechanobiology.* Developmental Cell, 2011. **21**(1): p. 35-47.
162. Kharkar, P.M., K.L. Kiick, and A.M. Kloxin, *Designing degradable hydrogels for orthogonal control of cell microenvironments.* Chemical Society reviews, 2013. **42**(17): p. 7335-7372.
163. Temenoff J.S., A.K.A., LeBaron R.G., Effect of poly(ethylene glycol) molecular weight on tensile and swelling properties of oligo(poly(ethylene glycol) fumarate) hydrogels for cartilage tissue engineering, J Biomed Mater Res, 59 (3) (2002), pp. 429-437, *Effect of poly(ethylene glycol) molecular weight on tensile and swelling properties of oligo(poly(ethylene glycol) fumarate) hydrogels for cartilage tissue engineering,.* Biomed Mater Res. **59**(3): p. 429-437.
164. Sah, R.L., Kim, Y. J., Doong, J. Y., Grodzinsky, A. J., Plass, A. H., and Sandy, J. D. , *Biosynthetic response of cartilage explants to dynamic compression.* D.J. Orthop. Res. , 1989. **7,** : p. 619- 636.
165. Weber, L.M., C.G. Lopez, and K.S. Anseth, *Effects of PEG hydrogel crosslinking density on protein diffusion and encapsulated islet survival and function.* Journal of Biomedical Materials Research Part A, 2009. **90A**(3): p. 720-729.
166. Burdick, J.A. and M.M. Stevens, *11 - Biomedical hydrogels*, in *Biomaterials, Artificial Organs and Tissue Engineering*, L.L. Hench and J.R. Jones, Editors. 2005, Woodhead Publishing. p. 107-115.
167. Sood, N., et al., *Stimuli-responsive hydrogels in drug delivery and tissue engineering.* Drug Delivery, 2016. **23**(3): p. 748-770.
168. Dinu, M.V., M.M. Perju, and E.S. Drăgan, *Porous Semi-Interpenetrating Hydrogel Networks Based on Dextran and Polyacrylamide With Superfast Responsiveness.* Macromolecular Chemistry and Physics, 2011. **212**(3): p. 240-251.
169. Berillo, D. and N. Volkova, *Preparation and physicochemical characteristics of cryogel based on gelatin and oxidised dextran.* Journal of Materials Science, 2014. **49**(14): p. 4855-4868.
170. Gökçeören, A.T., B.F. Şenkal, and C. Erbil, *Effect of crosslinker structure and crosslinker/monomer ratio on network parameters and thermodynamic properties of Poly (N-isopropylacrylamide) hydrogels.* Journal of Polymer Research, 2014. **21**(3): p. 370.
171. Karpushkin, E.A., *Anionic polymer hydrogel degradation by ascorbic acid.* Russian Journal of General Chemistry, 2013. **83**(8): p. 1515-1518.
172. Chatterjee, P., et al., *Thermal and mechanical properties of poly(N-isopropylacrylamide)-based hydrogels as a function of porosity and medium change.* Journal of Applied Polymer Science, 2015. **132**(45).
173. Přádný, M., et al., *Macroporous 2-hydroxyethyl methacrylate hydrogels of dual porosity for cell cultivation: morphology, swelling, permeability, and mechanical behavior.* Journal of Polymer Research, 2014. **21**(11): p. 579.
174. Annabi, N., et al., *Controlling the porosity and microarchitecture of hydrogels for tissue engineering.* Tissue engineering. Part B, Reviews, 2010. **16**(4): p. 371-383.
175. Yamane, S., et al., *Effect of pore size on in vitro cartilage formation using chitosan-based hyaluronic acid hybrid polymer fibers.* Journal of Biomedical Materials Research Part A, 2007. **81A**(3): p. 586-593.
176. Yuan, L., et al., *Migration of human mesenchymal stem cells under low shear stress mediated by mitogen-activated protein kinase signaling.* Stem Cells Dev, 2012. **21**(13): p. 2520-30.
177. Hartman, C.D., et al., *Vascular smooth muscle cell durotaxis depends on extracellular matrix composition.* Proceedings of the National Academy of Sciences of the United States of America, 2016. **113**(40): p. 11190-11195.
178. Kandow, C.E., et al., *Polyacrylamide Hydrogels for Cell Mechanics: Steps Toward Optimization and Alternative Uses*, in *Methods in Cell Biology*. 2007, Academic Press. p. 29-46.

179. Christ, A.F., et al., *Mechanical difference between white and gray matter in the rat cerebellum measured by scanning force microscopy.* Journal of Biomechanics, 2010. **43**(15): p. 2986-2992.
180. Mullen, C.A., et al., *The effect of substrate stiffness, thickness, and cross-linking density on osteogenic cell behavior.* Biophysical journal, 2015. **108**(7): p. 1604-1612.
181. Long, R., et al., *Effects of Gel Thickness on Microscopic Indentation Measurements of Gel Modulus.* Biophysical Journal, 2011. **101**(3): p. 643-650.
182. Yang, Z., et al., *Nonlinear Behavior of Gelatin Networks Reveals a Hierarchical Structure.* Biomacromolecules, 2016. **17**(2): p. 590-600.
183. Hattori, K., J.-i. Horinaka, and T. Takigawa, *Swelling behavior of a polyacrylamide gel in water/acetonitrile mixtures across the solvent phase separation temperatures.* Colloid and Polymer Science, 2020. **298**(4): p. 435-440.
184. Djabourov, M., J.-P. Lechaire, and F. Gaill, *Structure and rheology of gelatin and collagen gels.* Biorheology, 1993. **30**: p. 191-205.
185. Rudnicki, M.S., et al., *Nonlinear Strain Stiffening Is Not Sufficient to Explain How Far Cells Can Feel on Fibrous Protein Gels.* Biophysical Journal, 2013. **105**(1): p. 11-20.
186. Ma, X., et al., *Fibers in the extracellular matrix enable long-range stress transmission between cells.* Biophysical journal, 2013. **104**(7): p. 1410-1418.
187. Texter, J., *Templating hydrogels.* Colloid and polymer science, 2009. **287**: p. 313-321.
188. Shan, J., et al., *Anisotropic Structure and Properties of Chitin and Chitosan Nanofibril-Supported Starch Foams.* ACS Sustainable Chemistry & Engineering, 2020. **8**(47): p. 17387-17396.
189. Mohammadi, H., et al., *Inelastic behaviour of collagen networks in cell–matrix interactions and mechanosensation.* Journal of The Royal Society Interface, 2015. **12**(102): p. 20141074.
190. Motte, S. and L.J. Kaufman, *Strain stiffening in collagen I networks.* Biopolymers, 2013. **99**(1): p. 35-46.
191. Chen, J., et al., *Proanthocyanidin-crosslinked collagen/konjac glucomannan hydrogel with improved mechanical properties and MRI trackable biodegradation for potential tissue engineering scaffolds.* Journal of Materials Chemistry B, 2020. **8**(2): p. 316-331.
192. Leong, W.S., et al., *Thickness sensing of hMSCs on collagen gel directs stem cell fate.* Biochem Biophys Res Commun, 2010. **401**(2): p. 287-92.
193. Furlani, F., et al., *Strain Hardening in Highly Acetylated Chitosan Gels.* Biomacromolecules, 2021. **22**(7): p. 2902-2909.
194. Lee, C.H.S., A.; Lee, Y. , *Biomedical applications of collagen. .* Int. J. Pharm., 2001. **221**: p. 1-22.
195. Ramírez-Agudelo, R., et al., *Hybrid nanofibers based on poly-caprolactone/gelatin/hydroxyapatite nanoparticles-loaded Doxycycline: Effective anti-tumoral and antibacterial activity.* Materials Science and Engineering: C, 2018. **83**: p. 25-34.
196. Haug, I.J. and K.I. Draget, *5 - Gelatin*, in *Handbook of Food Proteins*, G.O. Phillips and P.A. Williams, Editors. 2011, Woodhead Publishing. p. 92-115.
197. Huang, Y.O., S.; Siewe, M.; Moshfeghian, A.; Madihally, S.V., *In vitro characterization of chitosan-gelatin scaffolds for tissue engineering. .* Biomaterials 2005. **26**: p. 7616-7627.
198. Tan, H. and K.G. Marra, *Injectable, Biodegradable Hydrogels for Tissue Engineering Applications.* Materials, 2010. **3**(3).
199. Kommareddy, S., D. Shenoy, and M. Amiji, *Gelatin Nanoparticles and Their Biofunctionalization*. 2007.
200. Langer, R. and D.A. Tirrell, *Designing materials for biology and medicine.* Nature, 2004. **428**(6982): p. 487-492.
201. Kuijpers, A.J., et al., *Characterization of the Network Structure of Carbodiimide Cross-Linked Gelatin Gels.* Macromolecules, 1999. **32**(10): p. 3325-3333.
202. Choi, Y.S., et al., *Study on gelatin-containing artificial skin: I. Preparation and characteristics of novel gelatin-alginate sponge.* Biomaterials, 1999. **20**(5): p. 409-417.
203. Zhao, M., et al., *Molecular composition of GAG-collagen I multilayers affects remodeling of terminal layers and osteogenic differentiation of adipose-derived stem cells.* Acta Biomater, 2016. **41**: p. 86-99.
204. Rehakova M, B.D., Vizarova K, Soldan M, Jurickova M. , *Properties of collagen and hyaluronic acid composite materials and their modification by chemical crosslinking. .* Biomed Mater Res 1996. **30**(3): p. 369-72.
205. Park SN, P.J., Kim HO, Song MJ, Suh H. , *Characterization of porous collagen/hyaluronic acid scaffold modified by l-ethyl-3- (3-dimethylaminopropyl)carbodiimide cross-linking. .* Biomaterials, 2002. **23**(4): p. 205-12.
206. Kim, S., et al., *Chitosan/gelatin-based films crosslinked by proanthocyanidin.* J Biomed Mater Res B Appl Biomater, 2005. **75**(2): p. 442-50.
207. Yao K., L.J., Yao F., , *Chitosan-based hydrogels: functions and applications,* . 2012 CRC Press, .
208. Lee, K.Y., W.S. Ha, and W.H. Park, *Blood compatibility and biodegradability of partially N-acylated chitosan derivatives.* Biomaterials, 1995. **16**(16): p. 1211-1216.
209. XH, W., *Crosslinked collagen/chitosan matrix for artificial livers.* Biomaterials, 2003. **24**: p. 3213-3220.
210. Islam, S., M.A.R. Bhuiyan, and M.N. Islam, *Chitin and Chitosan: Structure, Properties and Applications in Biomedical Engineering.* Journal of Polymers and the Environment, 2017. **25**(3): p. 854-866.

211. Prabaharan, M., *Review Paper: Chitosan Derivatives as Promising Materials for Controlled Drug Delivery.* Journal of Biomaterials Applications, 2008. **23**(1): p. 5-36.
212. Bhattarai, N., J. Gunn, and M. Zhang, *Chitosan-based hydrogels for controlled, localized drug delivery.* Advanced Drug Delivery Reviews, 2010. **62**(1): p. 83-99.
213. Caló, E. and V.V. Khutoryanskiy, *Biomedical applications of hydrogels: A review of patents and commercial products.* European Polymer Journal, 2015. **65**: p. 252-267.
214. Mao, J., et al., *Study of novel chitosan-gelatin artificial skin in vitro.* Journal of Biomedical Materials Research Part A, 2003. **64A**(2): p. 301-308.
215. Nagahama, H., et al., *Preparation and characterization of novel chitosan/gelatin membranes using chitosan hydrogel.* Carbohydrate Polymers, 2009. **76**(2): p. 255-260.
216. Chen, T., et al., *Enzyme-catalyzed gel formation of gelatin and chitosan: potential for in situ applications.* Biomaterials, 2003. **24**(17): p. 2831-2841.
217. Hoffman, A.S., *Hydrogels for biomedical applications.* Advanced Drug Delivery Reviews, 2012. **64**: p. 18-23.
218. Prata, A.S. and C.R.F. Grosso, *Production of microparticles with gelatin and chitosan.* Carbohydrate Polymers, 2015. **116**: p. 292-299.
219. Davoudi, Z., et al., *Development of chitosan/gelatin/keratin composite containing hydrocortisone sodium succinate as a buccal mucoadhesive patch to treat desquamative gingivitis.* Drug Development and Industrial Pharmacy, 2018. **44**(1): p. 40-55.
220. Wahba, M.I., *Enhancement of the mechanical properties of chitosan.* Journal of Biomaterials Science, Polymer Edition, 2020. **31**(3): p. 350-375.
221. Pereda, M., et al., *Chitosan-gelatin composites and bi-layer films with potential antimicrobial activity.* Food Hydrocolloids, 2011. **25**(5): p. 1372-1381.
222. Ng, W.L., W.Y. Yeong, and M.W. Naing, *Development of Polyelectrolyte Chitosan-gelatin Hydrogels for Skin Bioprinting.* Procedia CIRP, 2016. **49**: p. 105-112.
223. Ahmed, E.M., *Hydrogel: Preparation, characterization, and applications: A review.* Journal of Advanced Research, 2015. **6**(2): p. 105-121.
224. Maitra, J.a.S., V., *Cross-Linking In Hydrogels - A Review* American Journal of Polymer Science, 2014. **4** (2): p. 25-31.
225. Berger, J., et al., *Structure and interactions in covalently and ionically crosslinked chitosan hydrogels for biomedical applications.* European Journal of Pharmaceutics and Biopharmaceutics, 2004. **57**(1): p. 19-34.
226. Voron'ko, N.G., et al., *The chitosan–gelatin (bio)polyelectrolyte complexes formation in an acidic medium.* Carbohydrate Polymers, 2016. **138**: p. 265-272.
227. Singhal, R. and K. Gupta, *A Review: Tailor-made Hydrogel Structures (Classifications and Synthesis Parameters).* Polymer-Plastics Technology and Engineering, 2016. **55**(1): p. 54-70.
228. Tomihata K, I.Y.P.o.c.-l.h.a.f.o.l.w.c., Biomaterials 1997,18(3):189-95, *Preparation of cross-linked hyaluronic acid films of low water content,.* Biomaterials 1997. **18**((3)): p. 189-95.
229. Lu, P.-L., et al., *Carbodiimide cross-linked hyaluronic acid hydrogels as cell sheet delivery vehicles: Characterization and interaction with corneal endothelial cells.* Journal of biomaterials science. Polymer edition, 2008. **19**: p. 1-18.
230. Slusarewicz, P., K. Zhu, and T. Hedman, *Kinetic characterization and comparison of various protein crosslinking reagents for matrix modification.* J Mater Sci Mater Med, 2010. **21**(4): p. 1175-81.
231. Cheung, D.T., et al., *Mechanism of Crosslinking of Proteins by Glutaraldehyde IV: In Vitro and In Vivo Stability of a Crosslinked Collagen Matrix.* Connective Tissue Research, 1990. **25**(1): p. 27-34.
232. Nimni, M.E., *Glutaraldehyde Fixation Revisited.* 2001. **11**(3&4): p. 11.
233. Han B, J.J., Tang BW, Nimni ME. , *Proanthocyanidin: A natural crosslinking reagent for stabilizing collagen matrices. .* J Biomed Mater Res A, 2003. **65**: p. 118-124.
234. S., T., *Bioflavonoids: proanthocyanidins and quercetin and their potential roles in treating musculoskeletal conditions.* Orthop Sports Phys Ther 2002. **32**: p. 357-363.
235. Polyphenols, B.L., *Polyphenols: chemistry, dietary sources, metabolism, and nutritional significance. .* Nutr Rev, 1998. **56**: p. 317-333.
236. Cetta G, P.G., Tenni R, Bisi C. , *Influence of flavonoid-copper complexes on cross linking in elastin.* Ital J Biochem, 1977. **26**((4)): p. 317-327.
237. Rao CN, R.V., Steinmann B. , *Bioflavonoid-mediated stabi-lization of collagen in adjuvant-induced arthritis.* ScandJ Rheumatol 1983. **12**((1)): p. 39 -42.
238. Jing, Y., J. Huang, and X. Yu, *Preparation, characterization, and functional evaluation of proanthocyanidin-chitosan conjugate.* Carbohydrate Polymers, 2018. **194**: p. 139-145.
239. Akhavan-Kharazian, N. and H. Izadi-Vasafi, *Preparation and characterization of chitosan/gelatin/nanocrystalline cellulose/calcium peroxide films for potential wound dressing applications.* International Journal of Biological Macromolecules, 2019. **133**: p. 881-891.

240. Kan, J., et al., *Development of active packaging based on chitosan-gelatin blend films functionalized with Chinese hawthorn (Crataegus pinnatifida) fruit extract.* International Journal of Biological Macromolecules, 2019. **140**: p. 384-392.
241. Lee, K.Y. and D.J. Mooney, *Hydrogels for Tissue Engineering.* Chemical Reviews, 2001. **101**(7): p. 1869-1880.
242. Yu, X., Y. Jing, and Y. Jiang, *Preparation of proanthocyanidin–chitosan complex and its antioxidant and antibacterial properties.* Iranian Polymer Journal, 2018. **27**(9): p. 653-661.
243. Wichterle, O. and D. LÍM, *Hydrophilic Gels for Biological Use.* Nature, 1960. **185**(4706): p. 117-118.
244. Hunt, J.A., et al., *Hydrogels for tissue engineering and regenerative medicine.* Journal of Materials Chemistry B, 2014. **2**(33): p. 5319-5338.
245. Medical, F., M. Surgical, and Devices, *Standard Guide for Characterization of Hydrogels used in Regenerative Medicine*. 2011.
246. Mullen, C.A., et al., *The effect of substrate stiffness, thickness, and cross-linking density on osteogenic cell behavior.* Biophys J, 2015. **108**(7): p. 1604-1612.
247. Rao, R.R., et al., *Matrix composition regulates three-dimensional network formation by endothelial cells and mesenchymal stem cells in collagen/fibrin materials.* Angiogenesis, 2012. **15**(2): p. 253-264.
248. Wingate, K., et al., *Synergism of Matrix Stiffness and Vascular Endothelial Growth Factor on Mesenchymal Stem Cells for Vascular Endothelial Regeneration.* Tissue Engineering Part A, 2014. **20**(17-18): p. 2503-2512.
249. Mao, A.S., J.W. Shin, and D.J. Mooney, *Effects of substrate stiffness and cell-cell contact on mesenchymal stem cell differentiation.* Biomaterials, 2016. **98**: p. 184-91.
250. Lane, S.W., D.A. Williams, and F.M. Watt, *Modulating the stem cell niche for tissue regeneration.* Nature Biotechnology, 2014. **32**(8): p. 795-803.
251. Rice, A.J., et al., *Matrix stiffness induces epithelial-mesenchymal transition and promotes chemoresistance in pancreatic cancer cells.* Oncogenesis, 2017. **6**(7): p. e352.
252. Lachowski, D., et al., *Substrate Rigidity Controls Activation and Durotaxis in Pancreatic Stellate Cells.* Scientific reports, 2017. **7**(1): p. 2506-2506.
253. Lachowski, D., et al., *FAK controls the mechanical activation of YAP, a transcriptional regulator required for durotaxis.* Faseb j, 2018. **32**(2): p. 1099-1107.
254. Abramoff M, M.P., Ram S. , *Image processing with ImageJ.* Biophotonics International 2004. **11**(7): p. 36-42.
255. Parmenter, C., A. Baki, and K. Shakesheff, *Application of Cryogenic Focused Ion Beam Scanning Electron Microcopy to Hydrogel Characterisation.* European Microscopy Congress 2016: Proceedings, 2016: p. 682-683.
256. Gerecht, S., et al., *A porous photocurable elastomer for cell encapsulation and culture.* Biomaterials, 2007. **28**(32): p. 4826-4835.
257. Johnson, K.L., et al., *Surface energy and the contact of elastic solids.* Proceedings of the Royal Society of London. A. Mathematical and Physical Sciences, 1971. **324**(1558): p. 301-313.
258. Gavara, N. and R.S. Chadwick, *Determination of the elastic moduli of thin samples and adherent cells using conical atomic force microscope tips.* Nature nanotechnology, 2012. **7**(11): p. 733-736.
259. Smith, E.F., et al., *Ionic Liquids in Vacuo: Analysis of Liquid Surfaces Using Ultra-High-Vacuum Techniques.* Langmuir, 2006. **22**(22): p. 9386-9392.
260. Ratia, V.L., et al., *Sliding wear of a self-mated thermally sprayed chromium oxide coating in a simulated PWR water environment.* Wear, 2019. **426-427**: p. 1466-1473.
261. Liu, Y., et al., *The Properties of Chitosan-Gelatin Scaffolds by Once or Twice Vacuum Freeze-Drying Methods.* Polymer-Plastics Technology and Engineering, 2013. **52**(11): p. 1154-1159.
262. Murphy, S.V., A. Skardal, and A. Atala, *Evaluation of hydrogels for bio-printing applications.* Journal of Biomedical Materials Research Part A, 2013. **101A**(1): p. 272-284.
263. Rage, R., J. Mitchen, and G. Wilding, *DNA fluorometric assay in 96-well tissue culture plates using Hoechst 33258 after cell lysis by freezing in distilled water.* Analytical Biochemistry, 1990. **191**(1): p. 31-34.
264. Zernik, J., K. Twarog, and W.B. Upholt, *Regulation of alkaline phosphatase and alpha2(I) procollagen synthesis during early intramembranous bone formation in the rat mandible.* Differentiation, 1990. **44**(3): p. 207-215.
265. Kong, H.J., et al., *Controlling Rigidity and Degradation of Alginate Hydrogels via Molecular Weight Distribution.* Biomacromolecules, 2004. **5**(5): p. 1720-1727.
266. Peppas, N.A., et al., *Hydrogels in Biology and Medicine: From Molecular Principles to Bionanotechnology.* Advanced Materials, 2006. **18**(11): p. 1345-1360.
267. Han, B., et al., *Proanthocyanidin: A natural crosslinking reagent for stabilizing collagen matrices.* Journal of Biomedical Materials Research Part A, 2003. **65A**(1): p. 118-124.
268. Hsu, S.-h., et al., *Chitosan as Scaffold Materials: Effects of Molecular Weight and Degree of Deacetylation.* Journal of Polymer Research, 2004. **11**(2): p. 141-147.
269. He, Q., et al., *Preparation of chitosan films using different neutralizing solutions to improve endothelial cell compatibility.* Journal of Materials Science: Materials in Medicine, 2011. **22**(12): p. 2791-2802.
270. S. E. Noriega, A.S., *Consequences of Neutralization on the Proliferation and Cytoskeletal Organization of Chondrocytes on Chitosan-Based Matrices.* International Journal of Carbohydrate Chemistry, 2011. **2011**.

271. Cho, Y.-W., et al., *Preparation and Solubility in Acid and Water of Partially Deacetylated Chitins.* Biomacromolecules, 2000. **1**(4): p. 609-614.
272. McKenna, G.B., K.M. Flynn, and Y. Chen, *Swelling in crosslinked natural rubber: experimental evidence of the crosslink density dependence of χ.* Polymer, 1990. **31**(10): p. 1937-1945.
273. Eydelnant, I.A. and N. Tufenkji, *Cranberry Derived Proanthocyanidins Reduce Bacterial Adhesion to Selected Biomaterials.* Langmuir, 2008. **24**(18): p. 10273-10281.
274. Rhim, J.W., et al., *Preparation and characterization of chitosan-based nanocomposite films with antimicrobial activity.* Journal of Agricultural and Food Chemistry, 2006. **54**(16): p. 5814-5822.
275. Samuels, R.J., *Solid state characterization of the structure of chitosan films.* Journal of Polymer Science: Polymer Physics Edition, 1981. **19**(7): p. 1081-1105.
276. Kang, H.W., Y. Tabata, and Y. Ikada, *Fabrication of porous gelatin scaffolds for tissue engineering.* Biomaterials, 1999. **20**(14): p. 1339-1344.
277. Martin, I., et al., *Modulation of the mechanical properties of tissue engineered cartilage.* Biorheology, 2000. **37**(1-2): p. 141-147.
278. Lee, S.B., et al., *Study of gelatin-containing artificial skin V: fabrication of gelatin scaffolds using a salt-leaching method.* Biomaterials, 2005. **26**(14): p. 1961-1968.
279. Hayman, M.W., et al., *Growth of human stem cell-derived neurons on solid three-dimensional polymers.* Journal of Biochemical and Biophysical Methods, 2005. **62**(3): p. 231-240.
280. Kang, H.-S., et al., *Polyelectrolyte complex hydrogel composed of chitosan and poly(γ-glutamic acid) for biological application: Preparation, physical properties, and cytocompatibility.* Journal of Applied Polymer Science, 2007. **103**(1): p. 386-394.
281. Chen, K.Y., et al., *Novel bone substitute composed of oligomeric proanthocyanidins-crosslinked gelatin and tricalcium phosphate.* Macromol Biosci, 2008. **8**(10): p. 942-50.
282. Castellan, C.S., et al., *Solubility study of phytochemical cross-linking agents on dentin stiffness.* J Dent, 2010. **38**(5): p. 431-6.
283. Bigi, A., et al., *Stabilization of gelatin films by crosslinking with genipin.* Biomaterials, 2002. **23**(24): p. 4827-4832.
284. Jin, J., M. Song, and D.J. Hourston, *Novel Chitosan-Based Films Cross-Linked by Genipin with Improved Physical Properties.* Biomacromolecules, 2004. **5**(1): p. 162-168.
285. Hagerman, A.E. and K.M. Klucher, *Tannin-protein interactions.* Liss, 1986.
286. Hagerman, A.E. and L.G. Butler, *The specificity of proanthocyanidin-protein interactions.* J Biol Chem, 1981. **256**(9): p. 4494-7.
287. Wang, Z., Q. Hu, and Y. Wang, *Preparation of chitosan rods with excellent mechanical properties: One candidate for bone fracture internal fixation.* Science China Chemistry, 2011. **54**(2): p. 380-384.
288. Liu, Y., et al., *Preparation of pH-sensitive and antioxidant packaging films based on κ-carrageenan and mulberry polyphenolic extract.* International Journal of Biological Macromolecules, 2019. **134**: p. 993-1001.
289. Wang, X., et al., *Preparation and characterization of antioxidant and pH-sensitive films based on chitosan and black soybean seed coat extract.* Food Hydrocolloids, 2019. **89**: p. 56-66.
290. Sienkiewicz, A., et al., *Swelling effects in cross-linked polymers by thermogravimetry.* Journal of Thermal Analysis and Calorimetry, 2017. **130**(1): p. 85-93.
291. S.N. Molnes, *Physical properties of gelatin based solid emulsions: effects on drug release in the GI tract, ,* in *Dept. of Biotechnology, Norwegian*. 2013, Univ. of Science and Technology, : Trondheim. p. 145.
292. Cho, J., et al., *Physical gelation of chitosan in the presence of beta-glycerophosphate: the effect of temperature.* Biomacromolecules, 2005. **6**(6): p. 3267-75.
293. Mahdavinia, G.R., et al., *Modified chitosan 4. Superabsorbent hydrogels from poly(acrylic acid-co-acrylamide) grafted chitosan with salt- and pH-responsiveness properties.* European Polymer Journal, 2004. **40**(7): p. 1399-1407.
294. Choi, Y., H.-J. Kim, and K.-S. Min, *Effects of proanthocyanidin, a crosslinking agent, on physical and biological properties of collagen hydrogel scaffold.* Restor Dent Endod, 2016. **41**(4): p. 296-303.
295. He, L., et al., *Modification of collagen with a natural cross-linker, procyanidin.* International Journal of Biological Macromolecules, 2011. **48**(2): p. 354-359.
296. Moradi, M., et al., *Characterization of antioxidant chitosan film incorporated with Zataria multiflora Boiss essential oil and grape seed extract.* LWT - Food Science and Technology, 2012. **46**(2): p. 477-484.
297. Farris, S., et al., *Wetting of Biopolymer Coatings: Contact Angle Kinetics and Image Analysis Investigation.* Langmuir, 2011. **27**(12): p. 7563-7574.
298. Milleret, V., et al., *Alkali treatment of microrough titanium surfaces affects macrophage/monocyte adhesion, platelet activation and architecture of blood clot formation.* Eur Cell Mater, 2011. **21**: p. 430-44; discussion 444.
299. Lee, B.A., et al., *Surface characteristics and osteoblastic cell response of alkali-and heat-treated titanium-8tantalum-3niobium alloy.* J Periodontal Implant Sci, 2012. **42**(6): p. 248-55.

300. Kwon, O.H., et al., *Rapid cell sheet detachment from Poly(N-isopropylacrylamide)-grafted porous cell culture membranes.* Journal of Biomedical Materials Research, 2000. **50**(1): p. 82-89.
301. Schneider, G.B., et al., *The effect of hydrogel charge density on cell attachment.* Biomaterials, 2004. **25**(15): p. 3023-3028.
302. Bosworth, L.A., et al., *Enhancing Biocompatibility without Compromising Material Properties: An Optimised NaOH Treatment for Electrospun Polycaprolactone Fibres.* Journal of Nanomaterials, 2019. **2019**.
303. Gao, J., L. Niklason, and R. Langer, *Surface hydrolysis of poly(glycolic acid) meshes increases the seeding density of vascular smooth muscle cells.* Journal of Biomedical Materials Research, 1998. **42**(3): p. 417-424.
304. Wang, X., et al., *Procyanidins-crosslinked aortic elastin scaffolds with distinctive anti-calcification and biological properties.* Acta Biomaterialia, 2015. **16**: p. 81-93.
305. Castellan, C.S., et al., *Mechanical characterization of proanthocyanidin–dentin matrix interaction.* Dental Materials, 2010. **26**(10): p. 968-973.
306. Shavandi, A., et al., *Polyphenol uses in biomaterials engineering.* Biomaterials, 2018. **167**: p. 91-106.
307. Elizalde-Peña, E.A., et al., *Synthesis and characterization of chitosan-g-glycidyl methacrylate with methyl methacrylate.* European Polymer Journal, 2007. **43**(9): p. 3963-3969.
308. Liu, Z., et al., *Effects of chitosan molecular weight and degree of deacetylation on the properties of gelatine-based films.* Food Hydrocolloids, 2012. **26**(1): p. 311-317.
309. Qiao, C., et al., *Molecular interactions in gelatin/chitosan composite films.* Food Chemistry, 2017. **235**: p. 45-50.
310. Tan, Y.M., et al., *Functional chitosan-based grapefruit seed extract composite films for applications in food packaging technology.* Materials Research Bulletin, 2015. **69**: p. 142-146.
311. Lin, Y., et al., *Surface modification of poly(L-lactic acid) to improve its cytocompatibility via assembly of polyelectrolytes and gelatin.* Acta Biomaterialia, 2006. **2**(2): p. 155-164.
312. Wang, Y.K. and C.S. Chen, *Cell adhesion and mechanical stimulation in the regulation of mesenchymal stem cell differentiation.* J Cell Mol Med, 2013. **17**(7): p. 823-32.
313. Kim, C.H., et al., *An improved hydrophilicity via electrospinning for enhanced cell attachment and proliferation.* Journal of Biomedical Materials Research Part B: Applied Biomaterials, 2006. **78B**(2): p. 283-290.
314. Schwartz, M.A. and D.W. DeSimone, *Cell adhesion receptors in mechanotransduction.* Current Opinion in Cell Biology, 2008. **20**(5): p. 551-556.
315. Chau, D.Y.S., et al., *The cellular response to transglutaminase-cross-linked collagen.* Biomaterials, 2005. **26**(33): p. 6518-6529.
316. Freeman, F.E. and D.J. Kelly, *Tuning Alginate Bioink Stiffness and Composition for Controlled Growth Factor Delivery and to Spatially Direct MSC Fate within Bioprinted Tissues.* Sci Rep, 2017. **7**(1): p. 17042.
317. Ketelson, H.A., D.L. Meadows, and R.P. Stone, *Dynamic wettability properties of a soft contact lens hydrogel.* Colloids and Surfaces B: Biointerfaces, 2005. **40**(1): p. 1-9.
318. Maldonado-Codina, C. and N. Efron, *Dynamic wettability of pHEMA-based hydrogel contact lenses.* Ophthalmic and Physiological Optics, 2006. **26**(4): p. 408-418.
319. Read, M.L., P.B. Morgan, and C. Maldonado-Codina, *Measurement errors related to contact angle analysis of hydrogel and silicone hydrogel contact lenses.* Journal of Biomedical Materials Research Part B: Applied Biomaterials, 2009. **91B**(2): p. 662-668.
320. Cheng, L., S.J. Muller, and C.J. Radke, *Wettability of silicone-hydrogel contact lenses in the presence of tear-film components.* Current Eye Research, 2004. **28**(2): p. 93-108.
321. Xi, W., et al., *Material approaches to active tissue mechanics.* Nature Reviews Materials, 2019. **4**(1): p. 23-44.
322. Rothdiener, M., et al., *Stretching human mesenchymal stromal cells on stiffness-customized collagen type I generates a smooth muscle marker profile without growth factor addition.* Scientific Reports, 2016. **6**(1): p. 35840.
323. Tee, S.-Y., et al., *Cell Shape and Substrate Rigidity Both Regulate Cell Stiffness.* Biophysical Journal, 2011. **100**(5): p. L25-L27.
324. Thakur V.K., A.O.A., *History, Classification, Properties and Application of Hydrogels: An Overview.* , in *Hydrogels. Gels Horizons: From Science to Smart Materials.* , T.M. Thakur V., Editor. (2018), Springer, : Singapore.
325. Buxboim, A., I.L. Ivanovska, and D.E. Discher, *Matrix elasticity, cytoskeletal forces and physics of the nucleus: how deeply do cells 'feel' outside and in?* Journal of Cell Science, 2010. **123**(3): p. 297.
326. Winkelmann, M., et al., *Chemically patterned, metal oxide based surfaces produced by photolithographic techniques for studying protein– and cell–surface interactions I: Microfabrication and surface characterization.* Biomaterials, 2003. **24**(7): p. 1133-1145.
327. Lai, M., et al., *Surface functionalization of TiO2 nanotubes with bone morphogenetic protein 2 and its synergistic effect on the differentiation of mesenchymal stem cells.* Biomacromolecules, 2011. **12**(4): p. 1097-1105.
328. Donaldson, A.R., et al., *Photocrosslinkable Gelatin Hydrogels Modulate the Production of the Major Pro-inflammatory Cytokine, TNF-alpha, by Human Mononuclear Cells.* Front Bioeng Biotechnol, 2018. **6**: p. 116.
329. Shu, Y., et al., *A simple fabricated thickness-based stiffness gradient for cell studies.* Science Bulletin, 2017. **62**(3): p. 222-228.

330. Hillam RA, S.T., *Inhibition of bone resorption and stimulation of formulation by mechanical loading of the modeling rat ulna in vivo. .* J Bone Miner Res (1995)(10:): p. 683-689.
331. Grinnell F, Z.M., Carlson MA,, *Release of mechanical tension triggers apoptosis of human fibroblasts in a model of regressing granulation tissue. .* Cell Res, 1999. **248(2)**: p. 608-619.
332. Smitha K, H.S., Sunwooc M *The dependence of MG63 osteoblast responses to (meth)acrylate-based networks on chemical structure and stiffness, .* Biomaterials, 2010, . **Volume 31 ,** (Agust): p. 6131-6141. .
333. Solon J., L.I., Sengupta K., , *Fibroblast Adaptation and Stiffness Matching to Soft Elastic Substrates, .* Biophysical Journal 2007. **93:** : p. 4453-4461.
334. Khatiwala C., P.S., Putnam M.,, *The regulation of osteogenesis by ECM rigidity in MC3T3-E1 cells requires MAPK activation, J Cell Physiol, .* (2007). **211** ((3)): p. 661-672.
335. Carraher C., S.J., *Regulation of Matrix Assembly through Rigidity-dependent Fibronectin Conformational Changes, .* J of Biological Chemistry, 2013. **J Biol Chemv.** (21): p. 288.
336. Georges P. C., H.J.J., Gombos Z., McCormick M. Increased stiffness of the rat liver precedes matrix deposition: implications for fibrosis. Am. J. Physiol. Gastrointest. 2007, Liver Physiol. 293, G1147-G1154, *Increased stiffness of the rat liver precedes matrix deposition: implications for fibrosis. Am. J. .* Physiol. Gastrointest., 2007 **293,**: p. G1147-G1154.
337. Saha, K., et al., *Substrate modulus directs neural stem cell behavior.* Biophysical Journal, 2008. **95**(9): p. 4426-4438.
338. Douezan, S., J. Dumond, and F. Brochard-Wyart, *Wetting transitions of cellular aggregates induced by substrate rigidity.* Soft Matter, 2012. **8**(17): p. 4578-4583.
339. Song, W., N. Kawazoe, and G. Chen, *Dependence of spreading and differentiation of mesenchymal stem cells on micropatterned surface area.* J. Nanomaterials, 2011. **2011**: p. Article 6.
340. Kilian, K.A., et al., *Geometric cues for directing the differentiation of mesenchymal stem cells.* Proceedings of the National Academy of Sciences, 2010. **107**(11): p. 4872.
341. Hwang, J.-H., et al., *Extracellular Matrix Stiffness Regulates Osteogenic Differentiation through MAPK Activation.* PloS one, 2015. **10**(8): p. e0135519-e0135519.
342. van Eijden, T.M.G.J., L.J. van Ruijven, and E.B.W. Giesen, *Bone Tissue Stiffness in the Mandibular Condyle is Dependent on the Direction and Density of the Cancellous Structure.* Calcified Tissue International, 2004. **75**(6): p. 502-508.
343. Fekete, N., et al., *Bags versus flasks: a comparison of cell culture systems for the production of dendritic cell–based immunotherapies.* Transfusion, 2017. **58**.
344. Kim, T.H., et al., *Creating stiffness gradient polyvinyl alcohol hydrogel using a simple gradual freezing-thawing method to investigate stem cell differentiation behaviors.* Biomaterials, 2015. **40**: p. 51-60.
345. Nasrollahi, S., et al., *Past matrix stiffness primes epithelial cells and regulates their future collective migration through a mechanical memory.* Biomaterials, 2017. **146**: p. 146-155.
346. Oh, S.H., et al., *Wide-range stiffness gradient PVA/HA hydrogel to investigate stem cell differentiation behavior.* Acta Biomater, 2016. **35**: p. 23-31.
347. Donnelly, H., M. Salmeron-Sanchez, and M.J. Dalby, *Designing stem cell niches for differentiation and self-renewal.* Journal of The Royal Society Interface, 2018. **15**(145): p. 20180388.
348. Kuhn, N.Z. and R.S. Tuan, *Regulation of stemness and stem cell niche of mesenchymal stem cells: implications in tumorigenesis and metastasis.* J Cell Physiol, 2010. **222**(2): p. 268-77.
349. *<Directed Movement of Vascular Smooth Muscle Cells on Gradient-Compliant Hydrogels.pdf>.*
350. Wang, P.Y., W.B. Tsai, and N.H. Voelcker, *Screening of rat mesenchymal stem cell behaviour on polydimethylsiloxane stiffness gradients.* Acta Biomater, 2012. **8**(2): p. 519-30.
351. Uccelli, A., L. Moretta, and V. Pistoia, *Mesenchymal stem cells in health and disease.* Nature Reviews Immunology, 2008. **8**(9): p. 726-736.
352. Phinney, D.G. and D.J. Prockop, *Concise Review: Mesenchymal Stem/Multipotent Stromal Cells: The State of Transdifferentiation and Modes of Tissue Repair—Current Views.* STEM CELLS, 2007. **25**(11): p. 2896-2902.
353. Shi, Y., et al., *Mesenchymal stem cells: a new strategy for immunosuppression and tissue repair.* Cell Res, 2010. **20**(5): p. 510-8.
354. Li Jeon, N., et al., *Neutrophil chemotaxis in linear and complex gradients of interleukin-8 formed in a microfabricated device.* Nature Biotechnology, 2002. **20**(8): p. 826-830.
355. Chamberlain, G., et al., *Mesenchymal Stem Cells Exhibit Firm Adhesion, Crawling, Spreading and Transmigration across Aortic Endothelial Cells: Effects of Chemokines and Shear.* PLOS ONE, 2011. **6**(9): p. e25663.
356. Tai, G., M. Tai, and M. Zhao, *Electrically stimulated cell migration and its contribution to wound healing.* Burns & trauma, 2018. **6**: p. 20-20.
357. Park, J.Y., et al., *Cell morphological response to low shear stress in a two-dimensional culture microsystem with magnitudes comparable to interstitial shear stress.* Biorheology, 2010. **47**: p. 165-178.
358. Zhang, H., et al., *Gene expression of single human mesenchymal stem cell in response to fluid shear.* Journal of Tissue Engineering, 2012. **3**(1): p. 2041731412451988.

359. Wong, A.K., et al., *A Parallel-Plate Flow Chamber for Mechanical Characterization of Endothelial Cells Exposed to Laminar Shear Stress.* Cellular and Molecular Bioengineering, 2016. **9**(1): p. 127-138.
360. Salvi, J.D., J.Y. Lim, and H.J. Donahue, *Finite element analyses of fluid flow conditions in cell culture.* Tissue engineering. Part C, Methods, 2010. **16**(4): p. 661-670.
361. Riehl, B.D., et al., *Fluid-flow-induced mesenchymal stem cell migration: role of focal adhesion kinase and RhoA kinase sensors.* Journal of the Royal Society, Interface, 2015. **12**(107): p. 20150300.
362. Huang AH, F.M., Kim M, Mauck RL. , *Long-term dynamic loading improves the mechanical properties of chondrogenic mesenchymal stem cell-laden hydrogel.* Eur Cell Mater, 2010. **19**: p. 72-85.
363. Rouillard, A.D. and J.W. Holmes, *Mechanical boundary conditions bias fibroblast invasion in a collagen-fibrin wound model.* Biophysical journal, 2014. **106**(4): p. 932-943.
364. Kaushal, S., et al., *Functional small-diameter neovessels created using endothelial progenitor cells expanded ex vivo.* Nat Med, 2001. **7**(9): p. 1035-40.
365. Riehl, B.D., et al., *Fluid-flow-induced mesenchymal stem cell migration: role of focal adhesion kinase and RhoA kinase sensors.* Journal of The Royal Society Interface, 2015. **12**(104): p. 20141351.
366. Kreke, M.R. and A.S. Goldstein, *Hydrodynamic Shear Stimulates Osteocalcin Expression But Not Proliferation of Bone Marrow Stromal Cells.* Tissue Engineering, 2004. **10**(5-6): p. 780-788.
367. Gao, X., et al., *Regulation of cell migration and osteogenic differentiation in mesenchymal stem cells under extremely low fluidic shear stress.* Biomicrofluidics, 2014. **8**(5): p. 052008.
368. Dong, J.-d., et al., *Response of mesenchymal stem cells to shear stress in tissue-engineered vascular grafts.* Acta pharmacologica Sinica, 2009. **30**(5): p. 530-536.
369. Guo, W.-h., et al., *Substrate rigidity regulates the formation and maintenance of tissues.* Biophysical journal, 2006. **90**(6): p. 2213-2220.
370. Molladavoodi, S., et al., *Human corneal epithelial cell response to substrate stiffness.* Acta Biomater, 2015. **11**: p. 324-32.
371. Choi, J., et al., *Maturation of Adipocytes is Suppressed by Fluid Shear Stress.* Cell Biochem Biophys, 2017. **75**(1): p. 87-94.
372. Chandler, E.M., et al., *Stiffness of photocrosslinked RGD-alginate gels regulates adipose progenitor cell behavior.* Biotechnology and Bioengineering, 2011. **108**(7): p. 1683-1692.
373. Liu, L., et al., *Extracellular signal-regulated kinase1/2 activated by fluid shear stress promotes osteogenic differentiation of human bone marrow-derived mesenchymal stem cells through novel signaling pathways.* The International Journal of Biochemistry & Cell Biology, 2011. **43**(11): p. 1591-1601.
374. Lim, K.T., et al., *Synergistic Effects of Orbital Shear Stress on In Vitro Growth and Osteogenic Differentiation of Human Alveolar Bone-Derived Mesenchymal Stem Cells.* BioMed Research International, 2014. **2014**: p. 316803.
375. Maul, T.M., et al., *Mechanical stimuli differentially control stem cell behavior: morphology, proliferation, and differentiation.* Biomechanics and modeling in mechanobiology, 2011. **10**(6): p. 939-953.
376. Liu, L., et al., *The interaction between beta1 integrins and ERK1/2 in osteogenic differentiation of human mesenchymal stem cells under fluid shear stress modelled by a perfusion system.* J Tissue Eng Regen Med, 2014. **8**(2): p. 85-96.